

Traction Force-Speed Based Modelling for Hybrid Vehicle Energy Consumption
(ハイブリッド車のエネルギー消費計算のための
駆動力・車速ベースモデルに関する研究)

PITANUWAT, Siriorn

Doctor of Engineering
Graduate School of Environmental Studies, Nagoya University

2020

Traction Force-Speed Based Modelling for Hybrid Vehicle Energy Consumption

by

Siriorn Pitanuwat

Graduated School of Environmental Engineering

Nagoya University

Submitted in partial fulfillment
of the requirements for the degree of

Doctor of Engineering

Nagoya, Japan

September 2020

ABSTRACT

According to the coming of rapid hybrid-vehicles penetration, it is necessary to prepare effective tools to help projecting the directions of future developments on on-road transportation fuel consumption and greenhouse gas emissions. Thus, this study attempts to develop hybrid vehicles' energy consumption model for transportation research applications. I also present an inclusive modeling methodology which consisted of hybrid vehicles experiment, data acquisition, data processing, power-split hybrid powertrain operation control analysis, and the hybrid vehicles' energy consumption modeling. Based on the hybrid powertrain operation characteristics examined in this study, a microscopic analytical-empirical energy-consumption model called Traction Force-Speed based Energy Consumption Model (TFS model) is proposed.

Real-world experiments, private circuit experiments, and chassis dynamometer experiments are conducted to analyze and compare the advantages and disadvantages. According to the finding, real-world experiments are the most suitable approach for vehicles' fuel-consumption data acquisition. Meanwhile, chassis dynamometer experiments could provide the ability to sweep the powertrain operation points through all the regions. Thus, chassis dynamometer experiments are highly recommended for the data acquisition for the powertrain operation characteristics.

Next, this study investigates and validated the operation characteristics by applying the dataset to improve the powertrain operation models to become more realistic by using the Prius3 CRUISE AVL simulation platform. To obtain the requisite parameters, the power-flow path inside the power-split configuration is analyzed. Then, the powertrain's dynamic equations were derived and adopted in the parameter estimations and map calibrations. By applying the calibrated maps and models into the simulation, the fuel consumption and powertrain operation are significantly improved to be more realistic. According to the analysis, it indicated that the hybrid powertrain operated in multi-operation modes. The transition of the modes could be simplified and expressed by boundaries specified by vehicle speed and driving force as the X-Y axis. In addition, the boundaries also varies depending on the instantaneous available battery power.

One of the most important modeling processes is to estimate vehicle driving power. Firstly, a practical and cost-efficient approach to recalibrate coefficients of the vehicle-driving-power estimation equation for a specific vehicle model or fleet is proposed. This study implements the assessable CAN dataset to estimate the powertrain's total driving power via the powertrain's dynamic equation derived in the previous process. The coefficients in the vehicle-driving-power-estimation equation are calibrated with the powertrain's total driving power by applying stepwise multiple regression method. The results show that the calibrated equation significantly improved the driving power estimation compared to the conventional VSP (Jiménez et al., 1999). Particularly under heavy load driving (above 50kW) and high-speed driving (above 80km/h), the proposed method

substantially suppressed the prediction error by having the coefficient improved from 0.79 to 0.96.

Then, the TFS model is constructed based on the relationships between the vehicle speed and the average fuel consumption rate at specified traction force intervals. The trend of the vehicle speed and the fuel consumption rate monotonically increased as the traction force became more intense. The prediction results show that the TFS method efficiently reduced the error by 57% down to 23% compared to the conventional VSP energy consumption modeling method.

Furthermore, this study also explores hybrid vehicle fuel consumption characteristics in a different aspect. The objective of the project was to investigate the impact of winter tires and summer tires on hybrid vehicle fuel consumption. This study suggests a new parameter called instantaneous hybrid powertrain efficiency that incorporated the efficiency of the electric system and the engine system. The results show that this parameter provided the capability to analyze and visualize delicate factors that impacted the fuel consumption of the hybrid powertrains compared to fuel economy-oriented parameters, such as L/100km or km/L. Finally, the most significant remark is found that the summer tires tend to allow the powertrain system to operate at higher efficiency regions more frequently than the winter tires, particularly during deceleration under EV and HV regenerative braking and typical hybrid driving.

ACKNOWLEDGEMENTS

I would like to express my gratitude and appreciation to my supervisor, Prof. Hirofumi Aoki whose guidance, feedback, support, and encouragement has been invaluable throughout both my Ph.D. study and my student life in Japan. I also would like to thank the dissertation committee members, Prof. Satoru Iizuka, and Prof. Yasuhiro Mori for valuable advice on my dissertation. I want to express my appreciation to Prof. Takayuki Morikawa for his stimulating question and discussion on transportation research perspectives. I also would like to say special thank you to Tateishi Sadayoshi and the COI technical team for providing professional know-how and support on my vehicle experiment and data acquisition.

During my Ph.D., I am extremely grateful to participate in Michelin-Nagoya University collaborative research project. I would like to thank all the members especially Jung Woosang, Motohiro Asai, and Pierre Grange from Michelin. Throughout all three-year challenging research campaigns, I have developed both soft and hard skills including self-confidence. Most of all, I would like to express sincere gratitude to professor Tetsunori Haraguchi for the life-changing opportunities and experiences which are great steps toward my passionate hybrid powertrain development career path.

Many thanks to my supportive friends and professors, Dr. Li Yanyan, Dr. Mingyang Hao, Dr. Son Le Ahn, Nguyen Thanh Tung, Dr. Thomas Wilhelem, Dr. Ekim Yurtsever,

Patiphon Narksri, and Supatcha Chavalvechakul, and Assoc. Prof. Angkee Sripakagorn for encouraging and sharing ideas on my research.

I also would like to thank important people; Haruka Hirose, Mio Yamada, Temsiri Klissanawanich, Panwad Ritthisan, Thippachanh Souphihalath, Warittha Ratanacharee, Hiromi Takahashi, especially Izumi Araki, Makiko Kasuya, Suwalak Khanpruksa, and Ninnet Ongartthaworn, who always stand beside me sharing love and comfort through all good and bad time.

Last but not least, I would like to thank my family. Without their encouragement and unconditional support, I could not accomplish this work I have done.

TABLE OF CONTENT

TABLE OF CONTENT	I
LIST OF FIGURES.....	VI
LIST OF TABLES	XI
ABBREVIATIONS AND ACRONYMS	XII
Abbreviations.....	XII
Acronyms	XIV
CHAPTER 1 Introduction	1
1.1 Background	1
1.2 Problem Statement.....	5
1.3 Objective	7
1.4 Chapter organization	8
CHAPTER 2 Literature Review	10
2.1 Factors influencing vehicles’ energy consumption and GHG emissions.....	10
2.2 Vehicle energy consumption modeling methods	13
2.2.1 Vehicle energy consumption modeling methods in the transportation research field	15
2.2.2 Vehicle energy consumption modeling methods in the automotive research field	23
CHAPTER 3 Power-Split Hybrid Powertrain	29
3.1 Hybrid Vehicles Configuration.....	29
3.1.1 Series Hybrid.....	30
3.1.2 Parallel Hybrid	32
3.1.3 Series-Parallel Hybrid	34
3.2 Toyota Hybrid System of the Third Generation of Toyota Prius	36

3.2.1 Powertrain Configuration	36
3.2.2 Hybrid Powertrain Operation and Energy Management Strategy.....	38
3.3 Dynamic Equation Formulation and Power Transmission Analysis of the Third Generation of Toyota Prius.....	54
3.3.1 Power-Split Hybrid Powertrain Dynamic Equation Formulation.....	55
CHAPTER 4 Experiment and Data Acquisition for Hybrid Vehicles	66
4.1 Data Acquisition for Hybrid Vehicles	67
4.1.1 Controller Area Network (CAN) Signal.....	68
4.1.2 Fuel Consumption.....	74
4.1.3 High Voltage Battery	78
4.1.4 Electronic Circuit and Analog-Digital Signal Converter	79
4.1.5 Wind speed.....	80
4.1.6 Vehicle dynamics.....	81
4.1.7 Vehicle speed feedback display	82
4.1.8 Data acquisition system integration	83
4.2 Hybrid vehicle experiment.....	84
4.2.1 Real-world driving (NGO).....	85
4.2.2 Private circuit (JARI)	91
4.2.3 Chassis dynamometer (DYNO).....	98
4.2.4 Final conclusion for the three experimental approaches.....	106
CHAPTER 5 Quasi-Static Hybrid Powertrain Energy Consumption Modeling	109
5.1 Introduction	109
5.1.1 Simulation structure and component functions.....	110
5.1.2 Simulation flow and calculation algorithm	114
5.1.3 CRUISE Prius3 preliminary validation.....	118
5.1.4 CRUISE Prius3's problems identification.....	122
5.2 Scope of the improvement process.....	124
5.2.1 Hybrid operation control	125
5.2.2 Battery operation control	129

5.2.3 Engine operation control	132
5.2.4 Others	135
5.3 Methodology	136
5.3.1 Experiment	136
5.3.2 Data processing and filtering.....	137
5.3.3 Key parameter estimation	138
5.3.4 Map calibration and constant parameter tuning	138
5.3.5 Minor map adjustment.....	139
5.4 Key parameter estimation	139
5.4.1 High voltage battery	140
5.4.2 Engine	140
5.4.3 Motor/generator	140
5.4.4 Powertrain output	141
5.4.5 Energy equivalent conversion.....	142
5.4.6 Performance and efficiency.....	142
5.4.7 External observatory parameters.....	143
5.5 The dynamic model validation.....	144
5.5.1 Engine Dynamic Model	144
5.5.2 Powertrain Dynamic Model	147
5.6 Prius3 simulation calibrations and improvements	152
5.6.1 Hybrid operation control map calibration	152
5.6.2 Battery operation control	163
5.6.3 Engine operation control	167
5.6.4 Others	173
5.7 Results and Validation.....	176
5.7.1 Simulation condition set-up.....	176
5.7.2 Hybrid powertrain operation validation	179
5.7.3 Engine on time.....	188
5.7.4 Fuel consumption validation	189

5.8 Conclusion.....	192
CHAPTER 6 Microscopic Hybrid Vehicle Energy Consumption Modeling:.....	196
6.1 Development of Hybrid-Vehicle Energy-Consumption Model for Transportation Applications—Part I: Driving-Power Equation Development and Coefficient Calibration.....	196
6.1.1 Introduction and literature review	197
6.1.2 Methodology	204
6.1.3 Results and Discussion.....	215
6.1.4 Conclusions.....	230
6.2 Development of Hybrid-Vehicle Energy-Consumption Model for Transportation Applications—Part II: Traction Force-Speed Based Energy Consumption Modeling.....	232
6.2.1 Introduction and Literature review	233
6.2.2 Experimental set-up and data acquisition.....	238
6.2.3 Methodology	242
6.3.4 Results and discussions	250
6.3.5 Conclusion.....	255
6.3.6 Further improvement.....	256
CHAPTER 7 Hybrid Vehicle Energy Consumption Characteristic Analysis and Applications	257
7.1 An investigation of the impact of summer (Energy Saver +) and winter (ALPIN) tires on hybrid vehicle’s fuel consumption in real-world traffic driving.....	257
7.1.1 Introduction	257
7.1.2 Methodology	259
7.1.3 Result and discussion	262
7.1.4 Conclusion.....	266
CHAPTER 8 Conclusion and Future Work.....	268
8.1 Conclusion.....	268
8.2 Future Work.....	271
BIBLIOGRAPHY.....	272

LIST OF FIGURES

Figure 1 World Greenhouse Emission in 2016 classified by sectors-end use-emission gases.....	2
Figure 2 Green House Gases emission from the transportation sector (IPCC, 2014).....	3
Figure 3 Market trend of powertrain technology (Green Car Congress, 2017)	5
Figure 4 Dissertation structure.....	9
<i>Figure 5 Related factors dominating vehicle fuel consumption.....</i>	<i>12</i>
Figure 6 Fuel consumption modeling methods and the tread off between precision and computational load	15
Figure 7 Kinematic modeling approach.....	24
Figure 8 Quasi-static modeling approach	26
Figure 9 Series hybrid configuration	31
Figure 10 Parallel hybrid configuration.....	33
Figure 11 Series-parallel hybrid (Toyota Hybrid System)	35
Figure 12 Series parallel hybrid (Honda iMMD)	35
Figure 13 Toyota Prius3' power train configuration (Allouchery, 2012)	37
Figure 14 Driving force estimation.....	41
Figure 15 Requested battery charging power	43
Figure 16 Engine on/off judgment in Prius3	44
Figure 17 Relationship between available battery output power and battery soc.....	45
Figure 18 Prius3's dominant operation modes	48
Figure 19 THS operation modes described by vehicle speed and driving force	49
Figure 20 THS operation modes projected on engine operation region.....	52
Figure 21 Electrical power utilization during idling.....	54
Figure 22 Prius3's powertrain structure (Allouchery, 2012)	56
Figure 23 Prius3's powertrain free body diagram	57
Figure 24 Force free body diagram at the carrier for internal.....	58
Figure 25 Prius3's free body diagram at the carrier	59
Figure 26 Prius3's free body diagram at the sun gear.....	60
Figure 27 Prius3's free body diagram at ring gear	61
Figure 28 Prius3 Powertrain's nomographic chart.....	65
Figure 29 Power flow inside hybrid vehicles.....	68
Figure 30 Toyota DENSO Intelligent Tester 2 (IT2)	70

Figure 31 OTC Vehicle Interface Module (VIM).....	71
Figure 32 Fuel flow meter FMTD20	75
Figure 33 Flow meter installation equipment.....	78
Figure 34 High voltage battery's current sensor installation.....	79
Figure 35 External sensors' power supply and signal management module.....	80
Figure 36 Pitot tube wind speed sensor installation	81
Figure 37 Ninja Box IMU+GPS unite	82
Figure 38 Vehicle speed feedback display	83
Figure 39 Structure of the data acquisition system	84
Figure 40 Nagoya city center route	86
Figure 41 Nagoya highway route.....	87
Figure 42 Real-world experiment on highway driving.....	89
Figure 43 Real-world experiment on city driving.....	89
Figure 44 Winter-summer Tire displacement.....	90
Figure 45 JARI Shirosato outer-ring circuit layout.....	92
Figure 46 Constant acceleration speed pattern design method for a private circuit experiment	94
Figure 47 The operation points/region of HWFET on	94
Figure 48 Private circuit experiment.....	96
Figure 49 Data acquisition system.....	97
Figure 50 2-roller chassis dynamometer at Nagoya University.....	99
Figure 51 Powertrain operation points variation by using constant speed force mode	100
Figure 52 Vehicle set-up on chassis dynamometer	104
Figure 53 Constant speed and continuous speed test on Chassis dynamometer.....	104
Figure 54 Cooling fans for engine, exhaust pipe system including catalytic converter	105
Figure 55 AVL CRUISE Prius3	113
Figure 56 AVL CRUISE Prius3 simulation flow	117
Figure 57 Preliminary validation on engine on/off issue.....	119
Figure 58 Percentage of engine on prediction error.....	120
Figure 59 CRUISE Prius3 fuel consumption preliminary validation	121
Figure 60 Engine on/off control criteria maps in CRUISE Prius3.....	125
Figure 61 Boosting mode control maps in CRUISE Prius3	128
Figure 62 Battery operation control maps	130
Figure 63 Engine operation control maps	132
Figure 64 Engine IL4 16V fuel consumption map.....	Error! Bookmark not defined.

Figure 65 Key parameter estimation process.....	138
Figure 66 Comparison between $P_{ice_reqst_OBD}$ vs P_{ice_DynEq}	145
Figure 67 Comparison between $P_{ice_reqst_OBD}$ vs $P_{ice_DynEq_MultiRegress}$	146
Figure 68 Engine power compared among engine dynamic equation with CRUISE Prius3's coefficients (DynEq), dynamic equation with re-calibrated coefficients (DynEq+MR), and Engine Requested Power from HV ECU (OBD)	147
Figure 69 The characteristic of the chassis dynamometer error	149
Figure 70 Driving torque dynamic equation validation	150
Figure 71 Driving Power dynamic equation validation.....	151
Figure 72 STST, Tmax, Pmax maps classified by engine operation state	156
Figure 73 battery output power at different soc from JARI, DYNO, and NGO datasets	157
Figure 74 Data quality assurance for STST, Tmax, and Pmax maps	158
Figure 75 Re-calibration of STST, Tmap, Pmax map.....	161
Figure 76 BOOST pkW SOC map re-calibration	163
Figure 77 BATMAN rp MOT map recalibration.....	164
Figure 78 BATMAN rp Reкуп map recalibration	165
Figure 79 BATMAN rp eDRV map recalibration	166
Figure 80 , BATMAN pkW Alt map recalibration.....	167
Figure 81 2D-data screening process for engine maps re-calibration.....	169
Figure 82 2D-data screening applied to engine optimal operation curve.....	170
Figure 83 Engine optimal operation curve recalibration.....	170
Figure 84 2D-data screening applied to fuel consumption data	171
Figure 85 Engine fuel consumption map re-calibration for rpm [3,125-5,200]	172
Figure 86 re-calibrated full engine fuel consumption map.....	173
Figure 87 Hybrid control constant parameter re-calibration	174
Figure 88 Engine warm up deactivation.....	175
Figure 89 Naturalistic SOC calculation activation.....	175
Figure 90 Speed Profile input window.....	177
Figure 91 Road grade profile input window	177
Figure 92 Initial SOC input window	178
Figure 93 AUX power input window.....	178
Figure 94 Simulation results under JARI_a1b1_Constant Acceleration driving conditions	180
Figure 95 Simulation results under JARI Naturalistic acceleration from_0-100km/h and constant speed at 20 km/h driving conditions.....	182

Figure 96 Simulation results under NGO_CITY1_SummerTire(B) driving conditions	183
Figure 97 Simulation results under NGO_CITY3_SummerTire(B) driving conditions	185
Figure 98 Simulation results under NGO_HW2_Hongo-to-Komaki_SummerTire(B) driving conditions	187
Figure 99 Simulation results under NGO_HW2_Komaki-to-Hongo_SummerTire(B) driving conditions	187
Figure 100 Summary of the engine on time percentage	189
Figure 101 Summary of prediction error on the engine on time percentage	189
Figure 102 Summary of the fuel consumption prediction	191
Figure 103 Summary of prediction error on the total fuel consumption	191
Figure 104 Relationship between the engine on time error and fuel consumption prediction error	192
Figure 105 Analytical experiment on third-generation Prius (Prius3) at Japanese Automobile Research Institute (JARI) Shirosato	207
Figure 106 Prius3 powertrain structure	209
Figure 107 Figure 3. Free-body diagram of Prius3 powertrain	210
Figure 108 Validation of vehicle driving-power estimations compared to powertrain driving power (<i>PPTdrv</i>). (a) Light-load driving (<50 kW), and (b) heavy-load driving (≥ 50 kW)	220
Figure 109 Comparison of error residues from <i>DrvPwPrius3</i> , VSP Prius3Spec, and VSP LDV 1999. (a) Light-load driving (<50 kW) and (b) heavy-load driving (≥ 50 kW)	221
Figure 110 Prius3 driving-power prediction results at light-load driving during naturalistic acceleration and high-speed cruising	222
Figure 111 Figure 7. Prius3 driving-power prediction results during heavy-load driving during maximal acceleration	223
Figure 112 Driving-power-prediction error analysis on impact of driving speed on prediction errors from VSP LDV 1999, VSP Prius3Spec, and <i>DrvPw_Prius3</i>	225
Figure 113 Driving-power-prediction error analysis	227
Figure 114 Contribution of each driving-power term	229
Figure 115. Analytical experimental set-up and equipment	240
Figure 116. Real-world experiment routes' orientations and locations (Pitanuwat and Sripakagorn, 2015)	241
Figure 117. Analysis of the fuel consumption characteristics based on the conventional	243

Figure 118. Prius3's hybrid operation mode classification based on instantaneous driving.....	244
Figure 119. Traction Force-Speed Based Fuel Consumption Model.....	249
Figure 120 Fuel consumption prediction results of the third generation Toyota Prius (Prius3)'s traction force-speed based model.	252
Figure 121. Fuel consumption prediction validation among <i>DrvPwPrius3</i> and <i>TFS model</i>	253
Figure 122 Fuel consumption prediction error between <i>DrvPwPrius3</i> and <i>TFS model</i>	255
Figure 123 Comparison between fuel consumption of Prius3 driving with the summer and	259
Figure 124 Distribution of the driving force and power between the winter tires (Ta) and the summer tires (Tb) during the experiment.....	261
Figure 125 Comparison between the hybrid powertrain efficiency distribution	263
Figure 126 Comparison between the hybrid powertrain efficiency distribution during	264
Figure 127 Comparison between the hybrid powertrain efficiency distribution during active and inactive regenerative braking.....	266

LIST OF TABLES

Table 1 Literature review of Jimenez’s VSP LDT equation and VSP based modeling method	22
Table 2 Summary of automotive modeling methods.....	28
Table 3 Requisite dataset from HV ECU	72
Table 4 Flow meter installation information.....	76
Table 5 Vehicle condition preparation for the real-world experiment	88
Table 6 Speed patterns for private circuit experiment.....	95
Table 7 Vehicle condition preparation for private circuit experiment.....	96
Table 8 Test schedule for chassis dynamometer experiment.....	102
Table 9 Vehicle condition preparation for chassis dynamometer experiment	103
Table 10 Chassis Dynamometer experiment summary.....	106
Table 11 Advantage and disadvantage among real-world, private circuit, and chassis dynamometer experimental approaches	108
Table 12 Summary of CRUISE Prius3 established problem	124
Table 13 Information for engine on/off control criteria map calibration.....	127
Table 14 Information for Boost mode decision map calibration	129
Table 15 Information for battery operation control map calibration.....	131
Table 16 Information for engine operation control map calibration.....	134
Table 17 Hybrid control constant parameter tuning.....	135
Table 18 Engine operation state identification criteria based on HV ECU data	154
Table 19 Driving-power estimation classified by contributing factors.....	202
Table 20 Independent-variable (Indt var.) sets for stepwise variation process.	215
Table 21 Coefficient calibration for Prius3 driving-power equations.	218
Table 22 Hybrid powertrain instantaneous efficiency calculation	260

ABBREVIATIONS AND ACRONYMS

Abbreviations

A/C	Air Conditioner
ALL	Experimental database that includes JARI, DYNO, and NGO datasets
AUX	Auxiliary Power
BKK	Bangkok
CAN	Controller Area Network
CD	Chassis Dynamometer
CITY, city	City Experimental Database
Convnt	Conventional
CV	Conventional Vehicles/ Combustion engine vehicles
DYNO	Chassis Dynamometer
ECU	Engine Control Unit
eDrv, eDrive	Electric Driving Mode
EMS	Energy-Management System
ENG	Engine
EV	Electric Vehicle
GHG	Greenhouse Gases
GPS	Global Positioning System
HCU	Hybrid Control Unit
HV	Hybrid Vehicle
HVDrive	Hybrid Driving Mode
HW, hw	Highway Experimental Database
IMU	Inertia Measurement Unit
Indt var	Independent Variable
Inj	Injection Head Lift Duration Signal
ITS	Intelligent Traffic System
JARI	Japan Automobile Research Institute
LDV	Light-Duty Vehicle
MG, MOT	Motor/Generator
NGO	Nagoya
OBD	On-Board Diagnostics
Ori	Result related to the original simulation setting or equation
PHEV	Plug-In Hybrid Electric Vehicle
PI	Proportional–Integral
PID	Proportional–Integral–Derivative

PSM	Permanent Magnet Synchronous Motors
Prius3	Third-Generation Toyota Prius
PT	Powertrain
SAE	Society of Automotive Engineering
SD	Standard Deviation
SIM, Sim	Results obtained from simulation
SOC	State of Charge
TCO	Total Cost of Ownership
TFS model	Traction-Force-Speed-Based fuel-consumption model
THS	Toyota Hybrid System
US EPA	The United States Environmental Protection Agency
Vol	Volume
VSP	Vehicle-Specific Power

Acronyms

A	Vehicle frontal area	(m ²)
A_{front}	Vehicle's frontal area	(m ²)
AeroDrag	Aerodynamic drag	-
a_{veh}	Vehicle acceleration	(m/s ²)
C_d, C_{drag}	Aerodynamic drag coefficient	-
C_r, C_{roll}	Tire rolling-resistance coefficient	-
DrvPW_{Prius3}	Driving power calculated by calibrated Prius3 driving-power equation	(watt)
DynEq	Dynamic Equation	-
effi	Efficiency	-
FEqv	Fuel equivalent	-
fil	Filtered data	-
F_R	Force acting on the ring gear	(N)
F_S	Force acting on the sun gear	(N)
F_r	Force acting on the reduction speed's ring gear	(N)
F_s	Force acting on the reduction speed's sun gear	(N)
F_{wh}, F_{whl}	Wheel force	(N)
G_c, G_{counter}	Gear ratio at counter gear	-
G_f, G_{final}	Gear ratio at final gear	-
G_r, G_{reduction}	Gear ratio at MG2 speed-reduction gear	-
g	Gravitational acceleration	(m/s ²)
h, l	Slope rise and slope length	(m)
I_C	Moment inertia of counter gear	(kg·m ²)
I_{MG1}	MG1 moment inertia	(kg·m ²)
I_{MG2}	MG2 moment inertia	(kg·m ²)
I_R	Ring-gear moment inertia	(kg·m ²)
I_S	Sun-gear moment inertia	(kg·m ²)
I_{ice}	Engine moment inertia	(kg·m ²)
I_{trans2whl}	Transferred inertia at the wheel	(kg·m ²)
I_{wh}, I_{wheel}	Wheel moment inertia	(kg·m ²)
m	Gross vehicle mass	(kg)
MultiReg	Multi regression	-
Ori	Result related to the original simulation setting or equation	-
P_{aero}	Power contributed by the aerodynamic term	(watt)
P_{PT_drv}	Powertrain driving power calculated by powertrain's dynamic equation	(watt)
P_{roll}	Power contributed by the rolling-resistance term	(watt)
PT	Powertrain	-

R	Number of teeth at the ring gear	Teeth
R_{wheel}	Wheel radius	Teeth
r	Number of teeth at the speed reduction's ring gear	m
Regen	Regenerative braking	-
Rqst	Request	-
S	Number of teeth at sun gear	Teeth
s	Number of teeth at the speed reduction's sun gear	Teeth
sup	Supply power or torque	-
VSP LDV1999	Driving power calculated by conventional vehicle-specific-power (VSP) equation with light-duty-vehicle (LDV) coefficients	(watt)
VSP Prius3Spec	Driving power calculated by conventional vehicle-specific-power (VSP) equation with Prius3 vehicle-specific coefficients	(watt)
v_{veh}	Vehicle speed	(m/s)
$v_{veh,\omega_{MG2}}$	Vehicle speed computed by MG2 angular speed signal	(m/s)
v_{wind}	Relative wind speed	(m/s)
ϵ_i	Mass factor inertia term	-
$\mu_{surface}$	Road-surface friction coefficient	-
ρ_{air}	Air density	(kg/m ³)
$\rho_{fuel.E}$	Energy equivalent fuel density	(joule/m ³)
tot	total	-
τ	Torque	(N.m)
$\tau_{C>R}$	Torque transferred from the carrier to ring gear	(N.m)
$\tau_{C>S}$	Torque transferred from carrier to sun gear	(N.m)
τ_{MG1}	MG1 torque	(N.m)
τ_{MG2}	MG2 torque	(N.m)
τ_{PT_drv}	Powertrain driving torque at wheel calculated by powertrain's dynamic equation	(N.m)
τ_{ice}	Engine torque	(N.m)
$\tau_{brake,mech}$	Mechanical braking torque	(N.m)
τ_{drv_resist}	Driving resistance torque	(N.m)
$\tau_{roadload}$	Road load resistance torque	(N.m)
τ_{wh}, τ_{whl}	Wheel torque	(N.m)
Vol	volume	m ³
VSP_{kW, JM1999}	VSP with coefficients proposed by (Jiménez <i>et al.</i> , 1999)	kW
ω	Angular speed	(rad/s)
$\omega_{wh}, \omega_{whl}$	Wheel angular speed	(rad/s)
ω_{MG1}	MG1 rotational speed	(rad/s)
ω_{MG2}	MG2 rotational speed	(rad/s)
$\omega_{MG2@Wh}$	Wheel rotational speed calculated by MG2 speed	(rad/s)
ω_{ice}	Engine revolution	(rad/s)
$\omega_{wh}, \omega_{whl}$	Wheel rotational speed calculated by vehicle speed	(rad/s)
$\dot{\omega}$	Angular acceleration	(rad/s ²)
θ	Road grade angle	(rad)
$\theta_{gradeIT2_g,rad}$	Road grade angle measured from IT2	(m ² .rad)

CHAPTER 1

Introduction

1.1 Background

According to Global Warming of 1.5°C agreement issued by Intergovernmental Panel on Climate Change (IPCC). It indicates that a great number of evidence has confirmed that the rising of global temperature is a key factor that actuates high frequency and intensity of disasters caused from climate change and weather extremes. It increases the risk of flooding, drought, instability of ecosystem, food chain, species loss, extinction on both land and ocean. Furthermore, these problems affect human being such as health, livelihoods, food security, water supply, life security (IPCC, 2014).

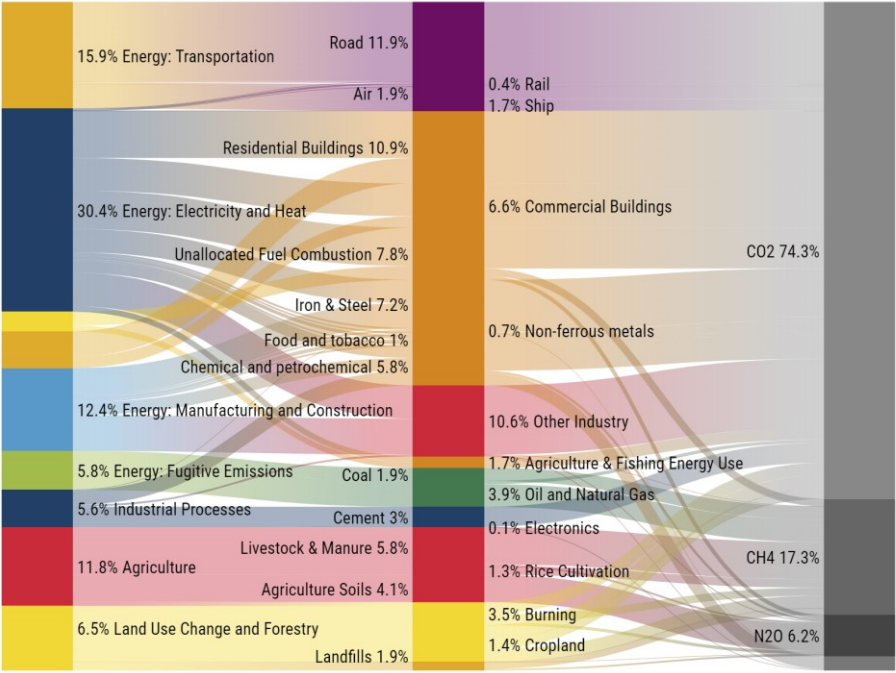
To mitigate this devastation caused by global warming, IPCC has proposed a roadmap to worldwide nations for appropriate responses to suspend the rising of global temperature above 1.5°C by 2100 compared to the pre-industrial level recorded in 1950 (Lah, 2017).

As reported by World Resources Institute, the top three world greenhouse gasses (GHG) and emissions contributors classified by sector are electricity & heat, transportation, and manufacturing & construction. The proportion of energy consumption is 30.4%, 15.9% and 12.4% respectively shown in Figure 1. The transportation sector is the second most

energy-consuming and GHG-emitting sector. At the end of every transportation process, all the energy consumed by vehicles is converted to a tremendous amount of carbon dioxide and emitted into the atmosphere (Ge and Friedrich, 2020).

World Greenhouse Gas Emissions in 2016 (Sector | End Use | Gas)

Total: 49.4 GtCO₂e



Source: [Climate Watch](#), based on raw data from IEA (2018), CO₂ Emissions from Fuel Combustion, www.iea.org/statistics; modified by WRI.

WORLD RESOURCES INSTITUTE

Figure 1 World Greenhouse Emission in 2016 classified by sectors-end use-emission gases

The statistical data of GHG emission emitted from the transportation sector is provided in Figure 2. Over the past 40 years from 1970 to 2010, on-road transportation has been considered as a major contributor in this sector. It has been accounted for more than half of the total GHG emitted by the transportation sector and gradually increased to 72% in

2010. The total amount of GHG emitted by this sector increased 2.3 times in the past 10 years and the trend continues to escalate. (IPCC, 2014)

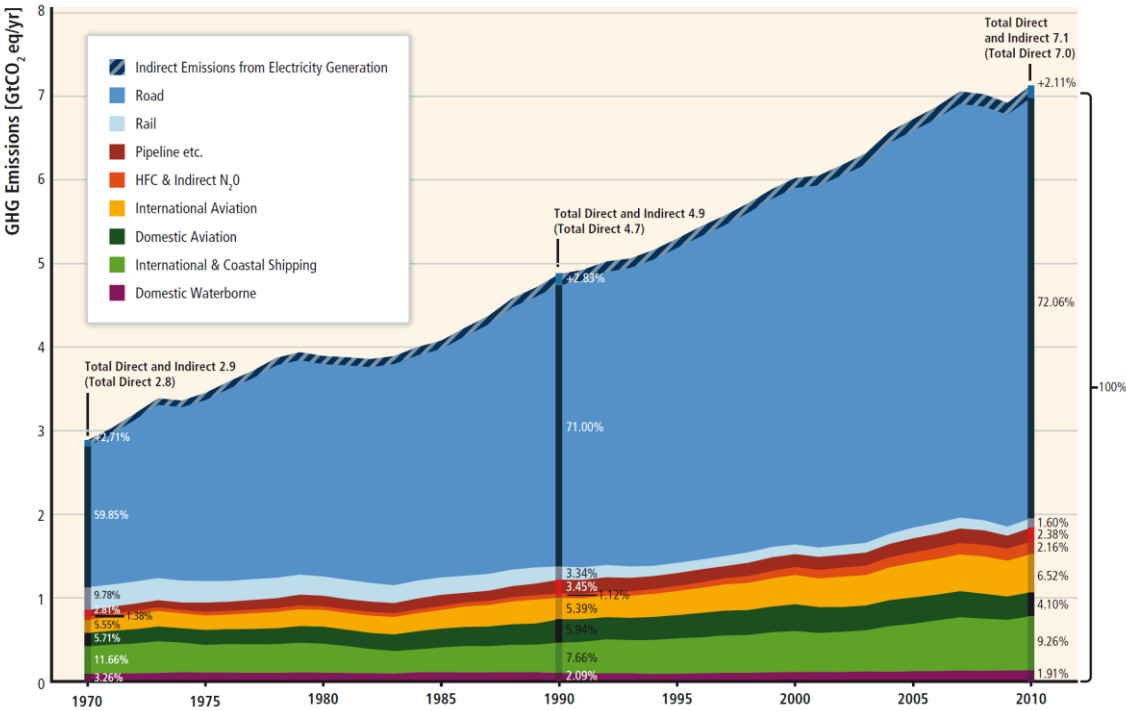


Figure 2 Green House Gases emission from the transportation sector (IPCC, 2014)

In an attempt to mitigate the risks of energy consumption and GHG from on-road transportation, IPCC divided the solutions into four schemes which are reducing the number of journeys, encouraging low carbon transportation, reducing energy intensity, and, developing low-carbon intensity fuel. (IPCC, 2014)

As vehicles are the major contributors to energy consumption and GHG emission from road transportation, reducing energy intensity is one of the solutions that can tackle the problem directly to the root cause. Reducing energy intensity means advancing the

propulsion system to be more efficient and developing energy-saving technologies, such as powertrain electrification, advanced fuel injection and combustion system, advanced transmission technology, heat recuperation and management, engine light-weighting and downswing, and others.

According to the research conducted by The Boston Consulting Group (BCG), the penetration of the electrified powertrain from 2015 to 2030 can be described into three phases. From 2015 to 2020, conventional vehicles (CVs) will remain as the primary powertrain. Even though there are some incentives and saving from fuel economy, the returns are still too long and are not attractive enough to invest for such a high total cost of ownership (TCO) vehicles while the infrastructure is not at a ready stage. In addition, CV powertrain technology at the moment still qualifies the emission regulations. (Green Car Congress, 2017)

The second phase will start from 2020 until 2025. As the emission regulations are becoming stringent, the automotive industry will be forced to shift to the electrified powertrain. Hybrid, and mild-hybrid will begin to gradually replace CV. (Enang and Bannister, 2017a) The market will be driven by the regulation, but there will be more attractive incentives provided to the users. (Green Car Congress, 2017)

The third phase will start from 2025 until 2030. Since battery technology has been continuously developed to reach the requirement in both price and specification. The TCO will become more affordable. Electrified vehicle sales will increase rapidly. Electrified vehicles will be a key element for future connected vehicles, autonomous driving, including car sharing since they provided longer mileage and capability for energy management. (Green Car Congress, 2017)

By 2030, the forecast projected that electrified vehicles will possess approximately 50% of the overall market share. Full hybrid and mild hybrid powertrains will dominate more than half of the electrified powertrain segment. (Green Car Congress, 2017)

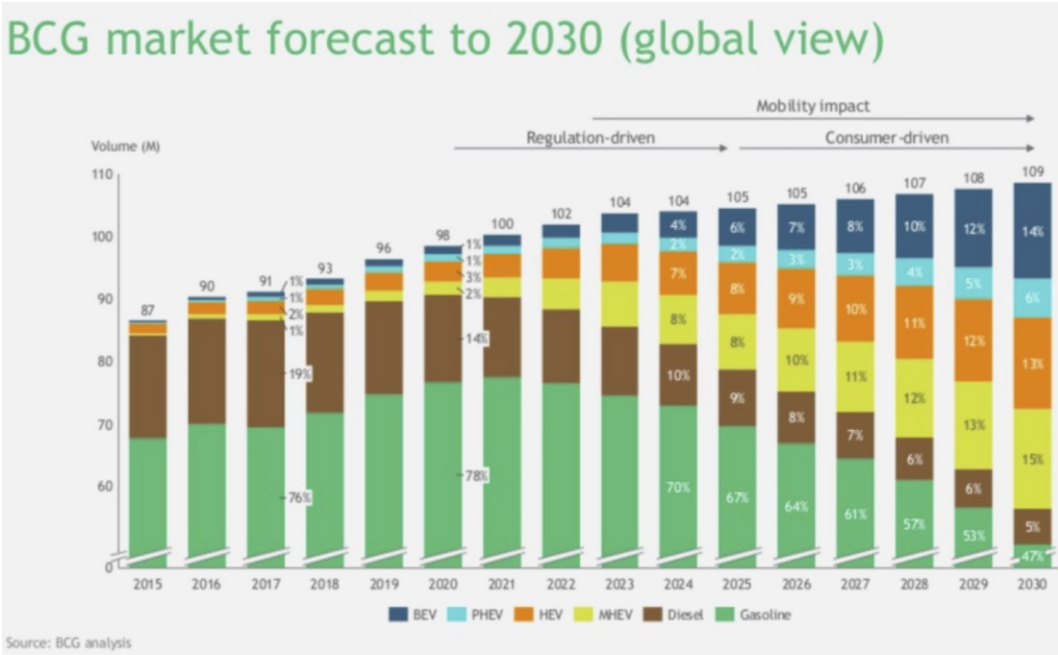


Figure 3 Market trend of powertrain technology (Green Car Congress, 2017)

1.2 Problem Statement

According to the coming of rapid hybrid-vehicles penetration, it is necessary to prepare for energy consumption and GHG emission prediction tools to help to project the direction of the future developments, and also a tool to help to evaluate the implemented policies and developments related to on-road transportation fuel consumption and GHG

emission issues. (Zhai, Christopher Frey and Roupail, 2011; Faris, Rakha and Elmoselhy, 2014; Mansour, Haddad and Zgheib, 2018)

Currently, there is a variety of hybrid powertrain configurations designed by world-wide automakers. The operating systems of these hybrid systems also contain different configurations, controls and energy management strategies. (Cunefare *et al.*, 2011; Sciarretta *et al.*, 2012; Faris, Rakha and Elmoselhy, 2014; De Cesare, Cavina and Brugnoli, 2019) Nevertheless, the only similarity is that the powertrains operate in multi-operation modes. These modes are switched and selected in an attempt to reduce inefficient engine operations and manage the balance between electric and engine power utilization. (Liu and Peng, 2008; Faris, Rakha and Elmoselhy, 2014; Pitanuwat *et al.*, 2020) Moreover, it is not only the complexity and variety of the systems that make the modeling becomes much more difficult than CV but also these controls and energy management strategies have been protected as confidential information. Thus, to understand the operation characteristics, it requires reverse engineering and a database that captures the characteristics of the powertrain operation.

For the modeling, the hybrid powertrain systems have become much more complicated than the conventional pure combustion engine powertrain since the powertrain systems combine electric and petrol power sources with sophisticated controls. (Liu and Peng, 2008; Murphey *et al.*, 2012; Sciarretta *et al.*, 2012; Lee *et al.*, 2013) However, the same modeling methods applied for conventional vehicles still have been adopted to hybrid vehicle energy consumption modeling. Thus, the modeling method for hybrid vehicle energy consumption prediction should be reconstructed and improved to be in accordance with the actual characteristic of hybrid powertrain operations. As the complexity increases, a good

model must be able to maintain the balance between computational load and accuracy that are appropriate for the objective application.

1.3 Objective

The first objective is to explore and suggest appropriate methods for hybrid vehicles' data acquisition and experimental procedures. The purpose is to collect a meaningful database that captures the characteristics of the powertrain operation and energy consumption in all significant powertrain operations.

The second objective is to investigate the hybrid powertrain operation logic and energy management control. This will be realized through developing a model of hybrid powertrain operation logic and energy management control of the third generation of Toyota Prius as a representative powertrain.

The third objective is to propose a new hybrid vehicle energy consumption modeling method. This objective aims to improve the model to be capable of representing the characteristics of hybrid powertrains. At the same time, it can offer a light computational load that suits large-scale transportation applications. This method will combine the advantage of a quasi-static modeling method that well captures the characteristics of the hybrid powertrain operation to the advantage of the microscopic modeling method that provides a reasonable computational load for large-scale applications. The model will be formulated based on the nature of the actual hybrid powertrain operations.

1.4 Chapter organization

This dissertation consists of eight chapters. Chapter 1 introduces the background and objectives of this research. Chapter 2 provides a summary of related works in the vehicle energy consumption modeling field. It mainly focuses on microscopic modeling and quasi-static modeling methods.

In chapter 3, it introduces the overview of available hybrid powertrain configurations. The dynamics model of a power-split hybrid configuration is derived. Then, it provides in-depth of hybrid powertrain operation controls and energy management of power-split hybrid powertrain.

Chapter 4 explains the procedure required for hybrid vehicle data acquisition. It provides technical knowhow, pros and cons obtained from three different experimental approaches: on-road experiment, private circuit experiment, and chassis dynamometer experiment.

Chapter 5 explains about modeling of hybrid operation logic and energy management of the third generation of Toyota Prius. The hybrid powertrain operation characteristics will also be observed via quasi-static modeling based on CRUISE AVL platform.

Chapter 6 explains about microscopic modeling method that adopts the quasi-static modeling technique and combines it with the microscopic modeling method. The first section will introduce a method to recalibrate a set of coefficients of the vehicle's driving power estimation equation. Then, the second section will propose a method called Traction Force-Speed model to construct an energy consumption model for Prius3.

Chapter 7 performs a special analysis of hybrid vehicles' energy consumption characters. The investigation was conducted to identify the impact of a difference of tire profiles on hybrid energy consumption and energy recovery during deceleration. Chapter 8 provides the executive summary of the overall dissertation.

Hybrid Vehicle Energy Consumption Modeling and Data Acquisition	
CHAPTER 1 Introduction	
CHAPTER 2 Literature review	
CHAPTER 3 Power-split hybrid powertrain	
CHAPTER 4 Experiment and data acquisition for hybrid vehicles	
CHAPTER 5 Quasi-static hybrid powertrain energy consumption modeling	CHAPTER 6 Microscopic hybrid vehicle energy consumption modeling
CHAPTER 7 Hybrid vehicle energy consumption characteristic analysis and application	
CHAPTER 8 Conclusion and future work	

Figure 4 Dissertation structure

CHAPTER 2

Literature Review

2.1 Factors influencing vehicles' energy consumption and GHG emissions

To construct an effective prediction model for vehicles' energy consumption and GHG, it is important to understand the impact of real-world driving activities on the mechanism of energy consumption and GHG emission of the vehicles. The factors that impact the energy consumption and GHG emission of vehicles can be classified into four main factors: vehicles and powertrain characteristics, drivers, infrastructure, and environmental conditions. The factors were synthesized and shown in Figure 5.

For the factor related to vehicles and powertrain characteristics, this factor includes all the factors regarding the sources that provide propulsion power to the vehicles. To obtain the propulsion power, the power sources consume energy in a form of fuel or electricity and produce propulsion power and GHG and emissions as by-products. In this group, the major contributors are powertrain configuration, engine, transmission specifications and technologies, and eco-driving assisting system. (US EPA, 2020) Vehicle specification includes factors related to vehicle appearance and features such as weight, size, shape, and tire. (Onori, Serrao and Rizzoni, 2016a) All these contributors directly related to road load (driving resistances) such as aerodynamics, rolling resistance, requested propulsion kinetic

and potential energy, and others. (Jiménez *et al.*, 1999; Onori, Serrao and Rizzoni, 2016a)

The example of powertrain configuration is the conventional powertrain, hybrid powertrain, electric powertrain, fuel cell powertrain. Even in hybrid powertrain class, there are abundant hybrid configurations available such as single-motor hybrid, 2-motor hybrid, series hybrid, parallel hybrid, combine hybrid, and other more. (Cunefare *et al.*, 2011; Onori, Serrao and Rizzoni, 2016a; Böhme and Frank, 2017; Enang and Bannister, 2017a) For the engine technologies, the potential contributors are fuel injection technology, turbo, exhaust gas recirculation (EGR), valve positioning and timing, intake manifold port design, cylinder deactivation, down sizing, weight reduction, and others. (US EPA, 2020) For engine specification, engine size and fuel type also reflect different fuel consumption behavior. For conventional vehicles, the transmission is the key component that indicates engine operation points. (US EPA, 2020) Currently, there are many technologies that provide more flexibility to avoid operating the engine at inefficiency region. The example is 7-speed automatic transmission, 10-speed automatic transmission, continuously variable transmission (CVT), and others. (US EPA, 2020)

For the factor related to driver, driver behavior, vehicle utilization, and maintenance have been found to be the most influential contributors that impact energy consumption and emissions. (Faris, Rakha and Elmoselhy, 2014; IPCC, 2014) Particularly, different driver behavior creates different driving speed, acceleration, and braking behaviors that correspond to different powertrain operation points and trajectories (steady or transient). Due to the different powertrain operations, energy consumption and powertrain efficiency will become different.

For the factor related to infrastructure, the major contributors are traffic conditions, road grade, speed limit, traffic light density and location, and the road surface condition. For the environment, weather conditions, season, and ambient temperature also directly contribute to powertrain operation such as heat loss, heat radiation, fuel combustion mechanism. (Faris, Rakha and Elmoselhy, 2014; Onori, Serrao and Rizzoni, 2016a) Temperature also plays an important role in lubricant viscosity which affects the friction of the engine. Moreover, temperature change also impacts the usage of air conditioning which is a device that consumes a significant amount of energy. (Böhme and Frank, 2017; Pitanuwat *et al.*, 2017)

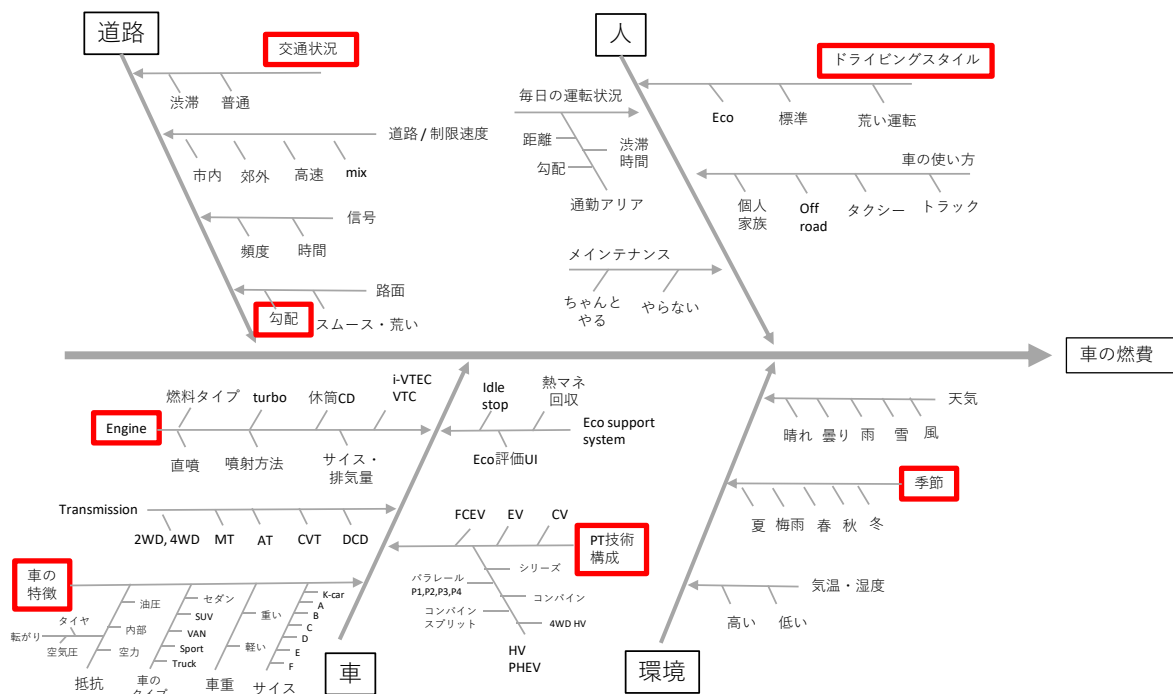


Figure 5 Related factors dominating vehicle fuel consumption

2.2 Vehicle energy consumption modeling methods

Due to the complexity of the factors affecting the vehicles' fuel consumption, taking all the parameters into account is not an effective way to construct the model. Because it will load the calculation process, and it will make the analysis much more complicated. (Enang and Bannister, 2017a)

The modeling process should start from clarifying the research questions and scope, then analyze the set of relevant factors that will be taken into account in the model.

To select a proper modeling method, it is necessary to consider the characteristic of the research problems, the requirement of the precision, and the acceptable computational load and time, the limitation of the database acquisition for modeling.

The modeling methods can be separated into two groups based on their applications which are modeling methods for transportation applications, and automotive engineering applications. These two methods require different comprehensive levels of input, output, and modeling techniques. They also provide different simulation accuracy and computational load. The tread-off relationship among modeling methods explained in Figure 6.

The model for transportation application requires inputs that are compact and general enough to acquire from a number of vehicles. The computational load should be light enough to deal with large-scale network calculations. The main purpose is to estimate the aggregate energy consumption and emissions. The modeling methods can be classified into three groups based on the scope of analysis and precision. The modeling methods are macroscopic scope, mesoscopic scope, and microscopic scope. (Faris, Rakha and Elmoselhy, 2014)

On the other hand, the model for automotive engineering application requires much higher detailed input related to the driving conditions and the vehicle specification. The modeling techniques are also done based on the fundamental of Dynamics and Control. Most of the models have been employed in the vehicle development process, for instance, powertrain control system design, energy management design, powertrain configuration design, optimization, and decision making. This type of model can provide precise and realistic powertrain dynamics and energy consumption. Nevertheless, it comes with a high computational complexity that does not suit for large-scale network applications. The modeling methods can be classified into three levels which are static method or backward modeling, quasi-static modeling, and dynamic modeling methods which provides a different level of precision and elaborate details. (Onori, Serrao and Rizzoni, 2016a; Enang and Bannister, 2017a)

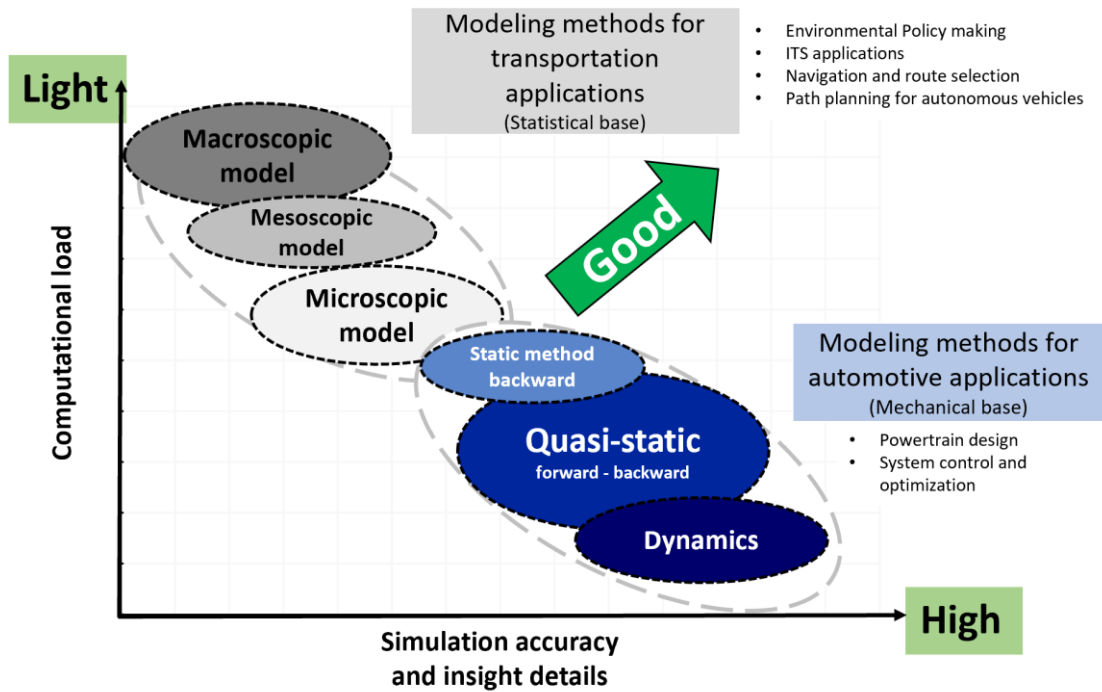


Figure 6 Fuel consumption modeling methods and the tread off between precision and computational load

2.2.1 Vehicle energy consumption modeling methods in the transportation research field

In the transportation area, the scopes of problem solving and problem visualization can be typically divided into three perspectives which are macroscopic scope, mesoscopic scope, and microscopic scope. In each scope, researchers have proposed various modeling techniques which also can be classified into analytical approach, empirical approach, and statistical approach. For more detailed explanation will be provided in the coming sections.

2.2.1.1 Macroscopic scope modeling

The macroscopic models view the transportation problems with the broadest perspective. It uses averaged and aggregate parameters to estimate large-scale network energy consumption and emissions. This type of model cannot provide high precision on a specific event or individual vehicle prediction. However, it is very useful for average trip fuel consumption prediction and large-transportation-network projects such as evaluating the impact of changing the control of traffic signal assignment, predicting the benefit of an infrastructure construction project. (Faris, Rakha and Elmoselhy, 2014; Song, Yu and Wu, 2016)

Macroscopic models are conventionally constructed based on the relationship between averaged fuel consumption rate and the vehicles' averaged speed or averaged driving power measured from a number of trips traveling a regional network. Some other statistical parameters such as averaged acceleration, the standard deviation of speed, and acceleration are also incorporated into the prediction process to capture particular characteristics of the study. (Faris, Rakha and Elmoselhy, 2014; Song, Yu and Wu, 2016)

The MOBILE is a macroscopic emission simulation developed by the United States Environment Protection Agency (US EPA). This simulation has been used in transportation planning to confirm and predict the impact of implemented measures on vehicles' emissions. The prediction is conducted based on the function of vehicles' average speed, vehicles' technology, vehicles' accumulated traveling distance, ambient temperature, fuel parameters, and vehicles' operating mode. The effect of temperature, gasoline type, and humidity can be compensated by an adjustment function equipped in the model. The output of the simulation

is eight emissions: HC, CO, CO₂, NO_x, PM, SO₂, NH₃, and hazardous air pollution(HAP). CO₂ is predicted by merely vehicle type, while speed, temperature, and gasoline type are neglected. Since fuel consumption which is one of the most concerned parameters cannot be predicted, this simulation has been replaced by Motor Vehicle Emission Simulator (MOVES) after 2004. (US EPA, 2016)

The computer programme to compute emissions from road transportation (COPERT) is another macroscopic simulation. This simulation has been adopted in a number of transportation applications in Europe. The emission rate is predicted based on average speed, and vehicle type. The simulation does not cover high-speed-driving scenarios and heavy-duty vehicle applications. (Giannouli, 2003)

2.2.1.2 Mesoscopic scope modeling

Mesoscopic model is a model that has the aggregation degree between macroscopic and microscopic models. It breaks down a trip into small micro-trips by road-link geometry or by vehicles' start-stop timing. Some studies stated that this approach is disaggregate enough to capture the effects of drivers' behavior on vehicles' fuel consumption and emissions in a large traffic network. As the calculation is conducted based on the road-link, it allows the interface between the fuel consumption simulation and traffic flow simulation to become more convenient and accurate. The approach has been found in traffic assignment and eco-routing projects. (Faris, Rakha and Elmoselhy, 2014)

Continuous Traffic Assignment Model (CONTRAM) was developed by Transportation Research Laboratory (TRL) in Europe. This simulation contains both mesoscopic fuel consumption and emission model with the traffic-flow model. The simulations were developed based on a real-world driving database, and it has been validated by several real-world applications. It can account for large-scale integrated traffic networks with long time period simulation scenarios. (Taylor, 2003)

Modeling of Emissions and Fuel Consumption in Urban Areas (MODEM) is a simulation that predicts fuel consumption and emissions of road links of light-duty vehicles. It is capable of predicting fuel consumption, CO, CO₂, HC, NO_x, and PM by using the vehicles' average speed as an input. However, the applications are limited to EURO3 and EURO4, European Emission Standard. Also, further, improvement is needed for a prediction on a severe road gradient condition. (CORDIS, 1994)

Vehicle Specific Power (VSP) modes-based model is a mesoscopic model approach that uses the data of road-and-facility type, road-link average speed, and vehicle driving power to estimate vehicles' fuel consumption and emission. VSP is an effective parameter for fuel consumption prediction as a strong correlation between VPS and fuel consumption has been reported by a number of researchers. However, VSP is a parameter that represents vehicles' driving power. To calculate this parameter, it requires vehicles specification. Thus, this application of this method is restricted to the vehicles that the dataset was used in the model construction. In addition, work for model recalibration is required for different datasets. (Frey, Zhai and Rouphail, 2009)

2.2.1.3 Microscopic scope modeling

Microscopic model is a model that provides the closest view of vehicles' energy consumption and emissions among all the approaches in the transportation field. It predicts instantaneous vehicles' energy consumption and emissions by using the instantaneous driving power, and vehicle specification. Typically, it is constructed based on the relationship between driving power and fuel consumption or emission rate. Therefore, it doesn't not only capture the impact of traffic flow, but it also can access the impact of driving behavior, road grade, wind speed and direction, and other individual vehicles' activities. (Faris, Rakha and Elmoselhy, 2014)

This modeling method deals with disaggregate datasets which contain larger size than those of macroscopic and microscopic approach. Thus, microscopic approach comes with a higher cost of computation load. However, thanks to the rapid growth of computers' processor technology, microscopic approach has widely been adopted by both individual and large-scale network projects. The ability of this modeling level is applicable to eco-root selection, driving behavior evaluation, traffic signal assignment, autonomous vehicles' fuel consumption optimization for path planning, and others. (Faris, Rakha and Elmoselhy, 2014)

The Passenger Car and Heavy Duty Emission Model (PHEM) is a microscopic based simulation for vehicles' emission prediction. It contains both passenger vehicles and heavy-duty truck models. The simulation requires vehicle speed and driving power as the primary input. The output is CO, CO₂, HC, and NO_x. This model introduces engine emission maps constructed in a form of engine speed-torque look-up-table map. The concept of the modeling method was derived based on the actual vehicles' operations. The most interesting feature of

this software is that it can interface with VISSIM and SUMO, traffic, and transportation simulation software. This software can yield analysis regarding traffic and transit operation with flexible size of the networks. (DRL, 2019)

Motor Vehicle Emission Simulator (MOVES) is a widely adopted fuel consumption and emission prediction software developed by US EPA. The newest version is MOVES 2014b. This model requires instantaneous vehicle speed and acceleration as the primary input. The output is fuel consumption rate, and emission rate: CO, CO₂, NO_x, PM, SO₂, and NH₃. MOVES implements a modal fuel consumption and emission rate approach that bins instantaneous fuel consumption rate into specified bin ranges of a parameter called vehicle specific power (VSP). Then, the correlation between the average fuel consumption rate collected at each bin and the specified VSP level is constructed as a model. Recently, VSP binning method has become the most conventional empirical method for microscopic transportation fuel consumption and emission modeling. (US EPA, 2019)

In the past decades, a number of researchers have been applying vehicle fuel consumption models to transportation research such as prediction and analysis. The conventional approach of vehicle fuel consumption modeling consists of two main processes, which are vehicle driving power estimation, and fuel consumption and driving power relationship construction (Frey, Zhai and Roupail, 2009; Graver, Frey and Choi, 2011; Zhai, Christopher Frey and Roupail, 2011; Song, Yu and Tu, 2012; Duarte *et al.*, 2014; Holmén and Sentoff, 2015; Duarte, Gonçalves and Farias, 2016; Song, Yu and Wu, 2016; Wang and Rakha, 2016; Zhou and Jin, 2017). In 1999, Jiménez et al. (Jiménez *et al.*, 1999) derived an equation for vehicle driving power estimation, and also provided a set of coefficients

specified for light-duty vehicles' (LDVs) application called vehicle-specific power (VSP). The equation is expressed in Equation (1).

$$VSP_{LDV1999} [watt] = m \left[1.1 a_{veh} v_{veh} + 9.81 \times \sin \left(\tan^{-1} \left(\frac{h}{l} \right) \right) v_{veh} + 0.132 v_{veh} + 0.000302 v_{veh}^3 \right], \quad (1)$$

The equation simply requires data that can be observed from outside of the vehicles, such as speed, acceleration, road grade, and wind speed. To construct the model, relationship between the estimated driving power and fuel consumption is defined by VSP-based modeling method that was also proposed by Jimenez in 1999. This method divides the total span of VSP into discrete VSP bins. Then, the vehicles' second-by-second fuel consumption data are classified and collected into the bin that has the VSP range matches with the data. Finally, the fuel consumption data within the same bin are averaged and established as the fuel consumption model. Table 1 provides a comprehensive literature review of research that incorporated Jimenez's VSP for LDT equation and VSP based modeling method including the applications. Furthermore, a large number of researchers adopting VSP in their research have reported on the monotonically increasing relationship between VSP and fuel consumption (Jiménez *et al.*, 1999; Frey, Zhai and Rouphail, 2009; Zhai, Christopher Frey and Rouphail, 2011; Graver, Frey and Choi, 2011; Song, Yu and Tu, 2012; Duarte *et al.*, 2014; Duarte, Gonçalves and Farias, 2014; Wu, Song and Yu, 2014; Duarte, Gonçalves and Farias, 2016; Holmén and Sentoff, 2015; Song, Yu and Wu, 2016; Wang and Rakha, 2016; Zhou and Jin, 2017).

Table 1 Literature review of Jimenez’s VSP LDT equation and
VSP based modeling method

Paper	Attractive aspects	Wheel power estimation method	Fuel consumption modeling method
(2002) Frey et al.	Proposed FC model for gasoline and alternative technology vehicles	VSP equation and coefficients [Jimenez et al. 1999]	14 discrete mode VSP binning
(2011) Graver et al.	Developed a FC model for PHEV during charging and discharging	VSP equation and coefficients [Jimenez et al. 1999]	1kW/ton discrete mode VSP binning
(2011) Zhai et al.	Developed HEV FC model, applied engine on/off criteria	VSP equation and coefficients [Jimenez et al. 1999]	14 discrete mode VSP binning [Frey et al., 2002]
(2014) Duarte et al.	Studied the impact of SOC to HEVs’ FC	VSP equation and coefficients [Jimenez et al. 1999]	14 discrete mode VSP binning [Frey et al., 2002]
(2015) Holmén and Sentoff	Studied fuel saving benefit for HEV in city, suburban and highway	VSP equation [Jimenez et al. 1999] , coefficients and actual vehicles’ mass	1kW/ton discrete mode VSP binning
(2016) Robinson et al.	Studied influence of driving patterns on vehicle emissions in Latin America	VSP equation [Jimenez et al. 1999] and input vehicle model’s coefficients	19 discrete mode VSP binning
(2016) Duarte et al.	Compare FC and emission of 6 vehicles with different powertrain technologies on NEDC and WLTP	VSP equation and coefficients [Jimenez et al. 1999]	14 discrete mode VSP binning [Frey et al., 2002]
(2016) Song et al.	Developed speed correction factors for macroscopic FC model	VSP equation and coefficients [Jimenez et al. 1999]	25 discrete mode VSP binning
(2017) Zhou & Jin	Proposed a transient correction module for FC model	VSP equation and coefficients [Jimenez et al. 1999]	1kW/ton discrete mode VSP binning

On the other hand, some researches also access the problem by using analytical methods such as machine learning, neural-network, and Kalman filter, stochastic model. These studies are more related to automotive fields. The research focuses were found on engine’s exhaust gas recirculation (EGR), Variable-geometry turbochargers (VGT), turbo charger, high-pressure direct injection, and others. (Faris, Rakha and Elmoselhy, 2014)

2.2.2 Vehicle energy consumption modeling methods in the automotive research field

The modeling methods that have been commonly implemented in the automotive research field can be classified into three approaches which are static approach, quasi-static approach, and dynamic approach. The characteristics and applications of these approaches will be explained in the following sections.

2.2.2.1 Static approach

The static modeling or backward modeling method is generally based on the relationship of kinematic motions among speed, force, rotational speed and torque at any individual moving components of vehicles. The simulation flow in this model starts from the input driving cycle which is a time-speed profile. For some models, they also include road grade and ambient temperature profiles. Based on the characteristics of the vehicles such as mass and road load and resistance, the required driving force at wheel is calculated in a sub-model called vehicle dynamics. The required driving force and vehicle speed will be fed to the drivetrain sub-model. It will calculate the requested engine speed and torque of the engine based on the drivetrain gear ratio. Once the engine speed and torque have been estimated, the engine model that contains a statistical fuel consumption model will be used to calculate the fuel consumption. The calculation flow is illustrated in Figure 7. Since the flow begins from

wheel back to the engine, sometimes this modeling method is called a backward-looking modeling method. (Onori, Serrao and Rizzoni, 2016a; Enang and Bannister, 2017b)

The simplicity of the model substantially helps reduce the computational load. Moreover, this type of model can ensure that the vehicle will exactly trace the driving cycle. The model is appropriate for vehicle fuel consumption emissions modeling. However, since there is no feedback loop in this model, there must be a measure to prevent the operation of the vehicle to exceed the actual maximum performance. Even though this method neglects all the transient events in the powertrain, it is accurate enough for the applications of energy consumption and emissions modeling, and preliminary determination of hybrid energy management design. (Cunefare *et al.*, 2011; Onori, Serrao and Rizzoni, 2016a; Enang and Bannister, 2017b)

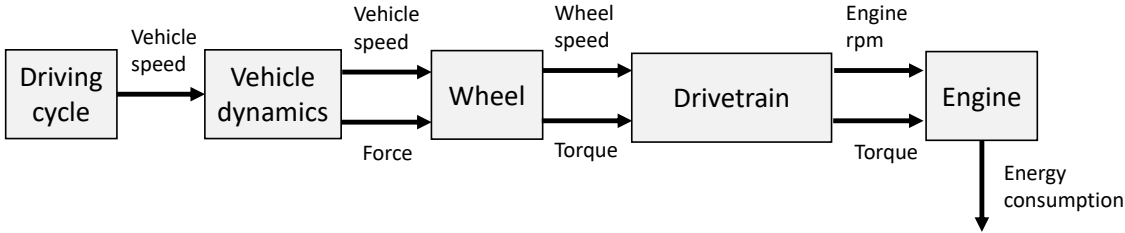


Figure 7 Kinematic modeling approach

2.2.2.2 Quasi-static approach

The fundamental of the quasi-static approach is accomplished based on the dynamic relationship of the vehicle components. The effect of inertia during transient will be taken

into account. Typically, the approach employed proportional–integral–derivative (PID) feedback control to ensure the target speed tracing function. (Liu, Peng and Filipi, 2005; Lee *et al.*, 2013; Yi *et al.*, 2016) To maintain the reasonable computational load, the components; engine, motor/generator, transmission losses, are modeled based on static efficiency maps or look-up table maps. This model combines the advantage of the differential dynamic equation with the advantage of the look-up table to provide a good balance model that suits for powertrain control design and hybrid energy management. (Sciarretta *et al.*, 2014; Yi *et al.*, 2016; Enang and Bannister, 2017a) Due to the sets of input, output, and essential powertrain component maps in the model and in the actual vehicles have several in common parts, the designed control logic can be directly implemented into the actual vehicles. (Enang and Bannister, 2017a) This type of model is sometimes called a forward-looking model. (Onori, Serrao and Rizzoni, 2016a; Enang and Bannister, 2017b)

The flow begins with driving cycle input. The vehicle speed will be fed to the driver model. Inside this model, it contains PI control that helps the vehicle to capable of tracing the target speed. In some models, they also contain a sub-model that converts vehicle speed, acceleration to acceleration pedal position, requested power. The drivetrain model will determine engine target speed and torque based on the gear ratio. Once the engine operation point has been determined, the energy consumption can be calculated. The flow of the simulation is illustrated in Figure 8. (Onori, Serrao and Rizzoni, 2016a; Yi *et al.*, 2016; Enang and Bannister, 2017a)

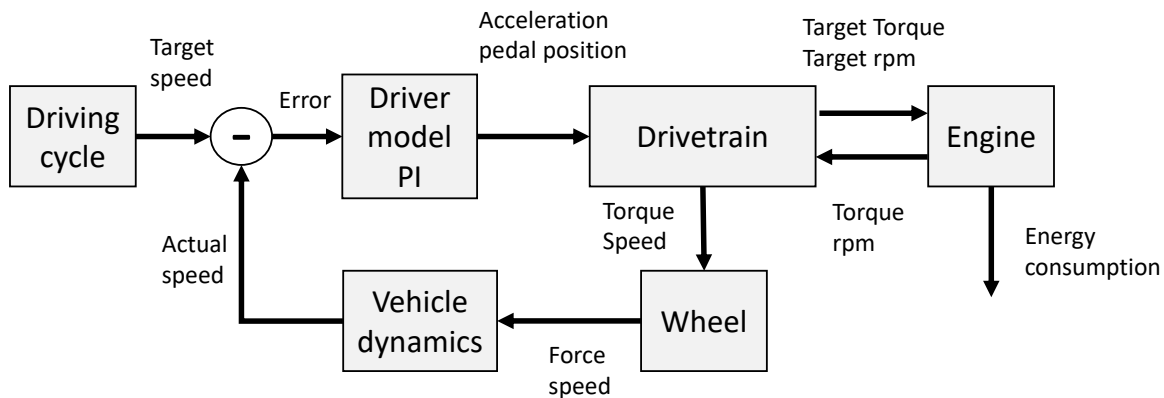


Figure 8 Quasi-static modeling approach

2.2.2.3 Dynamic approach

This approach is commonly implemented in a research field that requires the insight of the highly dynamic behavior during the transient of a specific component and research area. The problems related to combustion mechanism, fluid mechanics, thermodynamic, and heat transfer are usually tackled by the dynamic approach. The example of study topics is injection spray design, intake manifold, and valve port design, turbo blade design, turbo lag behavior investigation, torque convertor design, cooling system, and other. To solve the equations, governing equations and boundary conditions are usually established based on the conservation of mass, the conservative of energy, momentum principle. According to the complexity of the calculation, differential finite technique is usually introduced. (Enang and Bannister, 2017a)

2.2.2.4 Summary

Finally, the advantages and disadvantages of the three modeling methods and their applications are summarized and provided in Table 2. (Fazal U Syed *et al.*, 2006; Liu and Peng, 2008; Cunefare *et al.*, 2011; Murphey *et al.*, 2012; Lee *et al.*, 2013; Montazeri-Gh and Mahmoodi-k, 2015; Fiori, Ahn and Rakha, 2016)

Table 2 Summary of automotive modeling methods

Modeling methods	Pros	Cons	Applications found in former literatures
Kinematic modeling approach	<ul style="list-style-type: none"> • Low computational load • Ensure exact speed profile tracing • Enough accuracy for energy consumption and emission estimation and well capture static driving situations • Require statistical fuel consumption maps which ease the calculation load 	<ul style="list-style-type: none"> • No guarantee if the assigned speed exceeds the actual powertrain max power, but can be fixed by adding a logic to saturate powertrain's max/min power limit • Inadequate accuracy when dealing with problems regarding powertrain dynamics, control, and heat transfer, and transient stage 	<ul style="list-style-type: none"> • (P. John et al., 2011) developed energy consumption models of Toyota Prius (single-mode power-split hybrid) and General Motor (two-mode power-split hybrid). The objective of this study was to compare the fuel-saving potential, and the flexibility of power distribution between the two different hybrid configurations. • (C. Fiori et al., 2016) attempted to develop electric vehicles' energy consumption model that can be implemented in smartphone applications; eco-driving, eco-routing, and large-scale transportation network simulation. The model provided the ability to capture the characteristics of EV efficiency and regenerative braking benefit, unlike the transportation approaches that focus mainly on aggregate fuel consumption modeling level.
Quasi-static modeling approach	<ul style="list-style-type: none"> • Best suit for control development problems • Require statistical efficiency maps or energy consumption maps which ease the calculation. • Provide reasonable accuracy for energy consumption estimation, NOx, Soot. • Enable prediction during acceleration and transient operation of the overall powertrain • Due to all the input and output parameter sets of the model and the actual vehicles have much in common, the developed control is convenient to be implemented in real cars. 	<ul style="list-style-type: none"> • Require a driver model and PID control • Require differential dynamic equation of the vehicle and powertrain 	<ul style="list-style-type: none"> • (J. Lui and H. Peng, 2008; M. Montazeri and M. Mahmoodi, 2015; U. Fazal et al., 2006) attempted to develop an energy consumption model for Toyota Prius, power-split hybrid powertrain. Then, the models were adopted in the energy management strategy design and optimization. • (Y. Murphy et al., 2012) utilized Ford Escape Hybrid (power-split hybrid) model provided by Argonne National Laboratory's Powertrain Systems Analysis Toolkits (PSAT) to develop an online intelligent energy management system. The energy management strategy was constructed by applying machine learning and dynamic programming to learn about the effect of road-type and traffic conditions on energy consumption. • (S. Lee et al., 2013) developed The Advanced Light-Duty Powertrain and Hybrid Analysis tools (ALPHA), a freely-downloaded software provided by EPA. This study applied forward modeling techniques to construct and validate fuel consumption and GHG emission models for power-split hybrids and P2 parallel hybrid vehicles.
Dynamics modeling approach	<ul style="list-style-type: none"> • Suit for the research focusing transient stage and high dynamic events, such as internal combustion engine, insight combustion mechanism, abrupt acceleration 	<ul style="list-style-type: none"> • Require fluid dynamic or thermodynamic model which have a high computational cost • Require finite differential equation to solve the problems 	<ul style="list-style-type: none"> • (M. Pettiti et al., 2007) attempted to develop a diesel engine model to investigate the dynamic of the turbocharger in diesel engines and the response during acceleration caused by turbo lag.

CHAPTER 3

Power-Split Hybrid Powertrain

3.1 Hybrid Vehicles Configuration

Hybrid vehicles are vehicles that utilize more than one powertrain in the system. The most widespread combination is fuel and electricity. In general, combustion engines can only deliver maximum efficiency of 30-40%. The rest of 60-70% power is sacrificed in a form of heat loss, pump loss and mechanical loss. (Onori, Serrao and Rizzoni, 2016b; Böhme and Frank, 2017) Moreover, the high-efficiency operation region is located at only some specific torque-speed region at which does not completely match along with road load characteristic. Combustion engines deliver poor efficiency, particularly at low-speed stop & go, high torque at low-speed drive and instantaneous acceleration. (Enang and Bannister, 2017a; Pitanuwat *et al.*, 2018)

In order to improve the efficiency of combustion engine vehicles (CVs), electric powertrain has been introduced. Due to the characteristics of motors which can provide high torque at low speed with excellent efficiency and spontaneous response, it is capable of satisfying the driving road load required power while the overall efficiency varies within just a narrow range between 70-95%. In addition, implementing a generator/motor, it allows the powertrain to be able to recuperate braking and deceleration power instead of heat loss through the mechanical brake. (Onori, Serrao and Rizzoni, 2016b)

Therefore, electrical powertrain components are integrated into the conventional powertrain to compensate each other shortcoming. The engine tends to be more powerful and can provide a more reliable driving range while the battery power, which is considered as the main electric power source, is quite limited. On the other hand, the electric motor assists and absorbs engine power. It enables the engine to have more variation for operation point selection. (Onori, Serrao and Rizzoni, 2016b; Böhme and Frank, 2017; Enang and Bannister, 2017a)

Hybrid powertrain configurations can be classified into three main systems: series hybrid, parallel hybrid, and series-parallel hybrid system.

3.1.1 Series Hybrid

Series hybrid or sometimes called range extender is a system that the power flow from engine and generator/motor are allocated in the same line. The engine generates mechanical power, then this power is distributed to the generator. The generator converts mechanical power to electrical power and supply to the propulsion motor to drive the vehicle. The power shortage will be topped up by the battery power. (Çağatay Bayindir, Gözüküçük and Teke, 2011; Onori, Serrao and Rizzoni, 2016b; Enang and Bannister, 2017a) The power flow is illustrated in Figure 9.

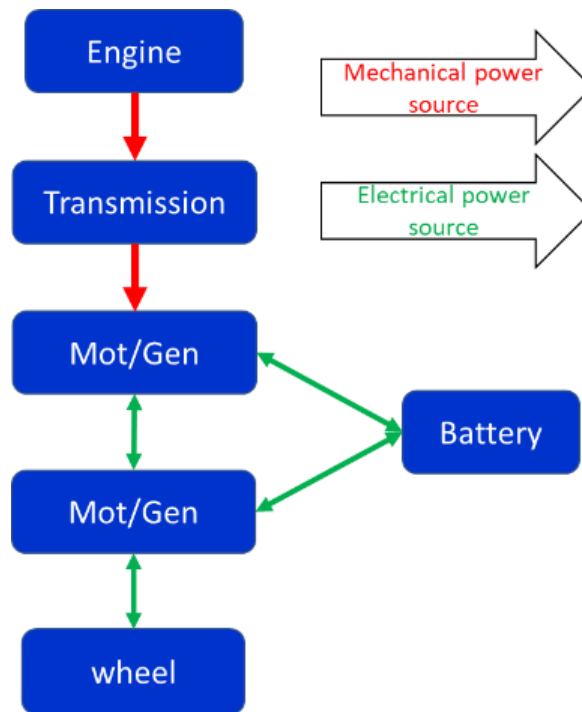


Figure 9 Series hybrid configuration

The merit of this configuration is that the engine can be operated independently from the instantaneous driving speed and requested power. As a result, the engine can operate constantly at its most optimal operation region with lower transient variation. This configuration significantly helps enhance the driving efficiency in city traffic. According to the powertrain configuration that disengages the direct connection between the engine and wheel speed, it allows the powertrain to shift inefficient operation points of the engine to a better region. The surplus or minus driving power is compensated by power from the battery via the motors. However, the mechanical power from the engine cannot be transmitted to wheels. Because the engine is only designed for electricity generation, the engine size can be smaller than the usual engines. This system also suffers from energy conversion loss among

engine-generator-motor. This design requires a large capacity of electrical components: motor, generator, and battery that are enough to propel the vehicle solely. (Onori, Serrao and Rizzoni, 2016b; Enang and Bannister, 2017a) The example of vehicles available in the current market is the BMW i3 and Chevrolet Volt.

3.1.2 Parallel Hybrid

Parallel hybrid system or sometimes called mild hybrid is the system that allows the engine power and motor power flow in parallel. Then, the two power paths are combined through transmission and pass through the wheels. Most of the parallel hybrid system utilizes only one small-medium size of the motor/generator to assist the engine and recuperate the braking energy. (Çağatay Bayindir, Gözüküçük and Teke, 2011; Onori, Serrao and Rizzoni, 2016b; Enang and Bannister, 2017a) The power flow is illustrated in Figure 10.

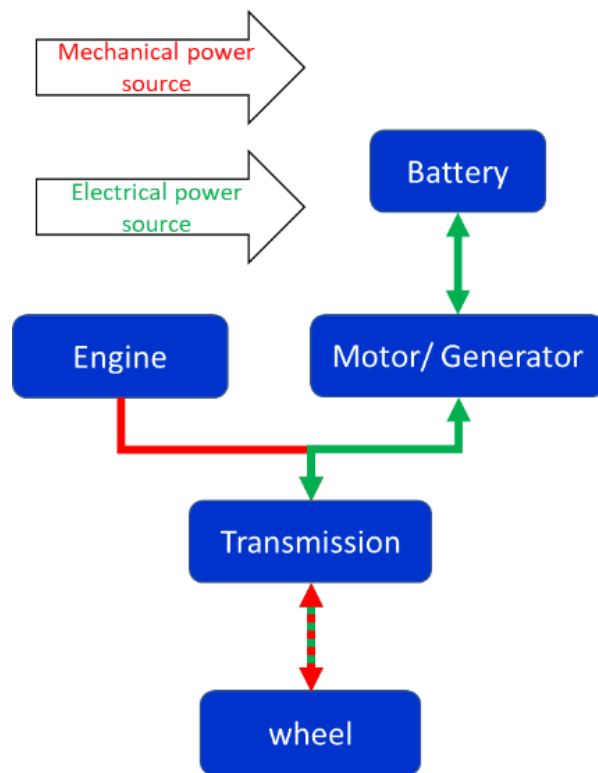


Figure 10 Parallel hybrid configuration

The merit of this system is that the loss from multiple energy conversion is eliminated since the engine and motor power is combined in parallel. The motor assists the engine during an engine power shortage, such as instantons acceleration, which significantly results in efficiency for highway driving. The motor also assists in engine control and braking energy recuperation. This system requires a smaller size and less number of powertrain components compared to series and combined hybrid systems. However, since the engine is still the main power source. The electric drive is utilized as a supplementary power assist. Thus, most of the time the vehicles operate more likely to CVs but low-efficiency engine operation can be partly reduced. The reason that it is called mild hybrid because the proportion between the

mechanical and electric driving power is smaller than other hybrid types. The example of vehicles available in the current market is Honda Inside, Honda Civic (IMA), Honda Fit (i-DCD), Mazda3 Hybrid, BMW 7 series (ActiveHybrid), and Chevrolet Malibu. (Enang and Bannister, 2017a)

3.1.3 Series-Parallel Hybrid

Series-parallel hybrid or combined hybrid is a system that merges the advantage from both series and parallel hybrid into a single system. As the configuration enables more power flow paths, it results in higher flexibility in power management and better powertrain efficiency. However, the overall efficiency of the powertrain system significantly depends on the design configuration and energy management system. Nowadays, several combined hybrid configurations have been introduced to the market, such as all Toyota & Lexus hybrid cars, Honda Accord, and Ford Escape. (Onori, Serrao and Rizzoni, 2016b; Böhme and Frank, 2017; Enang and Bannister, 2017a) The examples of the power flow paths are shown in Figure 11 and Figure 12.

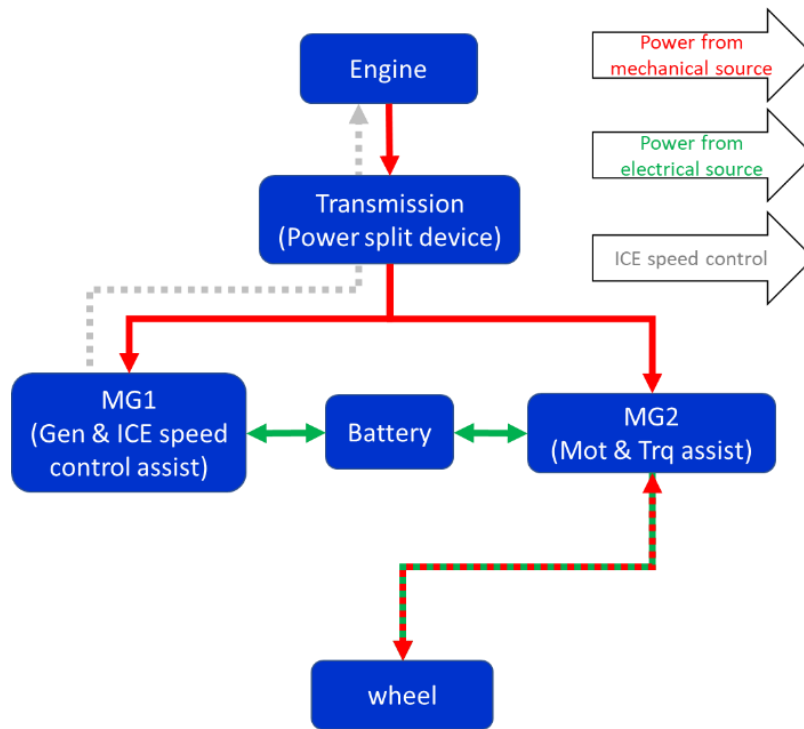


Figure 11 Series-parallel hybrid (Toyota Hybrid System)

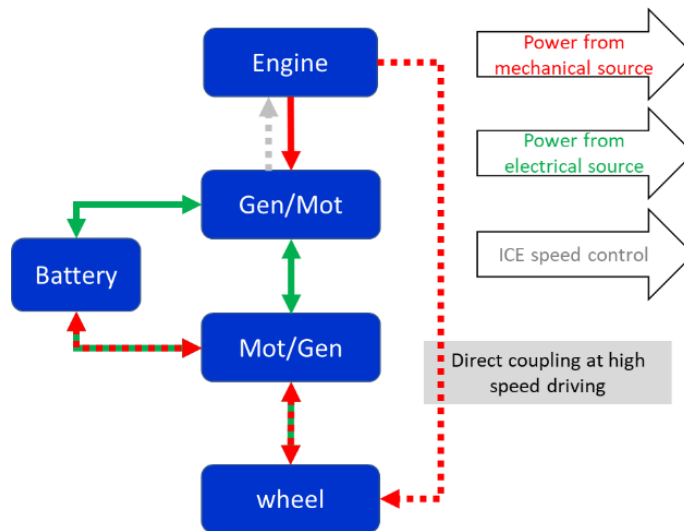


Figure 12 Series parallel hybrid (Honda iMMD)

3.2 Toyota Hybrid System of the Third Generation of Toyota Prius

This section describes fundamental of the powertrain configuration and important hybrid operation characteristics of Prius3. The information in this section is an important basis to understand CRUISE Prius3 improvement.

3.2.1 Powertrain Configuration

Power-split hybrid is one of the most widespread hybrid configurations at the present. (TOYOTA MOTOR CORPORATION, 2019) To combine and transmit the engine and two motor/generator (MG) power together, a planetary gear is used as conjunction called power-split device. Prius3's powertrain configuration is shown in Figure 13.

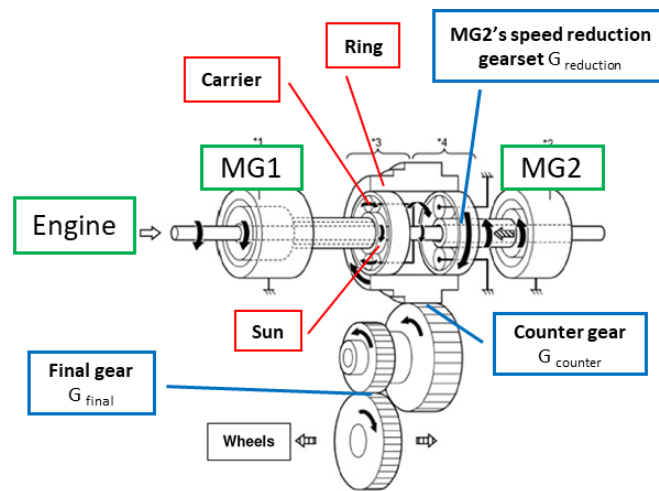


Figure 13 Toyota Prius3' power train configuration (Allouchery, 2012)

The engine power transmitted to the sun gear flows to MG1. MG1 mainly generates the engine power to electricity, then distributes the power to the battery, MG2, or auxiliary components, such as air conditioner, pumps, radio, and others. MG1 also acts as a starter and engine/vehicle speed controller. (Toyota, 2013)

The engine power transmitted to the ring gear flows directly to the wheels or to MG2. MG2 acts as the main driving motor, regenerative braking generator, and driving torque assisting motor. In some situation, the MG2 is also used as a generator to absorb the engine power residue and stores the power to the battery. (Liu and Peng, 2008; Toyota, 2013)

The main concept of this hybrid configuration is to maximize the engine and overall powertrain efficiency. The engine is controlled strictly to operate inside the optimal region, and to maintain the engine rpm at a constant as much as possible. However, in real-world driving, the requested driving power always fluctuates depending on the driving situation. To manage this, when requested driving power exceeds the engine power, MG1 and MG2

can act as a generator to absorb the engine power residue and save to the battery. Meanwhile, when the engine power is at shortcoming, MG2 can also act as a motor assisting driving torque. For driving speed fluctuation issue, MG1 can also act as a motor to adjusting the speed. (Toyota, 2013)

There is still one more constraint which is the limited battery capacity. For hybrid vehicles, the battery is relatively small compared to EVs and PHEVs. To balance the battery state of charge (SOC) in its suitable range, it is not possible to run the powertrain at the same operation mode at all time. The operation modes need to be switched in order to control the battery charging and depleting including the overall powertrain efficiency. As series-parallel hybrid configuration can enable multiple operation modes: EV, HV light load driving, HV medium-heavy load driving, and regenerative braking, and more, an appropriate operation mode need to be selected and operated intelligently for a specific driving situation. For Prius3, this operation mode selection logic is controlled based on an algorithm called rule-based control. These rules are used as criteria to manage the energy flow to maximize powertrain efficiency. This sophisticated and unique hybrid operation characteristic plays a significant role in hybrid powertrain operation which will be explained in the next section. (Toyota, 2013)

3.2.2 Hybrid Powertrain Operation and Energy Management Strategy

Hybrid powertrain operation and energy management strategy are the most critical component in hybrid powertrains. This section explains about the fundamental of THS

operation characteristics that are mandatory for ones who attempt to develop or tune hybrid powertrain models. Furthermore, this section will give the insight basis of operation mechanism in Prius3, Toyota hybrid vehicles.

According to the power-split hybrid powertrain that conveys driving power via a variety of configurations/operation modes. In another word, the vehicle can be driven by several operation modes, such as electric motor drive, engine & motor drive, and engine drives with battery charging mode. At each operation mode, MG1, MG2, engine, and battery also behave as a different combination, which means that energy efficiency and energy consumption are also different. Thus, when it comes to the modeling stage, these characteristics need to be properly extracted and simplified to a model.

For most of the hybrid vehicles, the operation modes are selected based on rule-based control energy management criteria. (Çağatay Bayindir, Gözüküçük and Teke, 2011; Enang and Bannister, 2017a) These criteria can be explained by the instantaneous driving force, total power request, speed, and state of charge (SOC). The purpose of these energy management is to 1) satisfy the request driving power, 2) optimize the engine and powertrain efficiency, and 3) maintain the battery level in a suitable range. (Onori, Serrao and Rizzoni, 2016b; Böhme and Frank, 2017)

To illustrate the insight explanation, we utilized experimental data from more than 530,000 samples, recorded from Prius3 in various driving situations to investigate the energy management criteria in Prius3. According to the data analysis results and literature reviews (Toyota, 2013), the hybrid operation can be summarized into two main determination processes. First is the engine on/off determination, and second is operation mode selection.

3.2.2.1 Engine on/off Determination

For conventional vehicles, the command that a driver can send to the powertrain is generally vehicle speed, gear position, and acceleration pedal position. Then, the vehicle interprets these signals into request driving force and driving power, and send to command the powertrain.

Nevertheless, in hybrid vehicles, the process becomes more complicated. In order to calculate the total request driving power, not only is the driving power taken into account but also required hybrid battery charging power, and electronic devices supply power (inverter, converter, auxiliary battery charging, steering pump, oil pump, and others).

First, the vehicle estimates the request driving force by using the command input from the acceleration pedal position and the vehicle speed. Figure 14 shows the effect of the input acceleration pedal and vehicle speed of Prius3 on the output requested driving force. Driving force is a force generated by the powertrain and transmitted to wheel to propel the vehicle. The color indicates the acceleration pedal position. To gain more acceleration, the driver needs to press the acceleration position deeper. The sensitivity of the acceleration pedal and the maximum acceleration performance change when the speed changes. At lower speed, the sensitivity of the acceleration pedal appears to be more responsive in terms of the output driving force increment compared to higher speed. In addition, in case that the driver requires sudden or hard acceleration by pressing the acceleration pedal deeper than approximately 80% (yellow zone), the powertrain will switch to boost mode, and draw the maximum power from both engine and battery to drive the vehicle. After obtaining the requested driving force and driving speed, the requested driving power can be calculated.

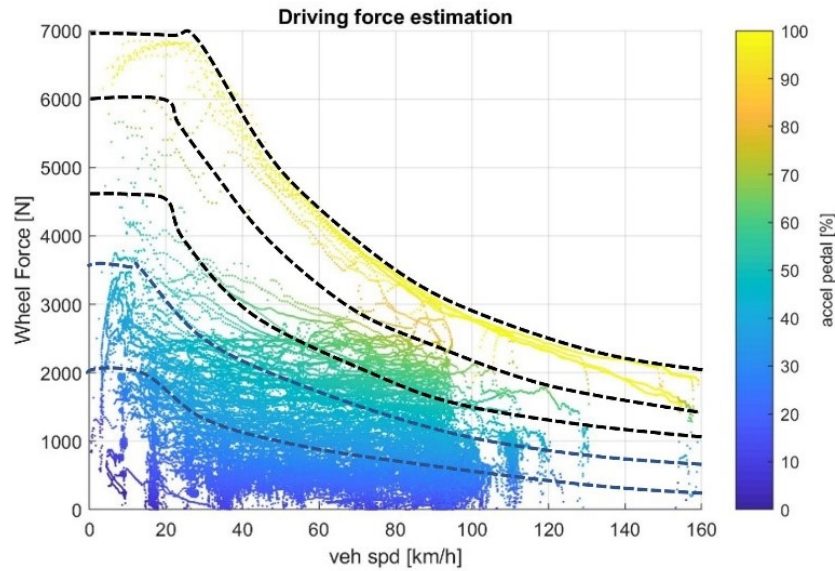


Figure 14 Driving force estimation

Second, the requested battery charging power need to be estimated. Figure 15 illustrates the actual battery charging activity in Prius3. The relationship between battery soc, battery power, and vehicle speed are shown with the distribution of battery soc.

At low-speed driving (blue cloud), such as city driving at which the speed lower than approximately 60 km/h, a pattern of battery charging was found during the actual driving. Prius3 often charges its battery as a cycle. When the battery soc depletes to approximately 38%, the engine is started to charge the battery (at the same time as providing power for driving) until the soc back to approximately 50%. At low-speed drive, there are more chances for the Prius3 to operate in eDrive mode. Thus, to prolong the electrical driving duration, it is better to recharge the battery from low soc to high soc at once to enable continuous

electrical drive. During this operation, the battery charging power supplied from the engine is constant around 5 kW as shown with a black line. In case that the battery soc is in the range between 45–60%, the battery charging power is diminished as shown by red line.

On the other hand, when the vehicle is driving at high speed, more than 64 km/h, the engine will be turned on. In order to maintain the engine to operate at the optimum efficiency region, the battery charging power and discharging power are varied to allow the engine to operate independently from the current requested driving power. Since the engine is usually on in such kind of driving situation, the battery charging occurs more often so the soc is usually operated in a range between 45-65%. This operation during high-speed driving is shown as a cloud of green data points surrounding the red line.

For boost driving that the vehicle utilizes full power of both engine and battery, Figure 15 shows the maximum discharging power and power assist of this battery during boosting labeled by gray lines. In other word, this figure shows allowance battery-operation region. The magenta line also shows the battery charging power limit of this battery established by Prius3 experimental data. Note that the maximum battery charging and discharging are also limited by the battery, inverter, and converter temperature which is neglected in this analysis. The black and red lines indicate the strategy of the general battery charging/discharging in Prius3. The gray line shows the maximum battery power assist during boosting. It is reasonable to conclude that the battery charging target is set at 60% soc. This battery charging strategy was designed to maintain the battery soc to operate within a suitable and safe range. From the data recorded from Prius3, the range was found between soc 35-70%, and the most operating region is in between soc 40-60%. After the requested battery charging power is

estimated, the next step is to sum the requested driving power, requested battery charging power, and electronic devices supply power to obtain instantaneous total power request.

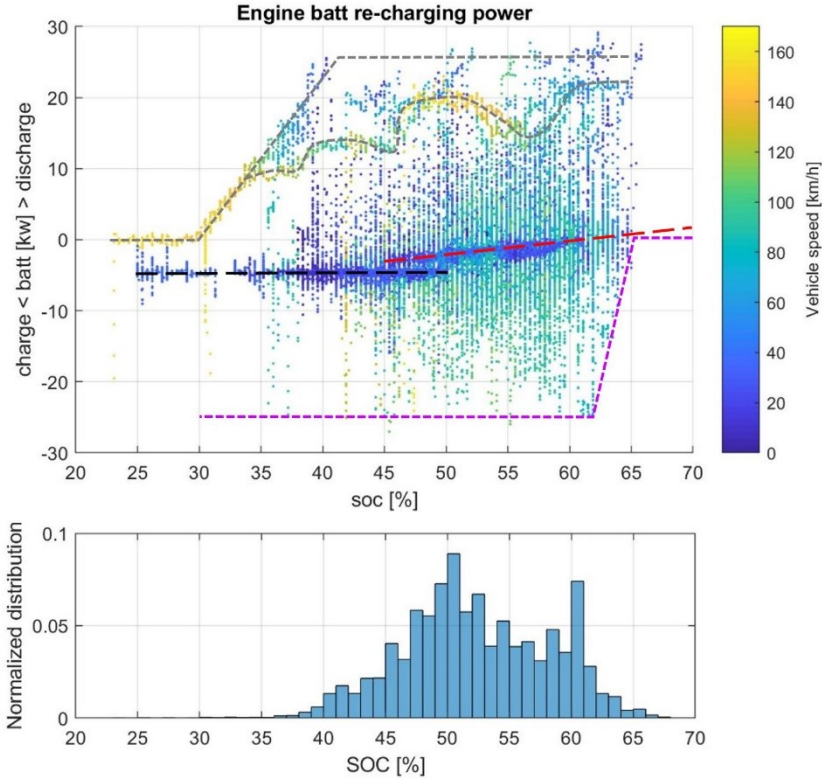


Figure 15 Requested battery charging power

Then, this total power demand is used as the main criterion for the engine on/off judgment. Figure 16 shows the data from Prius3 that were separated into engine on stage, engine off stage, engine start points, and engine shutdown point, and were plotted on vehicle speed and total power request axis. It is distinguishable that the engine off stage data points locate at low speed (<70km/h) and power (<10kW) area. Engine start point data align around a boundary of the engine off stage data points which shows the transition boundary between

engine off and on areas. Outside this area, the engine must turn on. In another word, Prius3 determines the engine on/off stage based on the area indicated by vehicle speed and total supply power.

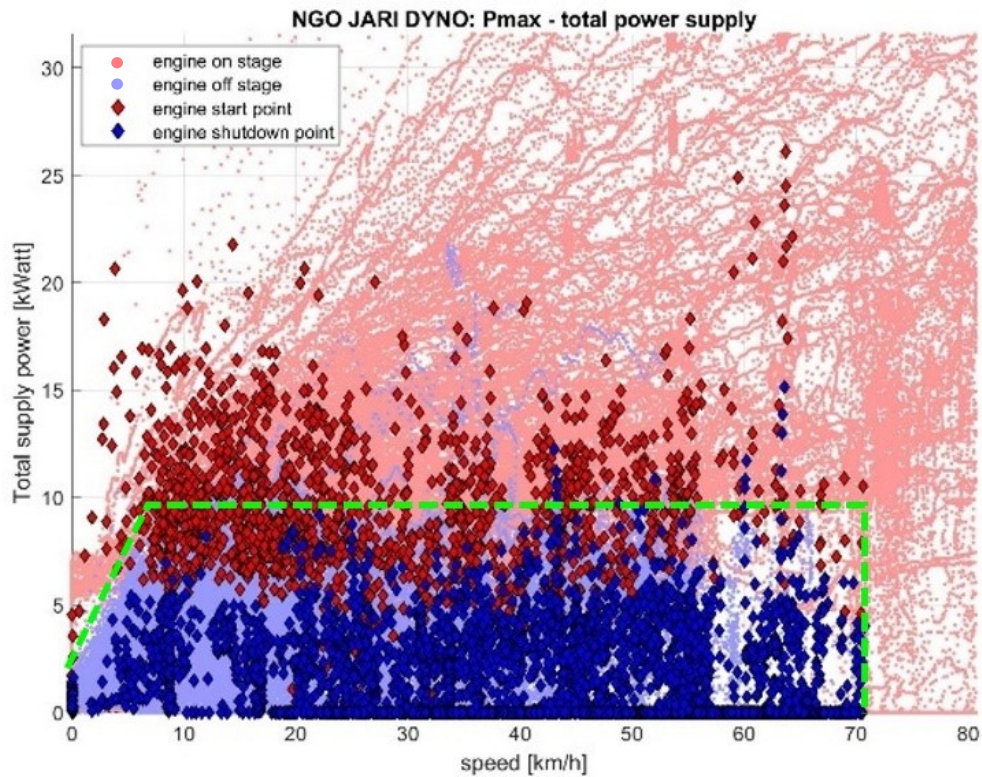


Figure 16 Engine on/off judgment in Prius3

Moreover, to determine the engine on/off stage, not only are the maximum capacity of the powertrain components taken into account but also the available battery power level should be considered. Because the available battery power varies according to the battery soc. Thus, the criteria describing the available battery power output and battery soc need to be included to the engine on/off judgment process.

Figure 17 shows the additional engine on/off judgment map in an aspect of the available battery power output at each battery soc level. This figure was plotted by the actual data recorded from Prius3 showing area of the engine off stage and engine start point data. The engine off stage data locate in a trapezoid shape, and the engine start point data align on top as a boundary at which imply to the maximum available battery output power. Furthermore, the boundary of this map is also subjected to the acceleration pedal position. If the acceleration pedal is slowly pressed under a certain threshold, the EV region (ice off region) can be slightly prolonged. This scenario is shown by the outlier ice-off data between soc 45-50% and total supply power between 10-20kW. However to maintain the vehicle's speed and acceleration, this acceleration-position threshold is considered too low in typical real-world driving.

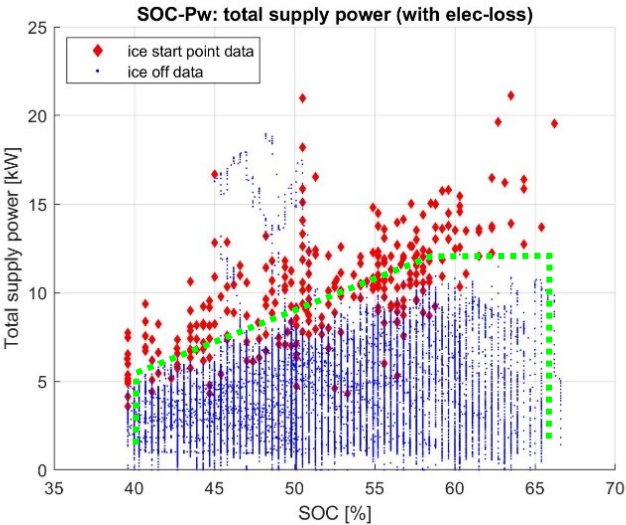


Figure 17 Relationship between available battery output power and battery soc

In summary, after the total power demand is calculated, the powertrain has to determine whether it is necessary to turn the engine on or not. In this process, two main criteria are required. First is the criteria that define the maximum power of the motor and battery because the drivability of motor depends on the battery power. Thus, the criteria that define the maximum available battery output power at different soc is mandatory. Second is the drivability of the powertrain system itself in which defined by vehicle speed and maximum driving force or torque.

3.2.2.2 Operation Mode Selection

Once the engine on/off stage is known, next the powertrain needs to determine the most efficient operation mode. Criteria of the operation mode selection are differed from automotive makers depending on powertrain design configuration. Moreover, every automotive maker protects these control criteria as high confidential data.

Most of the hybrid vehicles that are available on the market usually come with an operation mode control strategy called rule-based control. This strategy controls the powertrain operation to follow predefined operation mode selection rules/criteria that were carefully designed by experts. From literature, the operation mode selection criteria are usually defined as boundaries in terms of vehicle speed and driving force. These boundaries are usually designed in order to achieve high powertrain efficiency and drivability. Above all, the strategy design needs to consider the operation range of each powertrain component and the availability of the battery power.

In this section, we have performed an investigation to identify the criteria of Prius3 hybrid powertrain operation mode selection. The actual data from Prius3 containing more than 500,000 samples were classified into each operation mode that could be possibly available for this powertrain configuration. The data classification criteria were defined by the status of driving activities (driving, idling, braking), and MG1, MG2, engine battery activities (motoring, rest, generating).

As a result, it was found that Prius3 configuration frequently operates in 14 dominant modes as illustrated in Figure 18. During driving activity, which means gas pedal is pressed, the powertrain highly operates in two major modes: hybrid drive and electric drive. In electric drive mode, the powertrain highly operates in eDrive mode in which the battery discharges to supply electric power to MG2 for propulsion (batt-discharge/MG2-mot). In hybrid drive mode, the powertrain highly operates in High-Medium load mode (batt-charge or discharge depending on soc and driving conditions/MG1-gen/MG2-mot), Light load mode (batt-charge/MG1-gen/MG2-gen), Speed control mode (batt-charge/MG1-mot/MG2-gen), and Boost mode (batt-discharge/MG1-gen/MG2-mot/Full engine and electric power), respectively.

During braking activity, which means gas pedal is released, operation modes can be separated into two major groups: engine on while braking and engine off while braking. These modes are selected based on the current vehicle speed in order to maintain smooth driving. At high speed and heavy braking, the powertrain tends to brake with the engine on. During the engine off modes, the powertrain highly operates in Strong regenerative mode (batt-charge/MG2-gen) and Low-speed braking mode (batt-discharge/MG2-mot). At Low-

speed braking mode, MG2 acts as a motor to keep the car moving at low speed, such as driving with D gear position without pressing the gas pedal.

During idling, the vehicle mainly operates in two modes, which are battery depleting and battery charge sustaining. Once the battery level depletes to approximately 39%, the engine is on to generate the electricity via MG1 and charge to the battery all the way until soc increases up to 51%. This charging cycle usually occurs not only during the idle but also low-speed driving, when the battery charging moment is limited.

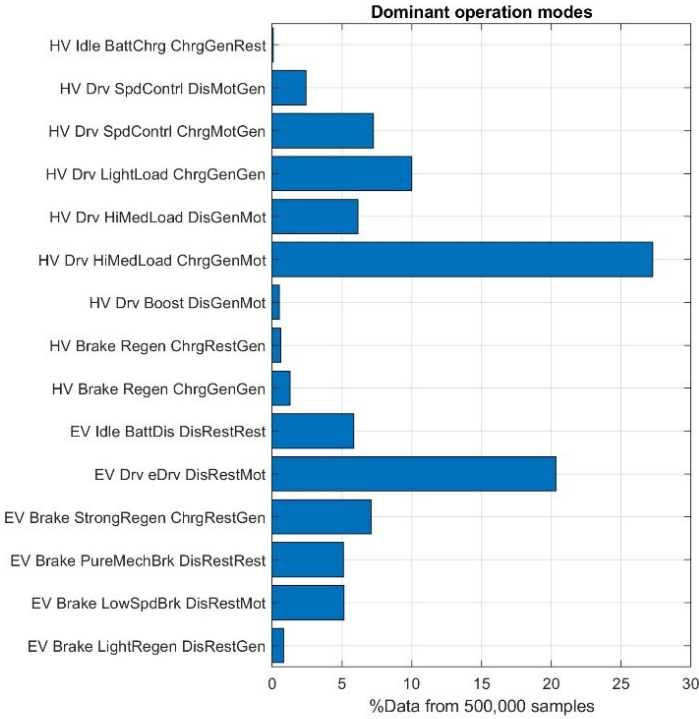


Figure 18 Prius3's dominant operation modes

After the operation modes in Prius3 were investigated and classified, the data in each mode were plotted on vehicle speed-driving force axis to illustrate operation mode regions and mode transition boundaries of Prius3's rule-based control energy management (operation modes) as shown in Figure 19. The operation mode can be categorized into three groups which are driving mode, braking mode, and idle mode.

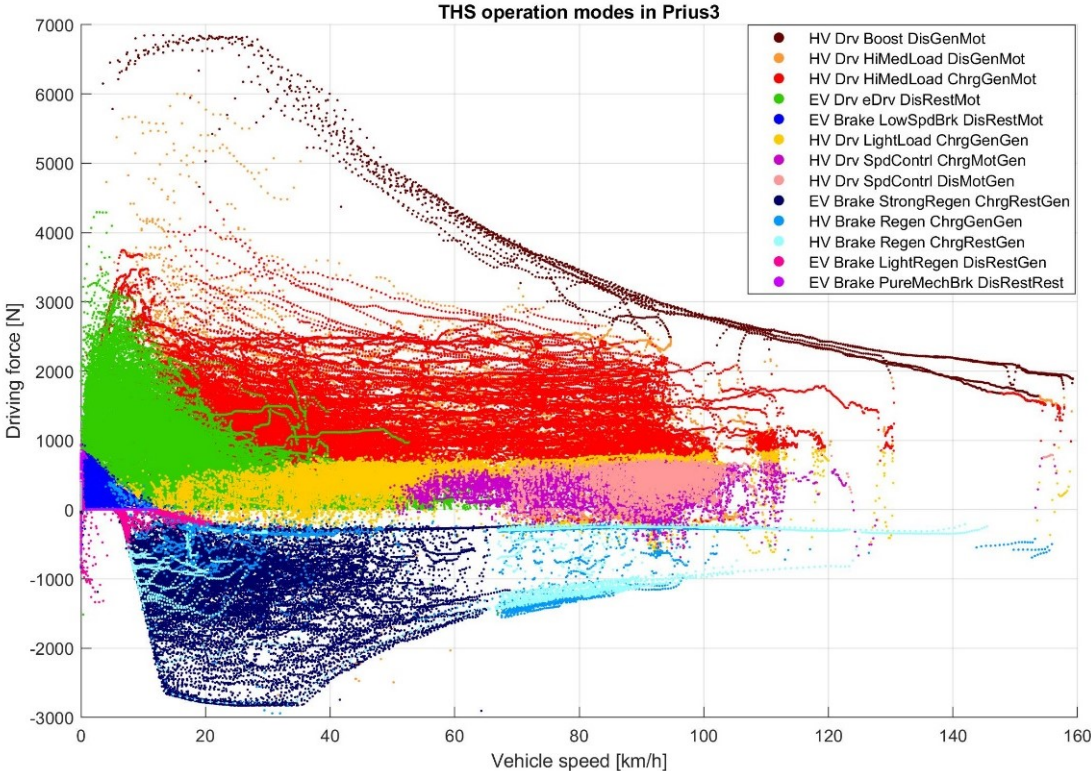


Figure 19 THS operation modes described by vehicle speed and driving force

Driving modes

eDrive mode is enabled only in a limited region of driving force and speed labeled in green. In case of high speed and high power demand, or insufficient battery power, the engine needs to turn on, and the operation mode needs to switch to hybrid modes. From Figure 19, we can see that some part of eDrive mode region overlaps with High-Medium load mode (red) and Light load mode (yellow). The eDrive and HVDrive overlapping occurs when extra power or battery charge are required.

At higher speed driving, High-Medium load mode (red) and Light load mode (yellow) are operated. The engine turns on to provide the driving force and battery charging.

Light load mode (yellow) is operated when the driving force is low. During this mode, the engine is operated at the most efficient region to supply the propulsion power. The engine speed was found between 1,000 – 3,500 rpm shown in Figure 20. Since the driving load is low, the engine power that exceeds the requested driving power is converted to electricity via MG1 and MG2, and store into the battery. When the vehicle speed starts to increase, the system rotates MG1 in the reverse direction to achieve the higher target wheel speed. Also, MG1 applies minus torque to allow direct engine torque to transfer to wheels. MG1 is typically operated as a speed controlling component, while MG2 is operated as a torque controlling component. For further explanation of the power-split mechanism, please refer to chapter3, Prius3 powertrain dynamic modeling.

As the requested driving force becomes higher, the powertrain switches the driving mode to High-Medium load mode labeled in red and orange in Figure 19. For these modes, the engine operates at wilder rpm range from 1,000 – 5,500 rpm shown in Figure 20.

Red refers to High-Medium load mode that MG1 acts as a generator and feeds the electricity to MG2 for driving torque assist. In case there is an electric power residual, it will be stored to the battery. In this mode, the driving power is mainly supplied by both MG2 and engine power (batt-charge/MG1-gen/MG2-mot).

However, in order to sustain the battery power to stay inside the appropriate region (20-80%), battery charging and discharging activities need to be balanced. Once the battery soc is getting too high or the vehicle requests higher power, the battery power will be utilized to assist driving during High-Medium load mode (batt-discharge/MG1-gen/MG2-mot) shown by the orange dataset. Thus, the clusters of red and orange data are overlaps.

In case that the driver requests full acceleration power by pressing acceleration pedal deeper approximately more than 80%. Maximum power from the engine and battery is utilized to accelerate the vehicle. The system will generate the engine torque by operating the engine along the maximum torque curve shown in Figure 20. Electricity generated via MG1 plus electricity from the battery is fed to MG2. As MG1 acts as generators, it allows a part of the engine torque to be transferred directly to wheels. This is the operation mode called Boost mode that provides an ultimate driving power from this configuration.

Figure 20 shows engine operation control paths and regions at each operation modes. The colors illustrate the dynamic of the engine by using rotational acceleration. For instance, the top left sub-figure shows the path for Boost mode that provides the most powerful and rapid control response. These paths were optimized and predefined to suit for the output performance characteristics.

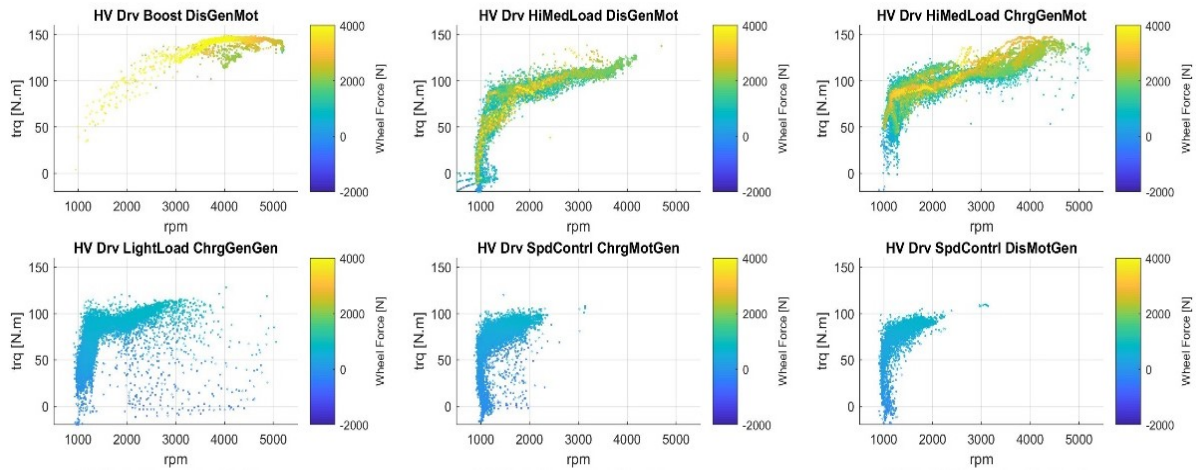


Figure 20 THS operation modes projected on engine operation region

Braking modes

The operation mode during the braking can be classified into categories which are braking with the engine on, and braking with engine off. When the braking occurs at speed higher than around 65km/h, the engine is always turned on, using the engine brake, MG2 regenerative braking together with mechanical braking power. In some case, this engine on braking can also occur at low-speed drive while battery charging. For the engine off braking, it usually occurs when speed lower than around 65km/h.

The most dominant operation mode during braking is Strong regenerative braking mode (dark blue). During this mode, the engine is off. MG2 recuperates the braking energy and charge to the battery.

Nevertheless, once the regenerative braking power is insufficient to supply the vehicles, especially when the speed becomes lower than 15km/h. The battery changes from the charge to the discharge stage. The MG2 also switches from generator to motor to maintain

the deceleration smoothly. This transition is shown by Light regenerative braking (red pink) and Low-speed braking (blue).

Note that the braking force that shows in Figure 19 does not include the mechanical braking force. This figure aims to show the operation mode regions and capable regenerative braking force.

Idle modes

During idle, though the powertrain does provide power for propulsion, the electric components inside the vehicle still continue to consume the energy. Thus, during idling, the powertrain needs to run by two operation modes, which are battery charging and battery discharging modes.

Most of the time, the powertrain operates in battery discharging mode. Electric power consumption was found in a range between 0.2 – 1.5 kW. Average electric power was at 0.6 kW. However, when the battery soc depleted to approximately 38%, the powertrain switched the operation mode to battery charging mode. During this mode, the battery was charge approximately at 4.6kW by the engine power. The engine operates around at 1,250 rpm and 48 N.m torque.

The intermittent engine on occurs due to these coming reasons: Engine warm-up when the coolant temperate less than 40 Celsius, catalytic warm-up when the engine starts for a short period, power request from Heater and A/C, low SOC, low battery temperature, and too high and low oil temperature.

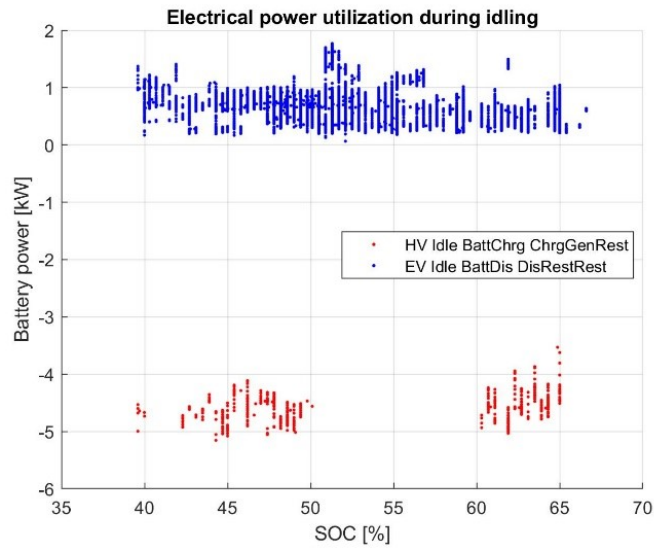


Figure 21 Electrical power utilization during idling

3.3 Dynamic Equation Formulation and Power Transmission Analysis of the Third Generation of Toyota Prius

This section focuses on how to make use of the limited available dataset from HV ECU, to estimate the key parameters. First, torque transfer in Prius3's power-split hybrid powertrain configuration is analyzed on a free body diagram. Based on the free body diagram, the powertrain equations were formulated by implementing the second law of Newton (law of motion) and Will's equation (planetary gears' speed relationship). In addition, further insight explanation on the control of Prius3's powertrain explained in the prior chapter will point out in this chapter.

3.3.1 Power-Split Hybrid Powertrain Dynamic Equation Formulation

This sub-section provides a basic force/torque analysis on power-split hybrid vehicle powertrain by using Prius3 as an example. The free body diagram of the system is presented. Then, based on the free body diagram, the powertrain equation is derived and implemented in the key parameters' estimation. Lastly, the validation of the estimated parameters will be performed to affirm the fidelity of both the estimation method and the reliability of HV ECU data.

3.3.1.1 Free Body Diagram and Power Transmission Analysis

Figure 22 illustrates Prius3's powertrain structure which consists of four parts, which are the main planetary gear, MG2 speed reduction gear, counter gear, and final gear. This transmission system connects and transfers power among the engine, MG1, MG2 and wheels. The powertrain components: engine, MG1, MG2, are labeled and indicated in green.

The main planetary gear, sometimes called power-split device, is labeled in red. The sun, carrier, and ring gears are mounted to MG1, engine, and MG2's speed reduction ring gear respectively.

According to the drawing, MG2 is mounted directly to the sun gear of the speed reduction planetary gear, while transmitting power through the fixed carrier throughout the ring gear. MG2 speed reduction's ring gear and the main planetary ring gear are coupled into

a single element contained inside the counter gear case. The features of the MG2 speed reduction gear are to reduce MG2 speed and increase torque to be suitable for driving.

The output torque from the two ring gears is transmitted to the counter gear to the reverse the rotating direction. Then, the torque is passed through final gear to adjust the force and speed into an appropriate driving range.

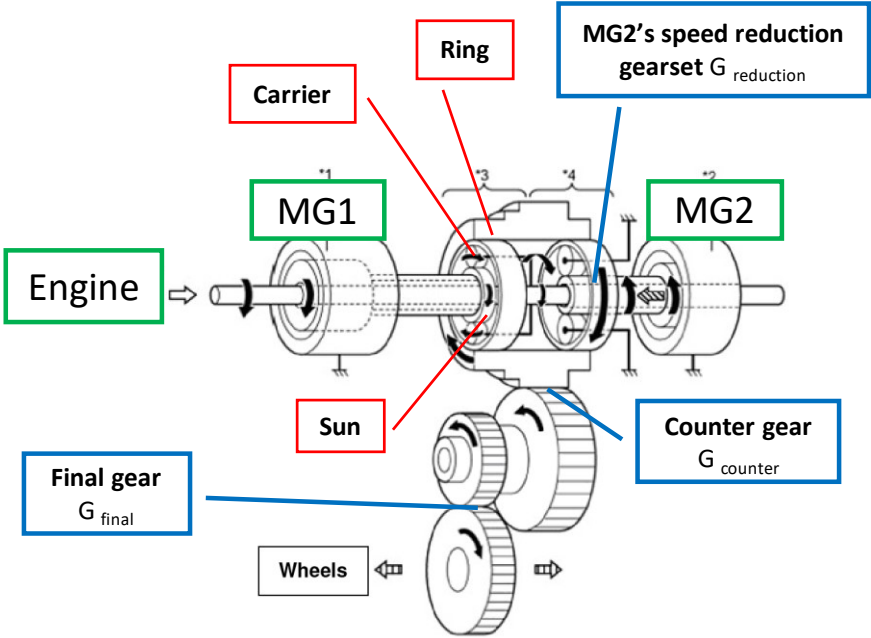


Figure 22 Prius3's powertrain structure (Allouchery, 2012)

After understanding Prius3's power-split hybrid powertrain structure, the torque and power transfer via the machine can be analyzed as shown in Figure 23.

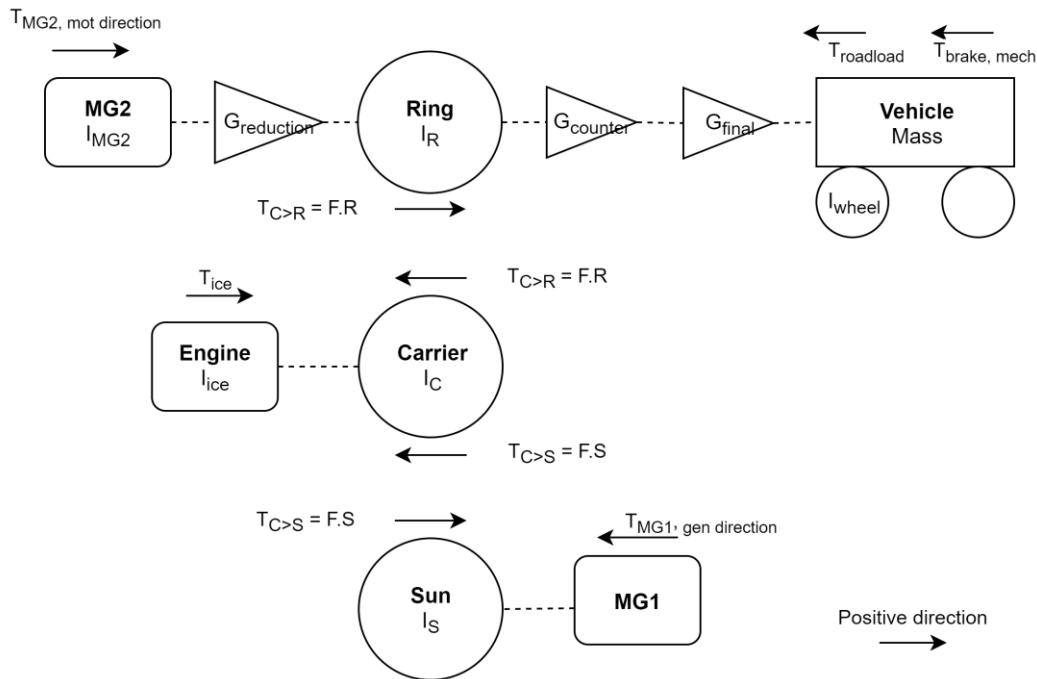


Figure 23 Prius3's powertrain free body diagram

The analysis starts with engine exerts torque to the carrier. It generates reaction forces described in terms of torque: torque transmitted from carrier to sun gear ($\tau_{C>S}$) and torque transmitted from carrier to ring gear ($\tau_{C>R}$). These engine torque are transferred to sun and ring gear. To analyze these torque terms, Figure 24 shows the free body diagram of the planetary gear during the engine force is acting on it. Once, we simplify the system by assuming steady state equilibrium moment at y point. It was found that $F_R = F_S$. Thus, the engine torque transfer can be labeled as $\tau_{C>S} = F \cdot S$ and $\tau_{C>R} = F \cdot R$. Caution that S and R are radius of the sun and ring gears, not the number of teeth.

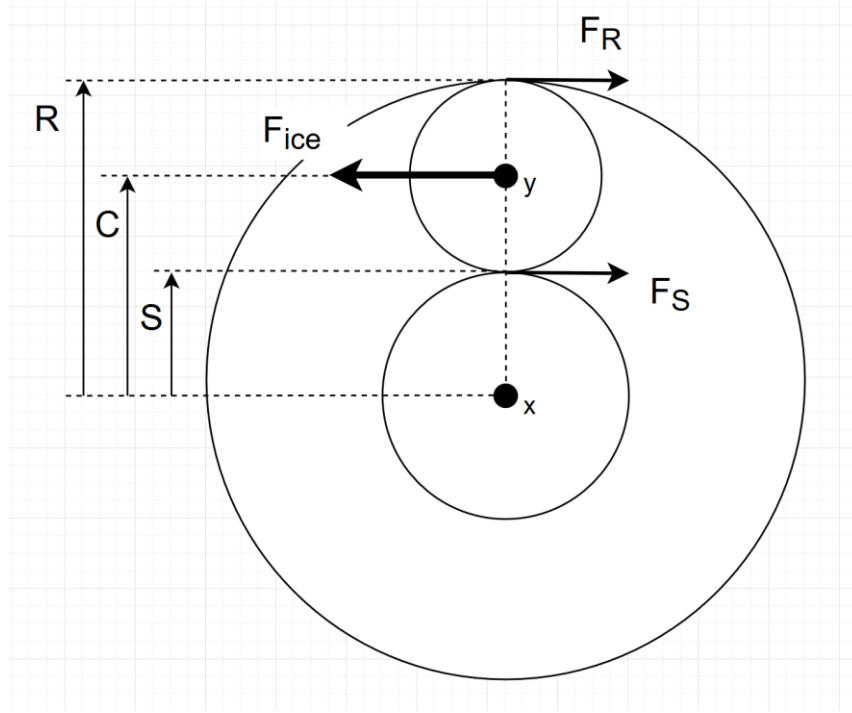


Figure 24 Force free body diagram at the carrier for internal

At sun gear and MG1 section, there is split engine torque $\tau_{C>S}$ acting on the system, meanwhile MG1 also exerts torque in the opposite direction. This case can be compared to when the engine is on and some part of the power is split to MG1 for electric generation. Thus, MG1 generation torque direction is labeled in a negative direction.

At ring gear section, it includes all the components from MG2, speed reduction gear, ring gear, counter gear, final gear, vehicle body, to wheels. $G_{reduction}$, $G_{counter}$, and G_{final} express the fix gear ratio at speed reduction gear, counter gear, and final gear respectively and I expresses moment of inertia at each component mass. There is torque $\tau_{C>R}$ acting on ring gear. From the left side, there is τ_{MG2} exerted in the positive direction which implies MG2 motoring torque. $\tau_{C>R}$ and τ_{MG2} represent the total driving power from the powertrain

that is used to overcome the resistances in terms of roadload $\tau_{roadload}$ acting on the vehicle. In case that the mechanical brake is applied, the torque also expressed by $\tau_{brake,mech}$ always pointing in negative direction. (Liu, Peng, and Filipi 2005; Liu and Peng 2008)

3.3.1.2 Dynamic Equation Model Formulation

Prius3's dynamic equation can be derived by starting from the carrier section. The free body diagram is illustrated in Figure 25.

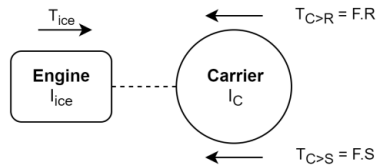


Figure 25 Prius3's free body diagram at the carrier

Once the second law of Newton is applied, the equation at carrier can be expressed in (2).

$$\sum \tau = I\dot{\omega}$$

$$\tau_{ice} - F \cdot R - F \cdot S = \dot{\omega}_{ice}(I_{ice} + I_C) \quad (2)$$

The internal force term F can be estimated by taking the second law of Newton on the sun gear section. The free body diagram of the sun gear section is illustrated in Figure 26

and the equation is written in (4). By plugging in ω_{MG1} and τ_{MG1} obtained from HV ECU, the internal force can be estimated.

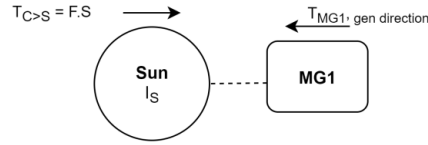


Figure 26 Prius3's free body diagram at the sun gear

$$\sum \tau = I\dot{\omega}$$

$$F \cdot S - (-\tau_{MG1}) = \dot{\omega}_{MG1}(I_s + I_{MG1}) \quad (3)$$

$$F = \frac{\dot{\omega}_{MG1}(I_s + I_{MG1}) - \tau_{MG1}}{S} \quad (4)$$

The direct engine torque split to sun and ring gear can be expressed by (5) and (6). These equations provide two options of the torque calculation which are dynamic torque, and steady-state torque split. The dynamic torque split can be obtained by input (4) in the F term in (5) and (6).

$$\tau_{C>S} = F \cdot S = \tau_{ice} \frac{S}{R + S} \quad (5)$$

$$\tau_{C>R} = F \cdot R = \tau_{ice} \frac{R}{R + S} \quad (6)$$

Next step is to calculate driving power, force, and torque that transmit to wheels. Base on free body diagram at the ring gear section's in Figure 27, the powertrain torque equation can be formulated by equation (7). G refers to gear ratio defined by N_{drive}/N_{driven} .

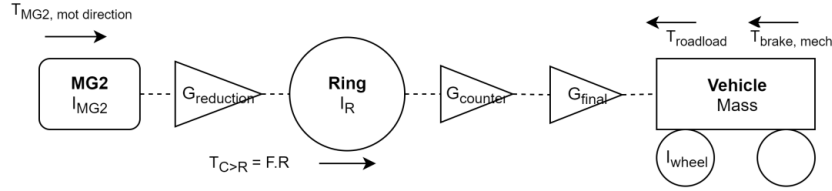


Figure 27 Prius3's free body diagram at ring gear

$$\left(\frac{\tau_{MG2}}{(G_r \cdot G_c \cdot G_f)}\right) + \left(\frac{F \cdot R}{G_c \cdot G_f}\right) - \tau_{roadload} - \tau_{brake, mech} = \dot{\omega}_{wheel} \left\{ \frac{I_R}{(G_c \cdot G_f)} + \frac{I_{MG2}}{(G_r \cdot G_c \cdot G_f)} + I_{wheel} \right\} \quad (7)$$

Road load consists of three terms: rolling resistance, aerodynamic drag, and road grade resistance, which can be calculated by equation (8).

$$\tau_{roadload} = R_{wheel} \left\{ mg C_{roll} + \frac{\rho_{air} A_{front} C_{drag} (v_{veh} - v_{wind})^2}{2} + mg \cdot \sin \left(\tan^{-1} \frac{h}{l} \right) \right\} \quad (8)$$

According to equation (7), the total torque that the powertrain propels the vehicle can be estimated by equation (9).

$$\tau_{wheel} = \left(\frac{\tau_{MG2}}{(G_r \cdot G_c \cdot G_f)}\right) + \left(\frac{F \cdot R}{G_c \cdot G_f}\right) - \dot{\omega}_{wheel} \left\{ \frac{I_R}{(G_c \cdot G_f)} + \frac{I_{MG2}}{(G_r \cdot G_c \cdot G_f)} + I_{wheel} \right\} \quad (9)$$

To convert torque to force and power, equation (10), (11), and (12) are required. v is vehicle speed.

$$P = \tau \cdot \omega = F \cdot v \quad (10)$$

$$F = \frac{\tau}{R_{wheel}} \quad (11)$$

$$\omega = v \cdot R_{wheel} \quad (12)$$

For the relationship of the rotational speed among sun, carrier, and ring gears, it can be expressed by equation (13) and (14).

$$(S + R)\omega_c = \omega_R R + \omega_s S \quad (13)$$

$$(S + R)\dot{\omega}_c = \dot{\omega}_R R + \dot{\omega}_s S \quad (14)$$

3.3.1.3 Nomographic Chart

There is another technique to analyze the motion of the planetary gear set called monographical chart technique. Since, the rotational speeds of sun, carrier, and ring gear always align on the same straight line, it is possible to implement a chart to explain. The nomographical chart of Prius3's powertrain is illustrated in Figure 28. The vertical axis indicates the magnitude of planetary gear element rotational speed. Each axis represents each

gear element labeled on top of the graph. Circle dots on the axis show whether the gear is fixed (black) or free (white).

The horizontal axis indicates the relationship of the number of sun and ring gear teeth. The left side and right side of the graph show nomographical charts of the main planetary gear, and MG2 speed reduction planetary gear set.

The consideration starts from the ring gear. Since the vehicle speed information is always available, the white dot is first placed on the ring gear axis at the current speed magnitude. Then, the actual MG2 speed can be calculated by equation (13) and the speed reduction gear ratio. Note that the carrier is fixed in place.

Based on vehicle current speed, acceleration pedal position, and battery soc, the powertrain determines the operation mode, and operation points of each powertrain components. Once, the speed of the engine is decided, the white dot can be placed on the engine axis. For planetary gear set, if the speed of two elements is known, the speed of the other element can be found. Thus, the planetary gear is recognized to have two degrees of freedom. By using this monographically chart, the speed of MG1 will be found by drawing a straight line through the dots on the ring and engine axis and find the position that the line crosses the MG1 axis. Equation (13) will also give the same answer.

According to the mechanism of THS power-split configuration, MG1 torque plays significant roles in the power-split powertrain speed control. Once it is actuated as a generator, it allows a part of the engine torque to transmit through wheels (ring gear) by producing reaction force on sun gear side. Without MG1 generation torque, the direct engine torque transfer to the wheels cannot be achieved yet the engine speed increases, such as

engine starting moment. Moreover, varying MG1 speed also results in wheel speed change. Thus, MG1 is sometimes called speeder because its capability to change engine speed and also the wheel speed.

For the torque analysis, it can be analyzed by using the same technique similar to a seesaw balancing. Figure 28 represents the operation of Medium-Heavy load driving mode. The colored arrows refer to torque and its direction, while the length indicates the magnitude. Starting with the engine supply torque to the system. The blue engine torque is split to MG1 and the ring gear. At this point, it is important to mention that the direct engine torque transfer can be achieved only if MG1 generation torque is active, or wheel slip does not occur. Otherwise, there is no reaction force to allow the pinion gears and carrier to transmit torque. In such a case, the engine speed will increase rapidly instead due to the free rotational of the sun or ring gears.

At the ring gear, the engine torque to sun gear will be equal to MG1 generation torque. At the ring gear which is the torque output gateway, the road load torque is balanced by the engine torque split to ring gear. Since the supplying torque is not sufficient, MG2 will provide the shortcoming amount to assist driving. (Toyota, 2013)

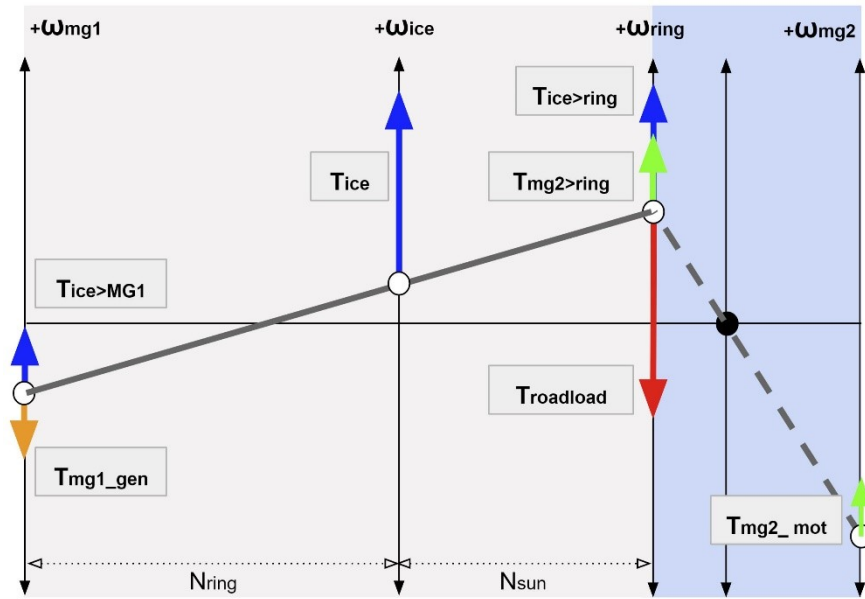


Figure 28 Prius3 Powertrain's nomographic chart

CHAPTER 4

Experiment and Data Acquisition for Hybrid Vehicles

The experiment is a common approach to peruse the desirable dataset. However, for hybrid vehicles, there are an abandon amount of data to be taken into account compared to conventional or electric vehicles. The objectives of the experiments during this project were to (1) study on hybrid vehicles' fuel consumption characteristics, and (2) to identify and understand the sophisticated operation of THS (Toyota Hybrid System) via Prius3.

The concept fuel consumption experiment is to design an experiment that can capture real-world driving consumption by designing/selecting the experimental conditions that reflex the typical driving scenario at that interested region. Based on this dataset, the frequently operated powertrain-operation region can be realized.

On the other hand, more experiments need to be conducted to obtain a suitable dataset for the hybrid powertrain operation investigation. The concept of the experimental design is to extend the powertrain operation region to cover all the area of vehicle speed-force map as much as possible. The experiment should also be designed to capture the operation mode overlapping (The data located at the same speed-force area but at different operation modes.). Furthermore, the operation points of each component, such as battery, engine, MG1, and MG2, should be extended to reach not only the typical usage but also the maximum performance.

Thus, this chapter provides comprehensive technique on how to design an experiment for hybrid vehicles based on three different experiment methods; public road, chassis dynamometer, and private circuit experiments. Advantages and disadvantages of each approach are also discussed and compared. In addition, the data acquisition and special concerns for hybrid vehicles are also provided in details.

4.1 Data Acquisition for Hybrid Vehicles

In hybrid vehicles, there are a long list of parameters to be monitored during the experiment compared to conventional and electric vehicles. In many cases, recording too many data causes a reduction of the sampling rate. To design the data list, it is recommended to begin with analyzing the power flow throughout the vehicle system, then select the input and output data that relate to the interested system.

For hybrid vehicles, the input power is in a form of petrol fuel and regenerative braking power. Depending on the driver command, the vehicles utilize the power from these two sources to energize the engine, motor/generators, and/or store the power in the battery. Finally, the output power from the powertrain is in a form of driving power, and electronic device output power. The overall power flow path in hybrid vehicles is illustrated in Figure 29.

For experiments related to the energy consumption experiment, the data list should focus on the input power source and output. On the other hand, All the four boxes on Figure 29 should be taken into account for hybrid operation characteristic investigation.

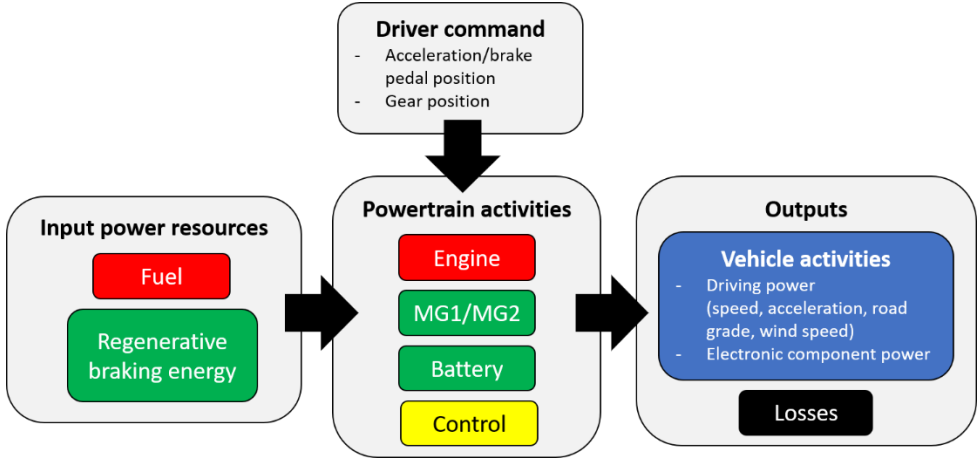


Figure 29 Power flow inside hybrid vehicles

The method to access the data may be different from vehicles to vehicles; however, the data acquisition for Toyota hybrid vehicles can be achieved by implementing equipment as described below.

4.1.1 Controller Area Network (CAN) Signal

In hybrid vehicles, there is a special control unit that monitors and controls synergic operation between the engine and electric powertrains called HV ECU (Hybrid Control Unit). This HV ECU receives substantial data from in-vehicle sensors, determine and send out the

control decisions to actuate the powertrain components. HV ECU provides 90% of the data in Input Power Sources, Powertrain Activities, and Output boxes described in Figure 29. These data are one of the most important datasets for energy consumption and hybrid operation characteristic investigation.

In order to access the data from HV ECU, ECU, others, we recommend Toyota DENSO Intelligent Tester 2 (IT2). This equipment works for not only the Toyota system but also Lexus and Suzuki's system without requiring any CAN ID. The data list can be customized; however, it can only access the data from one ECU at a time. Thus, while accessing HV ECU data, engine fuel injection and other specific parameters to the engine operation from ECU are not included in the data list. In addition, the exported CSV file also contains invalid redundant signal columns. An algorithm to distinguish and eliminate the invalid data columns must be applied. The maximum sampling frequency is approximately 7-8 Hz. This equipment is available on the online market at a reasonable price, 350USD. The picture is shown in Figure 30.



Figure 30 Toyota DENSO Intelligent Tester 2 (IT2)

Another option is OTC which is a vehicle interface module (VIM) officially used by TOYOTA. This equipment comes with a specific software called Global Tech Streme. Data accessibility is similar to IT2; nevertheless, the data list is not customizable and the sampling rate for HV ECU access was found approximately at 0.8Hz. The appearance is shown in Figure 31.



GTS TIS 3 OTC

Figure 31 OTC Vehicle Interface Module (VIM)

Table 3 provides an important data list, units, and definitions from HV ECU that can be accessed by IT2 and OTC. These data are substantially required for both energy consumption, and hybrid operation characteristic investigation particularly the bolded texts.

Table 3 Requisite dataset from HV ECU

Data Catagorty	no.	HV ECU data name	Unit	Definitions & notices
Time stamp	1	'TIME'	ms	Time stamp The sampling rate is not constant. The longer recording data list, the slower sampling rate.
	2	'Auxiliary Battery Vol'	V	The voltage of 12V battery
Electronic power consumption	3	'A/C Consumption Pwr'	Watt	Air conditioning power
	4	'Accelerator Degree'	%	Acceleration pedal position
Vehicle dynamics	5	'Gradient of Road Surface'	rad*g	rad is the angle between road surface to horizon level. g is gravity force 9.81 m/ss
	6	'Vehicle Spd'	km/h	vehicle speed 1km/h Resolution , In case tire diameter is different from the specification, this signal need to be compensted.
	7	'Ambient Temperature'	C	Outside vehicle temperature
Engine control	8	'Atmosphere Pressure'		Outside vehicle pressure
	9	'Engine Coolant Temp'	C	Engine coolant water temperature (80-100C)
	10	'Engine Fuel Cut'		1 = Fuel injection is deactivated. 0 = Fuel injection is active.
	11	'Engine Idling Request'		1 = request idle 0 = no need idle
	12	'Engine Revolution'	rpm	round per minute More recommended than Engine Rev (Sensor)
	13	'Intake Air Temperature'	C	
	14	'MAP'	gram/	Manifold absolute pressure
	15	Throttle Position'	%	For hybrid vehicle, throttle position does not vary accodring to accelration pedal position.
	16	'Target Engine Rev'	rpm	Engine rpm's control value
	17	'Aircon Request'		1 = engine on to supply A/C power 0 = no A/C power
	18	'Calculate Load'		Calculated engine load Activate only when the engine is on.
Hybrid control	19	'Charge Control Value'	kW	Power used to control HV battery charge
	20	'Discharge Control Value'	kW	Power used to control HV battery discharge
	21	'Drive Condition ID'		0 = electric drive (EV mode), 1 = engine triggling on 2 = engine triggling off, 3 = hybrid drive
	22	'Engine Stop Request'		1 = request engine to turn off 0 = no need engine off
	23	'Engine Warming Up Rqst'		1 = engine on for engine warm up 0 = no need engine warm up
	24	'ECO Mode'		1 = ECO mode is selected. 0 = ECO mode is off.
	25	'EV Request'		1 = EV drive is allowed. 0 = EV drive is not allowed.

	26	'Main Batt Charging Rqst'		1 = request battery charging 0 = no need battery charging
	27	'Request Driving Force'	N	Requested driving force during EV mode
	28	'Request Power'	Watt	Requested total driving power from engine
	29	'Rqst Regen Brake Torq'	N.m	Request regenerative braking torque
	30	'Stop Light Switch'		1 = Brake pedal is pressed. 0 = Brake pedal is free.
	31	'G(MG1) Trq Exec Val'	N.m	MG1 exact torque value
	32	'Generator(MG1) Rev'	rpm	MG1 revolution
Motor/Generator	33	'Generator(MG1) Torq'	N.m	MG1 torque (more robust than the exact value)
	34	'M(MG2) Trq Exec Val'	N.m	MG2 exact torque value
	35	'Motor(MG2) Revolution'	rpm	MG2 revolution
	36	'Motor(MG2) Torq'	N.m	MG2 torque (more robust than the exact value)
	37	'Regenerative Brake Torq'	N.m	Regenerative braking torque This signal is in active only when the major regenerative braking occurs, not every regenerative operation.
	38	'Inhaling Air Temp'	C	Inhaling air temperature for battery cooling system
High voltage battery	39	'Internal Resistance R01'	ohm	Internal resistance of battery module no. 1
	40	'Internal Resistance R02'	ohm	Internal resistance of battery module no. 2
	41	'Internal Resistance R03'	ohm	Internal resistance of battery module no. 3
	42	'Internal Resistance R04'	ohm	Internal resistance of battery module no. 4
	43	'Internal Resistance R05'	ohm	Internal resistance of battery module no. 5
	44	'Internal Resistance R06'	ohm	Internal resistance of battery module no. 6
	45	'Internal Resistance R07'	ohm	Internal resistance of battery module no. 7
	46	'Internal Resistance R08'	ohm	Internal resistance of battery module no. 8
	47	'Internal Resistance R09'	ohm	Internal resistance of battery module no. 9
	48	'Internal Resistance R10'	ohm	Internal resistance of battery module no. 10
	49	'Internal Resistance R11'	ohm	Internal resistance of battery module no. 11
	50	'Internal Resistance R12'	ohm	Internal resistance of battery module no. 12
	51	'Internal Resistance R13'	ohm	Internal resistance of battery module no. 13
	52	'Internal Resistance R14'	ohm	Internal resistance of battery module no. 14
	53	'Power Resource IB'	Amp	High voltage battery's current
	54	'Power Resource VB'	V	High voltage battery's voltage
	55	'State of Charge (All Bat)'	%	State of charge of high voltage battery
	56	'Status of Charge Max'	%	Recorded maximum SOC
57	'Status of Charge Min'	%	Recorded minimum SOC	
58	'Temp of Batt TB1'	C	High voltage battery temperature from sensor no.1	
59	'Temp of Batt TB2'	C	High voltage battery temperature from sensor no.2	
60	'Temp of Batt TB3'	C	High voltage battery temperature from sensor no.3	

For the WIFI/Bluetooth OBD scan tools, such as OBD link or ELM, the sampling rate was found slower, and less data list from HV ECU compared to the IT2 and OTC. However, it can access data from different ECUs at the same time. Please be caution that some of traditional OBD loggers do not support HV ECU data acquisition.

To avoid malfunction of the OBD scan tools and measurement noises, the most important tips is to always use the same power supply and ground generated by the vehicle. Using the power supply from home power socket while recording ECU data will cause malfunction and automatically disconnection. Since the vehicle's ground and home power socket's ground are different, it causes confusion to the measurement.

4.1.2 Fuel Consumption

According to the problem of lacking fuel consumption data from HV ECU, we solve the problem by installing external fuel flow meter. In order to select a proper fuel flow meter, it is recommended to consider not only sensor type, and performance, but also dimension of the sensor, operation range of pressure, flow rate, and temperature. Especially for hybrid vehicles that the engine turning on/off frequently, it creates fuel pressure shock to the sensors. Thus, the durability of the sensor should also be taken into consideration.

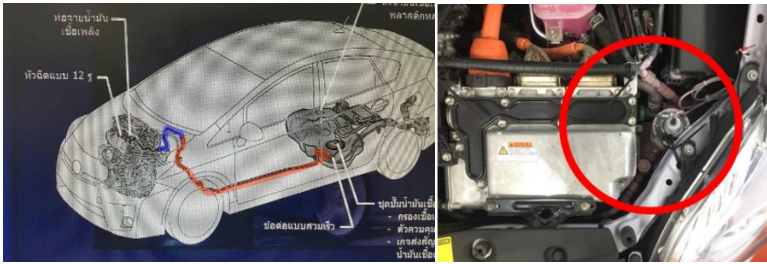
During this project, we implemented the propeller flow meter type to measure the fuel flow rate. The selected flow meter was FMTD20 model, DEA Engineering Company shown in Figure 32 Fuel flow meter FMTD20. The specification sheet is provided in Figure

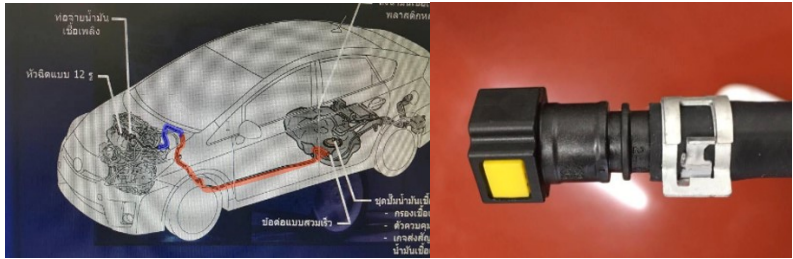
32. For the flow meter installation in Prius3, there are some additional gadgets and tips explained in Table 4.



Figure 32 Fuel flow meter FMTD20

Table 4 Flow meter installation information

Number Refer to Figure 33	Parts	Remarks
1	Flowmeter FMTD-20	<ul style="list-style-type: none"> - Max design pressure is at 3,000psi, and the design flow rate range is 0.30 – 67.5L/hr. - Prius3 has an indirect injection fuel system. The fuel return line is already equipped inside the tank. There is no need to measure the fuel on this line. Thus, installing the flowmeter in between the engine and the fuel tank is the most appropriate location for the measurement. - Possible installation position is at between blue and red tube in the picture below. - Prius3 fuel pump's maximum pressure is at 75psi, and the nominal pressure is at 42psi. - Prius3' measurable minimum and maximum flowrates were found at 0.5-13 L/hr. 
2	High-pressure injector fuel hose	<ul style="list-style-type: none"> - This fuel hose is used to connect/extend between the flow meter to the original fuel system. - For Toyota's product purchasing, the high pressure and low pressure (return) hoses are labeled with pink and white colors respectively. - The fuel hose inner diameter is 7.9mm.
3	Screw-to-nipple convertor (male end screw)	<ul style="list-style-type: none"> - This converter is connected at both ends of the flowmeter, and the high-pressure fuel hose. - The screw end diameter is 13.35mm., male type ¼ standard size. And the other end is a nipple 9mm. diameter.
4	Fuel hose ring clamp	<ul style="list-style-type: none"> - This clamp is used to lock and seal the high-pressure hose with connectors to prevent leakage. - It is recommended to use a clamp that is designed specifically to anti-leakage by distributing force equally around the clamp surface.

		<p>- The traditional clamp may cause wrinkle around on the rubber hose which leads to leakage problem.</p> 
5	Engine-side yellow plastic connector	<p>- The part is equated on the end of a middle fuel highlighted in blue below.</p> <p>- The connector can be separated by peeling the thermoplastic cover off.</p> <p>- This connector is used for connecting the inlet of the flowmeter to the end of the long tube (labeled in red) on the engine compartment side.</p> 
6	Metal fuel tank-side connector	<p>- The modification is required for this part by using some part of the long fuel tube labeled in red on the left picture shown in number 5.</p> <p>- Then, cut the tube at the end, on the engine compartment side, and modify the cut end to have a stopper ring for the hose clamping locker shown in right below.</p> 
7	Plastic cable tie	- These cable ties are used for tying the flowmeter system in place.
8	Wiring extender circuit board	- The board is located in the engine compartment to extend signal, power and ground cables from the compartment to the NI datalogger inside the vehicle.
Additional parts	Piping tape	- This piping tape should be applied around male screw before closing in order to prevent fuel leakage.

Additional parts	Fuel leakage monitoring spray	- This type of spray will change color when it detects any fuel leakage. For the safety, it is recommended to always check the leaking at every connection and gasoline smell to prevent serious accidents that may occur.
------------------	-------------------------------	--

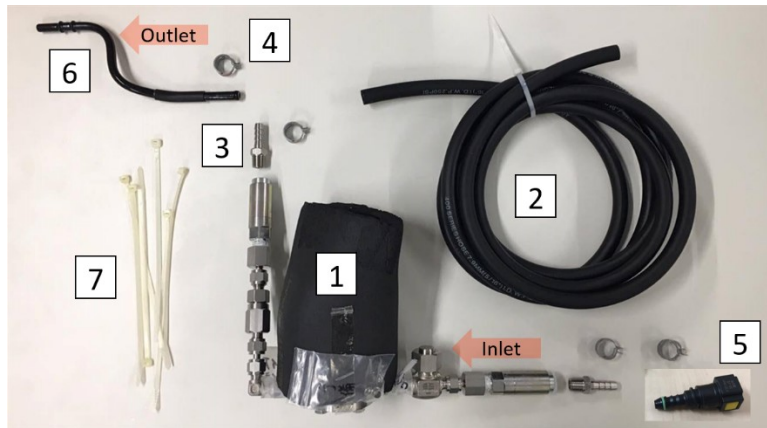


Figure 33 Flow meter installation equipment

4.1.3 High Voltage Battery

After the external flow meter installation, we installed current sensors at the high voltage battery for a purpose of IT2-external sensors time synchronization. High voltage battery current is selected due to its high fluctuation frequency that suits for cross-correlation signal synchronization method. In addition, we would like to calibrate the accuracy of the Prius3' on-board current sensor. However, there are also some other available options, such as vehicle speed, or trigger bottom, that can be used instead of the battery current. Prius3 battery current was found in a range of -150 – 150 Amp; however, the majority of the data distributes in a bell-shape liked distribution from -50 – 50Amp.

The sensor that we selected for Prius3's high voltage battery was Hall effect HOP200, LEM. This current sensor can measure both positive and negative current in a range of -200 to 200 Amp. The installation position is at the high voltage cable of the battery at which located in the back of the car shown in Figure 34. For more information about the sensor, please refer to the specification sheet provided in Figure 34. More importantly, safety procedures and cautions for high voltage system operation should be implemented as first priority concerns.



Figure 34 High voltage battery's current sensor installation

4.1.4 Electronic Circuit and Analog-Digital Signal Converter

Due to the output signals from the external sensors: fuel flow meter and current sensor, are generated as analog signals, we need to convert them to digital signals before

sending to a computer. Thus, we implemented NI-6001 as an analog-digital converter, and we used NI Signal Data Express to record the data.

For the sensors' power supply and signal management system, we fabricated a simple electronic circuit to supply power/ground, the bi-polar voltage for the current sensor, fuse, switch, a hub for the output signals before entering NI-6001. The module is shown in Figure 35.



Figure 35 External sensors' power supply and signal management module

4.1.5 Wind speed

During the experiment, we utilized pitot tube wind speed sensor type, DT-8920 ds-1592489 to measure the headwind speed. The measuring range is from 3.6 – 288km/h. The sensor was mounted on top of the roof. The inlet tube must both point in parallel with the vehicle longitudinal, and with the sea level. Figure 36 illustrates the mounting method. This

sensor comes with specific software called Mano. Thus, to synchronize the wind speed data to IT2 data, it can be achieved by comparing wind speed and vehicle speed. More specification is provided in Figure 36.



Figure 36 Pitot tube wind speed sensor installation

4.1.6 Vehicle dynamics

To affirm the accuracy of HV ECU vehicle speed signal (calculated from high precision MG2 rpm encoder signal), we implemented Ninja Box to measure the vehicle motion. Ninja Box consists of an inertia measurement unit (IMU), and GPS. The equipment is shown in

Note that the accuracy of the vehicle speed data mainly depends on GPS accuracy. IMU data are used to correct minor GPS error. In case of city driving or route passing through overhead obstacles may disturb GPS signal communication among satellites and the receiver.



Figure 37 Ninja Box IMU+GPS unite

4.1.7 Vehicle speed feedback display

For on-road speed pattern following the experiment, we prepared a vehicle speed feedback display to inform the driver about the speed pattern information and the current vehicle's speed shown in Figure 38. The speed comparison graph that was shown on the display was plotted by Matlab. Then, the current vehicle speed was taken from the vehicle CAN system via Vector CAN VN1610, compared to the desired vehicle speed, and shown on the display. The vehicle speed can also be taken from GPS; however, it may contain some delay and error depending on GPS signal condition.



Figure 38 Vehicle speed feedback display

4.1.8 Data acquisition system integration

Once all the sensors and equipment are installed into one single system, the data acquisition system is illustrated in Figure 39. The system was divided into three part. First is the data loggers that operate under Window10 time stamp: wind speed sensor (Mano), the external sensor (NI Signal Express), and vehicle speed feedback display (Matlab). Second is IT2, OBD scan tools that run by Intelligent Viewer in Window XP. The last one is Ninja Box IMU+GPS. Since the data came from three different systems, time synchronization and signal resampling are required.

To avoid malfunction of the OBD scan tools and measurement noises, the most important tips is to always use the same power supply and ground generated by the vehicle. Using the power supply from home power socket while recording ECU data will cause

malfunction and automatically disconnection. Since the vehicle's ground and home power socket's ground are different, it causes confusion to the measurement.

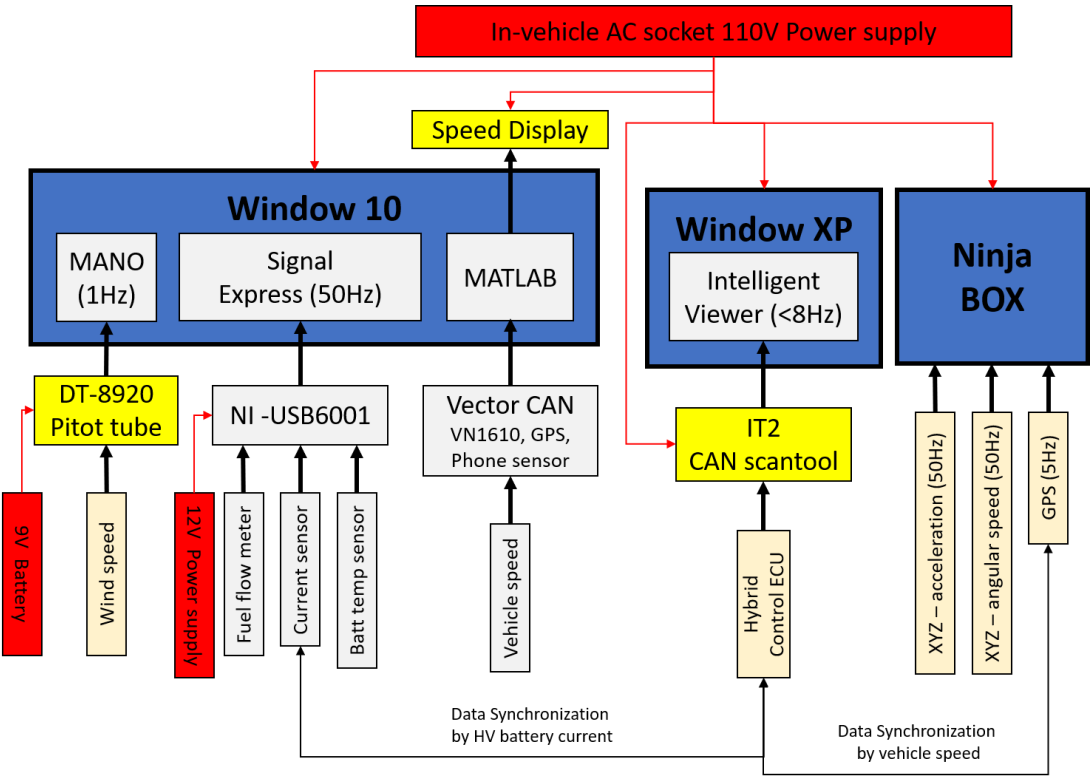


Figure 39 Structure of the data acquisition system

4.2 Hybrid vehicle experiment

In the Michelin project, the objectives of the experiment are to investigate (1) the hybrid powertrain fuel consumption, and (2) the hybrid powertrain control logic. In order to obtain substantial dataset for the analysis, this section explains about experiment method selection, speed pattern and test condition design, special concern for hybrid vehicle

experiment, data acquisition. We had conducted the experiments via three different approaches which were real-world driving, private test circuit, and chassis dynamometer. The advantages and disadvantages of these approaches are compared and summarized in this section.

4.2.1 Real-world driving (NGO)

The purpose of real-world driving is to evaluate and capture hybrid vehicles' fuel consumption and hybrid powertrain operation under a realistic driving scenario. To explain in more details, this database will be applied to study the characteristics of hybrid powertrain operation, fuel consumption characteristics under real-world driving in Nagoya. Based on this dataset, we recalibrated maps for CRUISE Prius3 and utilized the dataset for fuel consumption and hybrid operation characteristics validation.

More importantly, we also investigate the impact of summer (Energy Saver +) and winter (ALPIN) tires on hybrid vehicle's fuel consumption in real-world traffic driving. The special request from Michelin was if it is possible or not to investigate the effect of tire characters on vehicles' fuel consumption in real-world traffic. The challenging concern is that the impact of tire differences on fuel consumption is small compared to the impact of the uncertainty of traffic conditions. Thus, we have developed a new method for data visualization called hybrid powertrain efficiency distribution to analyze and extract the impact of tire difference. The results will be reported in chapter7.

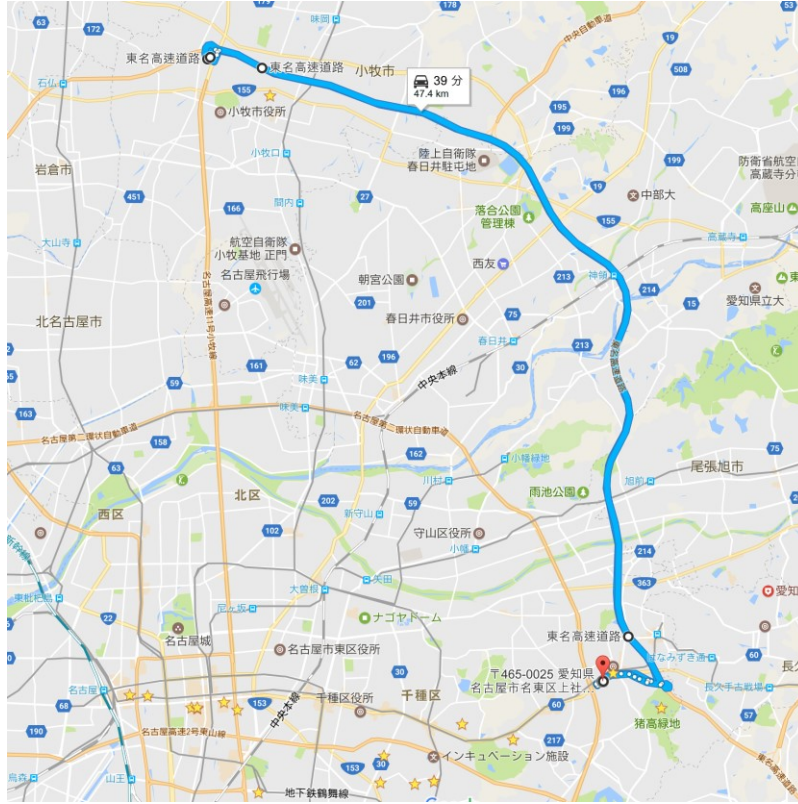


Figure 41 Nagoya highway route

Table 5 Vehicle condition preparation for the real-world experiment

Experimental conditions	City traffic	Highway traffic
Vehicle	White Prius3 2015	White Prius3 2015
Driver	Mr. Aoki Hirofumi	Mr. Tateishi Sadayoshi
Driving condition	Naturally driving	Naturally driving
Tire sets	<p>Summer tires (Energy save+ 195/65 R15) Winter tire (ALPIN 195/65 R15)</p> <p>Caution: 195/65 R15 has 30.8cm diameter; however, Prius3 tire specification is 30.8cm. Thus, vehicle speed needs to be adjusted.</p>	<p>Summer tires (Energy save+ 195/65 R15) Winter tire (ALPIN 195/65 R15)</p> <p>Caution: 195/65 R15 has 30.8cm diameter; however, Prius3 tire specification is 30.8cm. Thus, vehicle speed needs to be adjusted.</p>
Equipment	<ul style="list-style-type: none"> - Fuel flow meter - Current sensor - IT2 - Tire surface temperature thermometer 	<ul style="list-style-type: none"> - Fuel flow meter - Current sensor - IT2 - Tire surface temperature thermometer
Route	Sakae area	Hongo > Komaki Komaki > Hongo
Repetition	3 times/test condition/tire set	3 times/test condition/tire set
Initial soc	39%	50%
A/C set up	A/C on at 25C 3 rd level fan speed	A/C on at 25C 3 rd level fan speed
Tire warm-up duration	30mins	30mins
Experimental time	Middle of March 2017 16.00 – 20.00	Middle of March 2017 10.00 – 17.00



Figure 42 Real-world experiment on highway driving

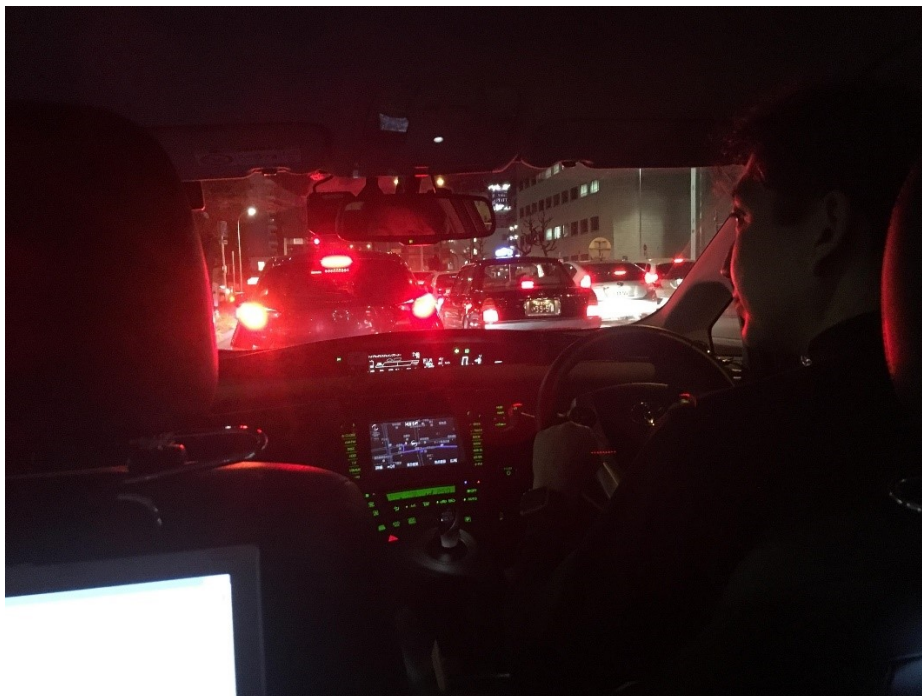


Figure 43 Real-world experiment on city driving



Figure 44 Winter-summer Tire displacement

4.2.1.2 Experiment summary

This dataset successfully provided actual driving conditions and Prius3 powertrain data in the most dominant region under Nagoya city traffic. This dataset was mainly used for both CRUISE Prius3 fuel consumption and hybrid powertrain operation validation. The total amount of dataset covered more than 400km raw data.

Nevertheless, it was realized that this dataset contained frequent speed fluctuation and transient operations which caused difficulties in CRUISE Prius3's hybrid operation control maps' calibration. Due to traffic safety, it was impossible to conduct maximum acceleration, deceleration tests to realize the vehicle's drivability. One more concern was about the data

repetition. A number of tests were required since identical driving conditions cannot be reproduced by real-world driving experiment.

4.2.2 Private circuit (JARI)

The purposes of the Private experiment at private test circuit are to obtain the data for Prius3 hybrid powertrain operation characteristics and obtain analytical dataset used for CRUISE Prius3' map calibration and hybrid powertrain operation validation. Furthermore, it also attempted to measure coast down test in Prius3 for road load function construction, and also to measure maximum drivability, such as maximum acceleration and deceleration.

The experiment was conducted at the outer-ring circuit (外周路), Japan Automotive Research Institute (JARI) in Shirosato, Ibaraki prefecture. The layout of the circuit is labeled in dark yellow indicated in Figure 45. This total distance for one round is 5.69km with 12m width. This circuit contains sever curves and hills. There are a long straight and flat profile starting from the start point to right before the u-turn illustrated in Figure 45. Acceleration, braking, and coast down tests were conducted on that area. The experiment was conducted at the end of October 2017.

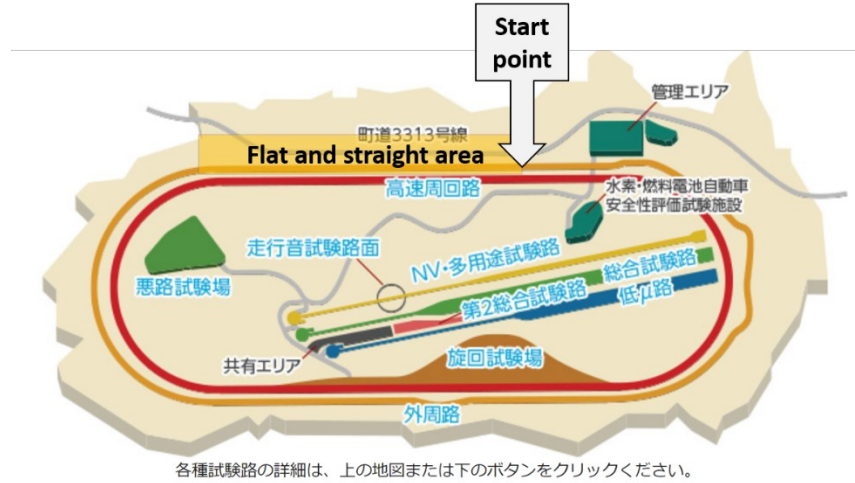


Figure 45 JARI Shiroshato outer-ring circuit layout

4.2.2.1 Driving pattern design for private circuit experiment

Since there is no traffic, the driving pattern need to be pre-determined. Particularly when the goals are to obtain the dataset for Prius3 hybrid powertrain operation characteristics investigation, it leads to important speed pattern design concepts. The concepts are (1) to force the powertrain to operate at the wider region as much as possible, and (2) the designed speed patterns have to force the operation point trajectory to pass through the hybrid operation modes' boundary as several points as possible.

To design the speed pattern, first, the real-world experiment dataset was utilized to find the approximate operation mode boundary. The operation stages of the engine, MG1, MG2, and battery were identified. Based on a combination of the components' stages, we categorized the powertrain operation into modes, and plot on speed and force axis map.

Then, speed profiles were designed/ selected from registration driving cycles. The most basic one is to design several constant acceleration speed patterns at several acceleration intervals. Since most of the hybrid vehicles' operation modes are defined in speed and driving force term, we introduced Vehicle Specific Power (VSP) equation (Jiménez *et al.*, 1999) to convert vehicle speed to force data.

After plotting the converted force and designed speed on the powertrain operation modes map, the speed patterns that pass through multiple boundaries, and located at a proper incremental interval were selected to be the speed profiles for this experiment.

Figure 46 shows a plot of speed patterns at different constant acceleration intervals on Prius3's powertrain operation modes map. The number of labels describe the acceleration level. For example, 50 kph means every 10 seconds vehicle speed increase 50 km/h, and so on. It can be seen that 2.5kph is a speed pattern that passes through several modes' boundaries the most at all.

Figure 47 shows how HWFET speed profile affects on Prius3's powertrain operation region. It can be interpreted that HWFET well captures the high-speed driving condition in Nagoya since the operation points of HWFET and the real-world experiment dataset overlap with each other. Based on Nagoya dataset, the acceleration is considered to be high; however, the deceleration seems to be high only at high speed and becomes mild at low speed.

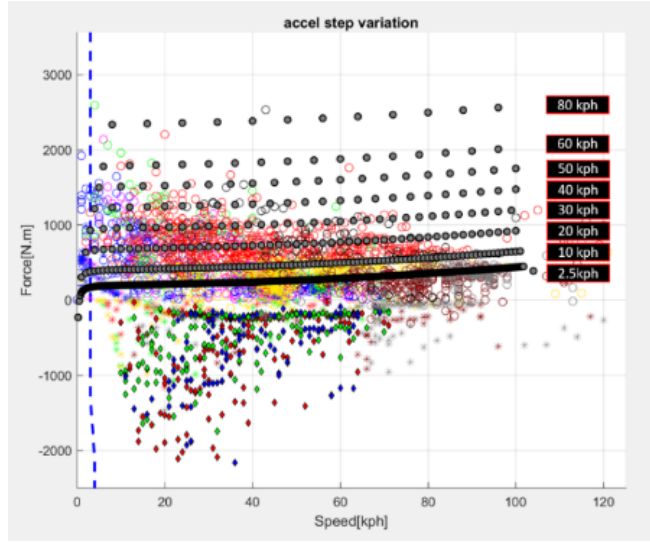


Figure 46 Constant acceleration speed pattern design method for a private circuit experiment

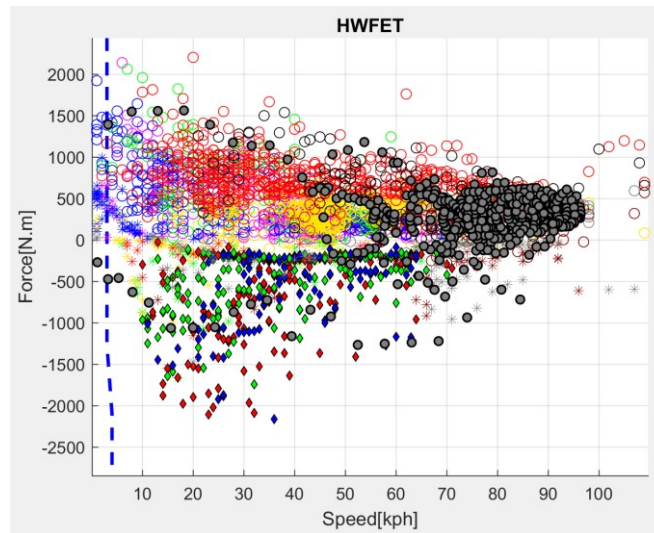


Figure 47 The operation points/region of HWFET on Prius3' powertrain operation modes map

Table 6 Speed patterns for private circuit experiment

Types of speed pattern	Definition/notice	In-used speed pattern
Constant acceleration/deceleration	<p>Acceleration (speed change with 10s)</p> <p>a1 : 2.5 km/h</p> <p>a2 : 20 km/h</p> <p>a3 : 40 km/h</p> <p>a4 : 60 km/h</p> <p>Deceleration (speed change with 10s)</p> <p>b1 : -2 km/h</p> <p>b2 : -6 km/h</p> <p>b3 : -10 km/h</p> <p>b4 : Maximum deceleration</p>	<p>'a1b1_dry</p> <p>'a1b2_dry</p> <p>'a1b3_dry</p> <p>'a2b1_dry</p> <p>'a2b2_dry</p> <p>'a2b3_dry</p> <p>'a3b1_dry</p> <p>'a3b2_dry</p> <p>'a3b3_dry</p> <p>'a3b4_dry</p> <p>'a4b1_dry</p> <p>'a4b2_dry</p> <p>'a4b3</p> <p>'a4b3</p> <p>'a1_wet</p> <p>'a1b1_wet</p> <p>'a1b2_wet</p> <p>'a1b3_wet</p> <p>'a1b4_wet</p>
Maximum acceleration – cruise speed – coast down	<p>Maximum acceleration: Acceleration pedal is 100% fully pressed.</p> <p>Cruise speed: Maintain constant speed at the assigned level</p> <p>Coast down: Gear in D position, free brake and acceleration pedal</p>	<p>'MaxAccel120Cruise120CoastFrm120</p> <p>'MaxAccel140Cruise100CoastFrm100</p> <p>'MaxAccel160Cruise80CoastFrm80</p> <p>'MaxAccel160Cruise60CoastFrm60</p> <p>'MaxAccel160Cruise40CoastFrm40</p> <p>'MaxAccel160Cruise20CoastFrm20</p>
Naturalistic acceleration – cruise speed – Naturalistic braking	<p>Naturalistic acceleration and deceleration: Accelerate and deceleration the vehicle at a level that the driver feels comfortable.</p>	<p>'NaturalAccel100Cruise20Brakefrm100</p> <p>'NaturalAccel100Cruise40Brakefrm100</p> <p>'NaturalAccel100Cruise60Brakefrm100</p> <p>'NaturalAccel100Cruise80Brakefrm100</p> <p>'NaturalAccel120Cruise100Brakefrm100</p> <p>'NaturalAccel120Cruise120Brakefrm100</p>
EV mode max acceleration	<p>EV mode max acceleration: trying to keep the vehicle in eDrive while applying maximum acceleration as much as possible.</p> <p>Tips: Try to control the acceleration pedal position to stay right in the middle of this bar</p> 	<p>'AccelEV1_dry</p> <p>'AccelEV2_dry</p> <p>'AccelEV3_dry</p> <p>'AccelEV4_dry</p>

Table 7 Vehicle condition preparation for private circuit experiment

Experimental conditions	Details
Vehicle	White Prius3 2015
Driver	Mr. Miyazaki, professional driver from Michelin
Driving condition	Speed pattern following, and naturally acceleration/deceleration
Tire sets	215/45 R17 87W Toyotire (30.4cm diameter. Follow the specification)
Equipment	<ul style="list-style-type: none"> - Fuel flow meter (failed) - Current sensor - IT2 - Ninja box - wind speed sensor - vehicle speed feedback display
Initial soc	45 - 50% Increase: slowly accelerate the vehicle to 60 km/h, then brake to recuperate the regenerative braking energy. Deplete: drive the vehicle in eDrive mode
A/C set up	off
Experimental date	The end of October 2017



Figure 48 Private circuit experiment

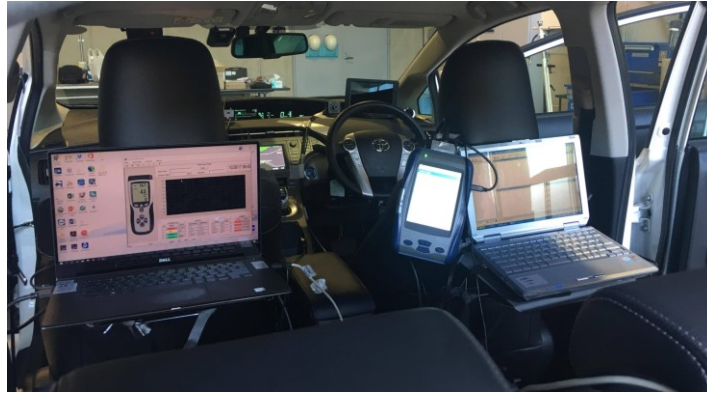


Figure 49 Data acquisition system

4.2.2.3 Experiment summary

The most interesting points obtained by circuit experimental approach are that (1) analytical driving, such as constant speed, acceleration, and deceleration, can be performed. This dataset significantly helps to understand sophisticated powertrain operations in hybrid vehicles compared to real-world test. Furthermore, basic vehicle specifications, such as maximum acceleration/deceleration ability, coast down test & road load function, can be

conducted safely in a closed environment. Powertrain operation region can be forced to operate outside the typical operation region depending on the pre-designed speed patterns.

On the other hand, this approach is not recommended for fuel consumption characteristic investigation since the driving patterns do not represent real-world driving. It requires a budget to rent the circuit, and professional driver to trace the speed patterns. The last point is that as the starting point located at a specific area, initial SOC adjustment was difficult to arrange to start at a precise level and at the specific position. Thus, a complete flat o-ring circuit is highly recommended.

4.2.3 Chassis dynamometer (DYNO)

The purposes of the chassis dynamometer test are (1) to obtain more data for Prius3 hybrid powertrain operation characteristics investigation, (2) to obtain analytical dataset to use for CRUISE Prius3' map calibration and hybrid powertrain operation validation, and (3) to obtain the data for Power-split hybrid powertrain dynamic model validation.

The experiment was conducted on 2-roller chassis dynamometer (CD) in Nagoya University. The facility is shown in Figure 50. The experimental concept is to utilize functions available in chassis dynamometer to allow us to sweep the powertrain operation points across vehicle speed-driving force fields.



Figure 50 2-roller chassis dynamometer at Nagoya University

In general, every CD usually provides three main functionalities for testing, which are constant force mode, constant speed mode, and simulation mode. The most useful mode is the constant force mode. CD generates constant force as a driving load via the front roller to resist the movement of the vehicle's wheels. Once, the vehicle starts acceleration/deceleration, CD will control the force to remain at constant along the wheel speed variation. In general speaking, this constant force mode is a tool to vary the powertrain operation points by setting a fixed force level and changing the vehicle speed. The example of the expected outcome is illustrated in Figure 51. The force levels were varied from 5 to 4,000 N. At each constant force level, the vehicle speed is (1) maintained at constant to capture the overlapping operation modes, and (2) varied to sweep the powertrain operation points from 0-95 km/h.

In addition, it is also important to prepare a mean to deactivate the vehicle's traction control. Since the rear wheels are fixed while the front wheels are moving, the vehicle will detect slip, and cut the powertrain power for safety reasons.

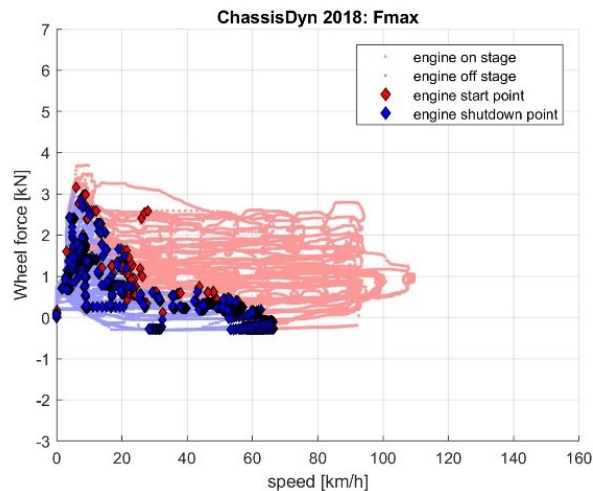


Figure 51 Powertrain operation points variation by using constant speed force mode

For the simulation mode, this mode can reproduce the real-world driving without the car moving. It is a basic facility to conduct registrations emission and fuel consumption tests since the test conditions are possible to be strictly controlled. However, to operate the vehicle in this mode, it requires the vehicle road load function in which the vehicle internal resistance has been excluded. To prepare for the vehicle road load function, first coast down test from high speed to completely stop needs to be conducted. Second is to input the coast down speed and time to the CD. Based on this data, we can use internal resistance identification function in CD (available in high standard CD) to exclude the internal resistance term. To achieve this, several coast down tests have to be performed on the CD. Then, CD will search for a proper compensation control to allow the vehicle speed coast down on CD to be equal to the actual road. The reason why the internal resistance must be excluded is that the road load function measured on the actual road always contains the internal resistance term. Thus, to

prevent the internal resistance redundancy (One is in the road load function, the other is from the vehicle.) this term must be excluded. Unfortunately, this feature is not available in our chassis dynamometer so the speed pattern following test was canceled.

4.2.3.1 Experimental conditions

The test schedule under constant force mode can be divided into constant speed and continuous speed test. The speed and force incremental interval are described in Table 8. According to performance limitation of the chassis dynamometer that designed for small vehicles, the operation force and speed ranges and test duration are limited by the facility and the cooling system performance, particularly for the exhaust pipe cooling system. Force 0-2000N. range and speed from 0-100 km/h are enough to cover the significant transition/overlapping between eDrive mode to Light load, medium-heavy load, and boost modes. The vehicle set-up and test conditions are described in Table 8.

Table 8 Test schedule for chassis dynamometer experiment

Constant force level (N)	Constant speed test	Continuous speed test
Notes	At speed < 60km/h, the test duration decides from the engine on/off complete one cycle. (Investigate the overlapping operation modes)	-
10	-	0 > 100 km/h
50	10: +10: 100 km/h	0 > 100 km/h
250	10: +10: 100 km/h	0 > 100 km/h
500	10: +10: 100 km/h	0 > 100 km/h
750	10: +10: 100 km/h	0 > 100 km/h
1000	10: +10: 100 km/h	0 > 100 km/h
1250	10: +10: 100 km/h	0 > 100 km/h
1500	10: +10: 100 km/h	0 > 100 km/h
1750	10: +10: 100 km/h	0 > 100 km/h
2000	10: +10: 100 km/h	0 > 100 km/h

Table 9 Vehicle condition preparation for chassis dynamometer experiment

Experimental conditions	Details
Vehicle	Purple Prius3 2015
Driver	Mr. Tateishi Sadayoshi, professional from Nagoya University
Driving condition	Constant speed and continuous speed increasing tests at several constant force mode
Tire sets	215/45 R17 87W Goodyear (30.4cm diameter. Follow the specification)
Equipment	Vehicle - Fuel flow meter - Current sensor - IT2 - vehicle speed feedback display (Chassis Dynamometer's display) Chassis dynamometer - wheel torque - wheel speed
Initial soc	39%
A/C set up	off
Experimental date	The end of October 2017



Figure 52 Vehicle set-up on chassis dynamometer



Figure 53 Constant speed and continuous speed test on Chassis dynamometer



Figure 54 Cooling fans for engine, exhaust pipe system including catalytic converter

4.2.3.2 Experiment summary

The summary of the hybrid vehicle experiment on chassis dynamometer is provided in Table 10.

Table 10 Chassis Dynamometer experiment summary

Experiment purpose Done / Fail	Procedure (Expected)	Experimental Results
1. Investigate hybrid operation map <u>Concept</u> : try to force the powertrain to run at wide/various operation regions as much as possible	Run the vehicle on ChassisDy in <u>constant force mode</u> at different constant speed levels (10,20,...,100 kph), and 0-100 kph moderate acceleration.	- The ChassisDy ran in this mode properly.
2. Validation of Power-split hybrid powertrain dynamic model <u>Concept</u> : utilize ChassisDy to measure wheel force and power, then validate the data to the dynamic model	Try to run the vehicle at the same condition until the engine on/off complete 1 cycle	Problems - <u>The wheel slipping on the roller surface</u> makes the comparison and several data points invalid. - At high load and speed, the ChassisDy will get <u>overheated</u> quickly. (Experiment sequence is important.) - The <u>cooling system for the vehicles</u> is insufficient, esp. exhaust pipe and catalytic.
3. Validation of hybrid powertrain hybrid characteristics and fuel consumption simulation <u>Concept</u> : run the vehicle in simulation mode follow an assigned speed pattern to maintain the same driving condition during the test	Run the vehicle on ChassisDy follow the speed pattern recorded from real-world and JARI experiment <u>in simulation mode</u>	- The machine could not provide a realistic roadload. The vehicle speed decreased rapidly, even though the 3 rd generation Prius roadload is already plugged in. - Vehicle's internal resistance compensation function is not available in this ChassisDy.

4.2.4 Final conclusion for the three experimental approaches

The content in this chapter can be used as a reference or guild line for data acquisition system design, test condition design, experimental approach determination, and also tips. The knowledge in this chapter is not applicable just only for hybrid vehicles, but also conventional and electric vehicles.

Finally, based on the experiences that have been obtained from the three experimental approaches: real-world, private circuit, and chassis dynamometer, the advantages, and disadvantages provided from each approach toward different hybrid powertrain experimental objectives are summarized in Table 11.

Table 11 Advantage and disadvantage among real-world, private circuit, and chassis dynamometer experimental approaches

Purpose	Real-world experiment	Analytical on-road experiment	Chassis dynamometer experiment
Fuel consumption modeling	Suitable - Realistic, actual traffic/ driving behavior / driving environment can be realized. - Require more equipment (wind speed sensor, IMU) - The same test condition cannot be reproduced. - Difficult to control initial SOC	Fair - Speed pattern following/ constant speed, acceleration - Require more equipment (wind speed sensor, IMU) - Costly, professional driver is required. -Possible to control the initial SOC	Fair - Speed pattern following/ constant speed, acceleration - The vehicle roadload function (w/o internal resistance) is required. - The driving test is limited by the chassis dynamometer specification. (Max accel and decel should be avoided.) - The test condition can be controlled. - Possible to control the initial SOC
Roadload measurement		Suitable - Coast down test, vehicle's maximum drivability can be conducted safely.	
Hybrid control logic investigation & mapping	Fair transient data > difficulty to analysis		Suitable - The analytical data can be obtained. - All the powertrain operation points can be obtained by using force constant mode. - Easy to manage the SOC issue

CHAPTER 5

Quasi-Static Hybrid Powertrain Energy Consumption Modeling

5.1 Introduction

This chapter attempts to examine a commercial quasi-static hybrid powertrain simulation, CRUISE Prius3 provided by AVL company, to extract the comprehensive hybrid operation characteristics that are essential for microscopic hybrid vehicle fuel consumption modeling in the next chapter. To achieve that, this chapter performs an improvement and validation on CRUISE Prius3.

Firstly, this study observed the component structure, internal data flow, and hybrid control models. Secondly, a preliminary validation was conducted to evaluate and identify inaccurate prediction issues. Lastly, the substantial solutions and improvement procedures corresponding to the problems found in the original CRUISE Prius3 simulation are proposed and performed.

5.1.1 Simulation structure and component functions

CRUISE Prius3 is the third generation of Toyota Prius' powertrain simulation that provides the estimation of vehicle fuel consumption, driving performance, and significant powertrain's operation data from the engine, MG1, MG2, battery, and others. Figure 55 shows the overall structure of CRUISE Prius3. The simulation consists of three main modules which are powertrain component, hybrid control, and driving performance output modules.

According to Figure 55, the powertrain component module is the part labeled by yellow color. Component boxes replicate Prius3 powertrain configuration. For the mechanical connection, engine, MG1 (42kW PSM) and MG2 (60kW PSM) are connected via planetary gear set. Then, the output from ring gear is transmitted through final gear and differential gear down to wheels. Inside the engine, MG1, MG2 boxes, it contains energy consumption maps of the corresponding machine. For the engine, there are four additional boxes (the yellow labeled part located inside the red labeled zone) used for the engine control and operation point selection of which the names start with ENG. The functionality of each box will be provided in the coming section.

For the electrical connection, MG1 and MG2 are connected to high voltage battery and low voltage network load. CRUISE Prius3 simplifies electrical configuration by omitting the existing of inverter and converter. To simplify the battery model, CRUISE Prius3 modified the battery structure form parallel to series. As a result, the battery capacity slightly changes from the actual 1.31 kWh to 1.495 kWh. The losses occur due to inverter and converter operation are compensated by the electric consumption load in the low voltage

network load. Note that inverter is an electronic equipment converting DC current from the battery side to AC current from MG side (both directions). Converter is electronic equipment that adjusts the voltage for motor/generator control purpose. In addition, auxiliary load, such as air conditioning, oil, and water pumps, also absences from the simulation. Thus, A/C load boxes are implemented to the model.

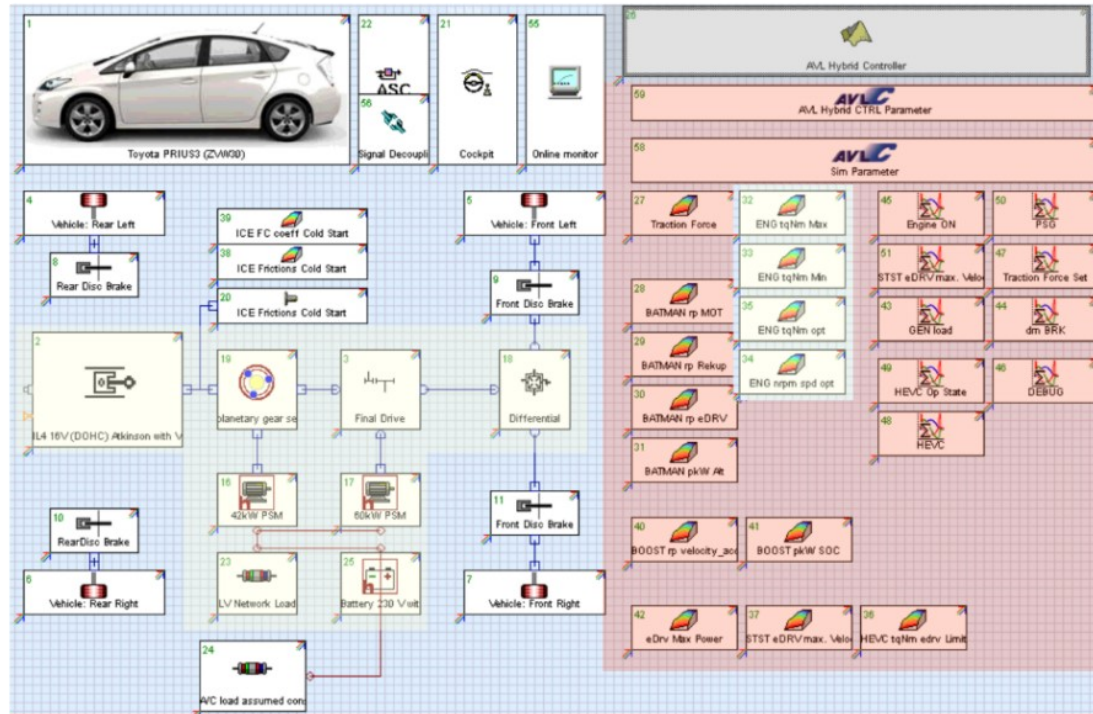
The hybrid control module is the most important module for hybrid vehicles. It is important to understand the operation characteristics in order to extract those characteristics and simplify them to a simulation. For CRUISE Prius3, the hybrid control module contains several boxes. The main functions of these boxes are to control the simulation to behave as similar as possible to the actual hybrid powertrain. According to the complexity of the hybrid operation characteristic, these boxes provide rules and criteria for the control of powertrain on/off, battery charging and discharging, regenerative braking, and powertrain operation point selection. The hybrid control module is separated into two parts which are open-accessed boxes (red label) and black box (black label). The open-accessed boxes mainly provide rules and criteria on powertrain on/off, battery charging and discharging, regenerative braking. Based on these rules and criteria, the black box performs decision making on powertrain operation point selection, and operation mode selection. Since the access to the black box is not available, the modification and tuning are not possible for this section.

The last part is driving performance output modules that are not highlighted. This module represents the vehicle body, wheels, mechanical braking system, and cockpit information.

In summary, if the powertrain model in the simulation performs inconsistently to the actual vehicle's hybrid characteristic, the outcome such as energy consumption prediction results will become invalid. Therefore, to reproduce realistic hybrid powertrain operations and high fidelity of fuel consumption prediction results, both of accurate energy consumption maps inside the powertrain boxes, and hybrid control are requisi

Powertrain Components (Open access)

- Engine
- MG1
- MG2
- HV battery
- Electrical loss
- Transmission (PSD)



Main Hybrid control decision box (Black Box)

- operation mode selection
- powertrain operation point decision

Hybrid control Criteria (open access)

- Battery power limit
- Boost power limit
- E-Drv limit
- Traction force limit
- HV constants

Figure 55 AVL CRUISE Prius3

5.1.2 Simulation flow and calculation algorithm

This section shows the overview of simulation flow in CRUISE Prius3 by explaining the calculation/process sequences, and the input and output signals at each component boxes. This section also projects the powertrain component, open-access hybrid control, and black-box hybrid control modules on the simulation flow diagram for the comprehensive understanding.

CRUISE Prius3 is a quasi-static forward-backward looking simulation. Quasi-static is a technique to analyze dynamic variation that happens so slowly that it is reasonable to assume uniform conditions across the study area. For powertrain simulations, the engine fuel consumption model and motor/generator loss model are simplified into a small-steady-step of changes called look-up tables. This will significantly help to increase the calculation speed compared to using the differential equations.

Forward-backward looking refers to the direction of the data flow in simulation. Therefore, most of the quasi-static forward-backward looking powertrain simulation usually obtains both dynamic modeling method and look-up table. Dynamic modeling is used to predict the dynamic motion that requires insight details and accuracy for control purposes, such as mechanical rotation, torque and force transfer, and battery model. On the other hand, table look up is used to simplify the high complexity mechanism, such as engine and motor energy consuming processes. Thus, the method is widespread among automotive powertrain modeling due to its sufficient accuracy with the reasonable computational load.

Figure 56 shows the simulation flow inside CRUISE Prius3. Colors highlight the major component. **Green** indicates preset input data that need to provide to the simulation before the start. The data are driving speed profile, road grade, AUX load, and ambient temperature. **Yellow**, **black** and **red** indicate the main modules: powertrain component, black-box hybrid control, and open-access hybrid control that were mentioned in the previous section.

After the preset input data is set up in the simulation. Vehicle speed signals are sent to the Driver model PI box. This box transforms the vehicle speed, wind speed, road grade, and speed error into acceleration pedal position. The function of this box is to maintain the vehicle speed at the same to the speed profile as much as possible.

Next, acceleration pedal position signal, vehicle speed, AUX, and A/C load signals enter to Power demand estimation box. This box estimates total requested power, total request driving torque and force. These output data are the main parameters for the hybrid control module to determine the powertrain operation activities.

Once the signals enter to EMS (hybrid controller), this box consists of two parts. The first part is the open-access boxes that provide rules/criteria for hybrid operation decision making. The second part is the black box. The box determines powertrain operation points and hybrid operation mode. The outputs from EMS (hybrid controller) are target revolution and torque of engine, MG1 ,and MG2. These signals are sent directly to the Efficiency map box.

Inside the Efficiency map boxes, it includes look-up tables that specify the relationship between operation points and energy consumption of engine, MG1, and MG2.

Since we know the operation points, we can calculate the energy consumed by each powertrain component based on the look-up table called map.

Then, the electrical energy consumption signals from MG1 and MG2 are sent to HV battery model box. The box calculates and updates battery SOC, and input it back to the model. For the fuel consumption, the signal is sent to the Fuel tank box to calculate the total fuel consumption.

Next, the operation points from engine, MG1, and MG2 are sent to Planetary gear dynamic model box. The box calculates output force/torque/power at wheels and vehicle speed corresponding to the selected operation points. Vehicle speed signal returns to the Drive model PI box as feedback of speed error.

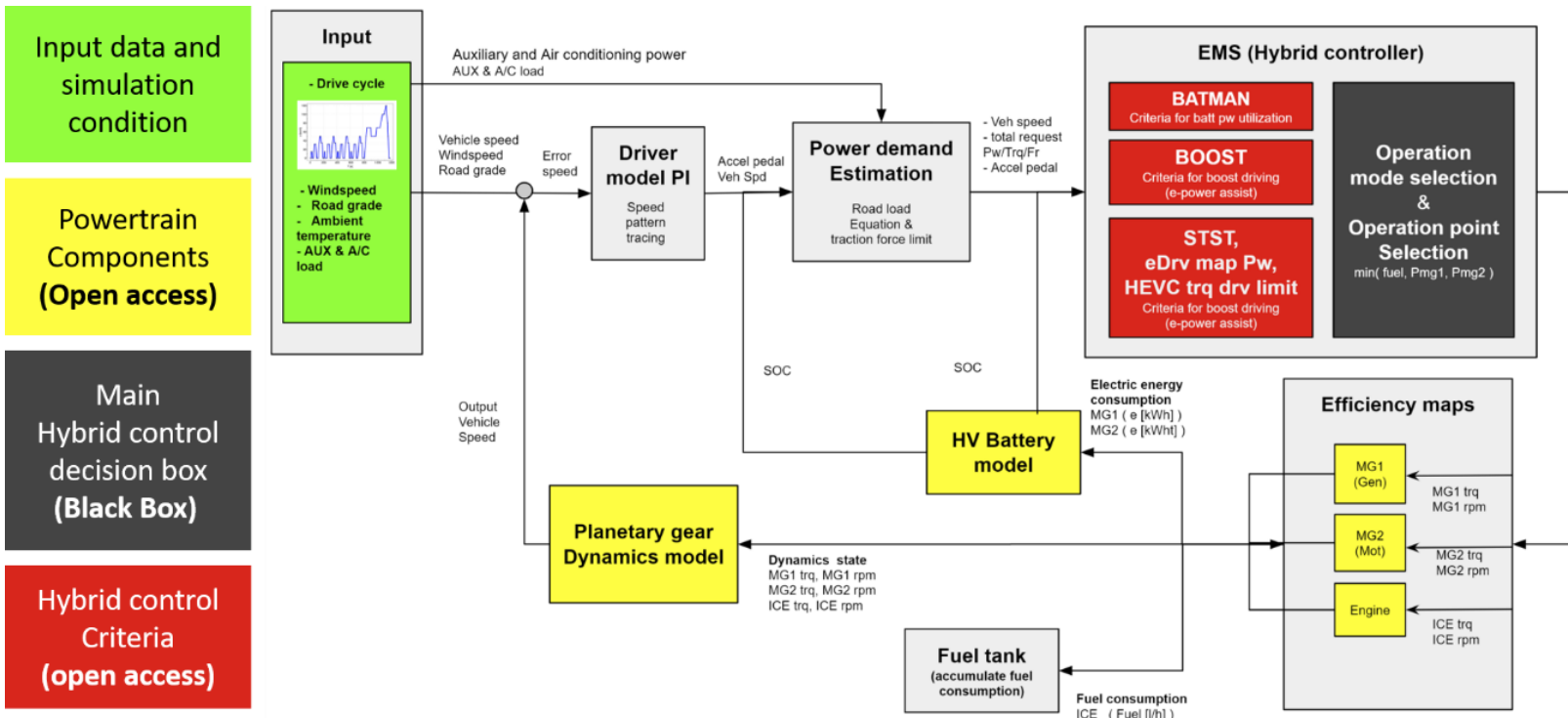


Figure 56 AVL CRUISE Prius3 simulation flow

5.1.3 CRUISE Prius3 preliminary validation

This section performs validation on CRUISE Prius3. Variety of speed profiles and test condition were input to the simulation. The results were compared to the measurement data recorded from Prius3 to evaluate the fidelity of fuel consumption and hybrid powertrain operation prediction from CRUISE Prius3. Based on these results, the problems established in CRUISE Prius3 were identified.

5.1.3.1 Preliminarily validation on hybrid powertrain operation

One of the main characteristics of the hybrid powertrain is the engine on/off. Thus, this section compares the engine on/off logic of the original CRUISE Prius3 to the actual vehicle. The data used in this validation were the highway driving condition. The speed profile and initial soc were set at the same as the actual data. AUX load was estimated approximately at 500W and input to the simulation. The result is showed in Figure 57. The upper graph shows the comparison between the measurement's and simulation's engine on/off characteristics. Blue line refers to vehicle speed, black and red refers to measurement and CRUISE Prius3 engine rpm respectively. From the graph, the engine on/off of the actual vehicle tends to be more sensitive to acceleration and deceleration. On the other hand, the CRUISE Prius3 engine seems to keep the engine on/off state for a longer period. For example, at the beginning of the trip when the speed increase from stop to 60 km/h. The actual vehicle turns the engine on/off frequency, while CRUISE operates in eDrive mode. As a result, the

battery soc of CRUISE’s depletes to 38%, and the engine turns on to charge the battery. At this point, it is obvious that the engine on/off in CRUISE Prius3 simulation fails to replicate the engine on/off, which is considered as one of the major features of hybrid vehicles.

After CRUISE engine turns on, it tends to maintain the engine rpm constant at 1000 rpm. However, the actual engine rpm fluctuates more during hard acceleration. It may be concluded that there is a discrepancy on the engine operation point, and also hybrid operation mode selection.

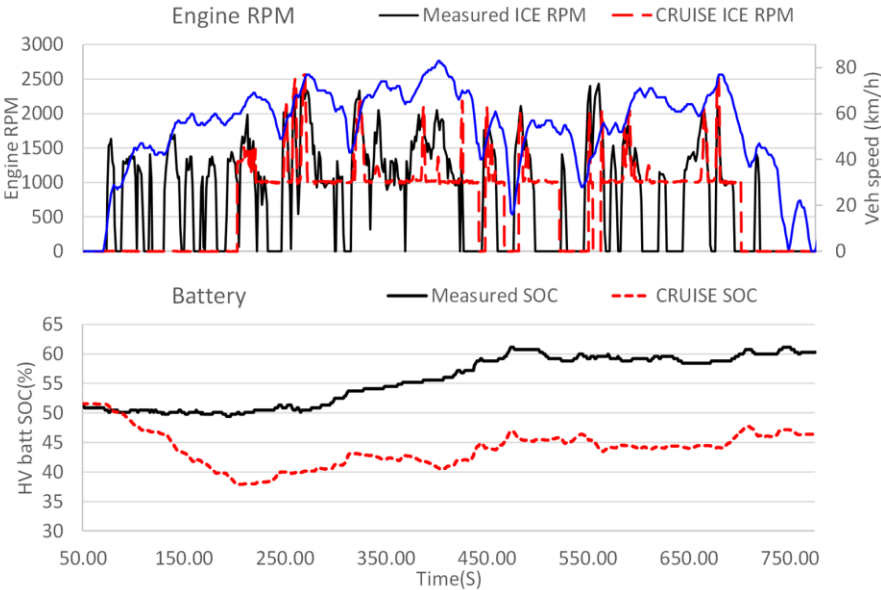


Figure 57 Preliminary validation on engine on/off issue

Further validation was also performed on a variety of real-world driving condition. Figure 58 shows the percentage of the engine on time prediction error. The total engine on time at each trip compared to the actual engine on time is described by % engine on time

error. For city driving, CRUISE Prius3’s engine on/off control criteria fails to capture the engine on/off behavior of the actual Prius3. CRUISE Prius3 excessively operates the engine as the error shows in a range of 46.5 - 98.9%.

For highway driving, the error is low compared to the city driving. The reason is that the possibility for the engine to off is much lower on the highway since it requires higher driving speed and power. The simulation operates the engine shorter than the actual vehicle does as shown by the error in a range of -1.4 - -4.3%.

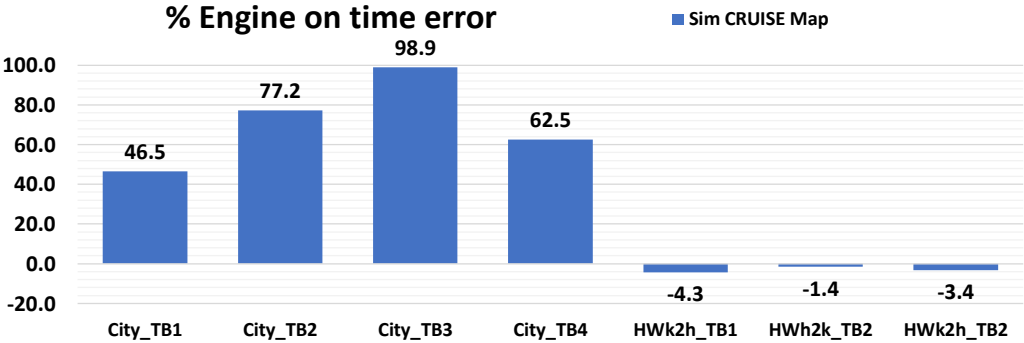


Figure 58 Percentage of engine on prediction error

In summary, CRUISE Prius3 does response to the battery charge request criteria, and engine off during deceleration. However, the engine on/off characteristic of the actual vehicle is far more sensitive to speed pattern fluctuation. Particularly in city driving, CRUISE Prius3 fails to capture the inherited hybrid characteristic. The comparisons in this section point out several critical problems of CRUISE Prius3 hybrid control logic that extensively require tuning and improvements.

5.1.3.2 Preliminary validation on fuel consumption prediction

For the fuel consumption prediction aspect, the results from CRUISE Prius3 were underprediction for both low speed (city) and high speed (highway) driving. The error was found in the range of -39.6 – -28.6%. Note that the fuel consumption results were compensated by taking the difference of the initial and final soc into account.

One interesting point is that CRUISE Prius3 performs significant error on the engine on time prediction in the city trips; however, the fuel consumption of the city trips was still underestimated. Therefore, it implies that the fuel consumption map of the engine requires improvement.

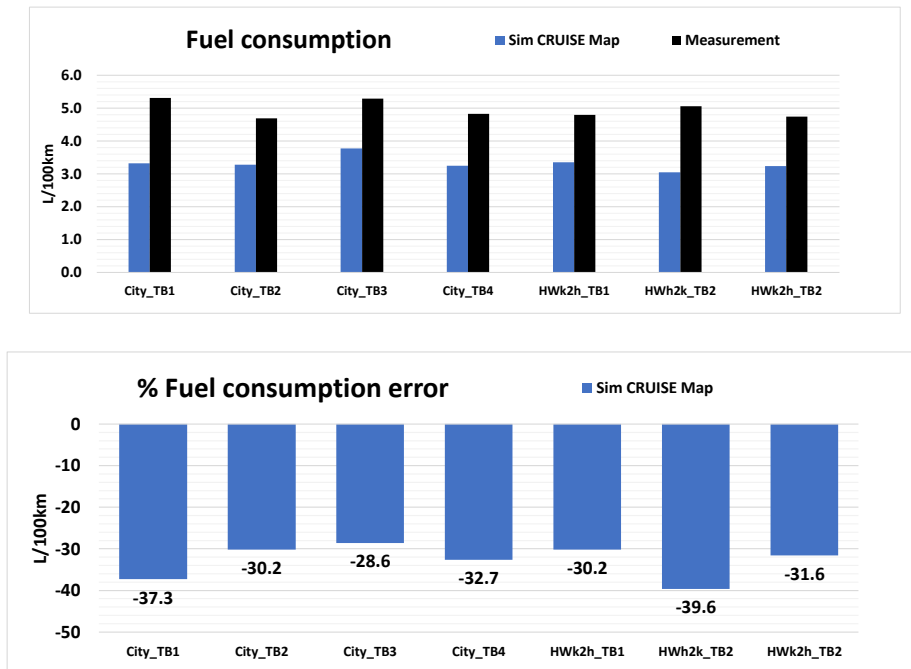


Figure 59 CRUISE Prius3 fuel consumption preliminary validation

According to the preliminary validation results, CRUISE Prius3 fails to perform realistic hybrid operation characteristics. Moreover, engine fuel consumption map seems to have a discrepancy that requires further improvement. The problems in CRUISE Prius3 will be explained in details in the next section.

5.1.4 CRUISE Prius3's problems identification

Results from the preliminary validation bring out a number of problems in CRUISE Prius3 that behaves unlikely to the actual Prius3. The problems were investigated based on the preliminary results, and CRUISE Prius3 modeling structure. Finally, the problems were identified and classified into four main groups.

First is the problems regarding hybrid operation control. The main problems were the unrealistic engine on/off criteria, missing battery alternative charging cycle at low speed, unrealistic Boosting mode selection, and unrealistic engine, battery, MG1 and MG2 controlling constant parameters.

Second is the problems regarding battery power control constraints which is unrealistic battery discharge and charge load.

The third is the problems regarding the engine operation. It is recommended to assure the engine optimal operation curves and the engine fuel consumption maps.

Last is miscellaneous problems. For instance, the engine on at the beginning of the simulation. This problem causes the CRUISE Prius3 soc to increase abnormally which make it impossible to compare the results to the rest of the trip. Another problem is that the soc

calculation in CRUISE Prius3 was set at Naturalistic SOC calculation. The definition is that the simulation will search the initial soc that makes the final soc ends at the same level as the initial soc, then use that soc to simulate the result. This mode is useful when testing a powertrain follow the reiterative scheme. However, in this project, this calculation algorithm needs to be deactivated to allow the soc to fluctuate freely as the actual vehicle. The problems established in the original CRUISE Prius3 are summarized in Table 12.

Results from the preliminary validation bring out a number of problems in CRUISE Prius3 that behaves unlikely to the actual Prius3. The problems were investigated based on the preliminary results, and CRUISE Prius3 modeling structure. Finally, the problems were identified and classified into four main groups.

First is the problems regarding hybrid operation control. The main problems were the unrealistic engine on/off criteria, missing battery alternative charging cycle at low speed, unrealistic Boosting mode selection, and unrealistic engine, battery, MG1 and MG2 controlling constant parameters.

Second is the problems regarding battery power control constraints which is unrealistic battery discharge and charge load.

The third is the problems regarding the engine operation. It is recommended to assure the engine optimal operation curves and the engine fuel consumption maps.

Last is miscellaneous problems. For instance, the engine on at the beginning of the simulation. This problem causes the CRUISE Prius3 soc to increase abnormally which make it impossible to compare the results to the rest of the trip. Another problem is that the soc calculation in CRUISE Prius3 was set at Naturalistic SOC calculation. The definition is that

the simulation will search the initial soc that makes the final soc ends at the same level as the initial soc, then use that soc to simulate the result. This mode is useful when testing a powertrain follow the reiterative scheme. However, in this project, this calculation algorithm needs to be deactivated to allow the soc to fluctuate freely as the actual vehicle. The problems established in the original CRUISE Prius3 are summarized in Table 12.

Table 12 Summary of CRUISE Prius3 established problem

CRUISE Prius3 problems	Details
Hybrid operation control	<ul style="list-style-type: none"> - Unrealistic ICE on/off threshold - Missing battery alternative charging cycle at low-speed drive - Unrealistic BOOST mode decision - Unrealistic ICE/Batt/MG min power constant limit
Battery power control	<ul style="list-style-type: none"> - Unrealistic battery discharge/charging load
Engine control	<ul style="list-style-type: none"> - engine optimal operation curves - Engine fuel consumption maps
Others	<ul style="list-style-type: none"> - Abnormal engine on at the beginning of the simulation - The initial and final soc are set at the same level.

5.2 Scope of the improvement process

This chapter proposes solutions toward the improvement on the problems established in the original CRUISE Prius3 presented in the previous chapter. Due to the sophisticated operation of the hybrid powertrain, a number of parameters, component operation maps, and hybrid control maps need to be calibrated. Thus, this chapter will provide the scope of the

substantial improvements that are limited by the black-box hybrid control accessibility and the structure of the original CRUISE Prius3 itself. For better understanding, this chapter also describes the features and definitions of the parameters and maps that require the calibration. Finally, the overview of CRUISE Prius3 improvement methodology is also mentioned.

5.2.1 Hybrid operation control

5.2.1.1 Unrealistic engine on/off criteria

The issue regarding unrealistic engine on/off criteria can be solved by recalibrating the engine on/off maps that provide information about which condition engine is allowed to turn off. In order to identify which maps provide engine on/off criteria, we assumed that CRUISE Prius3 probably uses similar criteria compared to the actual Prius3.

According to the section that explains about Engine on/off determination, Prius3 considers vehicle speed, total requested power, battery soc, battery available power. Then, we compared these data to the list of maps in CRUISE Prius3. The possible candidates are eDrv Max Power, STST eDRVmax. Velocity, and HEVC tqNm drv Limit shown in Figure 60



Figure 60 Engine on/off control criteria maps in CRUISE Prius3

eDrv Max Power (Pmax) is the map that provides engine on/off boundary based on vehicle speed and total requested power. It judges real-time speed and total requested power whether they fall inside or outside the boundary. This boundary represents the maximum power at a different vehicle speed that the powertrain can operate with engine off. If the speed and total requested power data fall inside the boundary, it means the engine off function is enabled. To recalibrate Pmax map, it requires vehicle speed and total requested power. Vehicle speed is available in HV ECU system (Vehicle Spd or Motor(MG2) Revolution); however, total requested power data is not available in the vehicle system. Thus, the estimation method will be provided in the coming section.

STST eDrv max Velocity (STST) is the map that provides engine on/off boundary based on battery soc and vehicle speed. How to implement this map is the same as Pmax. Both SOC and vehicle speed can be obtained via HV ECU system (State of Charge (All Bat), Vehicle Spd or Motor(MG2) Revolution).

HEVC tqNm drv Limit is the map that provides engine on/off boundary based on vehicle speed and driving torque. This map is implemented in the same way as Pmax. However, driving torque data is not available in the vehicle system. Thus, the estimation method will be also explained.

CRUISE Prius3 implements these three maps by judging if the real-time data fall outside one of at least these maps or not. If it is yes, the engine will turn on, but if it is no, the engine is allowed to stay off. Note that there are more criteria that cause the engine on; however, these three maps are the major criteria. The definitions and implementation of each map are summarized in Table 13.

Table 13 Information for engine on/off control criteria map calibration

No.	Map	Requisite data for map calibration	Definition (How it works?)	Data acquisition
1	eDrv Max Power (Pmax)	<u>Requested power</u> vehicle speed	Inside the map = eDrv is allowed.	HCU CAN data (Hybrid Control Unit)
2	STST eDrv max Velocity (STST)	SOC, vehicle speed	Inside the map = eDrv is allowed.	HCU CAN data
3	HEVC tqNm drv Limit (Tmax)	<u>Requested torque</u> vehicle speed	Inside the map = eDrv is allowed.	HCU CAN data

5.2.1.2 Unrealistic BOOST mode decision

The issue regarding Unrealistic BOOST mode decision can be solved by recalibrating the Boosting maps that provide information about when to allow the powertrain to enter the boost mode, and how much the energy can be drawn from the battery.

According to the section that explains about boosting mode, we presume that Prius3 considers acceleration pedal position, battery power, and soc as the main parameters for the determination. The possible candidates of the maps in CRUISE Prius3 are BOOST rp velocity accel pedal and BOOST pkW SOC shown in Figure 61.

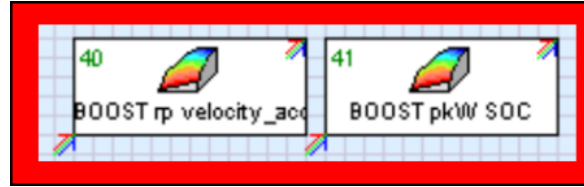


Figure 61 Boosting mode control maps in CRUISE Prius3

BOOST rp velocity accel pedal is the map that provides boosting mode allowance boundary based on vehicle speed, requested boosting power, and acceleration pedal position.

In this case, we assume that the operation mode will enter Boost mode when the acceleration pedal is pressed more than 80%. This assumption is affirmed by the data separation in Figure 18. Once we separated the boost mode data by using 80% acceleration pedal position, the data in boost mode align precisely on the maximum rim of the speed-force map.

In conclusion, we will try to input the logic that the Boost mode will be activated, when the acceleration pedal is pressed deeper than 80%. Vehicle speed and acceleration pedal position are available in HV ECU system (Vehicle Spd or Motor(MG2) Revolution, and Accelerator Degree); however, the battery power data is available in the vehicle system. The estimation method will be provided in the next chapter.

The issue regarding BOOST pkW SOC can be solved by recalibrating the Boosting maps that provide information about the maximum allowance battery power at different soc during boosting. The data that require for the map calibration are battery soc and battery power.

In summary, calibrating BOOST rp velocity accel pedal and BOOST pkW SOC will allow us to adjust the CRUISE Prius3 when to enable the Boost mode, and how much power can be drawn from the battery. The definitions and implementation of each map are summarized in Table 14.

Table 14 Information for Boost mode decision map calibration

No.	Map	Requisite data for map calibration	Definition (How it works?)	Data acquisition
1	BOOST rp velocity accel pedal	Vehicle speed, acceleration pedal position	Boost pw request at a specific speed and acceleration pedal position	Do not exist in Prius3 Boost pw is decided based on Force and speed.
2	BOOST pkW SOC	% SOC, <u>Boost pw max</u>	Max boost pw allowance at each SOC level	HCU CAN data It may result in engine operation point selection during HV drive.

5.2.2 Battery operation control

The issue regarding Unrealistic battery discharge/charging load can be solved by recalibrating maps relating to battery operation control. The possible candidate maps are BATMAN rp MOT, BATMAN rp Reкуп, BATMAN rp eDrv, BATMAN pkW Alt shown in Figure 62.

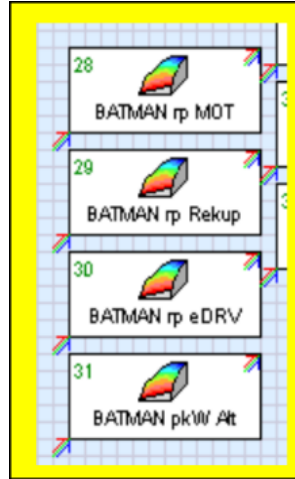


Figure 62 Battery operation control maps

BATMAN rp MOT is a map that defines the maximum allowance battery power for motoring at different soc. To calibrate this map, it requires battery soc data which can obtain via HV ECU; however, the maximum allowance battery power for motoring is not available in the vehicle system. Thus, we utilize the MG2 motoring power to represent the maximum allowance battery power for motoring, or we can screen the battery power data only when the MG2 is actuated as a motor.

BATMAN rp Reкуп is a map that defines the maximum allowance battery charging power during regenerative braking at different soc. Due to the accessibility of HV ECU data, the recuperative signal is not available in the ECU data list. In addition, recuperative braking is enabled during deceleration even when the driver does not press on the brake pedal. Thus, we utilize MG2 power data in engine-off generator mode to represent the maximum allowance recuperative power.

BATMAN rp eDrv is a map that defines the maximum allowance battery power supplying to MG2 at different soc during eDrive mode. To obtain the maximum allowance battery power supplying to MG2, the battery power data were extracted just only when eDrive mode is active (engine off and acceleration pedal is pressed).

BATMAN pkW Alt is a map that defines battery charging by alternative engine power at different soc. This data can be obtained by screening the battery power during charging while the engine is on without regenerative braking, or screening the battery power during charging while MG1 acts as a generator. The definitions and implementation requires for battery map calibration are summarized in Table 15

Table 15 Information for battery operation control map calibration

No.	Map	Requisite data for map calibration	Definition (How it works?)	Data acquisition
1	BATMAN rp MOT	SOC, <u>% MG2 motor pw</u>	MG2 motoring pw allowance at each SOC level	HCU CAN data
2	BATMAN rp Rekup	SOC, <u>% MG2 regen pw</u>	MG2 regen braking pw allowance at each SOC level	HCU CAN data
3	BATMAN rp eDrv	SOC, <u>% batt pw available for eDrv</u>	Batt pw available for eDrv at each SOC level	HCU CAN data
4	BATMAN pkW Alt	SOC, <u>% batt charging pw</u>	Batt charging pw allowance at each SOC level	HCU CAN data

5.2.3 Engine operation control

From the previous chapter, the issue regarding misprediction of fuel consumption, and engine operation point were established. This section will explain the problem-solving methodology engine operation control and fuel consumption map in accordance with CRUISE Prius3 platform. The data acquisition for the engine map calibration can be obtained via ECU data because it contains more data relating to the engine.

5.2.3.1 Engine optimal operation curve calibration

To solve the misprediction of engine operation point, it is recommended to confirm the fidelity of Engine optimal operation curve. The maps that correspond to the issue are ENG trNm Max, ENG tqNm Min, ENG tqNm opt, and ENG nrpm spd opt shown in Figure 63.

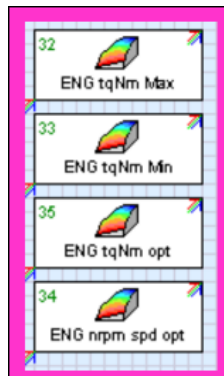


Figure 63 Engine operation control maps

ENG trNm Max and ENG tqNm Min are maps that specify the maximum and minimum torque produced by the engine. These maps require engine revolution and engine torque data. In other words, this map provides allowance engine torque range at specific engine speed. Even though the engine revolution signal is available in HV ECU, the engine torque data need to be estimated. The method in accordance with the engine torque estimation will be explained in more details.

ENG tqNm opt is a map that indicates the engine optimal operation curve based on engine revolution and engine torque. Method for engine curve identification will be explained later in the coming section. ENG nrpm spd op is also similar to ENG tqNm opt; however, it indicates the engine optimal operation curve based on engine revolution and engine power.

5.2.3.2 Engine fuel consumption maps calibration

To manage the problem regarding the discrepancy of engine fuel consumption prediction, the calibration on Engine IL4 16V fuel consumption map is necessary. The component box is shown in Figure 64. This map provides engine fuel consumption data in a function of engine torque, and engine fuel consumption rate [kg/h] and engine revolution. The relationship between engine torque and engine fuel consumption rate [kg/h] are separately explained in specified engine revolution interval ranges.



Figure 64 Engine IL4 16V fuel consumption map

Table 16 summarized the engine operation maps that require improvement calibration including requisite datasets, definitions, and data acquisition methods.

Table 16 Information for engine operation control map calibration

No.	Map	Requisite data for map calibration	Definition (How it works?)	Data acquisition
1	Engine IL4 16V Fuel consumption map	Ice rpm, trq, fuel [kg/h]	Fuel consumption at specified engine rpm range and continuous trq variation	ECU CAN data
2	ENG trNm Max	Ice rpm, trq	Max trq engine	ECU CAN data
3	ENG tqNm Min	Ice rpm, trq	Min trq engine	ECU CAN data
4	ENG tqNm opt	Ice rpm, trq	Engine's optimal operation curve (best efficiency line)	ECU CAN data
5	ENG nrpm spd opt	Ice pw, rpm	Engine's optimal operation curve (best efficiency line)	ECU CAN data

5.2.4 Others

Beside map calibrations, CRUISE Prius3 simulation also limits its hybrid powertrain control with several constant parameters. Significant constant parameters that require tuning are Batt Charge Pmax, Batt Discharge Pmax, Batt SOC min, Batt SOC max, HEVC Engine on min [s], Engine min power. Important details for the constant parameter tuning are provided in Table 17.

Table 17 Hybrid control constant parameter tuning

No.	Map	Requisite data for constant tuning	Definition (How it works?)	Data acquisition
1	Batt Charge Pmax Batt Discharge Pmax	<i><u>HV batt pw</u></i>	Max power limit for batt charge/ discharge	ECU CAN data (Engine Control Unit)
2	Batt SOC min Batt SOC max	HV batt SOC	Allowance batt SOC range	ECU CAN data
3	HEVC Engine on min [s]	<i><u>ICE rpm, or Drive condition ID=3</u></i>	The shortest duration that ICE is on.	ECU CAN data
4	Engine min power	<i><u>ICE pw</u></i>	Min ICE power at idle.	ECU CAN data

In conclusion, the unrealistic operations in CRUISE Prius3 can be improved by performing calibration on a number of maps and parameters. To achieve that the database recorded from the actual Prius3 is mandatory. Some data can be accessed via HV ECU or measured by external sensors. However, there is still a long list of data that need additional

data processing, and calculation. As mentioned before, insight data related to hybrid powertrain control are mostly protected as high confidential properties. Thus, how to obtain the data or key parameters that cannot be directly accessed or measured is one of the challenging issues for hybrid vehicle powertrain modeling. The next section will explain the map recalibration and the key parameter estimation methods in detail.

5.3 Methodology

This chapter proposes solutions toward the improvement on the problems established in the original CRUISE Prius3 presented in the previous chapter. Due to the sophisticated operation of the hybrid powertrain, a number of parameters, component operation maps, and hybrid control maps need to be calibrated. Thus, this chapter will provide the scope of the substantial improvements that are limited by the black-box hybrid control accessibility and the structure of the original CRUISE Prius3 itself. For better understanding, this chapter also describes the features and definitions of the parameters and maps that require the calibration. Finally, the overview of CRUISE Prius3 improvement methodology is also mentioned.

5.3.1 Experiment

The most important tool for hybrid powertrain simulation improvement or construction is databased. Without the database, the characteristics of the powertrain cannot

be extracted and sampled into a model. Thus, experiments need to be designed and conducted on hybrid vehicles to collect data from each hybrid powertrain component. To achieve that experimental conditions, environmental conditions, data acquisition, recording data list corresponding to the experiment objectives need to be considered carefully. The experimental procedures are explained in chapter4.

5.3.2 Data processing and filtering

Once, a number of trips and data were recorded, next is to organize the data into initiative format/structure, such as trip names, parameter name list, raw data, to facilitate the next data processing steps. Then, proper filters or data smoothing methods should be applied to eliminate noise from the data. The example of the data that require filtering is high voltage battery current/voltage, MG torque/rpm, discrete vehicle speed data, and others. For some data that contain low discrete resolution, such as vehicle speed, battery soc, data smoothing is recommended. After the noise elimination process, if more than one data logger used during the data acquisition, time synchronization must be applied to the database. To achieve this, the cross-correlation method can be implemented to match two data signals. However, it becomes more robust if apply this method with high-frequency data. In case of using vehicle speed data for time synchronization, it is recommended to differentiate and uses acceleration instead of vehicle speed.

5.3.3 Key parameter estimation

Most of the maps related to hybrid and battery control require parameters that are not available via the vehicle CAN system, or difficult to install sensors. Example of the key parameters that significantly influence the hybrid operation decision is total requested supply power, driving force and torque at wheels, engine torque, engine power, and others. In order to obtain these data, we derive Prius3's powertrain dynamic equation to estimate the key parameters based on the input of available HV ECU dataset. The data list is shown in Figure 65.

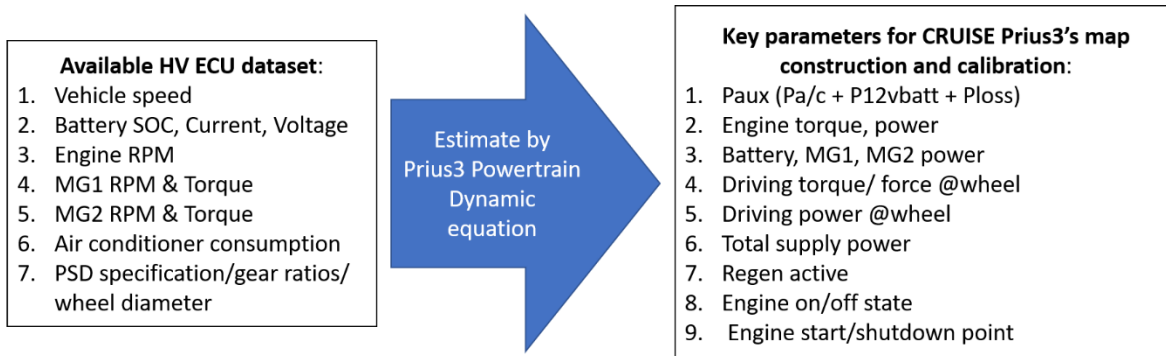


Figure 65 Key parameter estimation process

5.3.4 Map calibration and constant parameter tuning

After we have obtained the dataset required for mapping, next is to calibrate the maps and constant parameters in accordance with CRUISE Prius3 simulation platform

requirements. Most of the approaches that use for mapping are boundary identification, curve fitting, and some basic statistical analysis.

5.3.5 Minor map adjustment

Inside CRUISE Prius3, there are several parts that have been simplified and enclosed. Particularly for the black box, we barely know the exact process performing inside, as well as the issue from CAN data and external sensor accuracy. As a result, it is possible that the simulation may not perform in the same way as the actual vehicle for the first time. Therefore, once, the calibrated maps and constant parameters are input to the model, a simple validation needs to be investigated.

In case of that critical discrepancy was found, a minor adjustment must be applied. First is to identify the possible problems compared to the actual hybrid vehicles' characteristics. Then, it is recommended to search for the map that relates to the issue and makes an adjustment. In addition, CRUISE also provides a simple constant parameter optimization tool; however, it does not support 2D or 3D maps optimization.

5.4 Key parameter estimation

This section summarizes all the equations and calculation steps that necessary for the key parameter estimation. These parameters are not only implemented for CRUISE Prius3's

map calibration but also plays significant roles in the study of the impact of tire characters on hybrid vehicle fuel consumption discussed in chapter7.

5.4.1 High voltage battery

$$P_{batt} = V_{batt_fil} \cdot I_{batt_fil} \quad (15)$$

5.4.2 Engine

$$P_{ice.MultiReg} = -1.419(\dot{\omega}_{ice}\omega_{ice}) + 1.132(\dot{\omega}_{MG1}\omega_{ice}) - 3.804(\tau_{MG1}) - 1,038 \quad (16)$$

$$P_{ice} = \omega_{ice} \left\{ [\dot{\omega}_{ice}(I_{ice} + I_C)] + \left[\dot{\omega}_{MG1}(I_{MG1} + I_S) - \tau_{MG1} \cdot \left(\frac{R + S}{S} \right) \right] \right\} \quad (17)$$

$$\tau_{ice>MG1} = \tau_{ice} \cdot \left(\frac{S}{R + S} \right) \quad (18)$$

$$\tau_{ice>R} = \tau_{ice} \cdot \left(\frac{R}{R + S} \right) \quad (19)$$

5.4.3 Motor/generator

$$P_{MG1} = \tau_{MG1}\omega_{MG1} \quad (20)$$

$$P_{MG2} = \tau_{MG2} \omega_{MG2} \quad (21)$$

$$\tau_{MG2@R} = \tau_{MG2} \cdot (r/s) \quad (22)$$

$$\omega_{MG2@R} = \omega_{MG2} \cdot (s/r) \quad (23)$$

$$v_{veh.\omega_{MG2}} = \omega_{MG2} \cdot (G_c G_f G_r) \cdot R_{tire} \quad (24)$$

5.4.4 Powertrain output

$$\tau_{PT@ring} = \tau_{ice>R} + \tau_{MG2@R} \quad (25)$$

$$I_{trans2whl} = \frac{I_R}{(G_c G_f)} + \frac{I_{MG2}}{(G_c G_f G_r)} + (4 \cdot I_{whl}) \quad (26)$$

$$\tau_{whl} = \left[\frac{\tau_{PT@ring}}{G_c G_f} \right] - \left[\frac{\dot{v}_{veh.\omega_{MG2}} \cdot I_{trans2whl}}{R} \right] \quad (27)$$

$$F_{whl} = \tau_{whl} / R_{tire} \quad (28)$$

$$P_{whl} = F_{whl} \cdot v_{veh.\omega_{MG2}} = \tau_{whl} \cdot \omega_{whl} \quad (29)$$

5.4.5 Energy equivalent conversion

$$P_{FEqv.Watt} = \rho_{fuel.E} Q_{fuel} \quad (30)$$

$$E_{FEqv.j} = P_{FEqv.Watt} \cdot F_s = P_{FEqv.Watt} / \tau \quad (31)$$

$$Vol_{FEqv.battE} = \left(E_{batt.int} - E_{batt.fin} \right) / \rho_{fuel.E} \quad (32)$$

5.4.6 Performance and efficiency

$$P_{tot.sup.noRegen} = P_{ice.noRegen} + P_{batt.noRegen} \quad (33)$$

$$P_{tot.sup.Regen} = P_{ice.Regen} - P_{whl.Regen} \quad (34)$$

$$P_{tot.use.noRegen} = P_{whl.noRegen} - P_{batt.chg.noRegen} + P_{a/c.noRegen} \quad (35)$$

$$P_{tot.use.Regen} = -P_{batt.chg.Regen} + P_{a/c.Regen} \quad (36)$$

$$P_{tot.loss} = P_{tot.sup} - P_{tot.use} \quad (37)$$

$$P_{PT.effi} = \frac{P_{tot.use} \cdot 100}{P_{tot.sup}} \quad (38)$$

$$P_{ice.eff} = \frac{P_{ice} \cdot 100}{P_{fuel}} \quad (39)$$

$$P_{FEqv.tot.sup.noRegen} = P_{FEqv.ice.noRegen} + P_{batt.noRegen} \quad (40)$$

$$P_{FEqv.tot.sup.Regen} = P_{FEqv.ice.Regen} - P_{whl.Regen} \quad (41)$$

$$P_{FEqv.PT.effi} = \frac{P_{FEqv.tot.use} \cdot 100}{P_{FEqv.tot.sup}} \quad (42)$$

5.4.7 External observatory parameters

$$v_{veh.\omega_{MG2}} = \omega_{MG2} \cdot (G_c G_f G_r) \cdot R_{tire} \quad (43)$$

$$\theta_{grade_{rad}} = (\theta_{grade_{IT2.g.rad}} - 0.1) / 9.81 \quad (44)$$

$$F_{AeroDrag} = \frac{1}{2} \rho_{air} A_{front} C_{drag} (v_{veh.\omega_{MG2}} - v_{wind})^2 \quad (45)$$

$$\begin{aligned} VSP_{kW.JM1999} = & \{ [mass \cdot v_{veh.\omega_{MG2}}] \\ & \cdot [a_{veh}(E_{JM1999} + 1) + (g C_{r.JM1999}) \\ & + (g \sin \theta_{grade_{rad}})] \} + [v_{veh.\omega_{MG2}} \cdot F_{AeroDrag}] \end{aligned} \quad (46)$$

5.5 The dynamic model validation

To obtain accurate driving torque estimation, it is important to affirm the accuracy of the engine power estimation, since the total driving torque is a product of the torque from engine and MG2. As mentioned before because the engine power and torque signals are not available via HV ECU, the estimation method is needed to fulfill the total driving torque calculation.

This section will describe how to perform the validation on engine power estimation by using the available database. Then, the driving torque estimation will be validated based on the data measured from the chassis dynamometer. In addition, the content will mention further on the capability of utilizing sensors in the vehicle (ECU data) to perform a hybrid powertrain performance analysis and confirm quality of the ECU data.

5.5.1 Engine Dynamic Model

The engine is the main power source of hybrid vehicles for battery charging and propulsion. For Prius3's, Atkinson Cycle engine is adopted. The outstanding feature of this engine is that it can control the compression stroke volume and the expansion stroke volume separately by retarding the closing valve timing during the suction. Unlikely, the conventional engine that these two properties are usually varied proportionally or fixed. Thus, the compression ratio in Atkinson cycle engine can be varied. Meanwhile, the knocking

problem is reduced. As a result, the engine efficiency is improved, and the output power can be varied at a wider range.

To calculate the engine power, the engine dynamic equation in (17) is applied (P_{ice_DynEq}). We also developed a method using multi-regression to recalibrate the engine power dynamic model's coefficients to be optimal for Prius3's Atkinson cycle engine ($P_{ice_DynEq_MultiRegress}$). These two methods are compared to Engine Requested Power ($P_{ice_reqst_OBD}$) from HV ECU (OBD). Engine Requested Power is a target engine power that is sent to command the engine. Thus, there is a delay between the target signal and the actual engine power.

Figure 66 shows a comparison between $P_{ice_reqst_OBD}$ and P_{ice_DynEq} . The respond delay between $P_{ice_reqst_OBD}$ and P_{ice_DynEq} was found; however, the data oriented on the diagonal line. The r-square were found at 0.990.

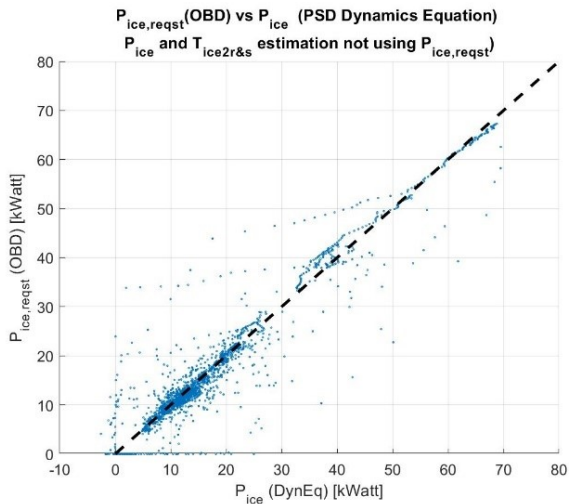


Figure 66 Comparison between $P_{ice_reqst_OBD}$ vs P_{ice_DynEq}

Figure 67 shows a comparison between $P_{ice_reqst_OBD}$ and $P_{ice_DynEq_MultiRegress}$. The delay between $P_{ice_reqst_OBD}$ and $P_{ice_DynEq_MultiRegress}$ was found; however, it was less than the engine dynamic equation method. The data located densely on the diagonal line with r-square at 0.996. The outlier data were found to be the data during the engine on/off, but the percentage is lower than 10%.

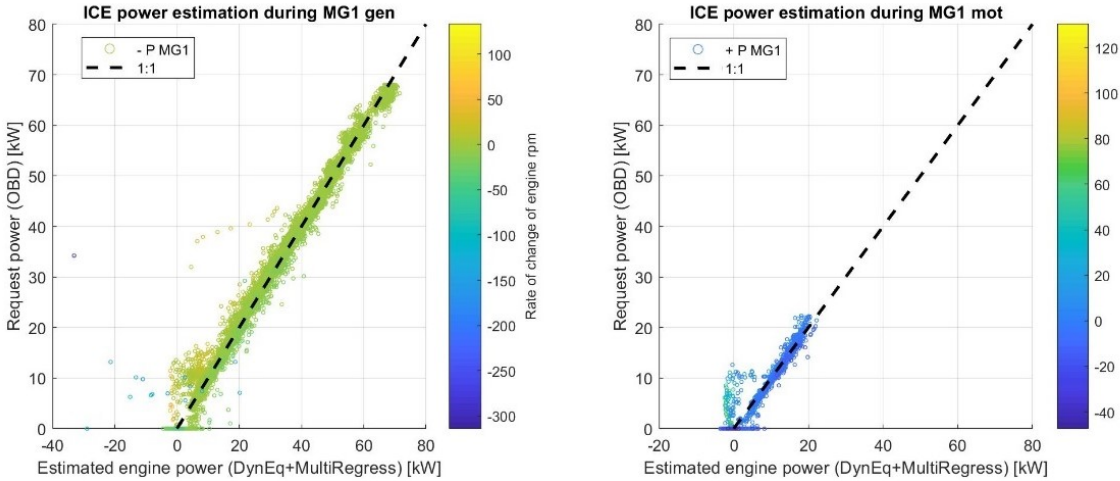


Figure 67 Comparison between $P_{ice_reqst_OBD}$ VS $P_{ice_DynEq_MultiRegress}$

Figure 68 shows the engine power prediction based on engine dynamic equation method and engine dynamic equation with multi-regression method compared to Engine Requested Power from HV ECU. The data was recorded during the chassis dynamometer experiment with constant force at different constant speed. The results indicate that the engine dynamic equation with calibrated coefficients provides more accurate prediction than just only using engine dynamic equation with coefficients suggested by CRUISE Prius3.

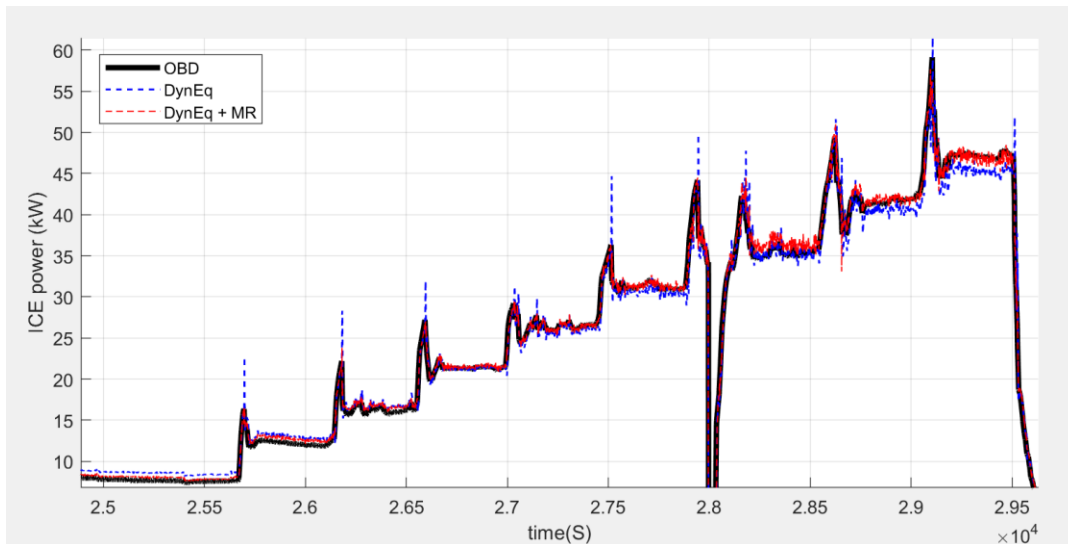


Figure 68 Engine power compared among engine dynamic equation with CRUISE Prius3's coefficients (DynEq), dynamic equation with re-calibrated coefficients (DynEq+MR), and Engine Requested Power from HV ECU (OBD)

5.5.2 Powertrain Dynamic Model

This section performs a validation of the powertrain dynamic model based on the data that was measured from the chassis dynamometer (CD), such as wheel torque, wheel speed, and wheel power. However, due to the CD's measurement accuracy issue, such as wheel slip and Force-Torque calculation, the purpose of this validation is just to affirm the prediction tendency of the estimation method that has been implemented in this work.

Figure 69 illustrates the error characteristic between the chassis dynamometer and the estimated data. The term error means the difference between the vehicle and CD measurements data. The colors of the data show a torque measurement error.

The upper figure implies that the higher driving speed is the larger power error become. The inclination rate of the power error changes proportionally to the torque error. The yellow color shows the data during speed change of which the torque is high. The green color shows the data during constant speed driving of which the torque was between 60-100 Nm. The blue color shows the data during deceleration of which the torque is negative. The discrepancy between the data during acceleration and deceleration is called CD's hysteresis which is a general characteristic of any CDs.

To solve the error problem, it is reasonable to select the data during constant speed to perform the validation because these data are at the most stable condition. It was found that the constant speed dataset has a torque error between 60-100 N.m. This low distortion data range is shown in Figure 69.

DynEq-Dyno torque error analysis

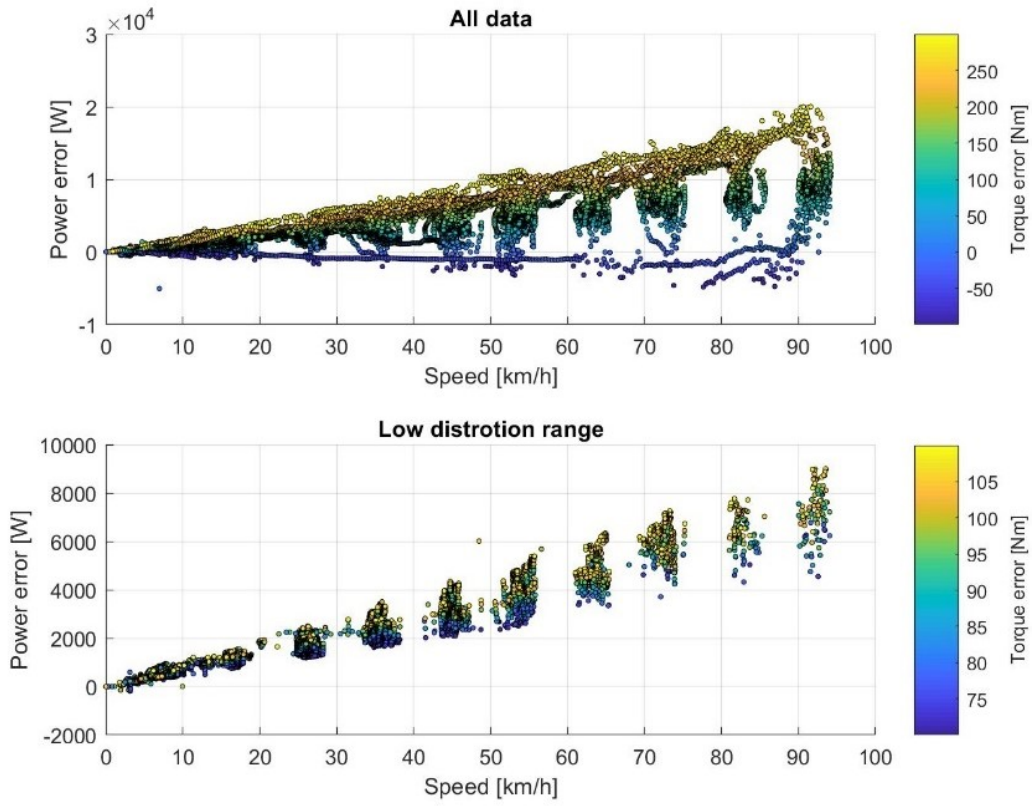


Figure 69 The characteristic of the chassis dynamometer error

Based on the constant speed data, the torque estimation validation result was plotted in Figure 70. The red data refer all dataset, and the green data refer to constant speed data called low distortion. The constant speed data located on the straight line that is parallel to the 1:1 line; however, there is some offset approximately 100N.m. discovered. There was an attempt of screening the data that have a low slip or small speed error, but the offset problem could not be solved.

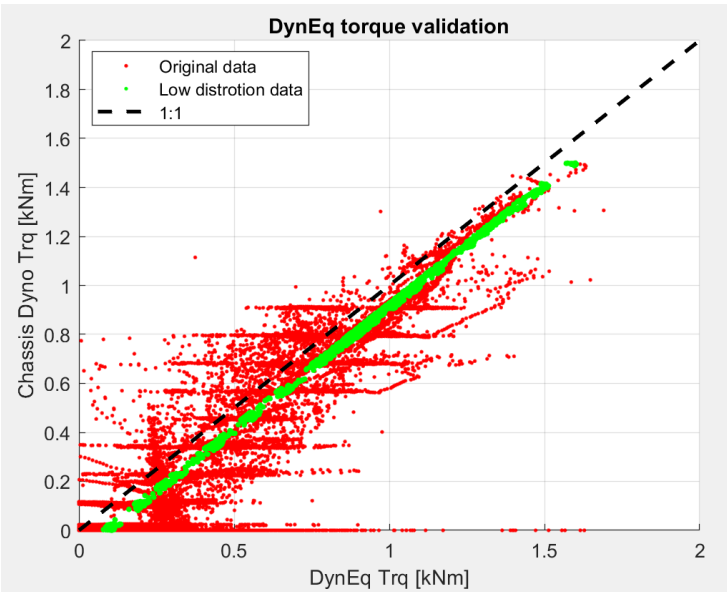


Figure 70 Driving torque dynamic equation validation

For the power estimation validation, the constant speed data (low distortion data) also aligned on mainly on the 1:1 line. To adjust the torque measurement offset, 0.86 was found to be the best value to adjust the data.

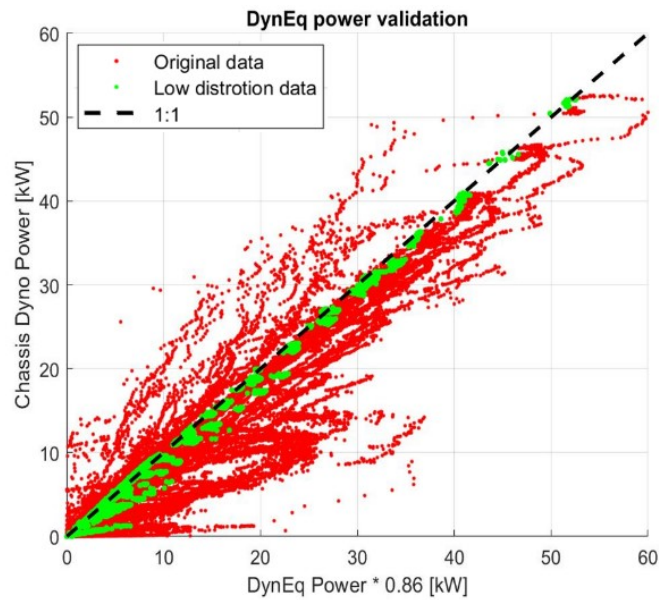


Figure 71 Driving Power dynamic equation validation

In summary, the validations in this section show that the dynamic model that has been derived is capable of providing a reasonable estimation tendency. Thus, the estimation data will be employed for CRUISE Prius3 maps re-calibration which will be explained in the coming sector.

5.6 Prius3 simulation calibrations and improvements

Once the key parameters have been estimated, this chapter attempts to provide an explanation on map calibration techniques for CRUISE Prius3. The concept of this task is to eliminate the outlier data and extract the significant features from them. The techniques that have been frequently used are curve fitting, boundary construction and other techniques. CRUISE Prius3 simulation platform is just an only one example. Even though the simulation platform is charged, the core techniques are still valid and applicable.

The maps in the section are constructed based on all the datasets conducted during a wide range of the experiments reported in chapter4. More than 500,000 of the data points were implemented into the map calibration process. For better understanding, it is recommended to apply the basic information provided in the previous section with the explanation in the coming section.

5.6.1 Hybrid operation control map calibration

This section explains techniques to correct the operation characteristics of CRUISE Prius3's virtual powertrain to operate similarly to the actual vehicles. This section also provides the method to recalibrate the engine on/off maps and boosting maps.

5.6.1.1 Engine on/off criteria and map construction

First is to construct the maps: STST eDrv max Velocity (STST), HEVC tqNm drv Limit (Tmax), and eDrv Max Power (Pmax). The requisite key parameters are vehicle speed, battery soc, requested total power and requested total driving torque.

Key parameters' estimation

Equation (33) is employed to estimate the total supply power of the powertrain and use estimated value to represent the requested total power. Also, equation (27) is employed to estimate the total driving torque from the powertrain and use the estimated value to represent the requested total driving torque. For more details please refer to Table 13.

Engine operation state classification

To distinguish the boundary between engine on/off transition, the engine operation states must be identified and marked to the key parameter dataset. The states can be identified by either Drive Condition ID or Engine Stop Request data from HV ECU. The identification criteria are explained in Table 18.

Table 18 Engine operation state identification criteria based on HV ECU data

Engine operation state	Drive Condition ID (x_i)	Engine Stop Request (x_i)
Engine on stage	$x_i = 3$	$x_i = 0$
Engine off stage	$x_i = 0$	$x_i = 1$
Engine start point	$1.99 \leq x_i \leq 2.01$	$x_i - x_{i+1} = 1$
Engine shut down point	$0.99 \leq x_i \leq 1.01$	$x_i - x_{i+1} = -1$

Then, the data were classified into each engine operation states. The results were discovered as illustrated in Figure 72. Red and blue colors refer to engine on and engine off states respectively. The dot and diamond shapes emphasize the state of the engine operation between engine on/off state (The operation remains at the same state), and engine starting/shutting down state (The operation changes the state.).

According to the orientation of the data, engine on and off state can be explicitly distinguished based on these key parameters presented in the fields of STST, Tmax, and Pmax maps. A cloud of the engine off data on each map locates densely inside a single specific region at which a fundamental geometry boundary can be identified. At the edge of the engine off region particularly on Tmax and Pmax maps, the engine start points align along and right at the edge which reasonably represents the engine operation transition boundaries between engine off and on state.

Outside the engine operation transition boundaries, the only one active engine operation is the engine on state data. It implied that the engine off, engine starting and shutting down activities are allowed only when the conditions stay inside the specified

boundaries. Once the conditions: vehicle speed, soc, wheel torque, wheel power exceed the boundaries, the engine has to be turned on and stays on at all time.

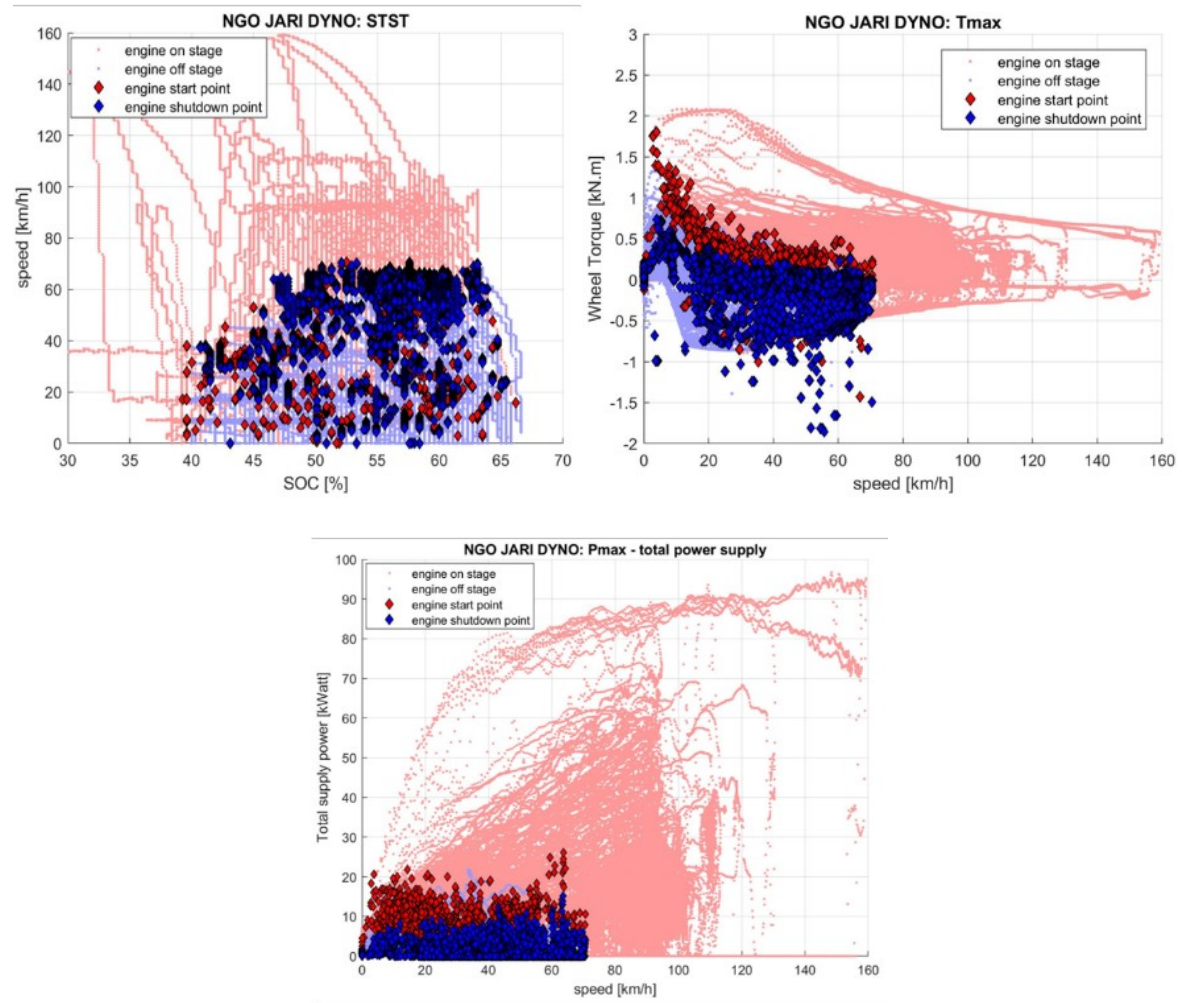


Figure 72 STST, Tmax, Pmax maps classified by engine operation state

Data quality assurance

Due to the accuracy uncertainties of the HV ECU data, key parameter estimation, including the actual vehicle operation itself, this section will provide a method to eliminate the outlier data in order to improve the confidence in the boundaries identification process.

According to the explicit relationship between battery soc and available battery output power during eDrive mode explained in Chapter3. We utilized the simple shape of the data alignment to construct the screening criteria. Figure 73 shows that this relationship remains in the same shape among three different experimental data and a wide range of driving conditions.

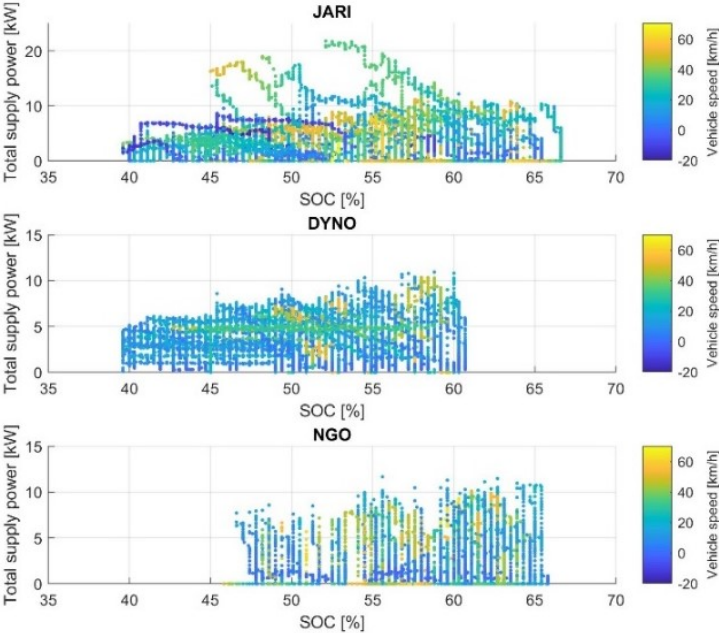


Figure 73 battery output power at different soc from JARI, DYNO, and NGO datasets

In Figure 74, trapezoidal shape was applied to identify the boundary that separates between engine on and off areas. Based on this boundary, the data that locate outside the boundary were eliminated. By using Matlab, it provides a function called *inpolygon* to classify whether the data are inside or outside of the boundary. Figure 74 shows the result. The eliminated data were shown in blue, while all red data locating inside the green boundary was taken into account for the STST, Tmax, and Pmax map construction.

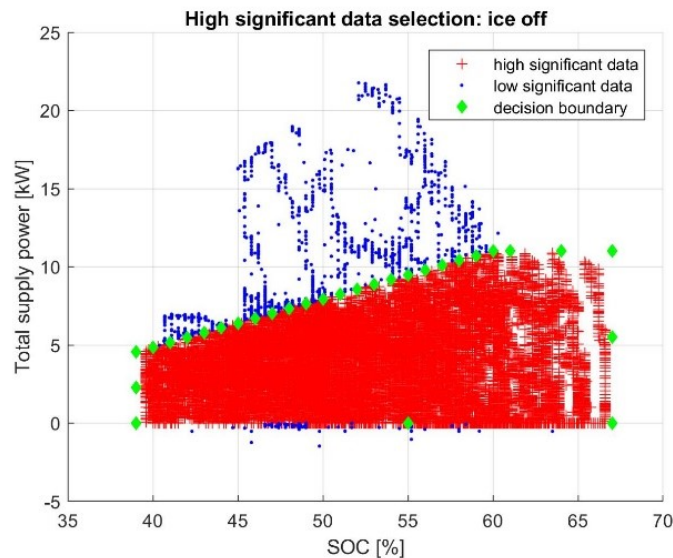


Figure 74 Data quality assurance for STST, Tmax, and Pmax maps

Engine on/off boundaries construction on STST, Tmax, and Pmax

After several investigations, this section selects two map construction methods that perform the best prediction. Figure 75 shows the comparisons among maps from the original CRUISE Prius3's, maps that were calibrated from Bangkok database (BKK), and maps that were calibrated from ALL database.

BKK database maps were constructed based on an experiment conducted in Bangkok Thailand. This dataset was implemented to investigate the possibility of CRUISE Prius3 improvement. This dataset contains a large amount of real-world driving data that covers a variety of powertrain operation and driving scenarios. At the preliminary stage, the idea of the map recalibration method was found to be effective. (Pitanuwat et al., 2017) Then, the additional experimental campaigns were conducted as called Nagoya dataset (NGO), analytical dataset conducted in JARI circuit (JARI), and chassis dynamometer dataset (DYNO). All the additional datasets are gathered and used as a dataset called ALL database (NGO+JARI+DYNO).

The map re-calibration was conducted by using the engine off, and engine start points data. First, the boundaries were constructed based on the engine off data by using *Boundary* function provided in Matlab. Then, the engine start points were also used as a reference trend for the boundary construction. Figure 75 shows the results of the identified boundary compared with the engine off and engine start points from ALL databased.

One noticeable point is that the difference between BKK and ALL boundaries. As ALL database contains a larger number of the data with higher variety of the operation points, it veils the operation area that was not found in BKK dataset. For example, on the STST map, ALL database map shows potential of eDrive that can be down to soc 39%, while BKK databased was limited at 44%. The reason was that A/C was on during BKK, but off during JARI and DYNO.

This issue indicates that the wider area that the driving conditions covers, especially the typical operation region, the more reliable the map re-calibration process becomes. Thus,

the proper design of driving condition, and electrical equipment operation during the experiment are mandatory for the map re-calibration.

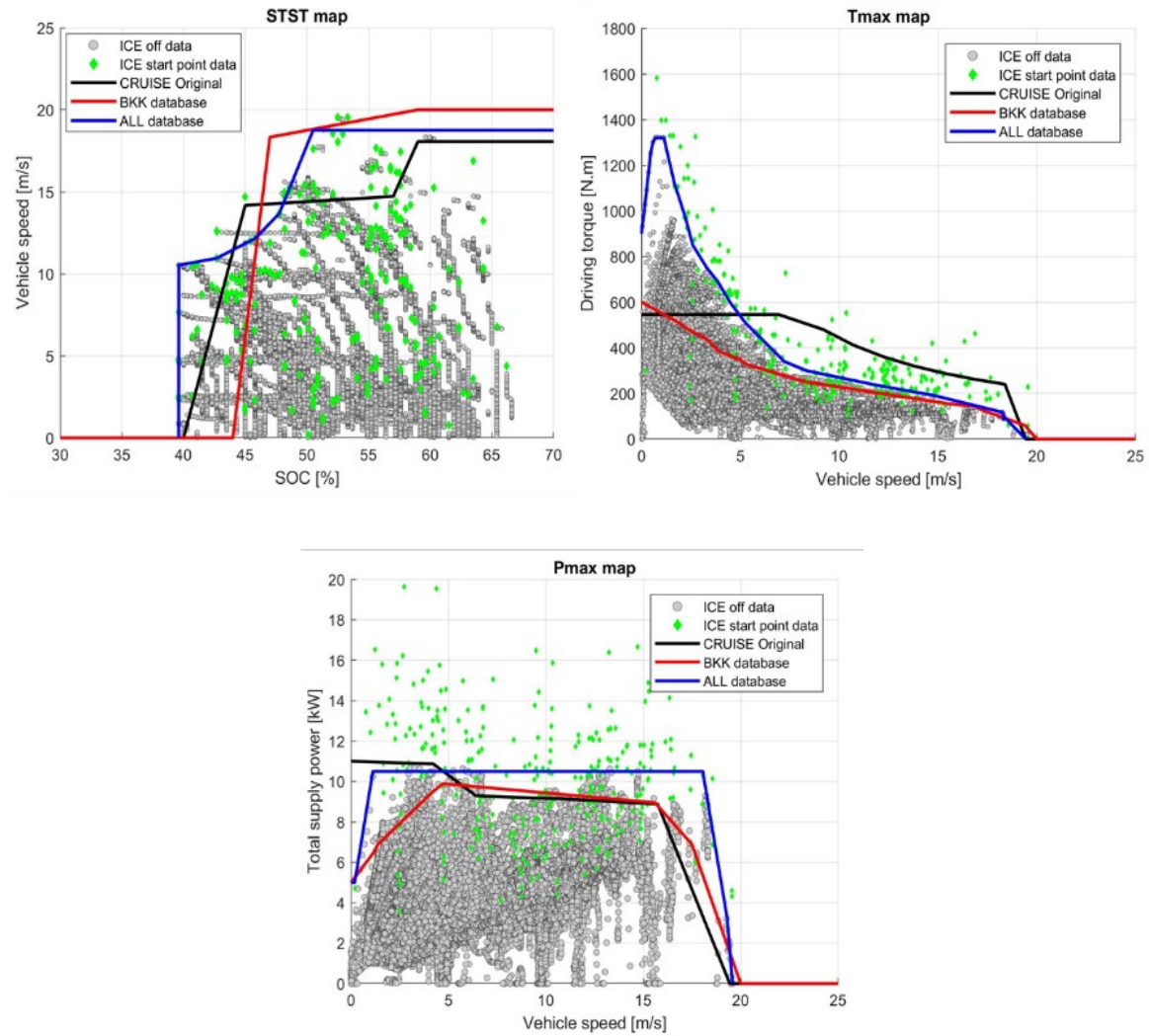


Figure 75 Re-calibration of STST, Tmax, Pmax map

5.6.1.2 BOOST mode decision

This section will explain the method to re-calibrate BOOST pkW SOC. Since the relationship between vehicle speed and acceleration pedal was not explicitly found in Prius3, the recalibration of BOOST rp velocity accel pedal map was estimated. The logic that is used for this map construction is once the acceleration pedal is operated more than 80%, the powertrain will enter to boost mode.

For BOOST pkW SOC recalibration, this map requires battery soc and Boost power max. This map was found to have a substantial influence on the engine operation point selection. To represent the Boost power max data, we implemented battery power data for the map construction. In this case, we are interested in the maximum battery discharge power. Thus, the boundary between boost mode and non-boost mode can be defined based on the line drawn on battery soc and battery power axis shown in Figure 76. For the map construction methodology, please refer to the previous section, Engine on/off criteria.

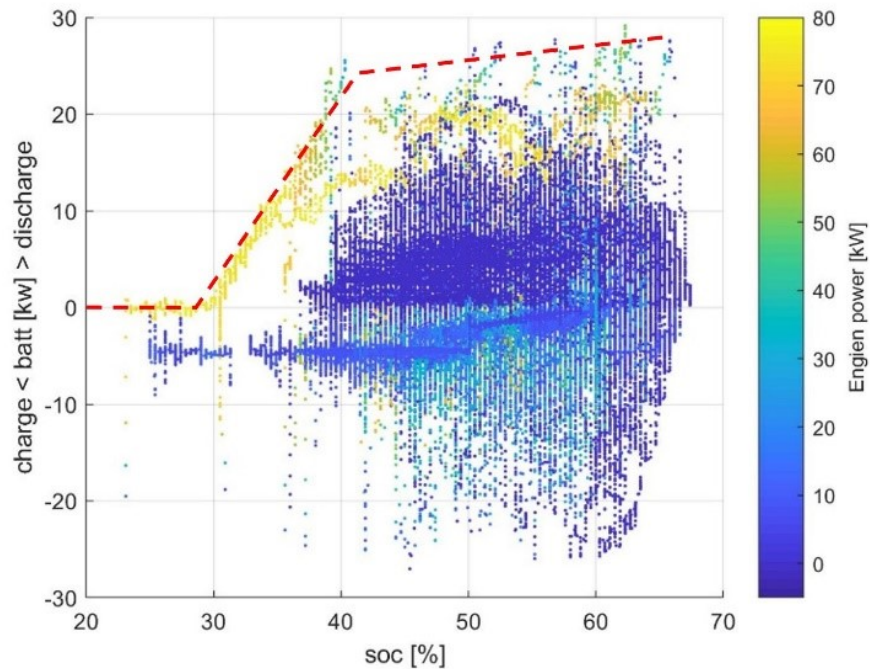


Figure 76 BOOST pkW SOC map re-calibration

5.6.2 Battery operation control

This section will re-calibrate battery operation control maps, which are BATMAN rp MOT, BATMAN rp Reкуп, BATMAN rp eDRV, and BATMAN pkW Alt. The requisite key parameters are battery soc, MG2 power during motoring and generating, battery power during eDrive and alternative battery charging. For more details and definitions of the parameters, please refer to Table 15. The map/boundary construction technique in this section is the same as the previous section, Engine on/off criteria; however, the important concept is highlighted on how to define the state of the machine and to interpret the meaning. For MG2 motoring and generating power, this machine state can be intuitively identified. However, it

is important to confirm the conventional sign and meaning of charge/discharge or motor /generator of HV ECU data by comparing MG to battery data.

To construct BATMAN rp MOT map, it requires the maximum allowance of battery power providing to MG2 at each soc level. First, the data at boost mode need to be excluded and remained only normal mode (acceleration pedal < 80%). Then, the map can be constructed as shown in Figure 77.

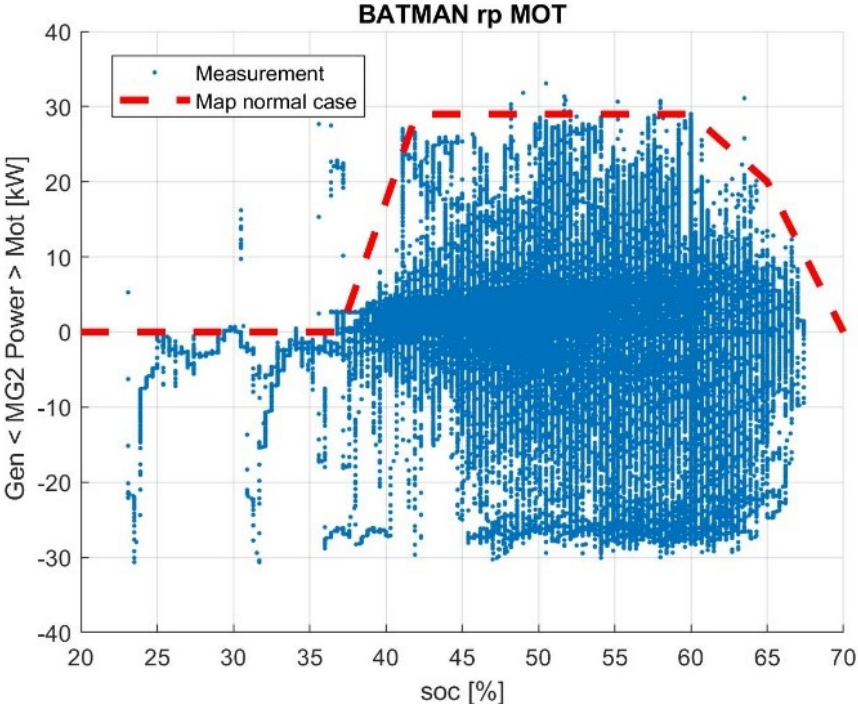


Figure 77 BATMAN rp MOT map recalibration

BATMAN rp Reкуп map is a map that quantifies the maximum allowance of regenerative braking power that the battery can absorb at each soc state. To obtain regenerative braking power, we utilize the MG2 power and the battery data during engine off, speed > 0km/h, and no acceleration peddle operation to construct the map. Finally, the map can be defined as shown in Figure 78.

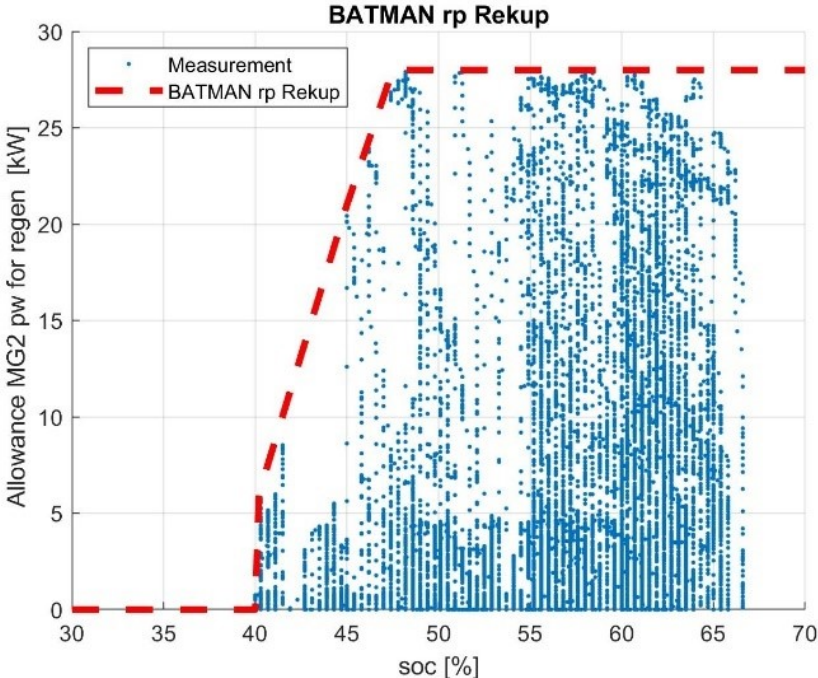


Figure 78 BATMAN rp Reкуп map recalibration

BATMAN rp eDRV is a map that quantifies the maximum allowance of the battery power for electric driving mode (eDrive mode). It requires battery power and soc data under the engine off, speed>0 km/h, and acceleration pedal is operated. The screened data are plot and the map is shown in Figure 79.

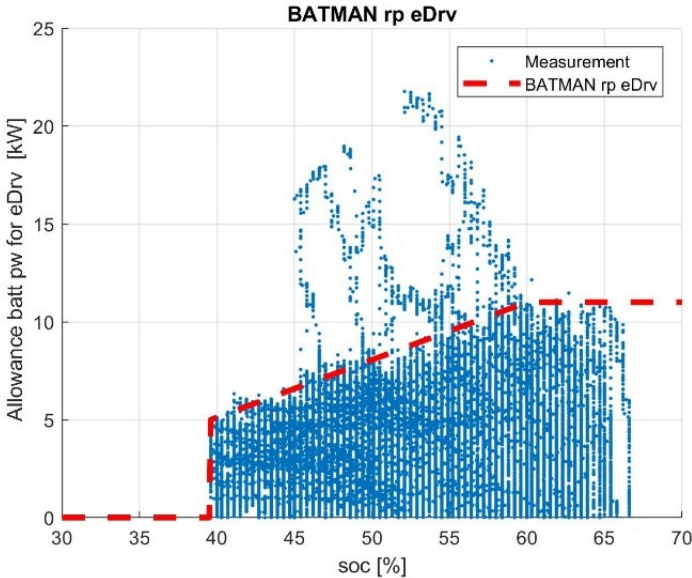


Figure 79 BATMAN rp eDRV map recalibration

At last, BATMAN pkW Alt is the map that quantified the maximum allowance of the engine alternative power (battery charging power) at each soc level. This map was found to have a substantial influence on the alternative engine power distribution for battery sustaining. To obtain the engine alternative power, the data can be extracted under the conditions of the engine on and no regenerative braking. The regenerative braking machine state can be indicated by the fact that when the MG2 generation power becomes larger than

the engine power, it means MG2 is absorbing braking power. The BATMAN pkW Alt map can be identified as shown in Figure 80.

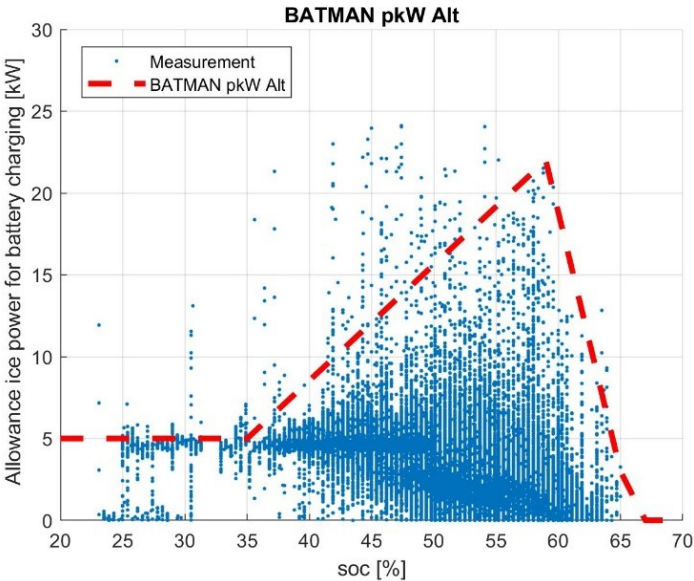


Figure 80 , BATMAN pkW Alt map recalibration

5.6.3 Engine operation control

The engine fuel consumption map and engine operation map were re-calibrated based on engine torque, speed and fuel injection data recorded from ECU. The map provides steady-state conditions of the engine fuel consumption characteristic specified by continuous engine torque and discretized engine speed ranges as the inputs. For the engine operation map, it contains the most efficient engine operation trajectory that the engine should theoretically operate along the curve. These two maps have significant influence and direct impact on fuel

consumption prediction and the engine operation point selection. Moreover, engine efficiency fluctuates much more than MG efficiency. Thus, it is important to confirm the validity of the maps.

This section provides the methodology for engine maps' data filtering. This method is capable of eliminating transient and noisy measurement data points. Then, the procedures for Engine IL4 16V Fuel consumption map, ENG trNm Max, ENG tqNm Min, ENG tqNm opt, and ENG nrpm spd opt are performed based on the filtered dataset.

5.6.3.1 Engine optimal operation curve

Due to the high variation in the engine operation including transient period, data filtering is needed. This section proposes 2D-data extraction. This method provides a capability of extracting data in which an area that the engine frequently operates and eliminate the outlier data points.

The main concept of 2D-data extraction is that first the data were divided into grids on x-y axis. Then, the number of data in each grid will be cumulated and compared to the number of total data in the same column. If the percentage of the count in that grid exceeds 20%, then all data points in the grid will be saved. The engine curve will be fitted based on these data. Note that, the grid interval on x and y axis can be judged by the data fitness values and the screening performance.

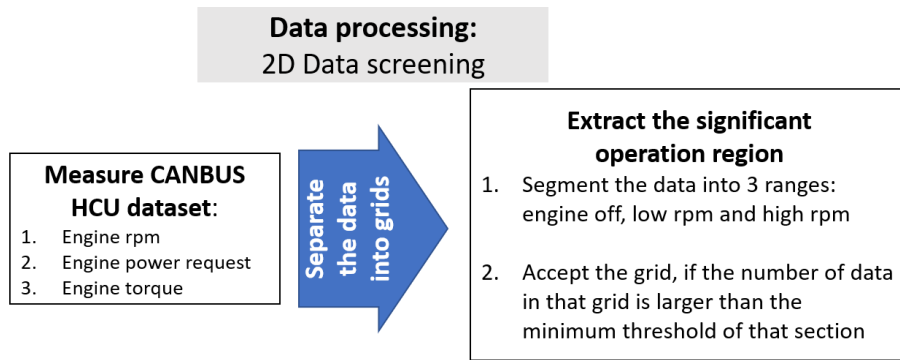
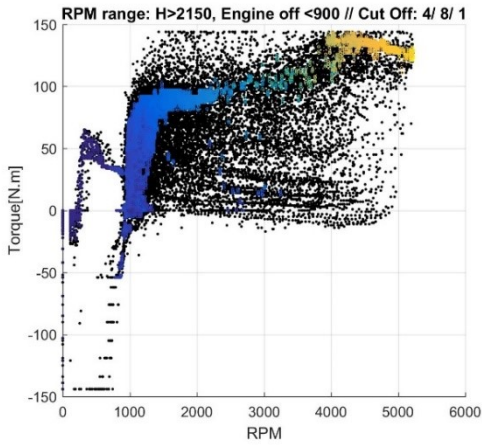
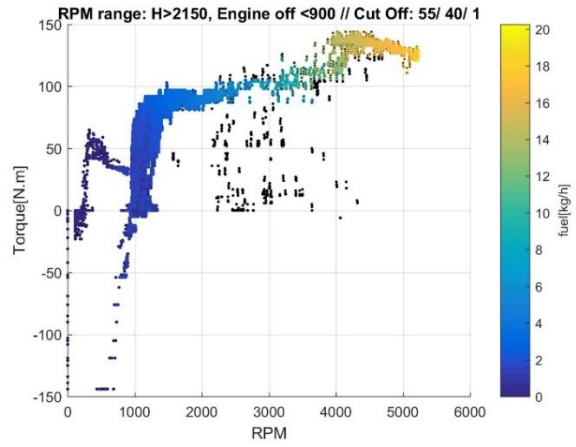


Figure 81 2D-data screening process for engine maps re-calibration

Figure 82 shows 2D-data extraction that was applied on Prius3's engine optimal operation map. The significant operating points were extracted two times with different screening set up. First 2D-data extraction with small-grid separation was applied in order to realize the shape of the data. Then, the second 2D-data extraction was applied with large-grid separation to eliminate the scattered data points. The results from each screening step are shown in Figure 82, where the black color refers to the data that were eliminated. Finally, the extracted data were fitted as a re-calibrated engine operation map and compared to the original Prius3 CRUISE's map in Figure 83.



(1st screen)



(2nd screen)

Figure 82 2D-data screening applied to engine optimal operation curve

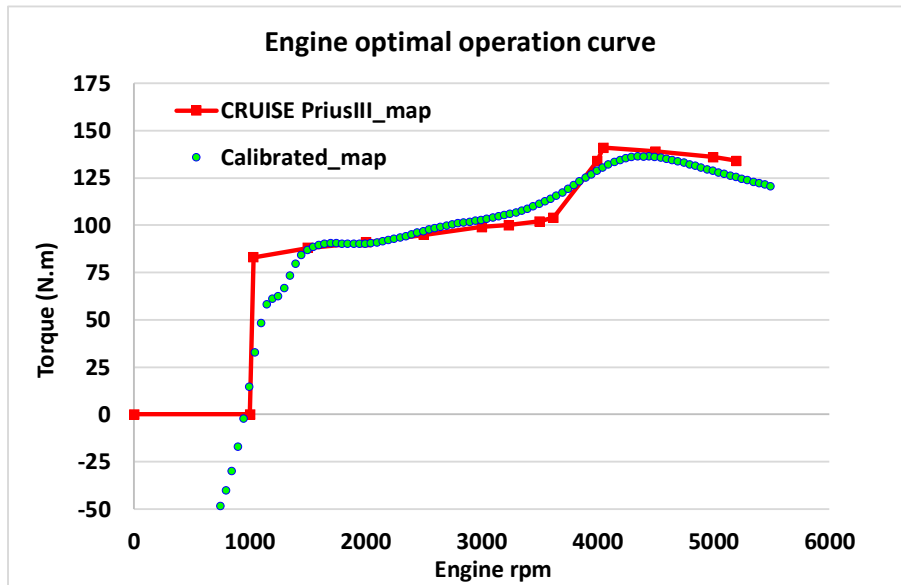


Figure 83 Engine optimal operation curve recalibration

5.6.3.2 Engine fuel consumption maps

2D-data extraction and derivative of engine rpm were applied on the fuel consumption mapping data to eliminate the transient data points. Figure 84 shows the comparison of the fuel consumption map at 4,500 rpm between without applying 2D-data extraction and with applying 2D-data extraction. The red and black dot curves show Prius3 CRUISE's map and the re-calibrated map respectively.

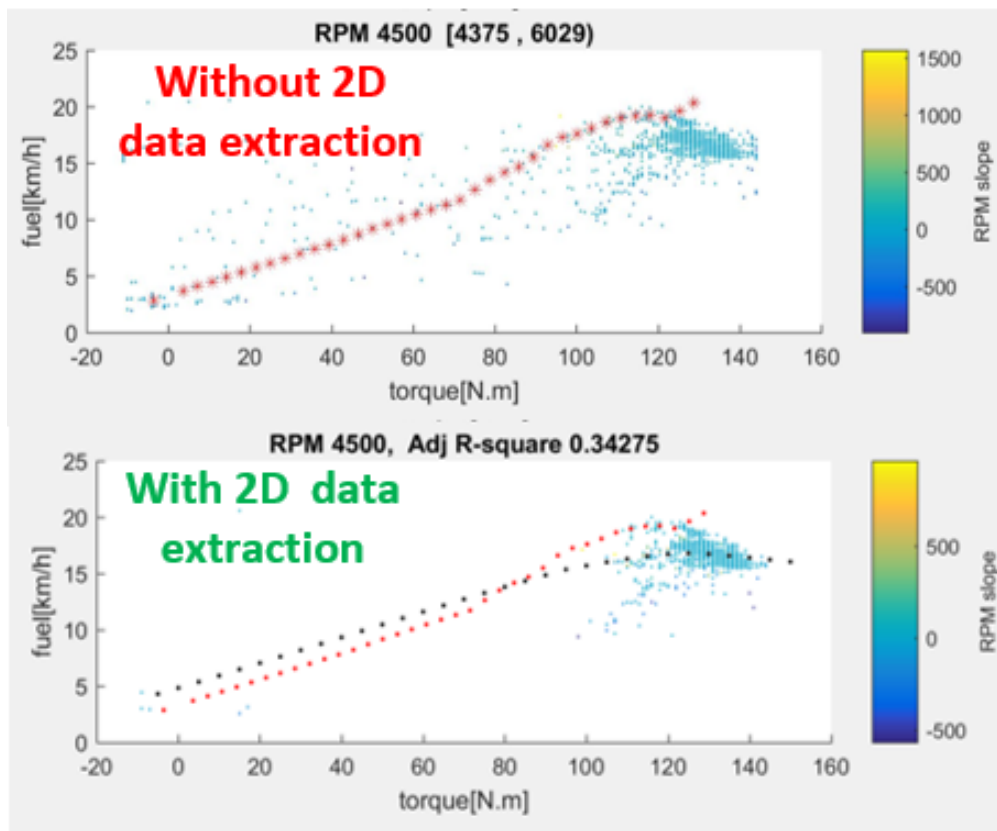


Figure 84 2D-data screening applied to fuel consumption data

After 2D-data extraction was applied through all the rpm ranges, the engine fuel consumption curves were fitted to the data. Figure 85 shows the comparison between the re-calibrated curves (black) and the original CRUISE Prius3 curves (red). The newly fitted curves tend to cut pass the majority of the data clouds.

Finally, all the fitted curves from each rpm ranges were combined. Then, the re-calibrated engine fuel consumption maps were plot as a contour diagram shown in Figure 86.

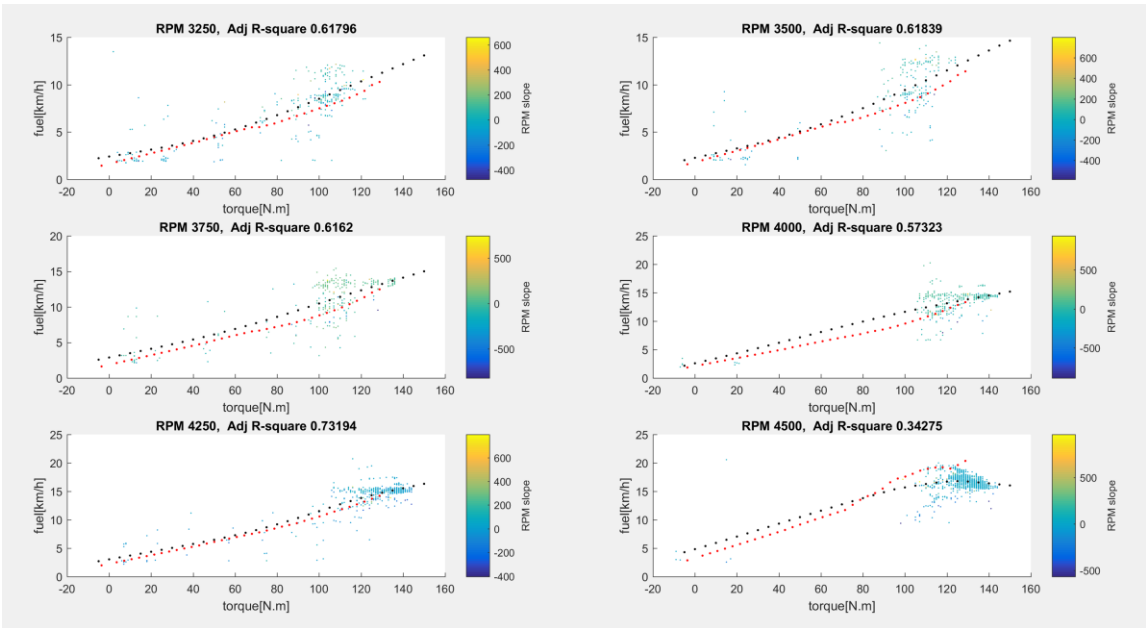


Figure 85 Engine fuel consumption map re-calibration for rpm [3,125-5,200]

Engine fuel consumption map

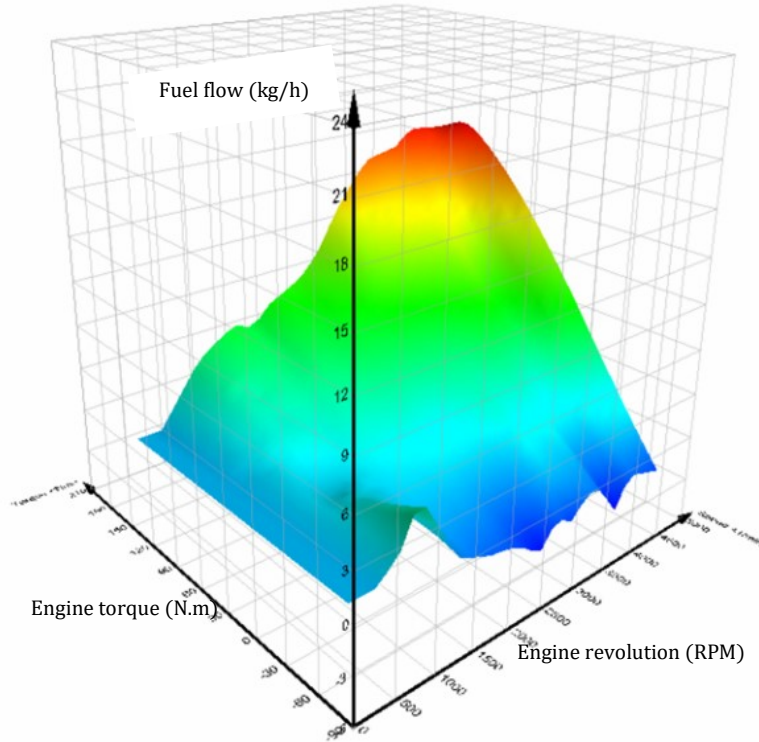


Figure 86 re-calibrated full engine fuel consumption map

5.6.4 Others

5.6.4.1 Hybrid control constant parameter tuning

This section provided re-calibrated hybrid control constant parameters based on the databased observation. The modification is highlighted in yellow shown in Figure 87.

Original CRUISE Prius3

Improved CRUISE Prius3

Data Bus Channel	Description	Value	Unit	Data Type	Data Bus Channel	Description	Value	Unit
Constant 0	eDrive Pmax (may change the	8	kW	double	Constant 0	eDrive Pmax (may change the	10	kW
Constant 1	Battery Charge Pmax	27	kW	double	Constant 1	Battery Charge Pmax 30	25	kW
Constant 2	Battery Discharge Pmax	27	kW	double	Constant 2	Battery Discharge Pmax 30	25	kW
Constant 3	Battery SOC min	38	%	double	Constant 3	Battery SOC min	39	%
Constant 4	Battery SOC max	70	%	double	Constant 4	Battery SOC max	65	%
Constant 5	Battery U HV nominal (nominal	100	V	double	Constant 5	Battery U HV nominal (nominal	650	V
Constant 6	Battery U LV nominal	14	V	double	Constant 6	Battery U LV nominal	14	V
Constant 7	Static Rolling Radius of Wheel	307.73	mm	double	Constant 7	Static Rolling Radius of Wheel	307.73	mm
Constant 8	Curb Weight of Vehicle - Nomi	1379.0	kg	double	Constant 8	Curb Weight of Vehicle - Nomi	1379.0	kg
Constant 9	Transmission Ratio of Single R	3.2677469135802		double	Constant 9	Transmission Ratio of Single R	3.2677469135802	
Constant 10	Base Ratio of Planetary Gear	2.6		double	Constant 10	Base Ratio of Planetary Gear	2.6	
Constant 11	eMOT coupling ratio	1.0	-	double	Constant 11	eMOT coupling ratio	1.0	-
Constant 12	Engine Idle speed	1000	1/min	double	Constant 12	Engine Idle speed	1000	1/min
Constant 13	Maximum Speed of Engine	5200.0	1/min	double	Constant 13	Maximum Speed of Engine	5200.0	1/min
Constant 14	eMOT nominal Power	60	kW	double	Constant 14	eMOT nominal Power	60	kW
Constant 15	eMOT nominal Torque	545.7	Nm	double	Constant 15	eMOT nominal Torque	545.7	Nm
Constant 16	eMOT U HV max	700	V	double	Constant 16	eMOT U HV max	700	V
Constant 17	eMOT U HV min	600	V	double	Constant 17	eMOT U HV min	600	V
Constant 18	eGEN nominal Power	42	kW	double	Constant 18	eGEN nominal Power (some ef	42	kW
Constant 19	eGEN nominal Torque	37,5	Nm	double	Constant 19	eGEN nominal Torque	37,5	Nm
Constant 20	HEVC Engine ON min	4	s	double	Constant 20	HEVC Engine ON min 30	5	s
Constant 21	HEVC GEN minimum speed	-13500	1/min	double	Constant 21	HEVC GEN minimum speed	-13500	1/min
Constant 22	Maximum Speed of Electric Ma	13500.0	1/min	double	Constant 22	Maximum Speed of Electric Ma	13500.0	1/min
Constant 23	HEVC ENG motoring torque	-6	Nm	double	Constant 23	HEVC ENG motoring torque	-6	Nm
Constant 24	HEVC Brake Faktor	250	-	double	Constant 24	HEVC Brake Faktor	250	-
Constant 25	HEVC edrive Temp Limit	323.15	K	double	Constant 25	HEVC edrive Temp Limit 323.2	323.25	K
Constant 26	STST Temp Limit	323.25	K	double	Constant 26	STST Temp Limit 323.25	323.25	K
Constant 27	STST Cycle Duration min	60	s	double	Constant 27	STST Cycle Duration min 10	10	s
Constant 28	FULL_eBrake	0	Pa	double	Constant 28	FULL_eBrake	0	Pa
Constant 29	Engine min power at warm-up	12	kW	double	Constant 29	Engine min power at warm-up	2	kW
Constant 30	Engine min power	2	kW	double	Constant 30	Engine min power (change ch	2	kW
Constant 31	LV Battery Voltage	12	V	double	Constant 31	LV Battery Voltage	12	V
Constant 32	LV Battery SOC	50	%	double	Constant 32	LV Battery SOC	50	%

Figure 87 Hybrid control constant parameter re-calibration

5.6.4.2 Engine warm-up deactivation

Engine warm-up at the beginning of the trip can be turned off by following the steps below and the deactivation window is shown in Figure 88.

1. Select at Cycle Run (of each input simulation condition)
2. Select Course
3. Adjust temperature(b) column to be higher than 45 degree Celsius.

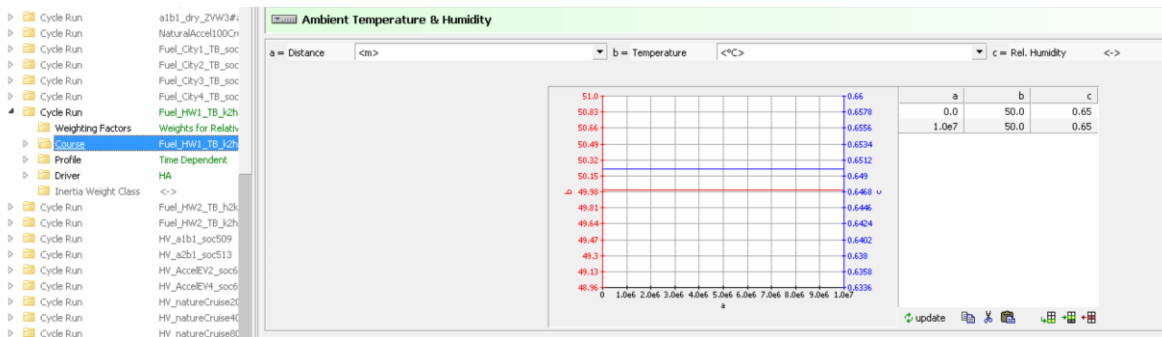


Figure 88 Engine warm up deactivation

5.6.4.3 Naturalistic SOC calculation activation

To deactivate the fixed soc calculation and activated the Naturalistic SOC calculation, it can be done by these steps below and the activation window is shown in Figure 89.

1. Select Cycle Run (of each input simulation condition)
2. Select weighting Factors
3. Under SOC Calculations, at Calculation Mode, select Deactivated.



Figure 89 Naturalistic SOC calculation activation

5.7 Results and Validation

This chapter provides simulation results and validations conducted and compared based on on-road (NGO) and private circuit (JARI) experiment dataset. It also mentions on the simulation condition input and control to ensure the consistency of the validations.

5.7.1 Simulation condition set-up

This section will explain the information that needs to be input to the simulation. For the fidelity of the simulation results, it is important to provide simulation conditions that correspond to the measurement conditions as much as possible. To control the simulation conditions, the requisite information is:

- Speed profile (Figure 90)
- Road grade profile (Figure 91)
- Initial SOC (Figure 92)
- AUX load (Figure 93)
- Wind speed effect (recommended)

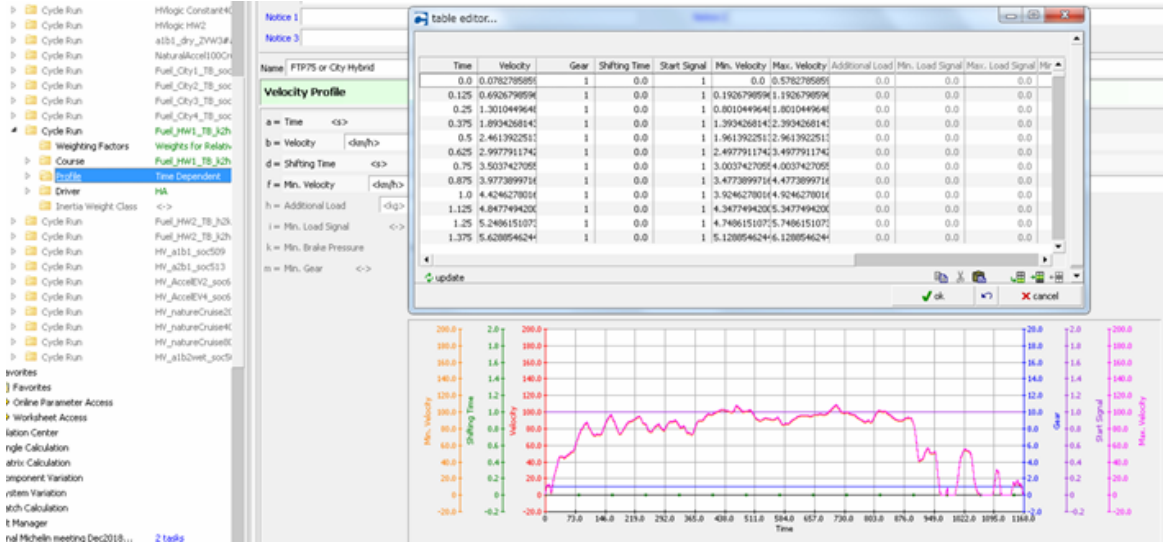


Figure 90 Speed Profile input window

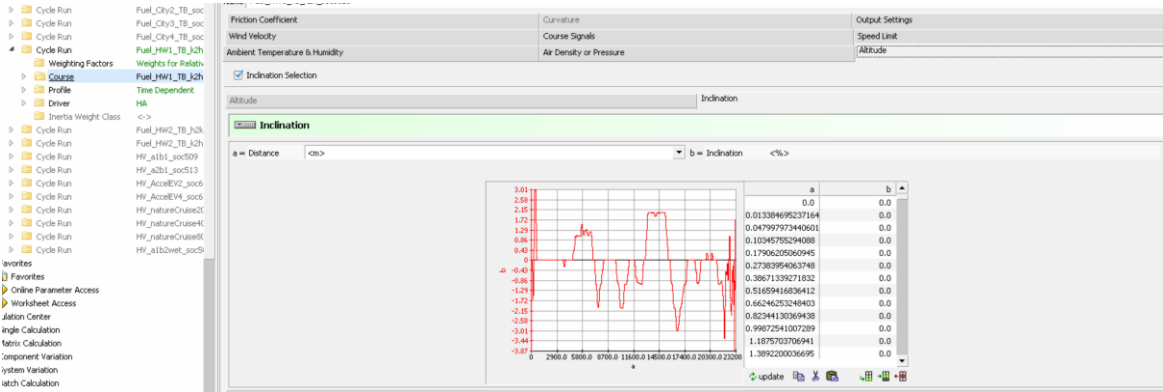


Figure 91 Road grade profile input window

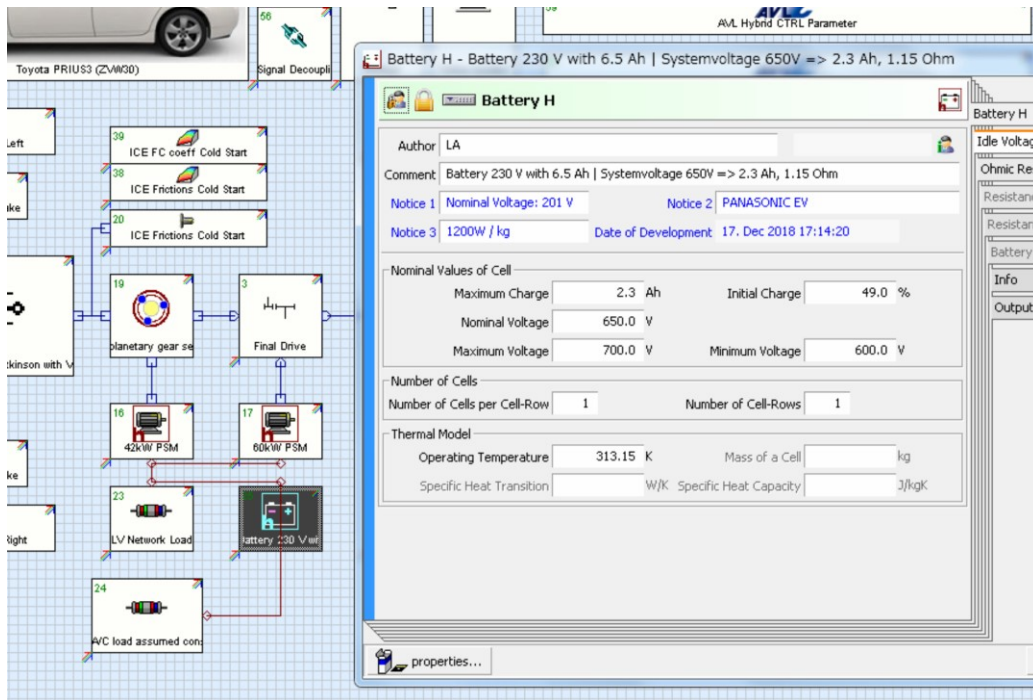


Figure 92 Initial SOC input window

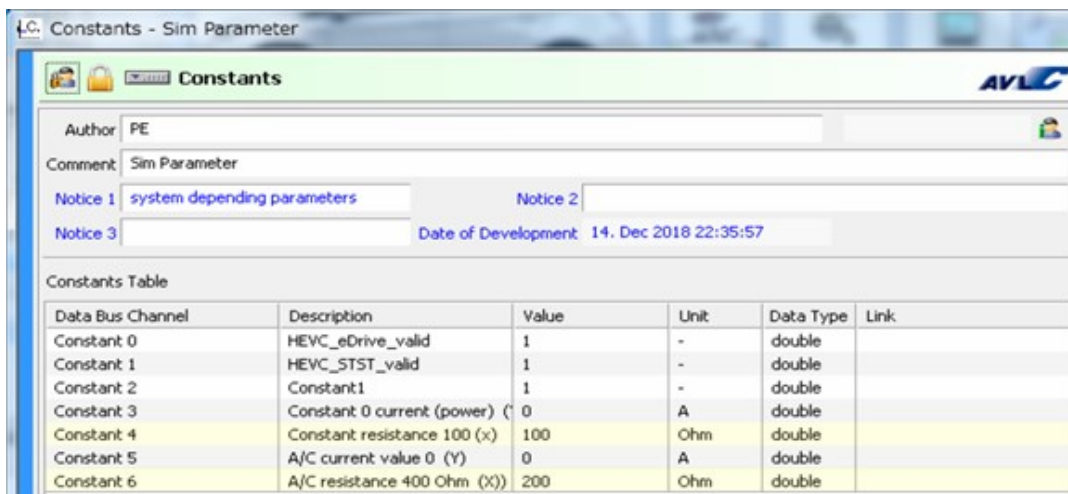


Figure 93 AUX power input window

5.7.2 Hybrid powertrain operation validation

This section presents simulation results from CRUISE Prius3 comparing among the measurement data, simulation results from the original CRUISE Prius3, and the simulation results from the recalibrated CRUISE Prius3. The results were plotted and named as Measurement, Sim CRUISEori, Sim ALL respectively. To evaluate the powertrain operation characteristics, the vehicle speed, engine rpm, and battery soc are compared. The validation was conducted based on three main driving scenarios: analytical driving, real-world city driving, and real-world highway driving.

5.7.2.1 Analytical driving scenarios

Figure 94 shows the simulation results of a1b1 driving pattern (JARI dataset). At 0-180s, all the powertrain operated in eDrive mode, and the battery soc depleted. The declination trend of the soc implies how the simulation interprets the input driving conditions to electrical energy. It also implies the accuracy of the battery and motor models. According to the results, Sim CRUISEori consumed a slightly lighter load than Sim ALL. Thus, we applied some adjustment on AUX power input to be more realistic compared to the measurement data.

Then, at 200s approximately, there was the main engine on. The Sim ALL turned the engine on at the same time as the actual engine, while the Sim CRUISEori's engine still remained off until 270s. As a consequence, discrepancy on soc prediction of Sim CRUISEori

was established. The second half of the trip Sim ALL also performs precise engine on/off in terms of engine start/shut down moment, and engine on/off state, while Sim CRUISEori still showed some minor misprediction at 400-460s. At 470-500s, the data shows that Sim CRUISEori failed to supply the power for the acceleration since the vehicle speed did not follow the assigned speed pattern strictly.

Considering the engine operation points, both Sim CRUISEori and Sim ALL presented the correlation between the measurement data only some extent; however, engine rpm was found underestimated at both high-speed driving peaks. As a result, the battery soc diverted from the measurement line.

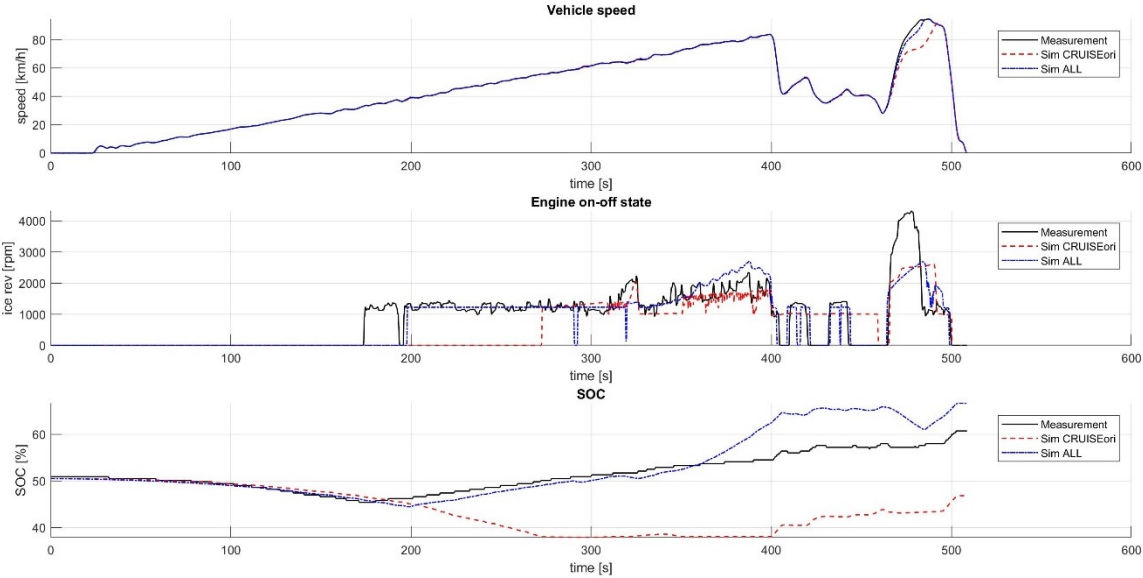


Figure 94 Simulation results under JARI_a1b1_Constant Acceleration driving conditions

Figure 95 illustrates another example of the simulation results conducted on naturalistic acceleration and constant speed driving at 20 km/h. This simulation aims to validate the transition between eDrive mode to light load driving mode (hybrid drive).

The acceleration at the beginning of the trip shows that Sim ALL provides more accurate engine start/shut down dynamic. Then, after the acceleration, the powertrains operated in eDrive mode. The soc depletion of Sim ALL compared to the measurement data implies that MG2 model, AUX load input, and driving power estimation are already well calibrated.

At 750s, the actual vehicle turned the engine on to charge the battery as a low speed charging cycle. However, CRUISE Prius3 simulation did not respond to this operation feature. As a result, the soc of both Sim CRUISEori and Sim ALL failed apart from the measurement data.

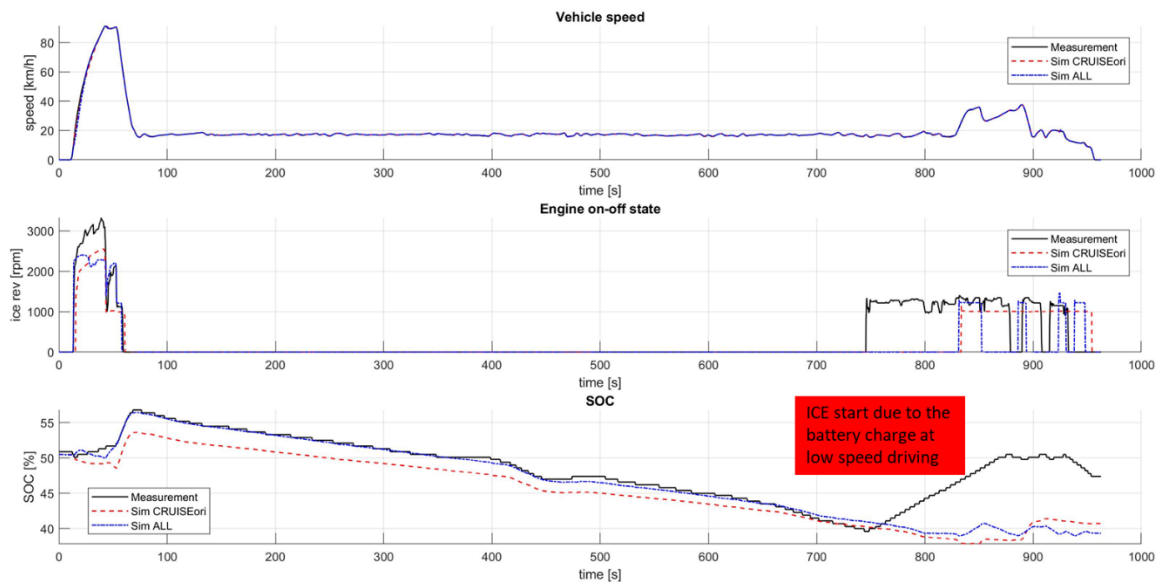


Figure 95 Simulation results under JARI Naturalistic acceleration from_0-100km/h and constant speed at 20 km/h driving conditions

5.7.2.2 Real-world city driving scenario

This section presents the simulation results under real-world driving conditions. The data contains a number of stop-and-go sessions at low-speed driving. These conditions allow the powertrain to operate in eDrive mode and light load mode. It is one of the most challenging conditions to observe the engine on/off characters of the powertrain simulation.

Figure 96 shows the simulation results under NGO CITY1 using the summer tire conditions. At the beginning of the trip, the actual engine turned on because of the low-speed battery charging cycle while both Sim CRUISEori and Sim ALL's engine did not turn into the charging session.

After 300s to the end of the trip, it shows that Sim ALL successfully adjusted the engine on/off characteristic of CRUISE Prius3 to behave more like to the actual vehicle. The engine start and shutdown points were precisely triggered at the exact moment with the actual vehicle. Even though there are some misprediction found, the results from Sim ALL show substantial improvement over the results from Sim CRUISEori. The engine on/off behavior of Sim CRUISEori appeared to be less dynamic, and less sensitive to the driving load fluctuation.

In another word, once the engine was operated at the right moment and the battery charging/discharging power was distributed correctly, the battery soc fluctuation became to have more similarly compared to the measurement data.

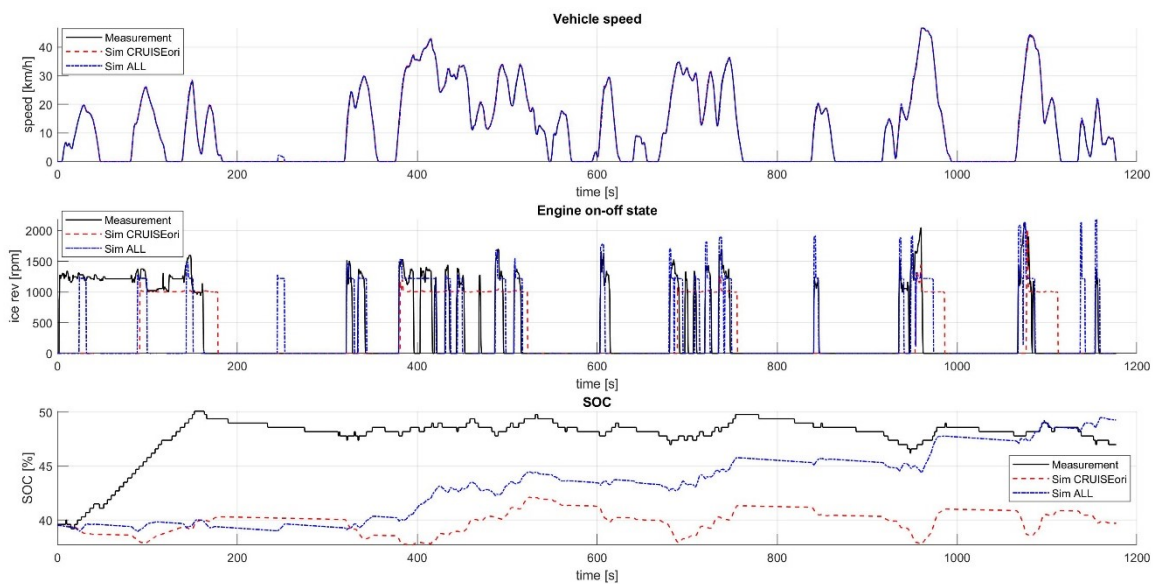


Figure 96 Simulation results under NGO_CITY1_SummerTire(B) driving conditions

Figure 97 shows comparative simulation results under NGO CITY3 using the summer tire conditions. According to the data, it also exhibits similar results compared to NGO CITY1. CRUISE Prius3 both Sim CRUISEori and Sim ALL failed to capture the low speed charging cycle at the beginning of the trip. Nevertheless, from 200ths, Sim ALL was capable of imitating all the major engine on/off operations, while the Sim CRUISEori did not show any corresponding engine operation compared to the measurement data.

For the engine's alternative power (battery charging power), Sim ALL was able to manage the battery power more similarly to the actual vehicle compared to Sim CRUISEori. However, some discrepancy was found as a gap between Sim ALL result and the measurement data. One of the reasons might be from the underestimated electrical auxiliary load. Since the A/C was turned on during the NGO experiment, and A/C generally consumed power as a duty cycle (on/off), but how A/C could be input to CRUISE Prius3 was just providing an average constant value. This problem can be noticed from Sim ALL which has smaller declination slop during depletion, larger inclination slope during charging.

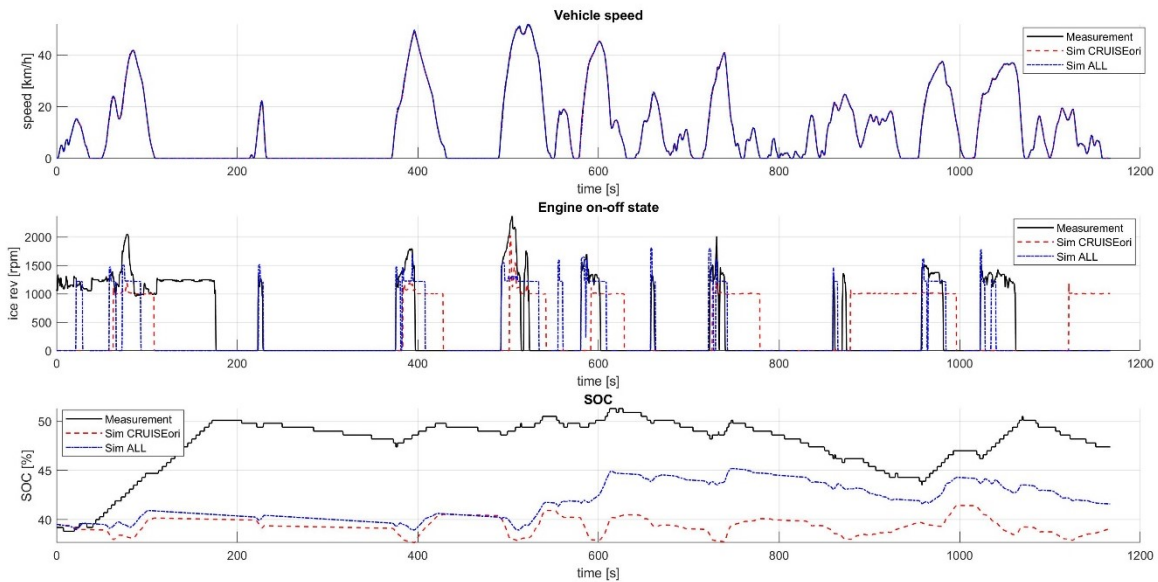


Figure 97 Simulation results under NGO_CITY3_SummerTire(B) driving conditions

5.7.2.3 Real-world highway driving scenario

This section presents the validation of the CRUISE Prius3 on real-world highway driving at which most of the time the speed is over 64 km/h. The engine is always on. Thus, these conditions are suitable for engine operation point selection and engine alternative power distribution monitoring.

Figure 98 shows the simulation results under NGO HW2 Hongo to Komaki using the summer tire. Both of Sim CRUISEori and Sim ALL showed a potential to capture the main engine on/off operation, though Sim ALL appeared to be more precise on the engine start and shut down moment.

For the engine operation point selection, Sim ALL could provide similar engine rpm fluctuation trend; however, it apparently contained underestimation in terms of magnitude. On the other hand, Sim CRUISEori seemed to provide a better engine rpm correlation compared to Sim ALL. However, in an aspect of the engine alternative power distribution, Sim CRUISEori seemed to establish inadequate battery power sustaining problem in which caused the abnormal battery soc depletion, and the battery remained at the minimum allowance soc almost 80% of the trip.

By observing Prius3 operation characteristics at high speed driving experiments, the powertrain dominantly operates at light load, medium-high load with battery charging, and medium-high load with battery discharging modes. Thus, some part of the engine power is distributed to sustain the battery. As a consequence, the battery soc usually remains high (50-70% approximately) during these high-speed driving conditions. These power management characteristics are also established in Sim ALL results as confirmed by Figure 98 and Figure 99.

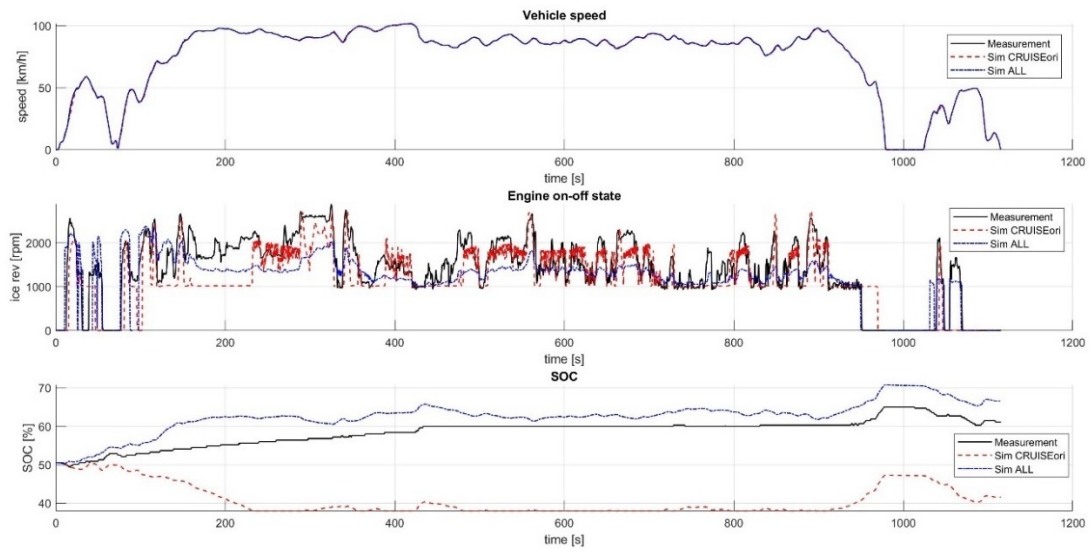


Figure 98 Simulation results under NGO_HW2_Hongo-to-Komaki_SummerTire(B)
driving conditions

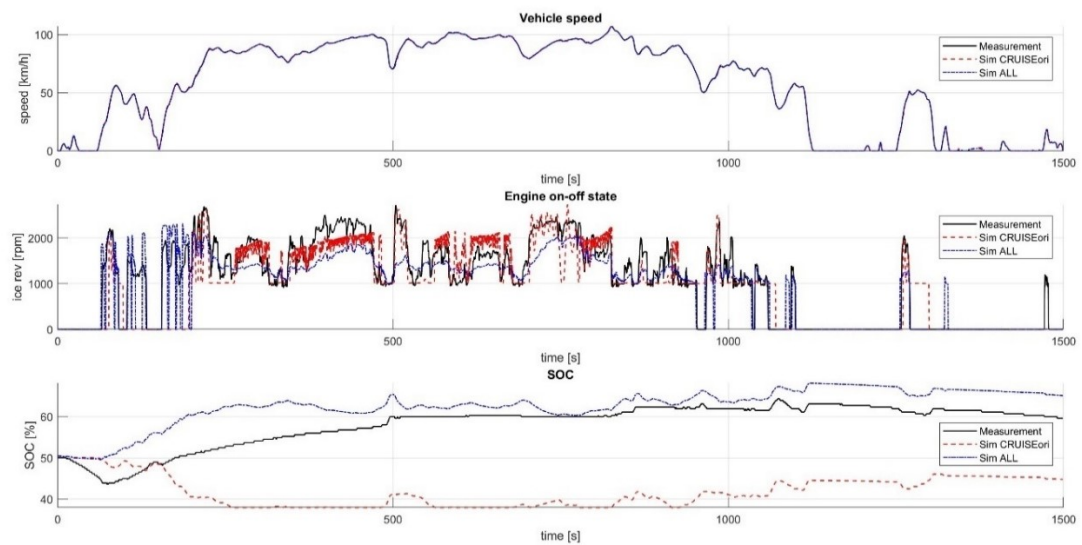


Figure 99 Simulation results under NGO_HW2_Komaki-to-Hongo_SummerTire(B)
driving conditions

5.7.3 Engine on time

In this section, the engine operation characteristics are evaluated in terms of percentage of the engine on time comparing among the measurement data, Sim CRUISEori, and Sim ALL results.

From Figure 100 and Figure 101, they illustrate the trend of Prius3's engine on the operation period. The engine operates less than 20% in the city driving, while the engine operates more than 60% on highway driving. Somewhat, the correct engine on time implies correct fuel utilization and powertrain operation.

For city driving conditions, Sim ALL significantly improved the engine on/off characteristics of the original CRUISE Prius3 simulation (Sim CRUISEori). Particularly in the city driving where the operation modes are switched frequently, Sim ALL properly captured the significant powertrain operations which resulted in the reduction of the engine on time prediction error from a range between 46.5-98.9% down to 5.4-21.5% or around 5 times. On highway driving, since the engine dominates the drive, the percentage of the engine on time does not show much difference. However, Sim ALL improved the prediction error from -1.4 - -4.3 to -1.3 – 0.8%.

The characteristic of the error of both Sim CRUISEori and Sim ALL seemed to produce overestimation on city driving, and underestimation on highway driving.

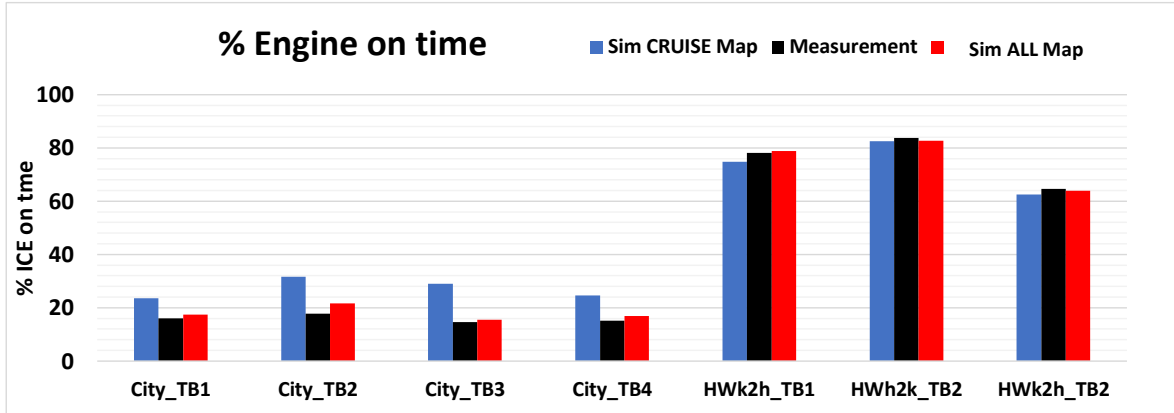


Figure 100 Summary of the engine on time percentage

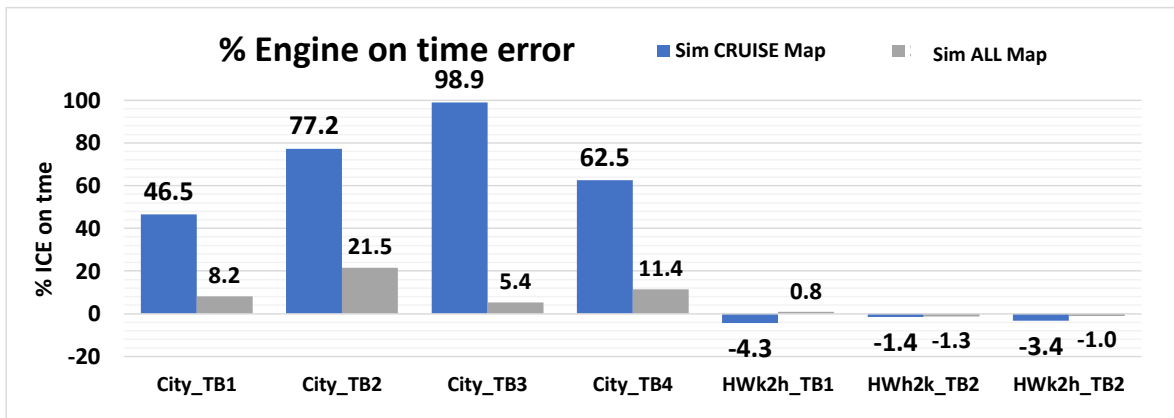


Figure 101 Summary of prediction error on the engine on time percentage

5.7.4 Fuel consumption validation

This section evaluates the fuel consumption prediction results by comparing the results among Sim CRUISEori, Sim ALL and the measurement data. Note that the difference between the initial and final soc was converted to equivalent fuel amount, and compensated

to the total fuel calculation. The total fuel consumption and percentage of the prediction error are shown in Figure 102 and Figure 103.

For Sim CRUISEori, the fuel consumption prediction were all found underestimated in both city and highway driving. The error was reported in a range between -28.6 - -39.6%. The average error in the city and highway were at 32.2% and 33.8% respectively.

Once the recalibration processed have been implemented, the fuel consumption prediction error was reduced and found in the range between 2.0 - -31.6. Particularly, for city driving condition, the fuel consumption results have been significantly improved. The error in the city was reported in a range between 2.0 - -2.7% (CITY Tb 3 was not included.). The average error was found at 1.8% which was 1/15 less than the error found in the original CRUISE Prius3.

For highway prediction, Sim ALL still has prediction error in a range between -13.4 - -21.7%. The average prediction error was found at 16.2% which is approximately 2 times more accurate. The error was suspected to be caused by the underestimate of the engine operation points and the unrealistic engine maps. Comparing the actual engine to CRUISE Prius3 simulation platform, the simulation defends the engine operation trajectory by a single curve input; however, the actual vehicle operates the engine on multi-operation trajectories depending on the operation modes.

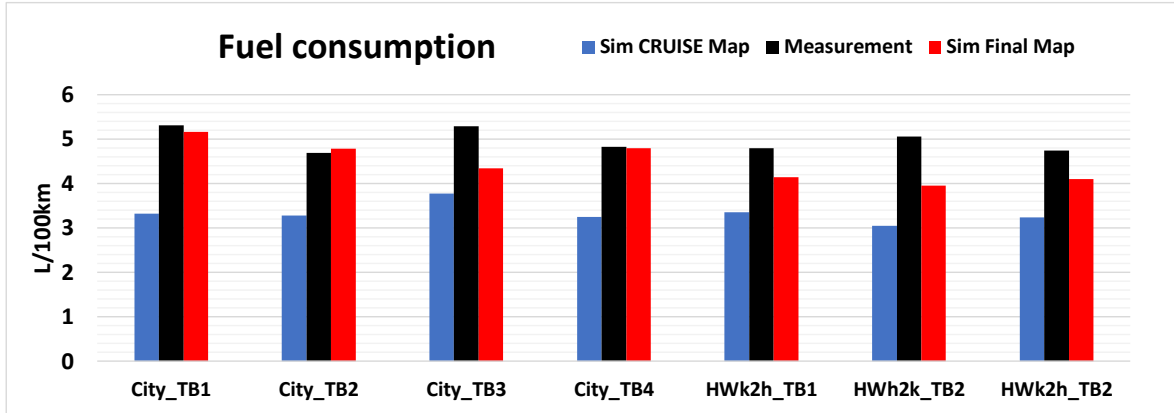


Figure 102 Summary of the fuel consumption prediction

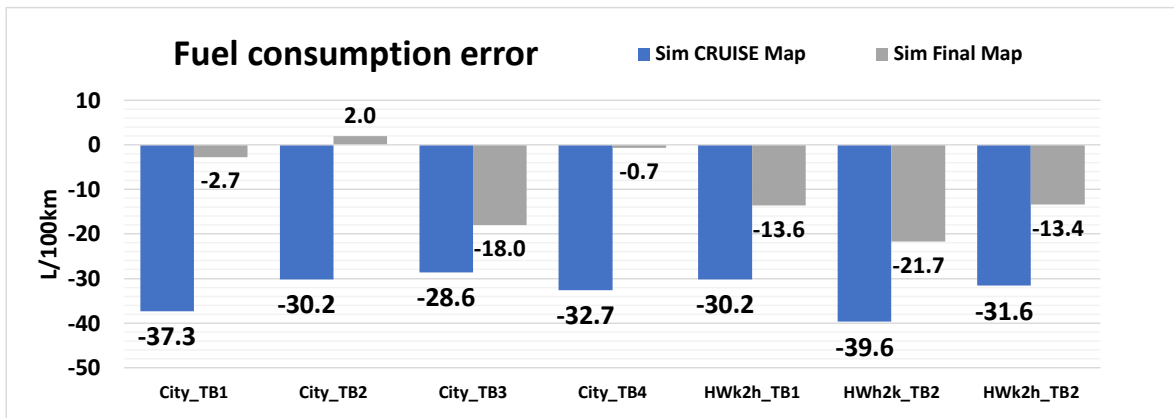


Figure 103 Summary of prediction error on the total fuel consumption

Figure 104 shows the relationship between the engine on time error and fuel consumption prediction error separated into the city and highway results. The error between fuel consumption and the engine on time seems to have a proportional relationship. The underestimated engine on time causes underestimated fuel consumption prediction. However, it is interesting to see that even the engine on time error is very small, the fuel

consumption is still offset approximately -15%. It indicated that the engine fuel consumption maps still required further improvement.

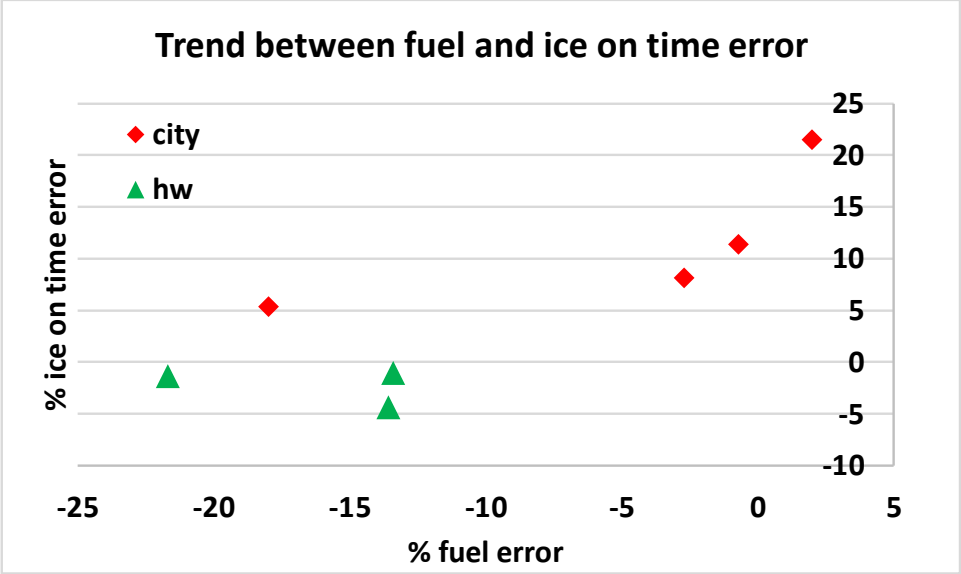


Figure 104 Relationship between the engine on time error and fuel consumption prediction error

5.8 Conclusion

This project had conducted a study on an investigation of hybrid vehicle powertrain operation mechanism, energy management, and performed an improvement on a commercial power-split hybrid powertrain simulation, AVL CRUISE Prius3. The 3rd generation of Toyota Prius was introduced to the study as a representative of the current hybrid vehicle fleet.

This study investigated the insight operation logic of Toyota Hybrid System (THS) by using the information available via HV ECU with some reverse engineering techniques. It was discovered that Prius3 operated its powertrain in 7 driving modes and 6 braking modes. These operation modes were selected and actuated based on several sophisticated pre-defined criteria that aimed to enable the engine to operate at the most efficient operation region.

Based on the characteristics of Prius3, AVL CRUISE Prius3 simulation was evaluated in terms of modeling structure, and prediction fidelity. Several limitations were discovered, such as limited access of the hybrid control in the black box, and the model structure platform that omits some important Prius3 features. A preliminary validation was performed to identify problems in the original powertrain simulation and to suggest for the possible solutions. The problems were prioritized based on their impact on the prediction fidelity and accessibility limitations. The problems were pointed out on unrealistic hybrid control, unrealistic battery sustaining and depleting unrealistic engine operation and fuel consumption underestimation. Thus, the solutions were proposed to recalibrated the maps that provided the criteria associated with these operation controls.

To achieve the map recalibration, data from Prius3 powertrain are the key. Thus, experiments were designed and conducted in order to acquire the dataset. It is important to design the experimental driving schedule to capture not only the dominant powertrain operation region in a tropical driving, but also extend the operation region of each component as much as possible. Moreover, selecting a proper experimental methodology will efficiently allocate an impeccable dataset.

Next step was to utilize the available dataset to construct the map; however, some of the key parameters required for the map construction were not acquirable. Thus, the power-split powertrain dynamic model was derived to estimate these key parameters. Moreover, some maps required data under specific conditioning, such as battery sustaining power, or regenerative braking. Thus, the knowledge on the powertrain operation is substantial for the interpretation of the data meaning. This step is considered to be one of the most important technique for the simulation improvement.

At the map recalibration state, most of the activities were to define the areas or curves that represented the major characteristics of the data. 14 maps and some other constant parameters were recalibrated and replaced into the original maps in CRUISE Prius3. A number of simulation set ups were tested for a purpose of minor map tuning, and validation.

According to the simulation results, the calibrated maps and parameters significantly improved the powertrain hybrid operation characteristics and also the fuel consumption prediction. The engine on/off behavior became more realistic in terms of engine start and shut down dynamic, especially in the city traffic driving. The prediction error range was reduced from 47 – 99% to 22 – 5.0%. For highway, the prediction error range was reduced from -4.3 – -1.4% to -1.30 – 0.8%.

According to the realistic prediction of the engine on/off and engine operation points in city driving, the fuel consumption results were significantly improved from the maximum error -37% to -2.7. Note that the CITY3 was excluded from the calculation due to excessive engine operation point misprediction. The average error was found at 1.8% at which the accuracy improved more than 15 times compared to the original CRUISE Prius3. For

highway data, the maximum fuel consumption prediction error was improved from -49 to -22%. The average prediction error was found at 16.2% which is approximately 2 times more accurate than the original CRUISE Prius3.

According to the results, it is confirmed that the methodology proposed in this study effectively improve CRUISE Prius3's powertrain operation to become more realistic, and represents the major unique features of Prius3. However, CRUISE Prius3 simulation still has several issues that require improvements. The further improvements could be suggested on engine operation point selection, engine fuel consumption map, and battery charging cycle at low speed. For the engine operation point selection and engine fuel consumption issues, the improvements can be partially done by adjusting BOOST pkW SOC map and Engine IL4 16V Fuel consumption map respectively. For the further improvements on the battery charging cycle at low speed and the engine operation point selection issues, they may need lower level modifications on the simulation platform or logic inside the black box.

Finally, we hope that the content in this study will allow you to be able to develop insight understanding based on one of the most promising hybrid configurations at the present of time, Toyota Hybrid System. Moreover, this study also provides the concepts of how to estimate, and extract those sophisticated hybrid powertrain features into a simulation state, including experimental techniques for hybrid vehicles that important for the modeling processes. Ultimately, this report will at least be a substantial guild line for powertrain simulation selection and validation for the future works.

CHAPTER 6

Microscopic Hybrid Vehicle Energy Consumption Modeling:

6.1 Development of Hybrid-Vehicle Energy-Consumption Model for Transportation Applications—Part I: Driving-Power Equation Development and Coefficient Calibration

This section is the first of a two-part of this research. The overall study presents a new methodology to improve the accuracy of hybrid vehicles' energy-consumption model over conventional transportation modeling methods. The first paper attempts to improve an equation for vehicles' driving-power estimation to be more realistic and specific for a particular vehicle model or fleet. The second paper adopts the driving-power equation to estimate the requested driving power. Then, the data are utilized to construct the hybrid-vehicle energy-consumption model, namely, the traction-force–speed-based energy-consumption model (TFS model). The main concept of the first paper is to utilize the power-split hybrid powertrain's accessible on-board diagnostics (OBD) dataset, and its dynamic model to estimate the total propulsion power. Then, propulsion power was applied as the main parameter for driving-power equation development and vehicle-specific coefficient calibration. For coefficient calibration, this study implemented the stepwise multiple regression method to select and calibrate an optimal set of coefficients. Results showed that

conventional driving-power equations Vehicle-Specific Power (VSP) LDV 1999 and VSP Prius3Spec provide low prediction fidelity, especially under high-speed (>80 km/h) and heavy-load driving (≥ 50 kW). In contrast, $DrvPW_{Prius3}$, proposed in this study, effectively improved prediction to become more accurate and reliable through all driving conditions and speed ranges. It dramatically helped to reduce prediction discrepancy over the conventional equations at heavy-load driving, from an R-square of 0.79 and 0.78 to 0.96. $DrvPW_{Prius3}$ also reduced the prediction error at high-speed driving from the maximal error of approximately -20 to -5 kW. This study also discovered that aerodynamics and rolling resistance were the primary factors that caused the prediction error of conventional VSP equations. In addition, results in this study showed that both of the approaches used to establish the P_{PTdrv} and $DrvPW_{Prius3}$ equations were valid for a power-split hybrid vehicle's driving-power estimation. For the coefficient-calibration part, the stepwise and multiple regression method is low-cost and simple, allowing to calibrate an appropriate set of optimal coefficients for a specific vehicle model or fleet.

6.1.1 Introduction and literature review

Vehicle driving power is one of the most significant parameters relating to vehicle operations that also directly affects emissions and energy consumption. In automotive powertrain control, the powertrain operation point, torque, and rotational speed are specified and controlled to achieve the desired instantaneous power demand (Wu, Song and Yu, 2014; Bohme and Frank, 2017). This parameter generally includes instantaneous driving power and

other types of power usage from auxiliary components, such as the air conditioner (A/C), headlight lamps, and liquid-circulation system (Pitanuwat *et al.*, 2017). Therefore, vehicle energy-consumption modeling initially estimates the requested driving power to identify the powertrain operation points, and then calculates the corresponding energy consumption (De Cesare, Cavina and Brugnoli, 2019).

In the transportation research field, vehicle energy-consumption modeling is a tool to estimate the impact of traffic conditions or vehicle driving activities on energy consumption and emissions. In the past few decades, several researchers have developed vehicle fuel-consumption models for microscopic transportation applications and intelligent-traffic-system (ITS) projects. For instance, real-time electrified-vehicle energy management, route selection, public-transportation management, powertrain-electrification policymaking, and autonomous vehicles' optimal fuel-driving-trajectory planning are active research fields.

The development of microscopic energy-consumption prediction models requires high prediction accuracy that is sufficient to capture the effect of driving fluctuations with a light computation load. Thus, modeling methods usually simplify the vehicle's energy-consumption characteristics by using statistical approaches and neglecting several details of the fundamental powertrain operation. One of the most conventional approaches throughout the past decades of research is to estimate instantaneous driving power and then establish the relationship between driving power and fuel-consumption rate (Faris, Rakha and Elmoselhy, 2014).

Jiménez, J. L. *et al.* (1999) formulated an equation for vehicle driving-power estimation called vehicle-specific power (VSP). This equation was derived on the basis of

Newton's second law. All substantial forces acting on the vehicle during driving were included, which are acceleration, road inclination climbing, aerodynamic drag, rolling resistance, and the vehicle's internal frictions. All these terms are expressed by Equation (47) in the form of a power unit:

$$\begin{aligned}
 VSP \text{ [watt]} = m & \quad (47) \\
 \times v_{veh} & \left[a_{veh}(1 + \varepsilon_i) + g \times \sin\left(\tan^{-1}\left(\frac{h}{l}\right)\right) + g \times C_r \right] \\
 + \frac{1}{2} \rho_{air} C_d A & \times v_{veh} (v_{veh} - v_{wind})^2
 \end{aligned}$$

The explanation of the variables are given in the following paragraph. The VSP equation has been incorporated in several fuel-consumption models, including the motor-vehicle emission simulator (MOVES) released by the United States Environment Protection Agency (EPA) (Yao *et al.*, 2013; Faris, Rakha and Elmoselhy, 2014; US EPA, 2019). Jiménez *et al.* also suggested a set of specific coefficients for light-duty-vehicle (LDVs) applications. The VSP LDV1999 equation is expressed as Equation (47):

$$\begin{aligned}
 VSP_{LDV1999} \text{ [watt]} = m & \quad (48) \\
 \left[1.1 a_{veh} v_{veh} + 9.81 \times \right. & \\
 \left. \sin\left(\tan^{-1}\left(\frac{h}{l}\right)\right) v_{veh} + 0.132 v_{veh} + 0.000302 v_{veh}^3 \right], &
 \end{aligned}$$

where ε_i is the mass factor inertia term (0.1); g is gravitational acceleration (9.81 m/s²); C_r is the rolling resistance coefficient (0.132); v_{veh} and a_{veh} are vehicle speed (m/s)

and acceleration (m/s^2); is and $\frac{1}{2}\rho_{air}C_dA$ is the aerodynamic drag coefficient term (0.000302). The effect of wind speed ($v_{wind} m/s$) is neglected.

A number of studies have reported high correlation between VSP and fuel consumption. Furthermore, the most prominent advantage of VSP is that it only requires externally measurable parameters, vehicle speed, acceleration, road grade, and wind speed, to calculate driving power (Faris, Rakha and Elmoselhy, 2014; Zhang *et al.*, 2014; Duarte, Gonçalves and Farias, 2016; Song, Yu and Wu, 2016). These parameters can be acquired by a global positioning system (GPS), inertia measurement unit (IMU), and wind-speed sensor, of which the installation does not require any additional vehicle modifications .

Since 1999, a great number of studies have applied the conventional VSP equation and coefficients for LDV to estimate the driving power of passenger cars regardless of vehicle model and technology. VSP has been utilized to estimate driving power to construct fuel-consumption and -emission models, and conduct further analysis on the influential factors or contributors to vehicle fuel consumption (Zhai, Christopher Frey and Roupail, 2011; Graver, Frey and Choi, 2011; Yao *et al.*, 2013; Duarte *et al.*, 2014; Zhang *et al.*, 2014; Wu, Song and Yu, 2014; Wyatt, Li and Tate, 2014; Zhang and Yao, 2015; Holmén and Sentoff, 2015; Duarte, Gonçalves and Farias, 2016; Hu, Frey and Washburn, 2016; Rodríguez *et al.*, 2016; Song, Yu and Wu, 2016; Zhou and Jin, 2017; Pitanuwat *et al.*, 2017). Nevertheless, before implementing the VSP equation and the LDV coefficients, none of them has performed validation to confirm prediction accuracy of whether the equation and coefficients estimated by the vehicles from the last 20 years can still accurately capture a vehicle or

studied vehicle fleet. Particularly at high-speed driving, the impact of an inaccurate aerodynamic coefficient may cause a dramatic error since it is multiplied with v_{veh}^3 .

Only some studies in the transportation research field have substituted actual vehicles' specific information, such as mass, aerodynamic-drag coefficient, rolling-resistance coefficient, and frontal area, into the driving-power equation (Pitanuwat and Sripakagorn, 2015). Some studies also implemented a more complex rolling-resistance term by introducing C_{roll} , C_1 , C_2 , and normal force action on the tires. They also neglected mass factor inertia and the wind-speed effect (Onori, Serrao and Rizzoni, 2016b; Al-Samari, 2017; De Cesare, Cavina and Brugnoli, 2019). The driving-power estimation equation is expressed as Equation (48):

$$P_{drv} [\text{watt}] = v_{veh} \left[ma_{veh} + mg \sin \theta + mg \cos \theta \times \frac{C_r}{1000} (C_1 v + C_2) + \frac{1}{2} \rho_{air} C_d A \times v_{veh}^2 \right] \quad (49)$$

In the automotive research field, driving-power equations are formulated by higher complex equations, and some of the coefficients or constants require particular measurement. For instance, some studies estimated the aerodynamic-drag and rolling-resistance terms with

$$P_{aero} + P_{roll} = v_{veh} (\beta_1 v_{veh}^2 + \beta_2 v_{veh} + \beta_3), \quad (50)$$

β_1 , β_2 , and β_3 , called the road-load coefficients, can be identified by a coast-down experiment. Some studies utilized direct estimation via Equation (46) or (48) and added

Equation (49) to capture other road loads (Fazal U. Syed *et al.*, 2006). Table 19 shows a summary of the available driving-power estimation methods classified by each contributor. (Fazal U. Syed *et al.*, 2006; Sciarretta *et al.*, 2014; Pitanuwat and Sripakagorn, 2015; Fiori, Ahn and Rakha, 2016, 2018; Al-Samari, 2017; Böhme and Frank, 2017; Pitanuwat *et al.*, 2017; De Cesare, Cavina and Brugnoli, 2019)

Table 19 Driving-power estimation classified by contributing factors.

Power Utilization	Estimation
Acceleration	$m(1 + \varepsilon)v_{veh}a_{veh}$ or $mv_{veh}a_{veh}$
Rolling resistance	$mg \cos \theta C_r(C_1v_{veh}^2 + C_2v_{veh})$ or mgC_rv_{veh}
Aerodynamic drag	$\frac{1}{2}\rho_{air}AC_dv_{veh}(v_{veh} - v_{wind})^2$
Road grade	$mgv_{veh} \sin \theta$
Road-surface friction	$mg \cos \theta \mu_{surface}v_{veh}$ or neglect
Others	$\beta_1v_{veh}^3 + \beta_2v_{veh}^2 + \beta_3v_{veh}$ or neglect

For automotive manufacturers, the Society of Automotive Engineers (SAE) has issued a standard procedure for road-load experiment and estimation called the SAE J2263 standard (US EPA, 2010; Kim *et al.*, 2016; Kühlwein, 2016). Procedures for the test-vehicle and -track preparation, minimal requirements for data acquisition, coast-down test procedure, and atmospheric-condition control are recommended (US EPA, 2010). After obtaining vehicle-speed–time data during the coast down, road-load coefficients (β_1 , β_2 , and β_3) can

be obtained by applying quadratic regression to driving-force and vehicle-speed data. Driving force can be calculated by vehicle-speed and time data (Ahlawat, Bredenbeck and Tatsuo Ichige, 2013; Kühlwein, 2016). Alternatively, direct wheel-force/torque measurement or wind-tunnel and rolling-resistance measurements on roller methods are also optional (Ahlawat, Bredenbeck and Tatsuo Ichige, 2013; Kühlwein, 2016).

According to earlier research, the VSP LDV1999 equation and its recommended coefficients have been conventionally incorporated for decades in a large number of studies and vehicle modeling in the transportation fields. Driving power is one of the most substantial parameters in vehicle fuel-consumption modeling. Several papers have stated that inaccuracy of road-load coefficients can lead to a discrepancy in fuel-consumption results (Ahlawat, Bredenbeck and Tatsuo Ichige, 2013; Kühlwein, 2016). Powertrain and transmission technologies have been progressively developed. Vehicle efficiency and performance have also been improved, especially for hybrid powertrains that contain highly sophisticated configuration. Thus, it is indispensable to update the conventional VSP equation so it is appropriate and realistic for the current vehicle models or fleets. Once fidelity of driving power is confirmed, it helps improve the accuracy of a calculation process or analysis.

Most traditional road-load-measurement methods require high standards of test facilities, equipment, and intensive labor for preparation and experiments, which come with a high cost and are time-consuming. Furthermore, these methods are not practical for applications in all the studied vehicle groups. As on-board-diagnostics (OBD) data are part of a basic dataset and are usually recorded during a transportation survey, this study proposes a method to utilize this dataset to calibrate the driving-power equation's coefficients. The

objectives of the study in Part I are to (1) develop and update the driving-power estimation equation for series-parallel hybrid vehicles; (2) propose an alternative methodology to calibrate the optimal set of coefficients for a particular vehicle model or fleet without any requirement of vehicle-specific information, but using only the OBD database; and (3) provide prediction-error analysis and comparative validation between conventional VSP methods and the newly developed driving-power equation.

The second part of this study (Part II) presents the energy-consumption prediction modeling for hybrid vehicles called the traction-force–speed-based model (TFS) (Pitanuwat, Aoki, Iizuka, *et al.*, 2019). This method was developed to suppress the prediction error caused by fluctuation of hybrid powertrain efficiency between multioperation modes. The driving-power equation established in Part I is utilized in hybrid-vehicle driving-power estimation and model construction in Part II.

6.1.2 Methodology

To develop the driving-power estimation equation and calibrate the optimal set of coefficients for hybrid vehicles, an analytical experiment was conducted on the third generation of Prius cars (Prius3) to collect a substantial database. According to existing equations in the earlier literature, all terms were reanalyzed. A stepwise algorithm was applied to evaluate the significance of each equation term and eliminate insignificant correlation terms from the equation. Then, this study applied multiple regression to calibrate an optimal set of coefficients for Prius3. This study aimed to acquire the dependent variable,

which is the hybrid powertrain propulsion power. To achieve that, this study applied the fundamental of dynamics of a power-split device to formulate the dynamic equation of Prius3's powertrain. On the basis of the Prius3 dynamic equation, we estimated the total output propulsion power from the hybrid powertrain, which combines power from the engine and motor/generator sources, and utilized it as the dependent variable. In other words, this study proposes a method to formulate the driving-power equation without direct measurement of vehicle-specific constants. Instead, it utilized accessible OBD data to estimate powertrain driving power, and then used them to calibrate an optimal set of vehicle-specific constants.

6.1.2.1 Data Acquisition and Experiment Design

An analytical experiment was designed and conducted at Japanese Automobile Research Institute (JARI) Shirosato, in the outer-ring test circuit. The circuit profile consisted of a long straight flat path, several corners, and slopes. The test vehicle was a Prius3 with 215/45R17 tires. Tire pressure was controlled according to the vehicle's standard value before the experiment. Total vehicle weight, including passengers and equipment, was 1625 kg, as measured on site.

In this study, the data-acquisition system was prepared to record two datasets. First, externally measurable parameters were recorded, including vehicle speed, acceleration, road grade, and wind speed, to formulate the driving-power estimation equation. An integrated GPS and IMU called Ninja Box was installed inside the middle console to measure vehicle

speed, acceleration, and road grade. A Pitot tube DT-8920 was equipped on top of the vehicle roof to measure wind speed. Second, the internally measurable parameters from the hybrid control unit (HCU) were measured, including the torque and rotational speed of the engine, and MG1 and MG2, to estimate the dependent variable for the multiple regression process. The hybrid powertrain data were accessed by Control Area Network (CAN) data via the on-board-diagnostics (OBD) port by using a Toyota Intelligent Tester II (IT2). This equipment provided a sevenfold higher sampling rate compared to other available Bluetooth/Wifi OBD scan tools available on the market. However, IT2 is not capable of simultaneously accessing HCU and fuel-consumption data. To achieve that, propeller-type fuel-flow meter DAE FMTD20 was installed in the engine compartment between fuel tank and engine. In order to synchronize the fuel-consumption data to the HCU data, we also installed external Hall effect current sensor HOP200 LEM at the high-voltage battery and recorded these two data types with the same data logger. Then, battery-current data were utilized to synchronize fuel and HCU data. To synchronize wind-speed and Ninja Box data with HCU data, we used vehicle speed as a median. The cross-correlation technique was implemented to synchronize these four data sources in the same timeline.

For the experiment schedule, the driver was instructed to follow analytical speed patterns, which were maximal acceleration and braking, cruise speed, coast down, constant acceleration and deceleration, naturalistic free driving, and e-drive maximum power driving. These speed patterns were deliberately designed to capture variety in powertrain activities, from typical driving to maximum drivability regions and hybrid operation logics, including realistic driving situations. The advantage of the analytical driving patterns is that they

contain simple driving activities that make it possible to understand operation transitions in hybrid vehicles, and experiment conditions are more controllable. At the beginning of the trips, the battery's initial state of charge was set between 45% and 50%. The sample size of this dataset was more than 135,000 data points, recorded at an 8 Hz sampling rate. Figure 1 shows the equipment setup and conduct during the experiment.

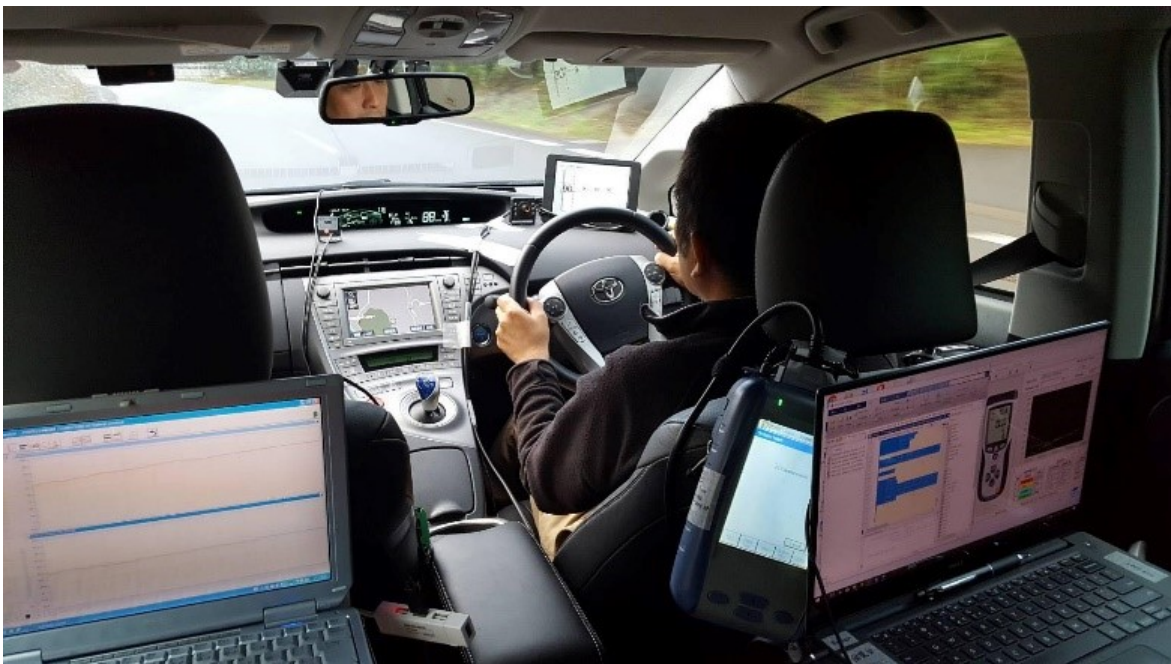


Figure 105 Analytical experiment on third-generation Prius (Prius3) at Japanese Automobile Research Institute (JARI) Shirosato.

6.1.2.2 Power-Split Hybrid-Powertrain Dynamic-Equation Formulation

This section explains the Prius3 hybrid powertrain's dynamic-equation derivation. These equations were utilized for calculating powertrain propulsion power by using input from accessible CAN data: ω_{MG1} , τ_{MG1} , ω_{MG2} , τ_{MG2} , and ω_{Ice} . Then, propulsion power was used to represent the vehicle's driving power as a dependent variable during the coefficient-calibration process.

The Prius3's powertrain configuration consists of three main powertrain components: Atkinson cycle engine, motor/generator 1 (MG1), and motor/generator 2 (MG2). MG1 is recognized as an electric generation motor, and MG2 is recognized as a propulsion motor. Power flows in these three components are integrated via a planetary gear set called a power-split device. Between the ring gear of the main planetary gear and MG2, Toyota added a speed-reduction gear, which is a planetary gear set with a fixed carrier to reduce MG2 speed and increase torque to be optimal for driving. The powertrain structure is shown in Figure 2. The engine is engaged with the carrier that holds all pinions inside the carrier case. MG1 and MG2 are mounted with the sun and ring gears, respectively.

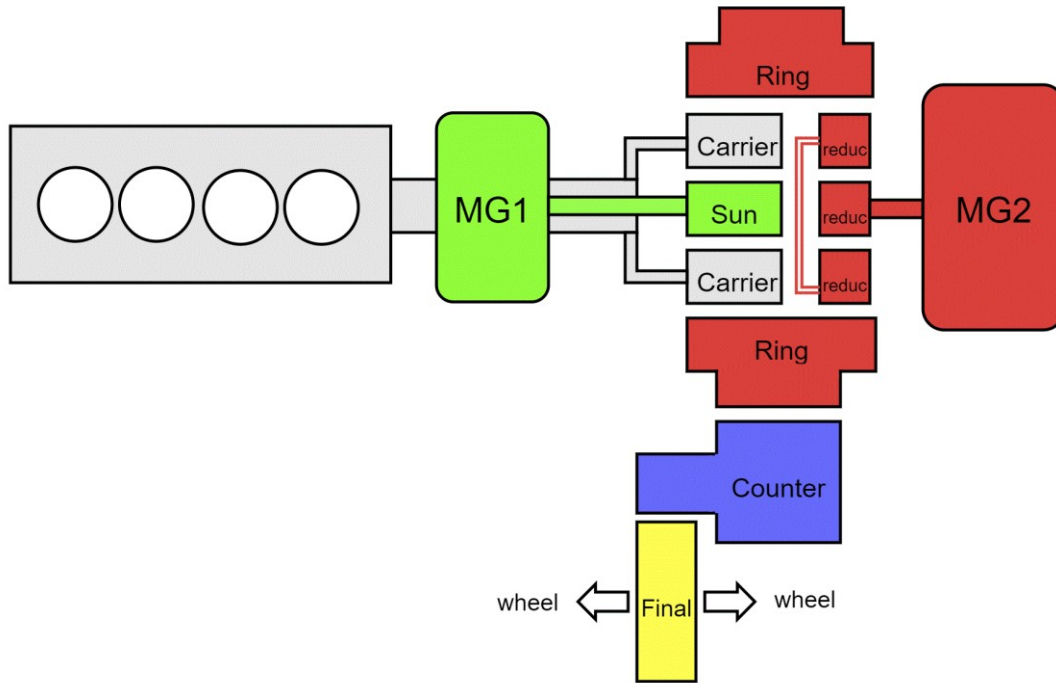


Figure 106 Prius3 powertrain structure.

The engine is considered as the primary power source for driving and battery recharging. Power from the engine is always split into two paths, sun and ring gear, via power-split device transmission. The engine power transmitted to the sun gear flows to MG1, which mainly generates engine power to electricity and distributes power to the battery, MG2, or auxiliary components, such as the air conditioner and pumps. MG1 also acts as a starter and engine-/vehicle-speed controller. The engine power transmitted to the ring gear flows directly to the wheel and/or to MG2, which acts as the main driving motor, regenerative braking generator, and driving-torque-assisting motor. In some situations, the MG2 is also used as a generator to absorb engine-power residue and store power in the battery. The

sun gear is balanced with the electricity-generation torque from MG1. This MG1 generation torque also enables the engine torque to transfer to the ring and wheels. However, this hybrid system also utilizes MG1 as an engine-speed controller by operating MG1 in the motor mode. All the torque components from the powertrain are denoted in a positive direction. By applying Newton's second law ($\sum \tau = I\omega$) at the carrier and sun gear, the engine torque (τ_{ice}) and torque transferred from the engine to the sun ($\tau_{C>S}$) can be expressed as Equations (50) and (51), respectively:

$$\tau_{ice} = \dot{\omega}_{ice}(I_{ice} + I_C) + \tau_{C>R} + \tau_{C>S}, \quad (51)$$

$$\tau_{C>S} = \dot{\omega}_{MG1}(I_{MG1} + I_S) - \tau_{MG1}. \quad (52)$$

Assuming a steady-state torque split from the engine to the sun and ring gear, the torque transferred from engine to ring ($\tau_{C>R}$) can be expressed as Equation (52)

$$\tau_{C>R} = \frac{R}{(R+S)} \tau_{ice} = \frac{R}{S} \tau_{C>S}. \quad (53)$$

Equation (53) represents the engine torque and can be obtained by substituting Equations (50) and (51) in Equation (52). This equation indicates that engine torque is a product of both engine and MG1 motion:

$$\tau_{ice} = \dot{\omega}_{ice}(I_{ice} + I_C) + \left(\frac{R+S}{S}\right)[\dot{\omega}_{MG1}(I_{MG1} + I_S) - \tau_{MG1}]. \quad (54)$$

At the ring gear, the engine-torque split to the ring gear is combined with the torque from MG2. Between MG2 and ring gear, there is MG2 speed-reduction planetary gear of which the carrier is stationary; the gear ratio is expressed by G_r . Then, total powertrain propulsion torque is transferred to wheels passing through the counter gear and final gear. Gear ratios are denoted as G_c and G_f . After applying $\sum \tau = I\omega$ to the wheels, Equation (54) is yielded. To calculate wheel rotational speed (ω_{wheel}), it is recommended to use MG2's rotational speed, since MG2's rotational speed sensor provides much higher precision than the vehicle-speed sensor does. The associated equation is expressed as Equation (55):

$$\left(\frac{\tau_{MG2}}{(G_r \cdot G_c \cdot G_f)}\right) + \left[\left(\frac{R}{R+S}\right) \tau_{ice} \cdot \frac{1}{G_c \cdot G_f}\right] - \tau_{drv_resist} - \tau_{brake,mech} = \dot{\omega}_{wh} \left\{ \frac{I_R}{(G_c \cdot G_f)} + \frac{I_{MG2}}{(G_r \cdot G_c \cdot G_f)} + I_{wh} \right\} \quad (55)$$

$$\omega_{wh} = (G_r \cdot G_c \cdot G_f) \omega_{MG2} \quad (56)$$

Thus, when mechanical braking is not being applied, powertrain driving torque (τ_{PTdrv}) must satisfy the required torque for driving acceleration and the required torque to overcome all driving resistances: rolling resistance, aerodynamic drag, road grade resistance, and other powertrain losses. This term aims to represent vehicle driving activity and is expressed by τ_{drv_resist} . Driving-torque and -power (P_{PTdrv}) equations are expressed as Equations (56) and (57), respectively:

$$\begin{aligned}
\tau_{PTdrv} &\cong \tau_{drv_{resist}} & (57) \\
&\cong \left(\frac{\tau_{MG2}}{(G_r \cdot G_c \cdot G_f)} \right) + \left[\left(\frac{R}{R+S} \right) \tau_{ice} \times \frac{1}{G_c \cdot G_f} \right] \\
&- \dot{\omega}_{wh} \left\{ \frac{I_R}{(G_c \cdot G_f)} + \frac{I_{MG2}}{(G_r \cdot G_c \cdot G_f)} + I_{wh} \right\},
\end{aligned}$$

$$P_{PTdrv} = \tau_{PTdrv} \omega_{MG2@Wh}. \quad (58)$$

P_{PTdrv} , calculated by the Prius3's powertrain dynamic equation, is used in VSP coefficient calibration and optimization.

6.1.2.3 Vehicle-Driving-Power Equation Formulation and Coefficient Calibration

This section presents a methodology for driving-power equation formulation and Prius3 coefficient calibration. First, the stepwise algorithm was applied to analyze the significance of each term and select the significant terms into the final driving-power equation. This step aimed to simplify the equation, and minimize the complexity of data acquisition and model updating. Then, coefficients and specific vehicle constants were calibrated on the basis of the multiple regression method as expressed in Equation (58):

$$Y = \beta_1 x_1 + \beta_2 x_2 + \beta_3 x_3 + \dots + \beta_n x_n + \epsilon. \quad (59)$$

To investigate the significance of the equation terms, the forward–backward stepwise algorithm was implemented with the multiple regression process. This algorithm

automatically eliminates and selects variables in the model on the basis of quality of fitness. The process begins with regressing each variable term (x_i) with the independent term (Y). The term that provides the lowest p -value, which must be lower than a specified entrance tolerance, was initially included into the equation. Next, multiple regression was applied to test the next candidate term. The term was selected into the equation by the same p -value criteria; however, the removal process also took place at this stage. In the removal process, if any terms that were included into the model were found to have a p -value larger than the removal-tolerance level, the term that contained the largest p -value was removed from the model. In this study, the entrance tolerance and the removal tolerance were set at a p -value smaller than 0.1 and larger than 0.15, respectively.

According to the equation terms frequently used in the literature in Table 20, this study arranged the equation terms into two different combinations described as Independent Variables (Indt var.) 1 and 2 in Table 2. Independent Variable 1 represents the basic driving-power equation that includes all conventional contribution terms. Independent Variable 2 represents the detailed estimation equation, which includes all contribution terms existing in the literature review. In the coefficients column, the left column describes the signs denoted for each coefficient term that is calibrated by the multiple regression method. The right column shows the definition of the derived coefficients from the theoretical conservative energy equation. The dependent variable (Y_1) was P_{PTdrv} . Data in this process excluded data from when reverse driving and mechanical braking were actuated. After the outlier was removed, the dataset obtained more than 98,000 samples. The best-candidate equation was selected on the basis of R-square and error-residue distribution.

Table 20 Independent-variable (Indt var.) sets for stepwise variation process.

Terms	Coefficients		Indt var. 1 (X ₁)	Indt var. 2 (X ₂)
Acceleration	β_{acc}	m	$v_{veh}a_{veh}$	$v_{veh}a_{veh}$
Road grade	β_{grd}	mg	$v_{veh} \sin \theta$	$v_{veh} \sin \theta$
Aerodynamic drag	β_{aero}	$\frac{1}{2}\rho_{air}AC_d$	$v_{veh}(v_{veh} - v_{wind})^2$	$v_{veh}(v_{veh} - v_{wind})^2$
Rolling resistance	β_{roll1}	mgC_rC_1	-	$v_{veh}^2 \cos \theta$
and road friction	β_{roll2}	mgC_rC_2	$v_{veh} \cos \theta$	$v_{veh} \cos \theta$
	β_{e1}	-	-	v_{veh}^3
Other road loads	β_{e2}	-	-	v_{veh}^2
	β_{e3}	-	-	v_{veh}

6.1.3 Results and Discussion

Table 21 shows the coefficient-calibration results found on the basis of P_{PTdrv} data. Results include the equations' coefficients, standard deviation (SD), and the p -value obtained from the two different sets of independent-variable equations (Indt var. 1 and 2). According to the results, p -values indicate that acceleration, road-grade climbing, and rolling resistance were the primary contributors to vehicle power utilization. This table also shows the comparison of the goodness of fit between Indt var. 1 and d 2's coefficients, the conventional VSP for LDV's coefficients (VSP LDV1999), and the conventional VSP with Prius3's specific parameters' coefficients (VSP Prius3Spec) by using R-square. R-square results were

separated into light-load-driving (<50 kW) and heavy-load-driving (≥ 50 kW) ranges to clarify the prediction accuracy of the four equations.

In the light-load-driving range, all four equations provided a high R-square at a satisfying level. R-squares associated with Indt var. 1 and 2 equations were found at 0.96, while the R-squares of VSP LDV 1999 and VSP Prius3Spec were found at 0.93 and 0.94, respectively. Nevertheless, this study discovered that the conventional VSP equation of VSP LDV1999 and VSP Prius3Spec provided significantly lower R-squares once they were under the heavy-driving load. The R-squares of VSP LDV 1999 and VSP Prius3Spec were reduced to 0.79 and 0.78, respectively, while the R-squares of Indt var. 1 and 2 remained at 0.96 throughout the light- and heavy-load-driving ranges. In other words, the new coefficient sets for Prius3 obtained in Indt var. 1 and 2 improved driving-power prediction during heavy-load driving by 21% to 22% compared to the conventional VSP equations.

Since Indt var. 1 and 2 provided R-squares at the same level during both light- and heavy-load driving, this study selected the Indt var. 1 equation to represent the Prius' driving-power estimation equation for further analysis, called $DrvPw_{Prius3}$. Furthermore, Indt var. 1 seemed to provide a good balance between prediction accuracy and calculation complexity. The newly calibrated driving-power equation is expressed as Equation (59). To some extent, results indicated that applying complex rolling-resistance terms $mg \cos \theta C_r (C_1 v_{veh}^2 + C_2 v_{veh})$, and the other road-load term, $\beta_1 v_{veh}^3 + \beta_2 v_{veh}^2 + \beta_3 v_{veh}$, included in Indt var. 2, did not seem to provide significant prediction improvement compared to Indt var. 1:

$$\begin{aligned} DrvPw_{Prius3} = & 0.9963 m \times v_{veh} \times a_{veh} + 1.168 mg \times v_{veh} \sin \theta \\ & + 1.523 \rho_{air} v_{veh} (v_{veh} - v_{wind})^2 \\ & + 0.0129 mg \times v_{veh} \cos \theta. \end{aligned} \quad (60)$$

Table 21 Coefficient calibration for Prius3 driving-power equations.

Equations	Coefficient	SD	<i>p</i> -Value	R ²	
Indt var. 1 (X ₁)	β_{acc}	1624	1.159	$\cong 0$	0.96 (<50 kW)
	β_{grd}	18,670	31.80	$\cong 0$	
	β_{aero}	0.912	0.0011	$\cong 0$	
	β_{roll2}	206.41	1.597	$\cong 0$	
		$DrvPw_{Indt var1} = \beta_{acc}v_{veh}a_{veh} + \beta_{grd}v_{veh} \sin \theta + \beta_{aero}v_{veh}(v_{veh} - v_{wind})^2 + \beta_{roll}v_{veh} \cos \theta$			kW)
Indt var. 2 (X ₂)	β_{acc}	1624	1.175	$\cong 0$	0.96 (<50 kW) 0.96 (≥50 kW)
	β_{grd}	18,900	36.87	$\cong 0$	
	β_{aero}	0.2567	0.0054	$\cong 0$	
	β_{roll1}	1163	284.5	4.379×10^{-5}	
	β_{roll2}	12320	6068	0.0424	
	β_{e1}	0.3362	0.0094	1.373×10^{-279}	
	β_{e2}	-1163	284.4	4.338×10^{-5}	
	β_{e3}	-1.214	6068	0.0454	
	$DrvPw_{Indt var2} = \beta_{acc}v_{veh}a_{veh} + \beta_{grd}v_{veh} \sin \theta + \beta_{aero}v_{veh}(v_{veh} - v_{wind})^2 + \beta_{roll1}v_{veh}^2 \cos \theta + \beta_{roll2}v_{veh} \cos \theta + \beta_{e1}v_{veh}^3 + \beta_{e2}v_{veh}^2 + \beta_{e3}v_{veh}$				
VSP LDV 1999	$VSP_{LDV1999} [\text{watt}] = m$ $\times v_{veh} \left[1.1 a_{veh} + 9.81 \times \sin \left(\tan^{-1} \left(\frac{h}{l} \right) \right) + 0.132 \right]$ $+ m \times 0.000302v_{veh}^3$			0.93 (<50 kW) 0.79 (≥50 kW)	
VSP Prius3Spec	$VSP_{Prius3} [\text{watt}] = m$ $\times v_{veh} \left[a_{veh}(1 + \varepsilon_i) + g \times \sin \left(\tan^{-1} \left(\frac{h}{l} \right) \right) + g \times C_{roll} \right]$ $+ \frac{1}{2} \rho_{air} C_{drag} A \times v_{veh}(v_{veh} - v_{wind})^2$			0.94 (<50 kW) 0.78 (≥50 kW)	

Figure 108 shows the validation results of the three driving-power estimation equations: $DrvPw_{Prius3}$, VSP Prius3Spec, and VSP LDV 1999, as compared to P_{PTdrv} . The validation results are from two different driving ranges: (a) light-load driving, in which driving power was less than 50 kW; and (b) heavy-load driving, in which the driving power was equal to or greater than 0 kW. Data incorporated in this analysis were data that had prediction error within the 95% confidential interval. The prediction error was calculated by the residue between prediction results and P_{PTdrv} .

In the light-load-driving condition, the data cloud from all three equations of VSP LDV 1999, VSP Prius3Spec, and $DrvPw_{Prius3}$ showed high correlation with P_{PTdrv} . The data clouds were densely aligned on the 1:1 diagonal line. VSP LDV 1999 and VSP Prius3Spec data showed similar alignment while $DrvPw_{Prius3}$ provided slightly less scattering and more symmetric results around the 1:1 line.

During heavy-load driving, these driving conditions were found in several driving scenarios, such as high-speed driving, aggressive driving, steep road gradient, strong head wind, or heavy cargo load. Even though these data do not represent typical driving situations in some countries or regions, heavy-load-driving conditions are the major factors that cause vehicles' energy consumption and emissions to dramatically increase. Results from Figure 108b illustrate that, during heavy-load driving, $DrvPw_{Prius3}$ provided more critically predictable results compared to both the VSP LDV 1999 and VSP Prius3Spec equations. Results from VSP LDV 1999 and VSP Prius3Spec showed significant discrepancy from the main diagonal line when compared to $DrvPw_{Prius3}$.

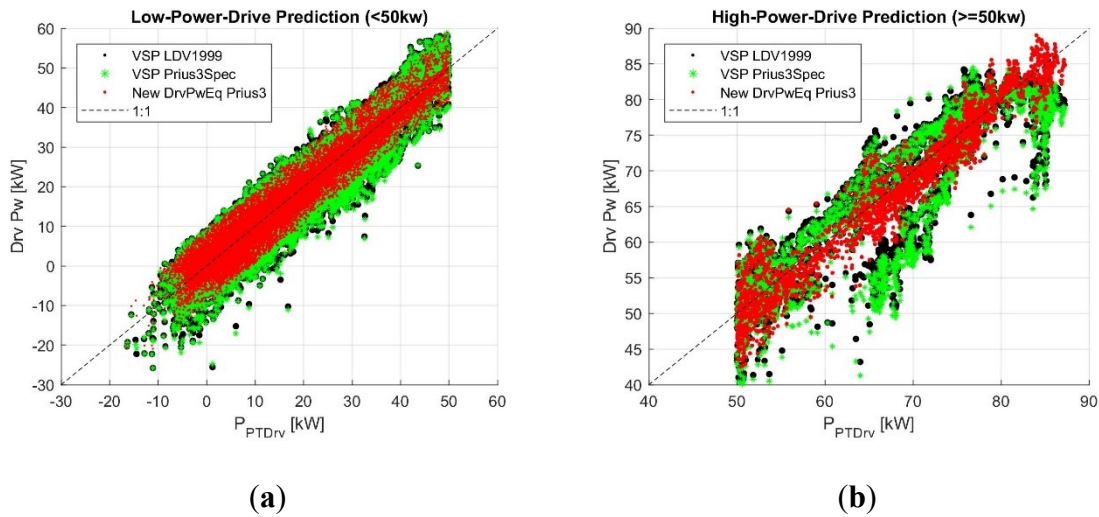


Figure 108 Validation of vehicle driving-power estimations compared to powertrain driving power (P_{PTdrv}). (a) Light-load driving (<50 kW), and (b) heavy-load driving (≥ 50 kW).

Due to the large size of the database plotted on Figure 109, it was difficult to distinguish the data-alignment concentration in the three datasets. Thus, Figure 109a, b presents the distributions of prediction-error residue of the three different driving-power estimation methods: $DrvPw_{Prius3}$, VSP Prius3Spec, and VSP LDV 1999, separated into light- and heavy-load-driving ranges. Error residues were computed on the basis of P_{PTdrv} .

In the light-load-driving condition, the error distributions of VSP LDV 1999, VSP Prius3Spec, and $DrvPw_{Prius3}$ presented normally shaped distributions. Nevertheless, the error distributions of VSP LDV 1999 and VSP Prius3Spec tended to shift to the left, which means that these conventional equations provided slightly underpredicted results. In the heavy-load-driving condition, $DrvPw_{Prius3}$ produced the prediction error in normally shaped distribution, and the peak was located at 0 kW. Maximal error was found at ± 5 kW.

On the other hand, the error distributions of VSP LDV 1999 and VSP Prius3Spec covered the range of -15 to 10 kW, which was 2.5-fold wider than the error range of $DrvPw_{Prius3}$. Moreover, the distribution peaks of VSP LDV 1999 and VSP Prius3Spec slightly shifted to the right and were located at approximately 1.25 kW.

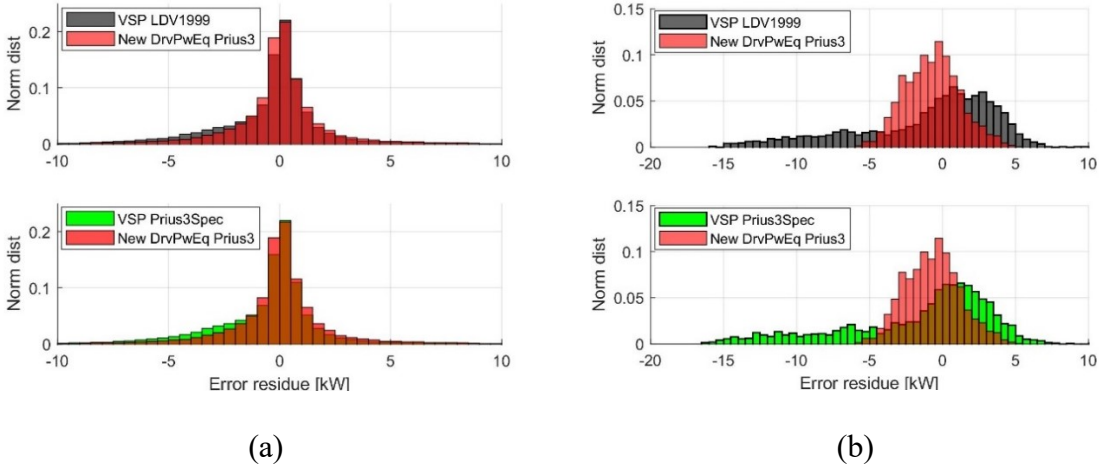


Figure 109 Comparison of error residues from $DrvPw_{Prius3}$, VSP Prius3Spec, and VSP LDV 1999. (a) Light-load driving (<50 kW) and (b) heavy-load driving (≥ 50 kW)

Furthermore, this study performed validation by analyzing prediction results and error analysis on the basis of actual driving datasets. Figure 110 shows the obtained results from naturalistic acceleration and a high-speed cruising speed profile. This dataset represents the light-load-driving condition in which driving-power utilization was less than 50 kW. Figure 110 is divided into three parts, namely, vehicle-speed profile, comparison between predicted driving powers to P_{PTdrv} , and prediction-error residues. At the initial naturalistic acceleration duration, all three equations provided slightly underpredicted results. However, the power-

utilization trajectories still captured the major driving-power utilization trend. Once speed became constant at around 110 km/h, $DrvPw_{Prius3}$ seemed to provide the best prediction results. There were some small fluctuations at some local spikes, but it still captured the tendency well. VSP LDV 1999 and Prius3Spec tended to provide underpredicted results at the high-speed- and light-load-driving conditions. For error-residue analysis, results showed that $DrvPw_{Prius3}$ produced an error fluctuating at around 0 kW, while VSP LDV 1999 and Prius3Spec produced an error fluctuating approximately at -3 kW, which accounts for 15% of driving-power level.

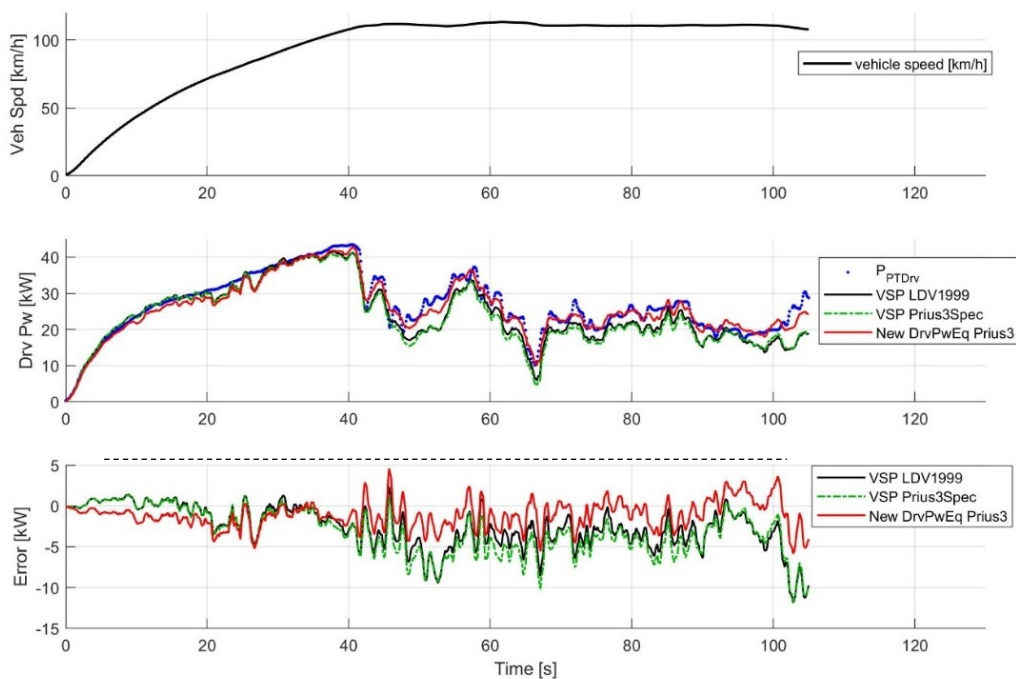


Figure 110 Prius3 driving-power prediction results at light-load driving during naturalistic acceleration and high-speed cruising.

Figure 111 presents the prediction results in the heavy-load-driving condition during the maximal-acceleration test. For Prius3, 0 to 60 km/h is the speed range in which the vehicle can provide the most powerful acceleration. As a result, driving power escalated sharply at the beginning. At this section, overshoots were found from the VSP LDV 1999 and Prius3Spec prediction results. These conventional equations provided similar prediction results, which were underpredicted during the first half of the acceleration. As vehicle speed increased, results became more underpredicted. Between the three equations, $DrvPw_{Prius3}$ was potentially the most accurate and reliable prediction. Through $DrvPw_{Prius3}$ produced some error, it fluctuated around the zero-error line.

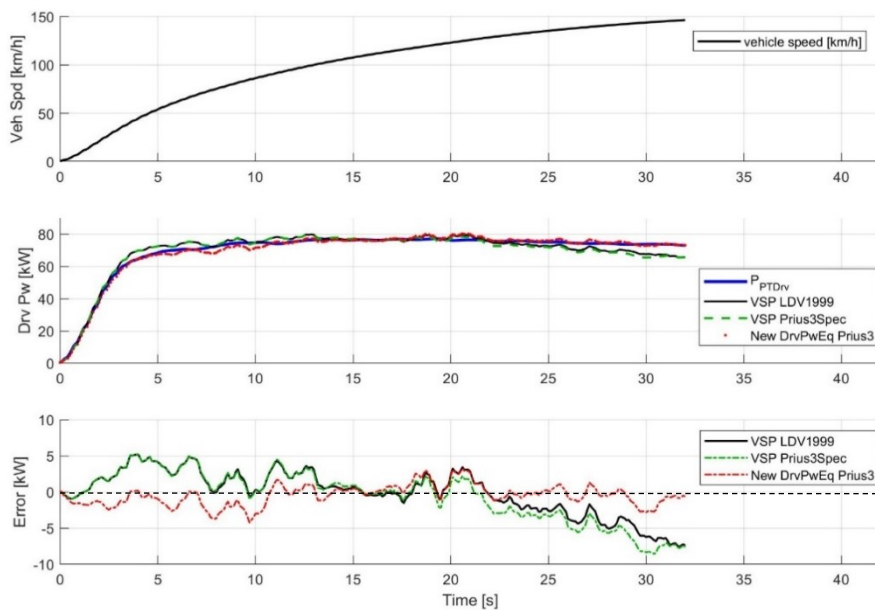


Figure 111 Figure 7. Prius3 driving-power prediction results during heavy-load driving during maximal acceleration.

This study also analyzed the impact of vehicle speed on the magnitude of prediction errors, discovering that the error generated by VSP LDV 1999 and VSP Prius3Spec is not only subject to the driving-power level, but also driving speed. When driving speed increased, VSP LDV 1999 and VSP Prius3Spec were prone to produce exponentially underpredicted results, as seen in the two top charts in Figure 112. Error residues started to deviate from the zero error line after vehicle speed reached 80 km/h. The data show that the prediction error of both conventional could increase up to -20 kW. Unlike $DrvPW_{Prius3}$, there was no significant deviation found from the driving-power prediction results shown in Figure 112 in the third chart from the top. The error was populated on the zero-error line from zero to maximal speed of 160 km/h. Furthermore, the width of the error cloud was also significantly reduced compared to both the VSP LDV 1999 and VSP Prius3Spec results.

In the bottom chart in Figure 112 is typical driving-speed distribution, recorded in Nagoya, Japan. The experiment was conducted for city (Sakae area) and highway (Tomei expressway from Hongo and Komaki) driving. The data showed that driving speed in city traffic was between 0 and 30 km/h, while top speed was recorded at roughly 55 km/h. On the highway, vehicle driving-speed range increased to between 80 and 100 km/h.

Results from Figure 112 indicated that, in the case of city driving, the three equations were appropriate for driving-power estimation. $DrvPW_{Prius3}$ only provided slightly higher prediction accuracy. Nevertheless, in the case of highway driving or higher-speed driving conditions, estimating driving power with VSP LDV 1999 and VSP Prius3Spec may cause a significant driving-power prediction error of up to -20 kW.

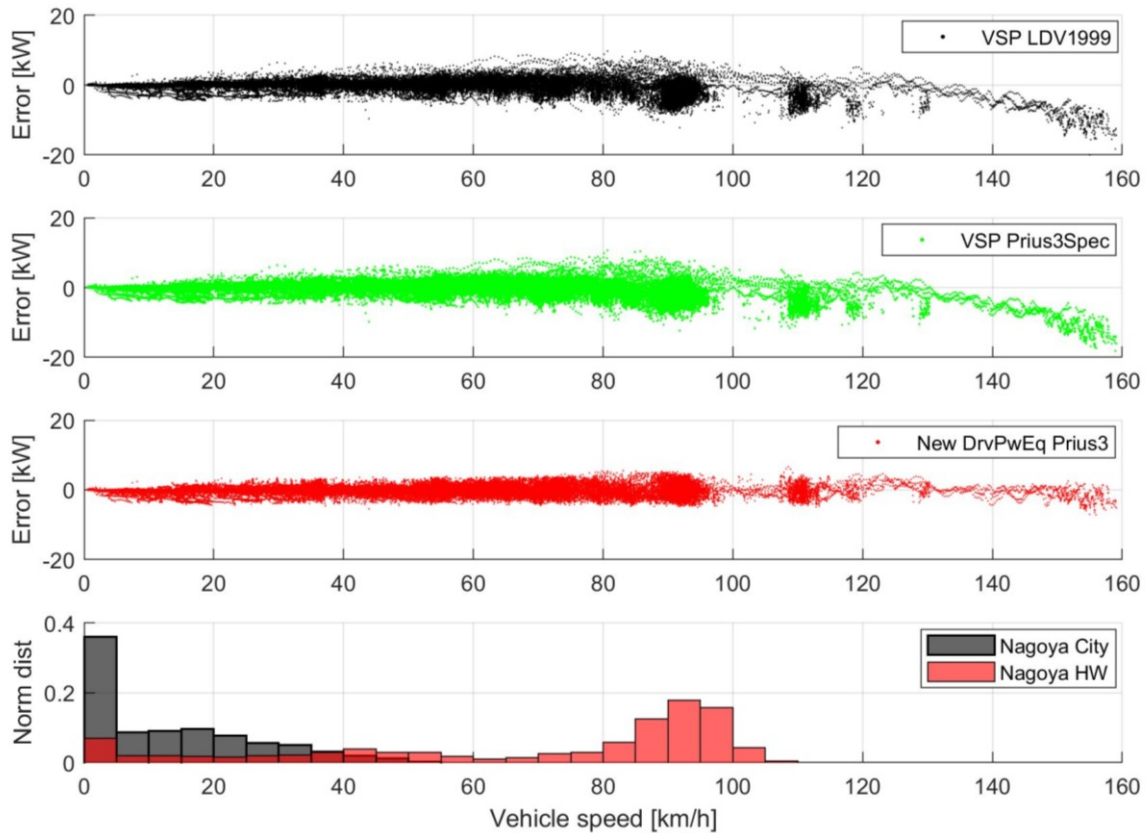


Figure 112 Driving-power-prediction error analysis on impact of driving speed on prediction errors from VSP LDV 1999, VSP Prius3Spec, and DrvPw_Prius3.

This study also provides an analysis on the cause of the error. Figure 113 shows the relationship between total prediction error and power-utilization magnitude of aerodynamics and rolling-resistance terms. Strong correlation implies that the particular term had significant influence on prediction-error occurrence, which was only found in aerodynamics and rolling-resistance terms. Results showed that the aerodynamics and rolling-resistance terms were the primary factors that contributed to the underpredicted error of VSP LDV 1999

and VSP Prius3. As the magnitude of the power utilizations of these two terms became larger, it resulted in the exponential growth of the total prediction error.

For the aerodynamics term, the prediction by VSP LDV 1999 and VSP Prius3 showed error deviation after the magnitude became larger than 15 kW. The possible maximal error caused by this term was found to be up to 15 kW. On the other hand, $DrvPW_{Prius3}$ was prone to mitigating the underprediction problems of the conventional methods. Prediction results only showed slight deviation after magnitude reached 23 kW. Maximal error was also effectively reduced to 3 kW.

The power utilization of the rolling-resistance term was found in the range of 0 to 8 kW, which was less than that of the aerodynamics term. The prediction by VSP LDV 1999 and VSP Prius3 showed a similar deviation trajectory. The error began to deviate at magnitudes larger than 5 kW. $DrvPW_{Prius3}$ significantly reduced the error caused by this term; however, it began to deviate after 7 kW.

Acceleration and road-grade terms could be considered as minor error contributors compared to the aerodynamics and rolling-resistance terms. No significant correlation was found between error and magnitude, which implies that the road-grade terms were not major factors that caused the driving-power prediction error.

For further improvement of the proposed $DrvPW_{Prius3}$ equation formulated by Indt var. 1, this study found that the trajectory of the error curve established a polynomial trend that could be properly fitted by a quadratic function of vehicle speed. In the case that high accuracy of driving-power estimation is required, this study recommends using the $DrvPW_{Prius3}$ equation formulated by Indt var. 2, which contains the quadratic function of

the vehicle-speed terms. This study also confirmed that the $DrvPw_{Prius3}$ equation formulated by Indt var. 2 is capable of suppressing the error caused by the aerodynamics and rolling-resistance terms. However, higher accuracy also comes with higher calculation complexity. The best practice is to select the equation that provides acceptable accuracy in a particular driving condition.

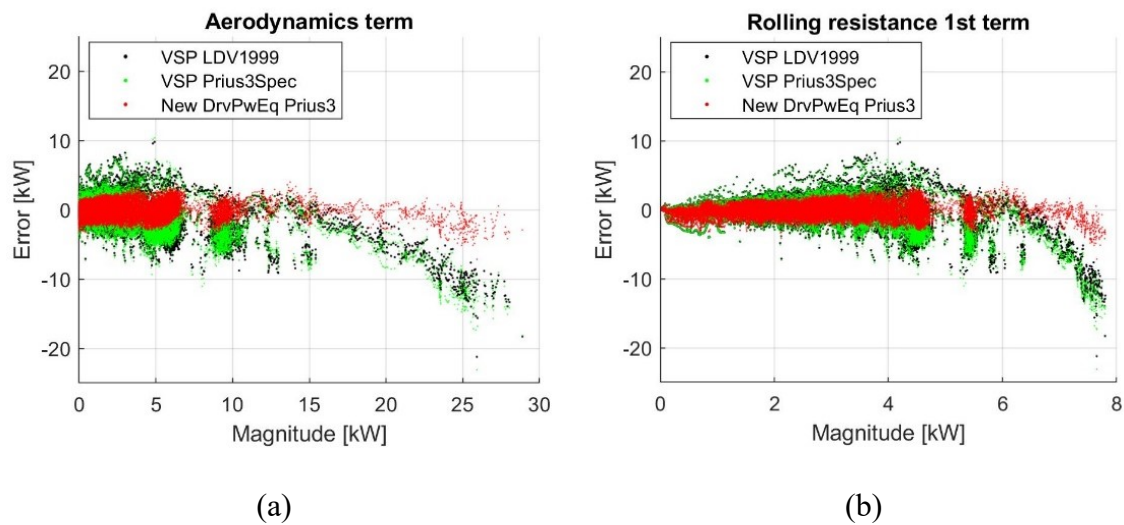


Figure 113 Driving-power-prediction error analysis.

Additionally, this study provides a summary of the impact of energy utilization classified by each acceleration and driving-resistance term based on Nagoya's city- and highway-driving conditions. Figure 114 shows the comparison of Prius3's driving energy utilization between city and highway driving. Data were classified into each contributor term: acceleration, road grade, aerodynamic, and rolling resistance, which were estimated by the terms in Equation (59). In the city, more than 70% of energy was utilized for acceleration,

which mostly took place during a stop-and-go situation. Approximately 20% of the energy was used to overcome rolling resistance. The effect of the road-grade and aerodynamic terms was comparatively small at 5% and 2%, respectively. On the other hand, energy utilization during highway driving showed that the proportion of the utilized energy by the acceleration term was decreased by half, while the effect of the road grade and aerodynamics increased 4- and 10-fold, respectively. In addition, only the acceleration and road-grade terms, which are surplus to the aerodynamic and rolling-resistance terms, could be recuperated during regenerative braking.

According to the impact of the energy utilization classified by each term, as shown in Figure 10, it can be concluded that, during city driving, it is recommended to ensure the accuracy of the acceleration and rolling-resistance terms. However, during highway driving, the contribution of all four terms fairly shares this significance. Thus, all coefficients in front of the four equation terms should be deliberately calibrated for accuracy of driving-power prediction.

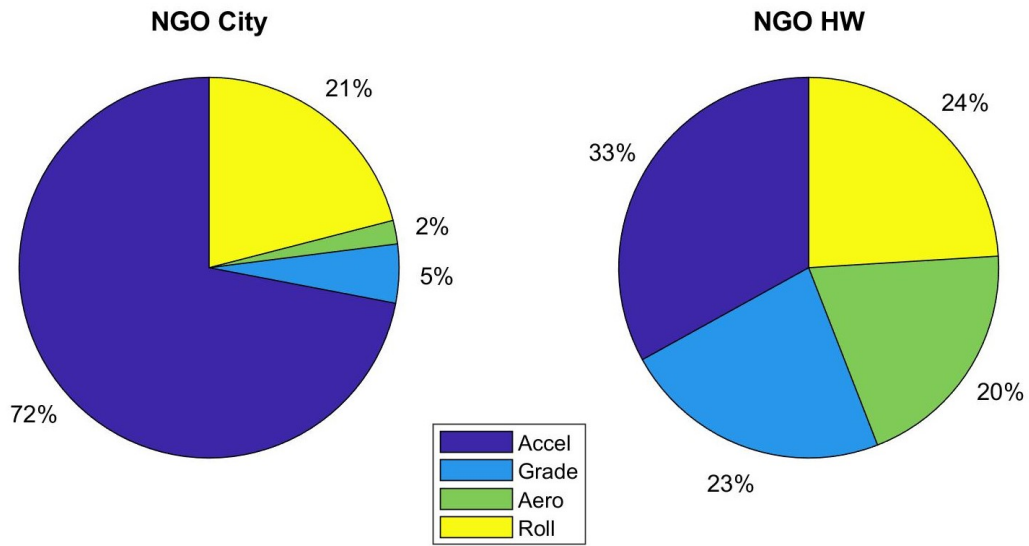


Figure 114 Contribution of each driving-power term in city and highway driving in Nagoya, Japan.

More importantly, this analysis also indicates two different vehicle driving-power calculation approaches, which are a direct calculation of powertrain propulsion output power and vehicle-specific power approaches. These two approaches require different sets of input parameters. One directly calculates driving power from the hybrid powertrain (P_{PTdrv}), and requires ω_{MG1} , τ_{MG1} , ω_{MG2} , τ_{MG2} , and ω_{Ice} as input parameters. The other calculates driving power from the vehicle's external observable parameters (VSP and $DrvPW_{Prius3}$), and requires v_{veh} , v_{wind} , a_{veh} , and θ (road grade) as input parameters. However, these two approaches established a significantly high correlation degree, thus confirming that these two calculation approaches are valid for hybrid-vehicle driving-power estimation. Moreover, it is reasonable to conclude that the driving-power equation-coefficient calibration method

proposed in this study is capable of providing an appropriate set of coefficients for any interested vehicle model or fleet.

6.1.4 Conclusions

Vehicle driving power is one of the most substantial parameters in vehicle energy-consumption modeling and analysis. This study developed a vehicle driving-power estimation equation for hybrid vehicles and proposed a procedure to calibrate an optimal set of vehicle-specific coefficients for acceleration, road-grade, rolling-resistance, and aerodynamics terms.

The approach utilized the power-split hybrid powertrain's accessible OBD dataset and its dynamic model to estimate the total propulsion power of the power-split hybrid powertrain in Prius3. Then, propulsion power was utilized as a key parameter for driving-power equation development and vehicle-specific coefficient calibration. The stepwise algorithm was introduced to determine the significance of each equation term. Then, this study implemented the multiple regression method to calibrate a set of coefficients that were optimal for a particular vehicle model or fleet.

Results showed that conventional driving-power equations VSP LDV 1999 and VSP Prius3Spec suffer from prediction error, particularly under heavy-load- and high-speed-driving conditions. During heavy-load driving, when power was greater than 50 kW, the correlation between VSP LDV 1999 and VSP Prius3Spec with P_{PT_drv} was found at an R-square of 0.79 and 0.78, respectively. During light-load driving, VSP LDV 1999 and VSP

Prius3Spec also tended to deliver slightly underpredicted results. Furthermore, at driving speeds higher than 80 km/h, VSP LDV 1999 and VSP Prius3Spec also caused underestimated prediction error. As speed increased, the error became more severe; maximal error ranged up to -20 kW. This error was primarily generated by the aerodynamics and rolling-resistance terms.

However, the new driving-power equation, $DrvPW_{Prius3}$, dramatically improved estimation accuracy over the two conventional VSP equations. It provided a consistent R-square of 0.96 in both light- and heavy-load-driving conditions. The error also established normally shaped distributions, which showed better reliability for prediction results. Moreover, $DrvPW_{Prius3}$ was also capable of suppressing error during high-speed driving, and significantly reduced the error generated by the aerodynamics and rolling-resistance terms. According to analysis, $DrvPW_{Prius3}$ is appropriate for application to all driving conditions, since it consistently provided a low prediction error from light- to heavy-driving power, and low- to maximal-speed driving compared to VSP LDV 1999 and VSP Prius3Spec.

For such an application, this study recommends that the coefficients be calibrated for the specifically studied vehicles or fleet, whether in city or highway driving. The reason is that, in city driving, the rolling-resistance term dominates 21% of total energy consumption. In highway driving, the aerodynamics and rolling-resistance terms dominate 20% and 24%, respectively, of energy consumption. Particularly during heavy-load driving, $DrvPW_{Prius3}$ can provide much more accurate prediction.

Lastly, results in this study showed that both of the approaches used to establish the P_{PTdrv} and $DrvPW_{Prius3}$ equations are rational for power-split hybrid-vehicle driving-power estimation. For the coefficient-calibration part, the stepwise and multiple regression method introduced in this study was capable of providing an appropriate set of coefficients that were optimal for a specific vehicle model or fleet. This coefficient-calibration method could be applied through all kinds of powertrains and vehicle types as long as driving power can be measured or estimated from the vehicles.

6.2 Development of Hybrid-Vehicle Energy-Consumption Model for Transportation Applications—Part II: Traction Force-Speed Based Energy Consumption Modeling

This section is the second part of the study. Part I captures the driving power equation development and the coefficient calibration for a specific vehicle model or fleet. Part II focuses on hybrid vehicles' energy consumption modeling, and utilizes the equation obtained in Part I to estimate the driving power. This study proposes a new methodology to improve the conventional energy consumption modeling methods for hybrid vehicles. Also, this research has discovered that driving power is not the only primary factor that influences hybrid vehicles' energy consumption. This study introduces a new approach by applying the fundamental of hybrid powertrain operation to develop a new modeling methodology. The method aims to reduce the errors and drawbacks of the conventional modeling methods. This study employs a new driving power estimation equation calibrated for the third generation

Toyota Prius from Part I. Then, the Traction Force-Speed Based Fuel Consumption Model (TFS model) is proposed. The combination of these two processes provides a significant improvement in fuel consumption prediction error compared to the conventional VSP prediction method. The absolute maximum error was reduced from 57% to 23%, and more than 90% of the predictions fell inside the 95% confidential interval. These validation results were conducted based on real-world driving data. Furthermore, the results show that the proposed model captures the efficiency variation of the hybrid powertrain well due to the multi-operation mode transition. The TFS model is also applicable throughout a variety of real-world traffic and driving conditions. It also provides a supporting analysis indicating that the driving mode transition in hybrid vehicles significantly affects the energy consumption. Thus, it is necessary to consider these unique characteristics to the modeling process.

6.2.1 Introduction and Literature review

Dominating around 45% of the global fuel consumption each year, the transportation sector is one of the primary contributors that emit a tremendous amount of carbon dioxide to the atmosphere (Organization of the Petroleum Exporting Countries, 2017). To address the problem, several measures and policies have been enforced. The regulation of tailpipe emissions and fuel consumption is one of the most explicit examples. It forces the penetration of hybrid and electric powertrain vehicles to the market (Duarte, Gonçalves and Farias,

2016). The evaluation of the impact of the transition of the powertrain technologies on the environment, fuel consumption, and emission models has become substantial.

Recently, there have been several hybrid powertrain configurations introduced into the market and on the road. A power-split hybrid vehicle is one of the most widespread series-parallel hybrid powertrain configurations (Toyota Motor Corporation, 2019). The remarkable concept of this powertrain is that it detaches the speed between the wheels and the engine. Thus, the engine can operate regardless of the driving speed (Liu and Peng, 2008; Murphey *et al.*, 2012). The system also takes advantage of the electric motor/generators (MG) which deliver quick response and high efficiency to assist and absorb the engine power. As a result, it allows more flexibility for the engine to operate onto the optimum regions. This configuration also provides multi-power flow paths that are known as multi-operation modes, such as electric drive, hybrid drive with battery charging, hybrid drive with electric motor assist, regenerative braking, and others. Each mode also provides different operation efficiency ranges. To achieve the maximum efficiency of the system, the energy management system (EMS) is a key component. It contains powertrain operation logic that controls and switches the operation mode to satisfy the driving condition and power usage. The EMS of most hybrid vehicles is constructed by a rule-based control algorithm. This algorithm contains a constraint that defines the conditions for the driving mode selections. It generally determines instantaneous wheel driving force at vehicle speed (Liu and Peng, 2008; Sciarretta *et al.*, 2014).

In the past decades, a number of researchers have been applying vehicle fuel consumption models to transportation research such as prediction and analysis. The

conventional approach of vehicle fuel consumption modeling consists of two main processes, which are vehicle driving power estimation, and fuel consumption and driving power relationship construction (Frey, Zhai and Roupail, 2009; Graver, Frey and Choi, 2011; Zhai, Christopher Frey and Roupail, 2011; Song, Yu and Tu, 2012; Duarte *et al.*, 2014; Holmén and Sentoff, 2015; Duarte, Gonçalves and Farias, 2016; Song, Yu and Wu, 2016; Wang and Rakha, 2016; Zhou and Jin, 2017). In 1999, Jiménez *et al.* (Jiménez *et al.*, 1999) derived an equation for vehicle driving power estimation, and also provided a set of coefficients specified for light-duty vehicles' (LDVs) application called vehicle-specific power (VSP). The equation simply requires data that can be observed from outside of the vehicles, such as speed, acceleration, road grade, and wind speed. Furthermore, a large number of researchers adopting VSP in their research have reported on the monotonically increasing relationship between VSP and fuel consumption (Jiménez *et al.*, 1999; Frey, Zhai and Roupail, 2009; Zhai, Christopher Frey and Roupail, 2011; Graver, Frey and Choi, 2011; Song, Yu and Tu, 2012; Duarte *et al.*, 2014; Duarte, Gonçalves and Farias, 2014; Wu, Song and Yu, 2014; Duarte, Gonçalves and Farias, 2016; Holmén and Sentoff, 2015; Song, Yu and Wu, 2016; Wang and Rakha, 2016; Zhou and Jin, 2017).

For hybrid vehicles, the powertrains consist of two propulsion power sources that result in more complexity for the energy consumption modeling process. Also, hybrid vehicles deliver the propulsion power in multi-operation modes. Each mode delivers the output efficiency at different ranges. To capture the energy consumption characteristics of hybrid vehicles, Frey *et al.* (Frey, Zhai and Roupail, 2009) proposed an approach to model fuel consumption and emissions for alternative vehicle technologies. First, the model

estimated the vehicles' driving power by using the conventional VSP equation with the coefficients for LDV. The fuel consumption data were binned into 14 discrete VSP ranges. The average fuel consumption rate at each VSP bin was calculated and established as a fuel consumption model. Since then, this method has been adopted by several transportation energy consumption and emission studies, and has become a conventional method among this field. In a related study, Zhai et al. (Zhai, Christopher Frey and Rouphail, 2011) attempted to develop a fuel consumption model for a hybrid vehicle, the Toyota Prius generation 3 (Prius3). The study quantified the engine on/off criteria by setting the maximum power threshold for each speed and acceleration range. Then, the conventional VSP modeling method was employed to construct the fuel consumption and emission models during the engine-on state period.

Duarte et al. (Duarte *et al.*, 2014) applied exactly the same convention VSP equation as a tool to evaluate the effect of the battery state of charge (SOC) on the fuel consumption of the 2011 Toyota Prius. Based on the 14 VSP bin basis, this study classified the data into four different SOC ranges. The results were analyzed based on the time-spent distribution, the average fuel consumption rate, and the average emission rate. Graver et al. (Graver, Frey and Choi, 2011) also applied the same methodology for plug-in hybrid vehicles by using the conventional VSP equation with the coefficients for LDV, but using 1 kW/ton bin intervals. However, this study classified the data into two groups: engine on and off, instead of SOC. Then, it also took both electricity and fuel energy usage into account instead of fuel consumption.

Holmén, B. A. and Sentoff, K. M. (2015) utilized the conventional VSP equation with LDV coefficients and the 1-kW VSP binning method to analyze the benefit of hybrid vehicles compared to internal combustion engine vehicles. This study separated the model into three driving scenarios—city, suburban, and highway—in an attempt to investigate the benefit factors for hybrid vehicles' fuel savings at each driving scenario. On the other hand, this research pointed out a significant drawback of the conventional VSP method. It is interesting to note that VSP models constructed from the same vehicle cannot provide similar model outcomes when they experience different traffic or driving conditions. It implied that the conventional VSP fuel consumption modeling that has been adopted in a tremendous number of research studies may lack some key parameters. The driving power might not be the only primary parameter that contributes to vehicles' fuel consumption. Zhou and Jin (Zhou and Jin, 2017) attempted to improve the fidelity of the conventional VSP binning modeling method by introducing a transient fuel consumption model. This model consisted of two sub-modules: steady-state and transient modules. To classify the transient data, boundaries were fitted to a scattered plot of speed and acceleration data slightly below the rim of the data cloud. Then, the transient model was constructed by fitting a curve on the speed and fuel consumption data at different discretized acceleration levels.

According to the previous literature, an enormous number of studies has actively adopted the conventional energy consumption modeling method. Nevertheless, only a small number of studies have made an attempt to improve the conventional VSP modeling. Applying the VSP equation and the LDV coefficients proposed since 1999 to estimate the driving power of the current vehicle models can cause a significant error to the estimation

and the following modeling process (Pitanuwat, Aoki, Morikawa, *et al.*, 2019). Moreover, there were some studies that pointed out that driving power might not be the only primary parameter contributing to vehicles' fuel consumption. Particularly for hybrid vehicles, the powertrain is capable of enabling multi-operation modes that deliver different energy efficiency. Thus, to develop a fuel prediction model for hybrid vehicles, it is necessary to take these unique characters of hybrid vehicles into account. However, there are no researchers or studies addressing this issue in the current literature. Thus, the objectives of this study are:

- 1.) To investigate and analyze hybrid vehicles' powertrain operation and energy consumption characters in order to suggest further improvement on the conventional VSP energy consumption modeling method.

- 2.) To organize and develop an energy consumption prediction model that can capture hybrid vehicles' energy consumption characteristics based on the fundamental of the actual hybrid operation, and to extend the application ability of the model to be more captive in various driving conditions.

6.2.2 Experimental set-up and data acquisition

6.2.2.1 Analytical experiment

This dataset is applied for analysis on hybrid powertrain operation characteristics and the conventional VSP fuel consumption model accuracy. Then, the improvement suggestions

are made based on the analysis. For this dataset, an experiment was conducted in the Japan Automotive Research Institute (JARI) at Shirosato Test Center. On-road analytical speed patterns were designed in an attempt to capture the characteristics of the power-split hybrid operation and drivability. The third generation of Toyota Prius (Prius3) was selected as a representative test vehicle. This vehicle contains a series-parallel hybrid powertrain using power-split hybrid configuration. The vehicle has been recognized as one of the most remarkable hybrid vehicle icons. The powertrain system consists of a 1800cc Atkinson cycle engine, MG1, and MG2. The high-voltage battery provides electrical power at 201.6 V and 6.5 Ah. The powertrain maximum output power is delivered at 134 hp. During the experiment, the vehicle's powertrain operational data, such as engine, MG1, MG2, and battery data, were collected via the on-board diagnostics (OBD) port accessing the Controller Area Network (CAN) from the hybrid control unit. To measure the road grade, wind speed, and vehicle dynamics, an inertia measurement unit with GPS and a Pitot tube wind speed sensor were also installed. The experimental equipment set-up is shown in Figure 115. During the experiment, the driver was assigned to follow the analytical speed patterns, which were maximum acceleration, maximum braking, cruise speed, coast down, constant acceleration/deceleration, free driving, and e-Drive maximum power. These speed patterns were deliberately designed to capture the varieties of powertrain activities and hybrid operation logics, including realistic driving situations. In addition, at the beginning of the trips, the battery's state of charge was controlled to start in between 45–50%. The sample size of this dataset was more than 50,000 data points recording at 8 Hz. The gross vehicles'

weight including the driver, two passengers, and equipment was measured on the measurement site and found at 1625 kg.

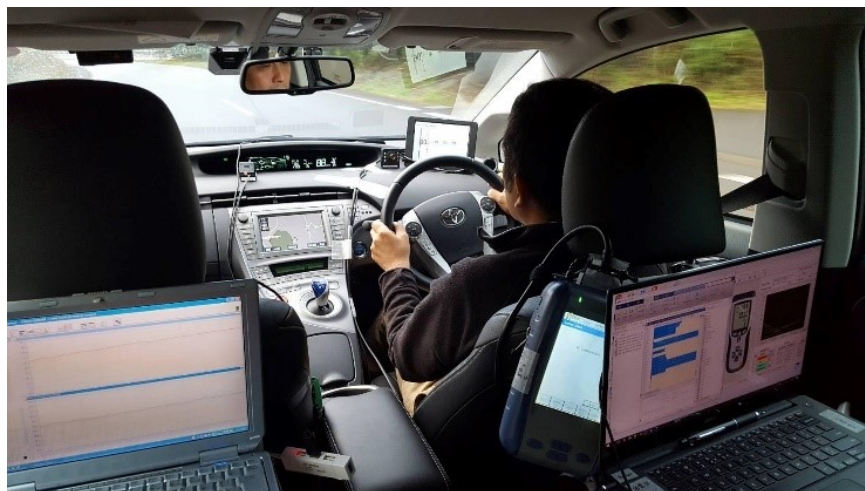


Figure 115. Analytical experimental set-up and equipment.

6.2.2.2 Real-world experiment

This dataset is implemented in the fuel consumption model construction and the result validation. This second dataset was collected under real-world traffic conditions in Bangkok, Thailand in 2015. The selected routes were Silom-Sathon Nuea, Rama 3, and Motorway 7, which represented Bangkok's typical city, suburban and highway traffic conditions well, respectively. Figure 116 shows the orientations and locations of the experimental routes. The colors illustrate the population density from high to low as labeled by red, brown, orange, and yellow, respectively. The same Prius3 model was used as the test vehicle. The CAN data were accessed from the engine control system by the vehicle interface module and Global

TechStream software. Vehicle speed, vehicle acceleration, and fuel consumption data were the primary dataset recorded during the experiment. The sampling rate was 1 Hz. This experiment covered more than 400 km of the OBD data amount with at least three repetitions per route (Pitanuwat and Sripakagorn, 2015).

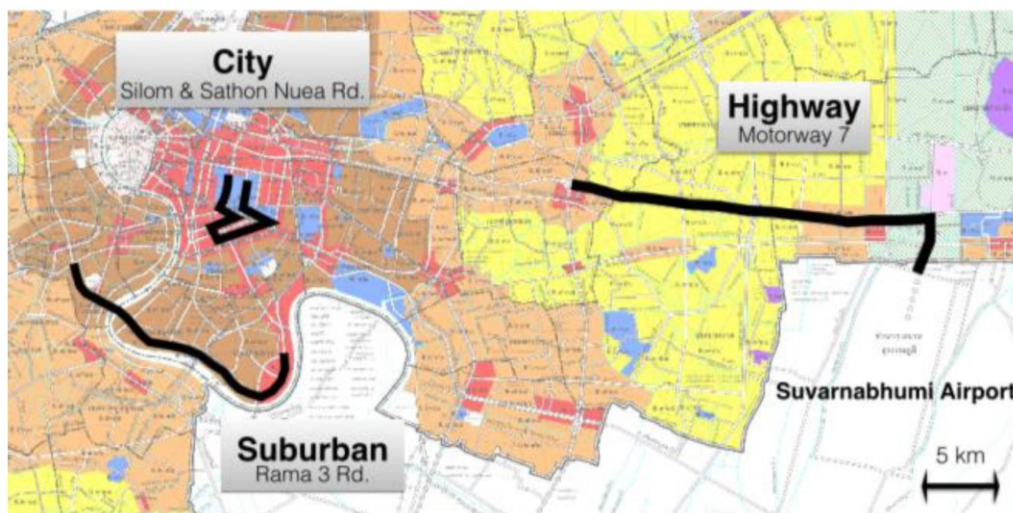


Figure 116. Real-world experiment routes' orientations and locations (Pitanuwat and Sripakagorn, 2015).

6.2.3 Methodology

6.2.3.1 Investigation of Hybrid vehicles' powertrain operation and energy consumption characteristics

Power is a function between force and speed. Thus, at one constant power level, it is possible to have multiple pairs of combinations between force and speed data. In general, vehicles operate the powertrain by choosing an optimal operation point that can satisfy the driving force while providing the desired speed. Even though the output power is the same, different force and speed means different powertrain operation points, which result in different energy consumption. Figure 117 shows the insight analysis of the conventional VSP fuel consumption modeling method. This analysis is generated from the analytical experiment dataset. VSP is annotated as the driving power. The color shows the fuel consumption rate at any recorded operation point. This figure attempts to illustrate the fuel consumption variation that occurs at any constant VSP level. From the data, at any layer of a horizon with a constant VSP, the faster the speed, the greater the amount of fuel consumed by the vehicle. Particularly, when the driving power is above 25 kW, the fuel consumption variation becomes more dramatic. This analysis confirms that using only VSP is not sufficient to capture the fuel consumption characteristics of a vehicle. There is still a significant variation of fuel consumption inside a VSP bin.

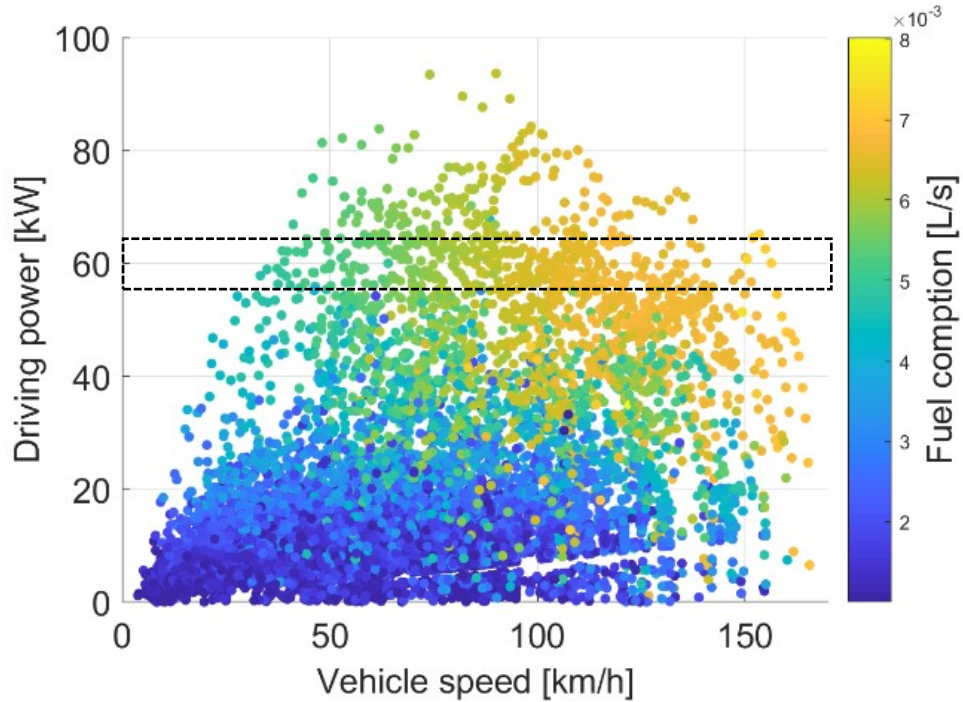


Figure 117. Analysis of the fuel consumption characteristics based on the conventional vehicle-specific power (VSP) fuel consumption modeling method.

In addition, according to the fundamental of the powertrain operation mechanism, the driving force and vehicle speed are the primary factors that are used for vehicle driving demand power calculation, and indicate the target of the powertrain's operation points. Most of the hybrid vehicles that are available at the present also use rule-based logic control to determine the hybrid powertrain operation modes. The rule-based control basically selects the driving mode based on the instantaneous driving force and vehicle speed (Liu and Peng, 2008; Sciarretta *et al.*, 2014). Each driving mode also delivers different efficiency depending on the active powertrain components and power flow paths. Moreover, according to the analytical experiment data in Figure 118, the analysis supports the statement that the hybrid

powertrain operation modes in the Prius3 are also selected based on the driving force and vehicle speed. This study also believes that the criteria are also applied through all Toyota Hybrid System vehicles. Further information on hybrid vehicles' EMS map identification and measurement procedure will be provided in a separate coming paper.

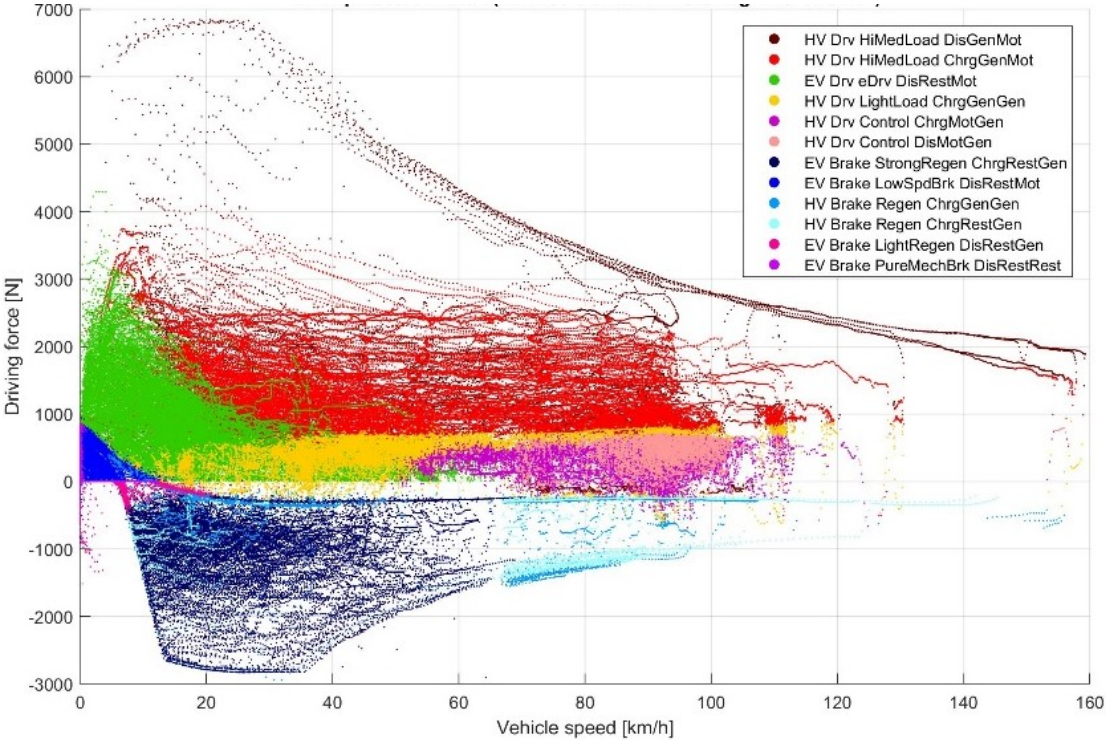


Figure 118. Prius3's hybrid operation mode classification based on instantaneous driving force at wheel and vehicle speed.

Due to the powertrain operation modes being switched mainly based on driving force and speed criteria, it implies that hybrid powertrain fuel consumption and efficiency are suitable to be modeled by driving force and speed rather than by driving power. Thus, this

study proposes the Traction Force-Speed Based Fuel Consumption Model (TFS model), which attempts to improve the limitations of the conventional VSP fuel consumption modeling methods. The basic concept of the model construction is designed based on the fundamental of hybrid vehicles' powertrain operation. The construction process of the TFS model can be divided into two main parts. The first part is to estimate the vehicle's driving power and force (traction force). The second part provides the model construction methodology.

6.2.3.2 Driving power and driving force estimation

This section introduces a newly developed driving power equation for Prius3 called $DrvPW_{Prius3}$. All the coefficients were deliberately calibrated to be specifically optimal for Prius3's characteristics. The equation for Prius3's driving power estimation is expressed in Equation (60). The equation development and coefficient optimization processes were provided in Part I of these series papers (Pitanuwat, Aoki, Morikawa, *et al.*, 2019).

$$\begin{aligned}
 DrvPW_{Prius3} = & 0.9994(m \cdot v_{veh} \cdot a_{veh}) + \\
 & 1.1705(mg \cdot v_{veh} \sin \theta + 0.2168(\rho_{air} \cdot v_{veh}(v_{veh} - v_{wind})^2) + \\
 & 0.0111(mg \cdot v_{veh} \cos \theta),
 \end{aligned} \tag{61}$$

To confirm the estimation fidelity of the new Prius3 driving equation ($DrvPW_{Prius3}$), Figure 5 illustrates the comparison of Prius3' driving power estimated by two different methods: the conventional VSP equation with the LDV coefficients ($VSP_{LDV1999}$)

proposed by Jiménez et al. (Jiménez *et al.*, 1999), and $DrvPw_{Prius3}$ (Pitanuwat, Aoki, Morikawa, *et al.*, 2019). In Figure 5, the driving power estimated by the two driving power equations are validated to the driving power calculated by Prius3's powertrain dynamic modeling method, which can be referenced in Part I. Comparing the correlation between $VSP LDV1999$ to $DrvPw_{Prius3}$, the correlation is improved from 0.77 up to 0.95. Furthermore, the prediction accuracy of $DrvPw_{Prius3}$ was improved by 23%, and it effectively suppressed the driving power prediction discrepancy at high-speed driving compared to $VSP LDV1999$.

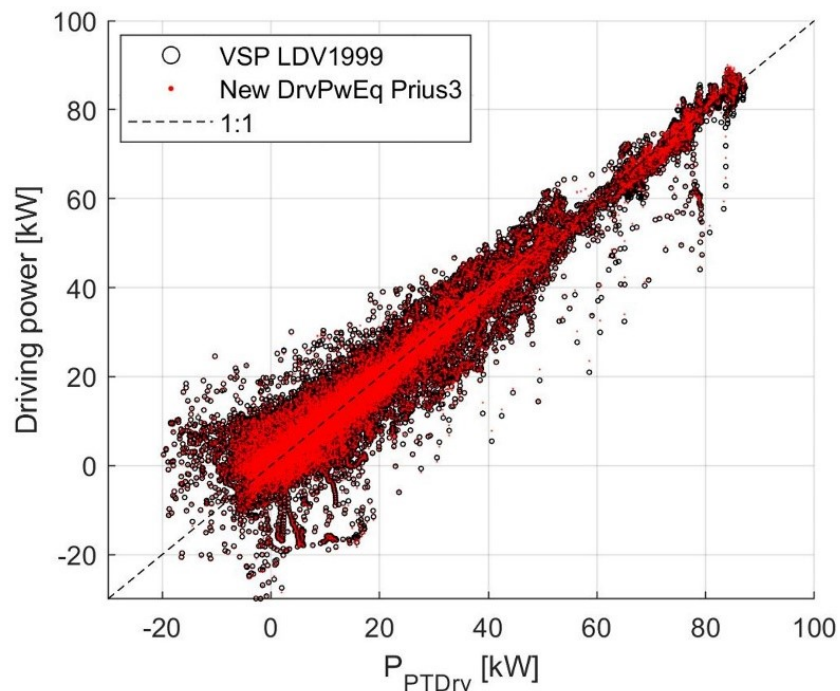


Figure 5. Comparison and validation of Prius3' driving power estimated by two different methods: $VSP LDV1999$ and $DrvPw_{Prius3}$

6.2.3.3 Construction of Traction Force-Speed Based Fuel Consumption Model

The TFS model is intentionally designed according to the fundamental of an actual powertrain's control mechanism and fuel consumption characteristics. First, the driving force and vehicle speed axes are divided into two-dimensional grids. The grid sizes are considered based on the variation of the fuel consumption, the number of data in the grid, and the consistency of the incremental fuel interval of the TFS model. The grid boundaries of the driving force and vehicle speed are set up as specified in Equation (61) and Equation (62).

$$V_{bound} = [-100, -0.5: 1: 0.5, 20, 50: 10: 100, 120: 20: 180, 200], \quad (62)$$

$$F_{bound} = [-10000, -5, -0.5, 0.5, 1, 1.5, 3, 10000], \quad (63)$$

Then, the database, including the vehicle speed, driving force, and fuel consumption, is prepared based on the real-world experiment dataset. Vehicle speed can be obtained from the experiment dataset; however, driving force and fuel consumption need to be calculated. Equation (63) is used to estimate the driving force. It should be cautioned that the average auxiliary load and air conditioning power need to be included into this term before binning. This study inputs 350 W estimated based on the database. For the fuel consumption, the injection head lift duration signal (Inj) is employed to calculate for the fuel consumption rate. The calculation equation is expressed by:

$$Fuel[l/s] = \frac{n \cdot \omega_{ice} \cdot (Inj/10)}{k \cdot 60 \cdot 1000}, \quad (64)$$

where n is the number of cylinders, and k is the number of engine rotations per one injection. For Prius3, n is 4, and k is 2.

Next, the fuel consumption data are binned into the grids, where the specified driving force and vehicle speed range match with the binning data. After this process, the average fuel consumption of all the data in each grid is computed. Then, the complete TFS model is presented in Figure 119. Each line shows the relationship between fuel consumption rate (liter/sec) at different speeds within a specified range of the driving force. The dots on the lines show the average fuel consumption amount that will be used for the prediction. The missing data points indicate the area that the vehicle does not frequently operate. Note that the data analysis and modeling construction conducted in this study were programmed in MATLAB.

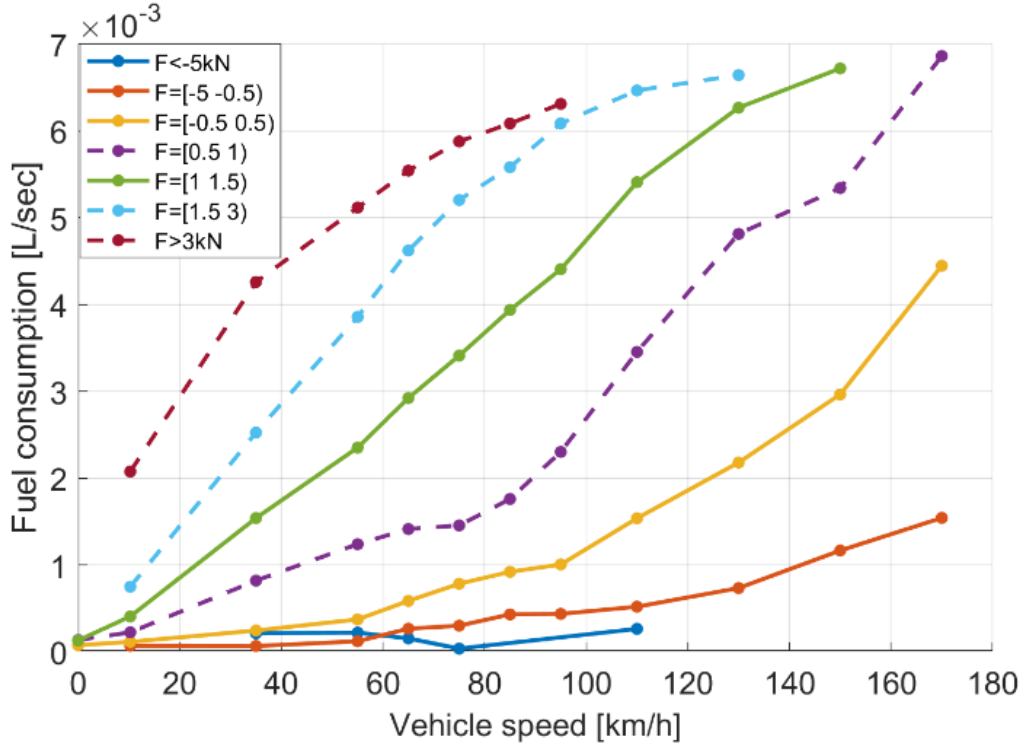


Figure 119. Traction Force-Speed Based Fuel Consumption Model.

6.2.3.4 Model implementation

For the model prediction implementation, the requisite input data are the vehicle speed, vehicle acceleration, road grade, wind speed, average auxiliary load, and air conditioning power data. Then, the fuel consumption prediction procedures are explained:

1. Calculate the driving power by using Equation (60); then, sum up with the average auxiliary load and air conditioning power data.
2. Divide the total power by the vehicle speed (m/s) in order to obtain the driving force.

3. Predict the fuel consumption by using the calculated driving force and speed to find the grid position that is satisfied with the calculated driving force and speed level, and then collect the fuel consumption rate of the grid from TFS model shown in Figure 119. Note that the driving force and speed boundaries were specified in equations (61) and (62).

4. Multiply the fuel consumption rate with the time interval of the input data, and calculate the total fuel consumption of the overall trip.

6.3.4 Results and discussions

Referring to Figure 118, the boundary of the electric vehicle (EV) driving mode (lime green) covers the area up until the maximum speed, which is approximately 64 km/h. It illustrates the boundary at which the Prius3 switches the driving mode from EV to hybrid vehicle (HV), which is either when the operation point falls outside the EV boundary, or the battery power is insufficient. Projecting these characteristics onto the model in Figure 119, at speeds below 64km/h and when the driving force is lower than 0.5 kN, the average fuel consumption is comparatively small compared to the models of the driving force higher than 0.5 kN. This also includes the first two modes of the driving force ranges at 0.5–1 kN, 1–1.5 kN, and 1.5–3 kN. The overall fuel consumption trend shows that the higher the driving force, the more fuel the vehicle consumes. The relationships between the vehicle speed and the fuel consumption rate at different driving force ranges all present fine curve trajectories except for the force range between 0.5–1 kW. The supporting reason is that the data at the driving force between 0.5–1 kW pass through six different operation modes. Since the power flow

path and operation of the engine, MG1 and MG2, are different at each mode, it is possible to cause the fluctuation of the fuel consumption curve. The final TFS map exhibits a significant impact of the hybrid vehicle's operation mode transition on the energy consumption characteristics. Moreover, the proposed grid boundaries— V_{bound} and F_{bound} , which were carefully divided based on the fuel consumption variation—eventually found that the bands of all the farce ranges appropriately cover all the significant hybrid vehicles' operation mode transitions.

For the validation process of the Prius3's TFS model, the real-world experiment dataset recorded in Bangkok traffic conditions is employed. Figure 121 shows a plot between the prediction results and the measurement average fuel consumption of 24 driving trips from various driving behaviors and traffic conditions in Bangkok. The correlation was found at R-squared at 0.96, and 92% of the overall prediction results were aligned inside the 95% conference interval band.

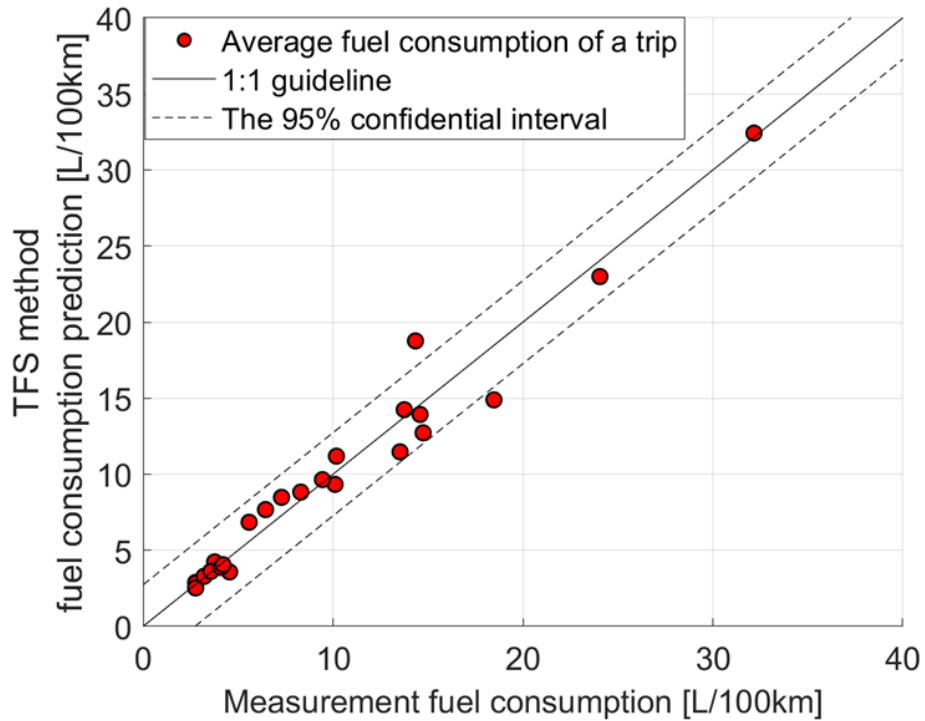


Figure 120 Fuel consumption prediction results of the third generation Toyota Prius (Prius3)'s traction force-speed based model.

Furthermore, this study also investigates the advantages of the new driving power equation combined with the TFS model over combining the conventional VSP equation with the conventional VSP fuel consumption model under real-world driving fuel consumption prediction conditions on the Prius3. Figure 121 shows a comparison of the average fuel consumption among the measurement data and the data from two prediction methods. The red bars illustrate data that were predicted by implementing the new driving power equation model, in order to estimate the instantaneous driving force; then, the driving force was input into TFS model to calculate the fuel consumption ($DrvPw_{Prius3}$ and TFS model). The gray

bars illustrate the data that were predicted by the conventional VSP with LDV coefficients to estimate the driving power; then, the fuel consumption results were generated based on the conventional VSP fuel consumption model (*VSP LDV1999* and *Convvt. VSP model*). Both methods provide a rational fuel prediction trend from low to high average driving speed compared to the measurement shown in Figure 121. The measurement data show that hybrid vehicles deliver fuel economy from high to low in suburban, highway, and city driving conditions, respectively. The average driving speed between 36–66 km/h was prone to be the most optimal driving conditions in terms of the hybrid vehicles’ fuel consumption.

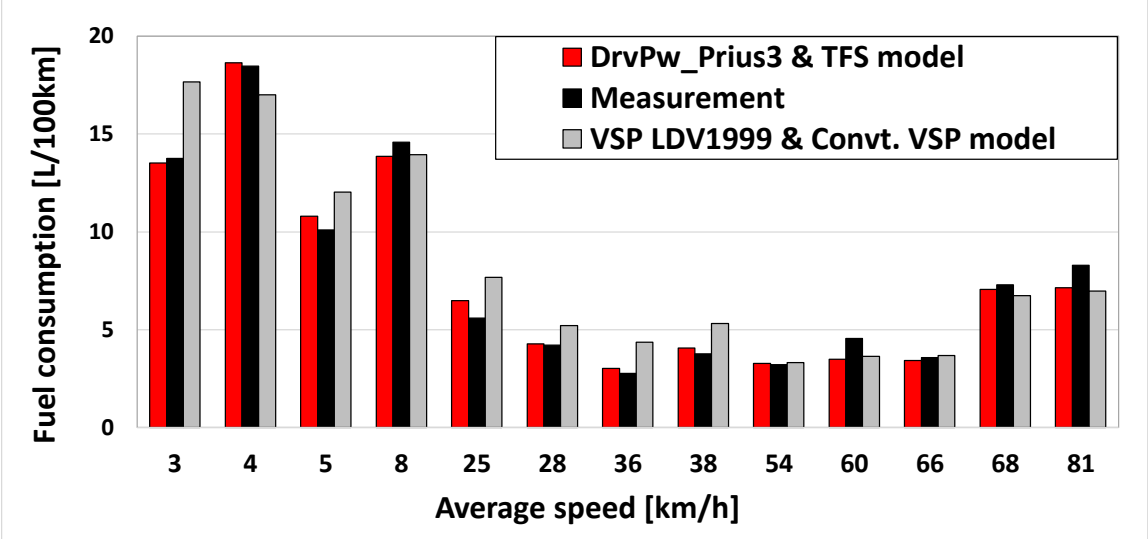


Figure 121. Fuel consumption prediction validation among *DrvPw_{Prius3}* and *TFS model* method, measurement data, and *VSP LDV1999* and *Convvt. VSP model* method

Figure 122 shows the error generated by the two comparative methods in various real-world driving conditions in Bangkok from 14 trips of which the average speeds vary from 3

km/h to 81 km/h. From the data, the new method proposed in the study significantly reduces the error from the conventional VSP method. The fluctuation of the fuel consumption prediction is reduced from a range of -20 to 57% down to -23 to 16%. Particularly, at low to moderate average driving speed, which reflects city and suburban traffic conditions, the conventional VSP fuel consumption model performs an unreliable prediction with the error in a range of -8 to 57% compared to the measurement. On the other hand, the new method provides much more stability and reliability on the prediction results. It provides sufficient accuracy to capture the complexity of hybrid powertrain fuel consumption characteristics. Moreover, this model is applicable to various driving conditions. Nevertheless, this model requires a larger amount of data than the conventional VSP fuel consumption modeling method. The database used in the model construction should be able to cover a variety of driving incidents.

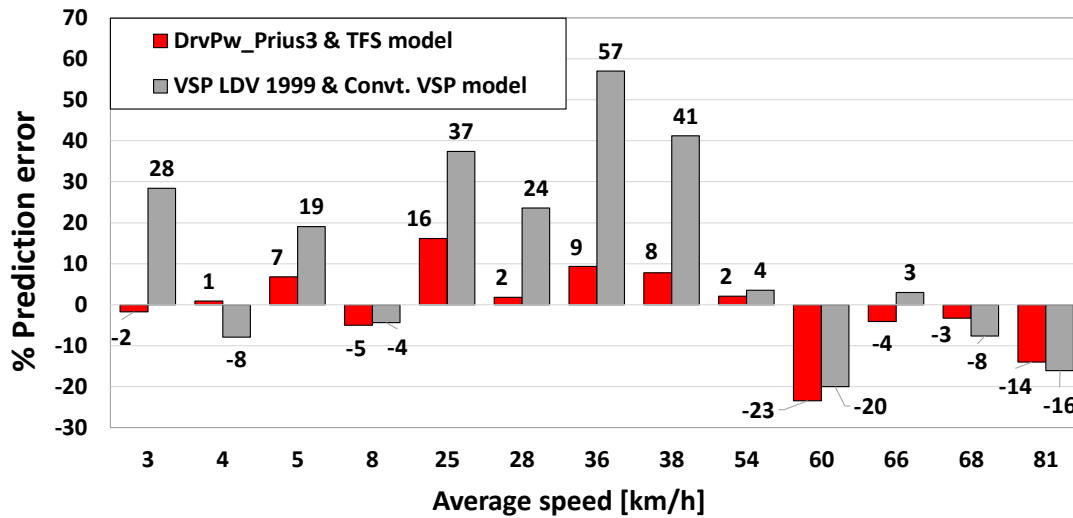


Figure 122 Fuel consumption prediction error between *DrvPw_{Prius3}* and *TFS model* method, and *VSP LDV1999* and *Convrt. VSP model* method

6.3.5 Conclusion

This study proposed a new methodology to model the fuel consumption of a hybrid vehicle based on the fundamental of the powertrain operation mechanism. For the vehicle's driving force estimation, this study applied the new driving power equation with a set of coefficients that was specifically calibrated for the Prius3. The new equation provided accurate estimation at r-squared 0.95.

For the model construction, this study provided a comparative analysis on the fidelity of the conventional VSP fuel consumption modeling method and the fundamental of the hybrid powertrain operation mechanism. This paper discovered that vehicle driving power is not the only primary factor that influences hybrid vehicles' fuel consumption. According to

the analysis, this study constructs the energy consumption model based on vehicle's driving force and speed called Traction Force-Speed Based Model. The results show that this model provided a promising capability on real-world fuel consumption estimation for hybrid vehicles. More than 90% of the prediction results fell inside the 95% confidential interval. The Traction Force-Speed Based Model also improved the prediction error from the conventional VSP modeling method from the absolute error at 57% to 23% by using the same data acquisition effort. Taking driving force and speed into the model significantly suppressed the fluctuation of the prediction error. Also, it extended the application limitations of the conventional models to be able to capture a variety of driving situations and the impact of hybrid vehicles' operation mode transition on the energy consumption characteristics. In addition, this study has presented evidence that the driving mode transition in hybrid vehicles significantly affects their energy consumption. Thus, it is necessary to consider these unique characteristics to the modeling process.

6.3.6 Further improvement

This version of the TFS model is not yet the final version. This model still has not included the electric consumption model of the hybrid vehicle. In addition, the criteria of hybrid vehicles' operation mode switching is primarily determined based on vehicle speed, driving force, and battery SOC. Therefore, the further improvement will also be focusing on battery modeling to predict the real-time SOC and the current operation mode.

CHAPTER 7

Hybrid Vehicle Energy Consumption Characteristic Analysis and Applications

7.1 An investigation of the impact of summer (Energy Saver +) and winter (ALPIN) tires on hybrid vehicle's fuel consumption in real-world traffic driving

7.1.1 Introduction

According to Michelin's request, this study attempted to investigate the impact of tires on hybrid vehicle fuel consumption. The research questions also identify whether it is practical to conduct this experiment under real-world traffic conditions. In this context, the effect of the tires on vehicle fuel consumption is comparatively small, once the test conditions were interfered by predominate contributors, such as traffic condition, driving behavior, road grade, and wind speed. (Pitanuwat and Sripakagorn, 2015)

Thus, this section will propose a data visualization technique to analysis the tire effect on hybrid vehicle fuel consumption. NGO real-driving database was employed in this analysis. Two tire sets: summer tires (Energy Saver +) and winter tires (ALPIN), were compared. City and highway traffic conditions were selected for the driving scenario. At the same traffic condition, the same professional driver was employed to maintain the

consistency of the driving behavior. The test repetition was conducted 3 rounds per one test condition. The tire-surface temperature was measured and found between 23-28°C during the experiment. For more experimental set-up procedure, please refer to section chapter4.

The conventional visualization technique usually evaluates the vehicle fuel economy based on total fuel consumption and total driving distance, such as L/100km or Km/L. Figure 123 shows the fuel consumption comparison by using the L, L/100km unit and average speed of the trips. Note that the difference between initial and final battery soc was compensated into the fuel consumption equivalent term. The results between the winter and summer tire datasets are labeled as Tire A (red) and Tire B (blue) respectively.

On the left figure, the relationship between fuel consumption amount (L) and average speed (km/h) was displayed. The data separated into two clusters which are low average speed in city driving, and high average speed in highway driving. On the right figure, it shows the data in a form of fuel consumption (L/100km) and the average speed of the trips. Both of tire A and B datasets exhibit the same trend that in city driving, the lower the traveling average speed is, the more fuel that the hybrid vehicle will dramatically consume per 100 km of driving. However, in highway driving, lower average speed seems to provide a better fuel consumption result. In addition, the incremental trend of fuel consumption is less severe in higher average speed driving. It appears the hybrid vehicle might be designed to perform the best fuel efficiency in traffic that has an average speed around 40-60km/h.

From Figure 123, these conventional data visualization methods have a potential to visualize the effect of traffic; however, these analysis methods are too coarse to interpret the

delicate effect of tires on vehicle fuel consumption. Since the most dominating factors such as traffic conditions cannot be well managed under the real-world driving environment.

Thus, this study developed a new data visualization method to analyze the effect of the tires on vehicle fuel consumption under multi-influential factors of real-world driving conditions. This method aims to view fuel consumption from the powertrain efficiency perspective.

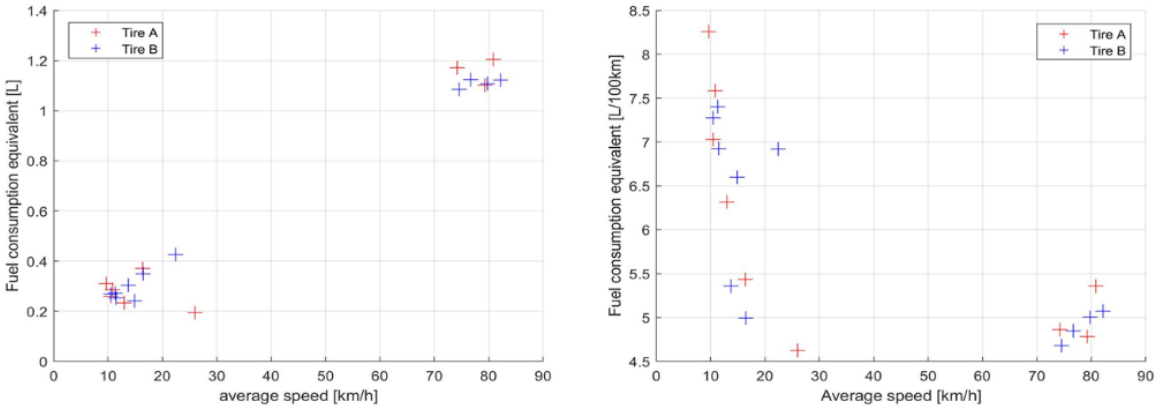


Figure 123 Comparison between fuel consumption of Prius3 driving with the summer and winter tire sets based on conventional data visualization technique

7.1.2 Methodology

The new data visualization method had been developed based on instantaneous powertrain efficiency. The related equations used for the hybrid powertrain efficiency calculation are described in Table 22.

Table 22 Hybrid powertrain instantaneous efficiency calculation

NO regenerative braking	Input = Fuel_Pw + Batt_discharge_Pw
(Acceleration)	Output = Drv_Pw + Batt_charge_Pw + AUX_Pw
	PT eff = Output / Input
Regenerative braking	Input = Fuel_Pw + Braking_Pw
(Deceleration)	Output = Batt_charge_Pw + AUX_Pw
	PT eff = Output / Input

This section analyzes the powertrain efficiency with the driving force and vehicle speed. For driving force and power consumption, these parameters were not directly measured at the tire surfaces but the driving they were estimated from the powertrain dynamic model.

During the experiment, the test conditions were controlled to be consistent between the two tires. Distribution of the driving force and power between the winter tires (Ta) and the summer tires (Tb) during the experiment are shown in Figure 124. The distributions are slightly different but the shapes of both driving force and power are significantly similar. According to the data, it may indicate that the traffic and driving conditions of the experiment on Ta and Tb are identical to some extent. In addition, AUX power usage and Initial SOC were also set up to follow the same procedure. Thus we assumed that the only major differences were tires that created an impact on the powertrain operation point selection.

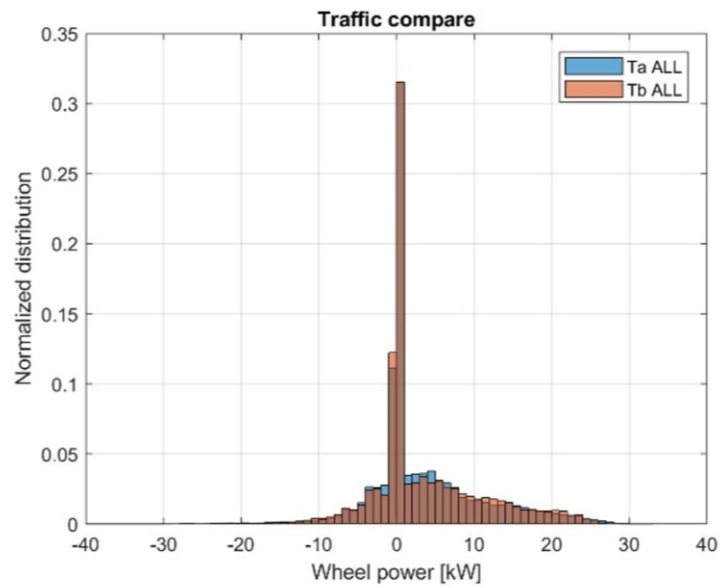
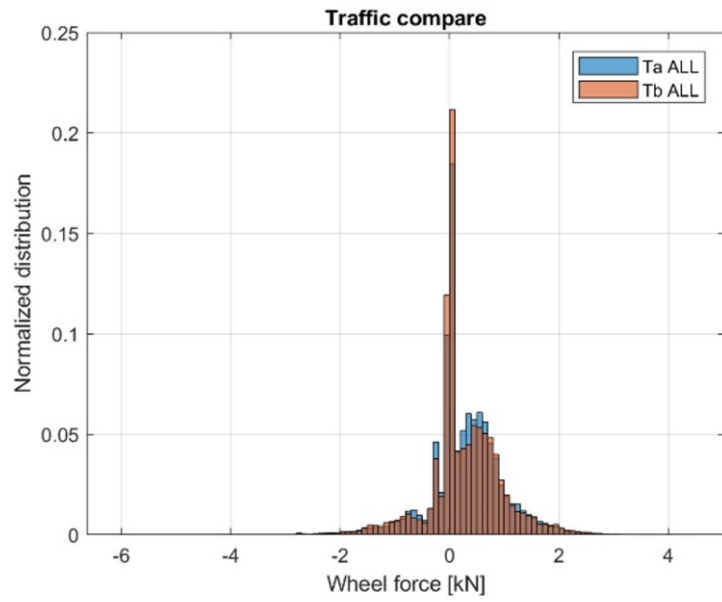


Figure 124 Distribution of the driving force and power between the winter tires (Ta) and the summer tires (Tb) during the experiment

7.1.3 Result and discussion

Figure 125 illustrates the hybrid powertrain efficiency with winter tire (Ta) and summer tire (Tb) during inactive regenerative braking. The data are classified into two modes which are electrical driving mode (EV) and hybrid driving mode (HV). The variation of the efficiency is displayed by the colors. At EV mode, the maximum efficiency of both Ta and Tb were found approximately at 90%, located at the area that is far from the zero speed and torque lines, while at HV mode were found at 50%, located at 80-100 km/h driving. At EV mode driving, Ta and Tb operated at the similar regions, while at HV mode, the only apparent difference was at low-speed driving indicated by the dash line shape. Ta seemed to operate at low-speed in HV more frequently and in a wider region. It might imply that using Tb allowed the powertrain to stay in EV mode longer than Ta. EV is usually operated at low speed driving and stop-and-go situation at which the rolling resistance is dominate. Since, Ta provides less rolling resistance compared to Tb, EV driving range of Ta tends to be longer.

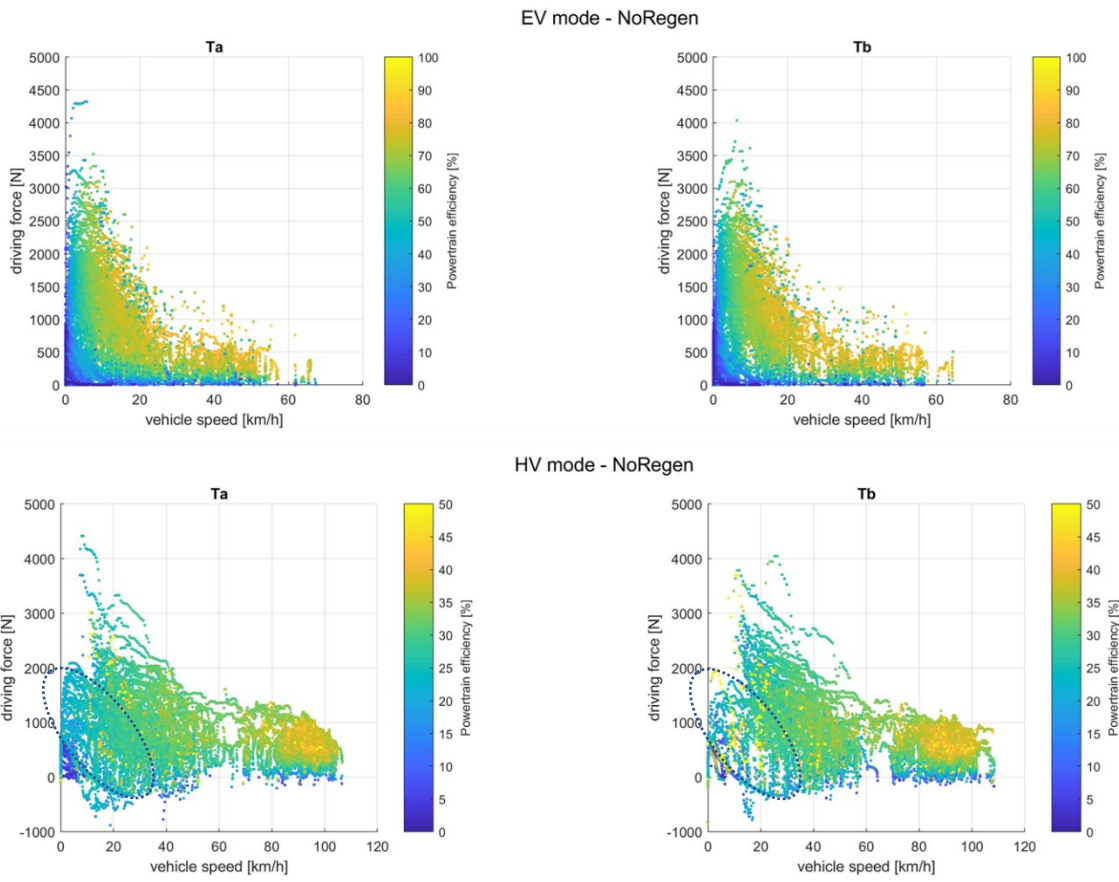


Figure 125 Comparison between the hybrid powertrain efficiency distribution during inactive regenerative braking

Figure 126 shows the data during regenerative braking is active. During the deceleration, the powertrain frequently operates in EV mode. Comparing the data between Ta and Tb, Tb tends to have more data operating at a wider range as labeled in the dash-line shapes. In addition, Tb also operated at higher efficiency more frequently than Ta during braking.

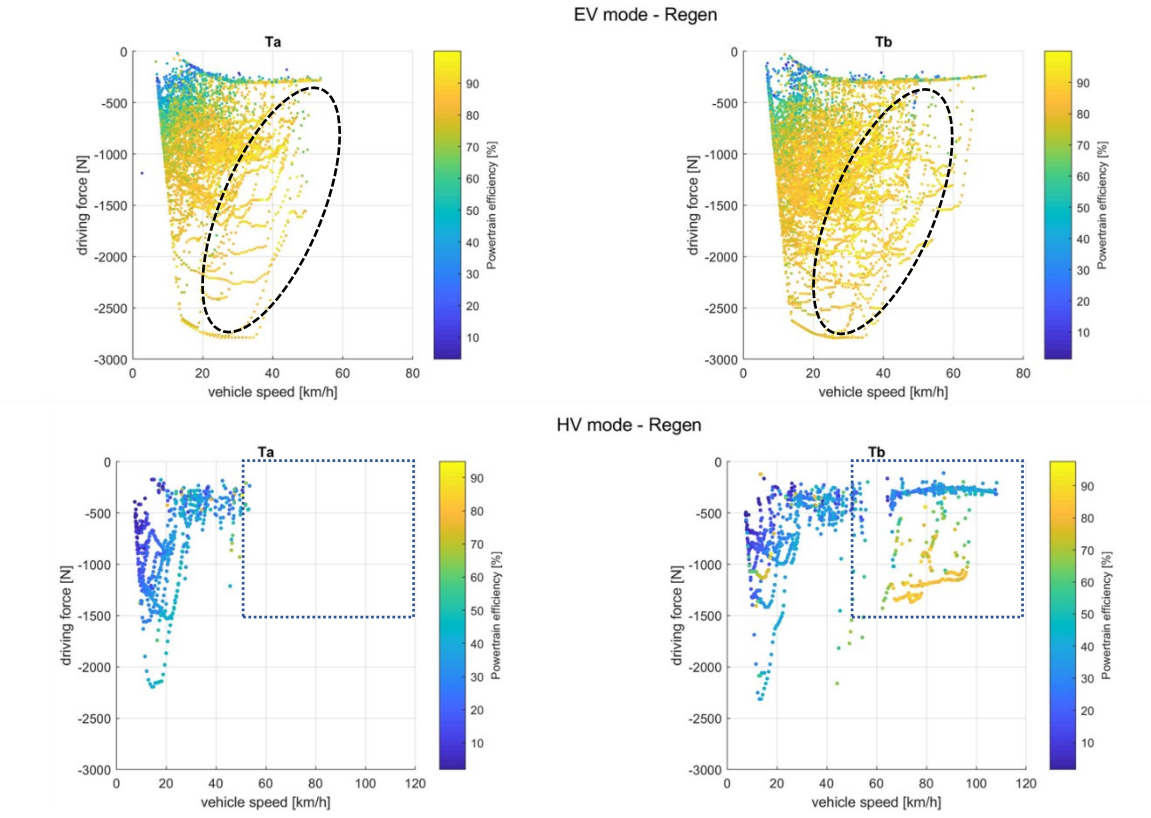


Figure 126 Comparison between the hybrid powertrain efficiency distribution during active regenerative braking

To analyze the efficiency of the powertrain in more detail, Figure 127 shows the comparison of the distribution of the powertrain efficiency between Prius3 using the winter tires (Ta) and summer tires (Tb). The data were categorized by two criteria; powertrain state which is electric drive (EV) /hybrid drive (HV), and regenerative braking state which are active regenerative braking (regen)/inactive regenerative braking (no-regen).

At EV no-regen mode, the results show that the shapes of the powertrain distributions between Ta and Tb are similar. The efficiency of Ta and Tb varied between 20-90%. However, there are some shifts observable. At the first and second peaks, Ta seemed to have higher distribution, while Tb slightly shifted to the middle between the peaks.

At HV no-regen, the result shows that Tb slightly shifted towards the higher efficiency direction compared to Ta. The overall powertrain efficiency varied between 5-50%. It may imply that using Tb allows the powertrain to operate at the higher efficiency region compared with using Ta during HV no-regen mode.

At EV regen, this figure shows the most distinguishable shift between Ta and Tb. According to the former analysis, it affirmed that EV regen is a significant operation mode during deceleration. The distributions show that Tb data populated at higher efficiency during EV regenerative braking compared to Ta data. It indicates that Tb allows the powertrain to perform a better efficiency of braking energy recuperation compared to Ta. At HV regen, the data also show similar results.

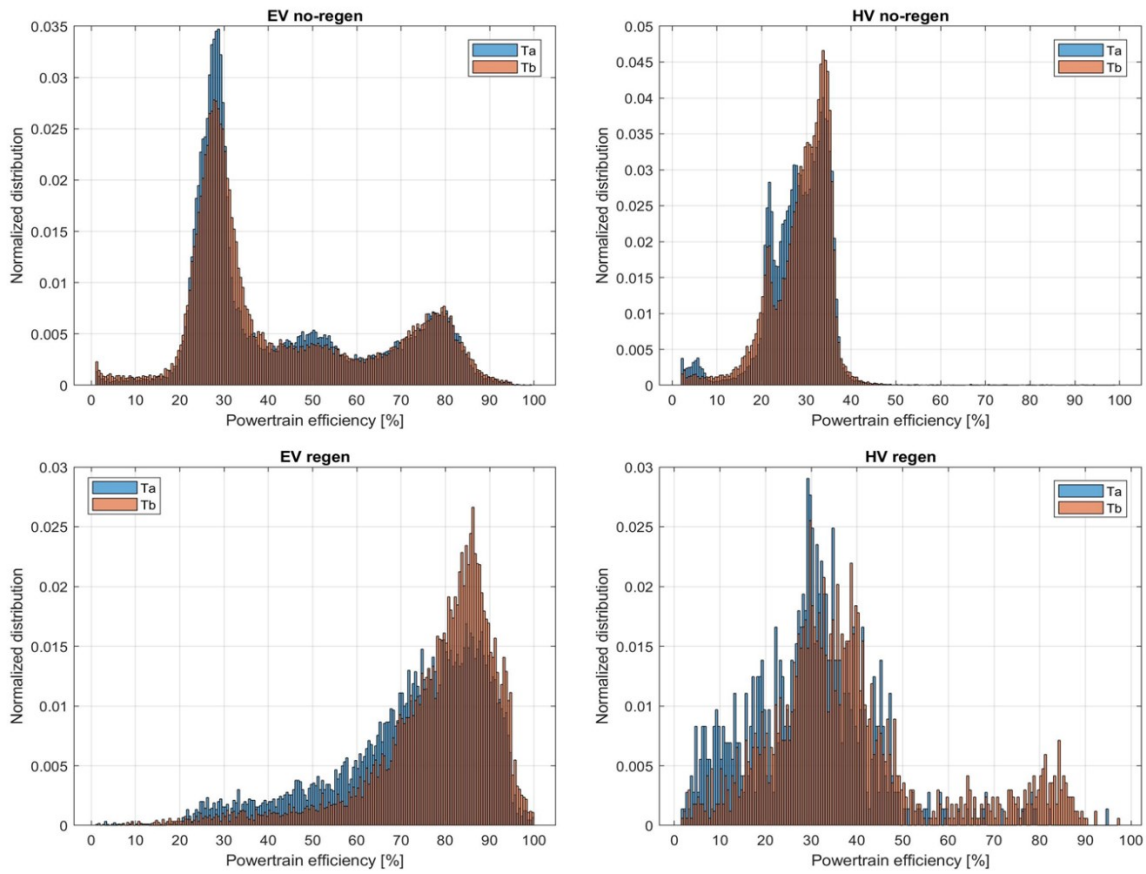


Figure 127 Comparison between the hybrid powertrain efficiency distribution during active and inactive regenerative braking

7.1.4 Conclusion

The effect of tires on vehicles' fuel consumption is quite small compared to the uncertain/diversity of the real-world traffic flows. Thus, the conventional comparison by using L/100km and average speed are too rough to capture and analyze the tire effect. Thus, we implement hybrid powertrain efficiency as a parameter to analyze the impact of tires on

a vehicle's instantaneous energy consumption characteristics. Due to the characteristic of hybrid vehicles which have multi-operation modes delivering different PT efficiency, it is important to separate the analysis cases into EV and HV driving / Regen and no-Regen modes.

According to the results, it showed that both of the Ta (winter tire, ALPIN 195/65 R15) and Tb (summer tire, Energy save+ 195/65 R15) delivered the powertrain efficiency roughly at the same range. The powertrain efficiency in EV modes was found between 5 – 95%, while in HV modes were found between 5 -50%. For the powertrain distribution analysis, Tb tends to have a potential to allow the powertrain to operate at higher efficiency regions more frequently than Ta, particularly during deceleration (EV and HV regen) and hybrid driving (HV no-regen).

This data visualization concept is just at a pilot study state. There are several parts that require further improvements. For instance, the number of samples needs to be increased to statistically manage the uncertainty of the traffic flow. Also, the experimental conditions should be properly controlled in terms of the temperature, tire warm-up duration, and others. Nevertheless, according to the presented results, it is convincing that the instantaneous powertrain efficiency analysis method proposed in this study has the potential to capture such a delicate effect of tires on vehicle fuel consumption.

CHAPTER 8

Conclusion and Future Work

8.1 Conclusion

This dissertation attempted to construct analytical-empirical hybrid vehicles' energy consumption model for transportation research applications. This study also presented step-by-step modeling processes that started from hybrid vehicles experiment, data acquisition, data processing, combine hybrid powertrain operation control investigation, and modeling. Based on the hybrid powertrain operation characteristics investigated in this study, a microscopic analytical-empirical energy-consumption model called Traction Force-Speed based Energy Consumption Model (TFS model) was constructed.

To acquire a representative dataset for hybrid powertrain operation and fuel consumption characteristic investigation, experimental design, and data acquisition must be conducted. In this study, real-world experiments, private circuit experiments, and chassis dynamometer experiments were conducted. The advantages and disadvantages were analyzed and compared. According to the finding, real-world experiment was the most suitable approach for vehicles' fuel-consumption data acquisition. On the other hand, to acquire the dataset that covered a significant of the complex powertrain operation characteristics, this study suggested using chassis dynamometer experiment operating under constant force mode.

The next process was the powertrain operation characteristic investigation. This study investigated and validated the operation characteristics by applying the dataset to improve the logics of the powertrain operation models in Prius3 CRUISE AVL simulation. To obtain the requisite parameters, the power-flow path inside the power-split configuration was analyzed. Then, the powertrain's dynamic equations were derived and adopted in the parameter estimations and map calibrations. By applying the calibrated maps and models into the simulation, the fuel consumption and powertrain operation were significantly improved to be more realistic. According to the analysis, it indicated that the hybrid powertrain operated in multi-operation modes. The transition of the modes could be simplified and expressed by boundaries specified by vehicle speed and driving force as X-Y axis. In addition, the boundaries also varied depending on the instantaneous available battery power.

Based on these substantial operation characters, the TFS model had been built to capture those hybrid powertrain features. In this process, the contributions of the research were, first to propose a practical and cost-efficient approach to recalibrate coefficients of the vehicle-driving-power-estimation equation to be specific for the studied vehicle models or fleets. This study implemented the assessable CAN dataset to estimate the powertrain's total driving power via the powertrain's dynamic equation derived in the previous process. The coefficients in the vehicle-driving-power-estimation equation were calibrated with the powertrain's total driving power by applying stepwise multiple regression method. The results stated that the calibrated equation significantly improved the driving power estimation compared to the conventional VSP with the LDV coefficients. Particularly under heavy load

driving (above 50kW) and high-speed driving (>80km/h), the proposed method substantially suppressed the prediction error by having the coefficient improved from 0.79 to 0.96.

Then, the TFS model was constructed in MATLAB based on the relationships between the vehicle speed and the average fuel consumption rate at specified traction force intervals. The trend of the vehicle speed and the fuel consumption rate monotonically increased as the traction force became more intense. The prediction results showed that the TFS method efficiently reduced the error by 57% down to 23% compared to the conventional VSP modeling method.

Furthermore, this study also explored hybrid vehicle fuel consumption characteristics in a different aspect. The objective of the project was to investigate the impact of winter tires and summer tires on hybrid vehicle fuel consumption. This study suggested a new parameter called instantaneous hybrid powertrain efficiency that incorporated the efficiency of the electric system and the engine system. The results showed that this parameter provided capability to analyze and visualize delicate factors that impacted the fuel consumption of the hybrid powertrains compared to fuel economy-oriented parameters, such as L/100km or km/L. Finally, the most significant remark was found that the summer tires tended to allow the powertrain to operate at higher efficiency regions more frequently than the winter tires, particularly during deceleration under EV and HV regenerative braking and typical hybrid driving.

8.2 Future Work

This version of the TFS model still has not included the electric consumption model of the hybrid vehicle. Since the criteria of hybrid vehicles' operation mode transition are primarily determined based on vehicle speed, driving force, and battery SOC, the further improvements are suggested to continue on developments of light-computational-load models of battery modeling to precisely predict the real-time SOC, and operation mode transition. Furthermore, to reduce labor intensive on the modeling process, the hybrid vehicles' fuel consumption models must be generalized to be more aggregate so that a single model can represent the substantial characteristics among a drastic diversity of hybrid vehicle configurations. This study also recommends to make use of big data (floating car dataset) and modeling automation to increase the modeling capacity.

BIBLIOGRAPHY

- Ahlawat, R., Bredenbeck, J. and Tatsuo Ichige, M. (2013) 'Estimation of Road Load Parameters via On-road Vehicle Testing g Tire Technology Expo 2013 February 5-7 Cologne Germany', pp. 1–44. Available at: www.aanddtech.com.
- Al-Samari, A. (2017) 'Study of emissions and fuel economy for parallel hybrid versus conventional vehicles on real world and standard driving cycles', *Alexandria Engineering Journal*. Faculty of Engineering, Alexandria University, 56(4), pp. 721–726. doi: 10.1016/j.aej.2017.04.010.
- Allouchery, L. (2012) 'Modeling of prius iii with cruise 2011.2'.
- Bohme, T. J. and Frank, B. (2017) *Hybrid Systems, Optimal Control and Hybrid Vehicles, Advances in Industrial Control*. doi: 10.1007/978-3-319-51317-1.
- Böhme, T. J. and Frank, B. (2017) *Hybrid Systems, Optimal Control and Hybrid Vehicles*. Cham: Springer International Publishing (Advances in Industrial Control). doi: 10.1007/978-3-319-51317-1.
- Çağatay Bayindir, K., Gözüküçük, M. A. and Teke, A. (2011) 'A comprehensive overview of hybrid electric vehicle: Powertrain configurations, powertrain control techniques and electronic control units', *Energy Conversion and Management*. Pergamon, 52(2), pp. 1305–1313. doi: 10.1016/J.ENCONMAN.2010.09.028.
- De Cesare, M., Cavina, N. and Brugnoli, E. (2019) 'Conceptual Design and Analytic Assessment of 48V Electric Hybrid Powertrain Architectures for Passenger Cars', in. doi: 10.4271/2019-01-0353.
- CORDIS (1994) *Modelling of Emission and Consumption in Urban Areas | MODEM Project | FP2 | CORDIS | European Commission*. Available at: <https://cordis.europa.eu/project/id/V1053> (Accessed: 5 May 2020).
- Cunefare, K. *et al.* (2011) 'Backward-Looking Simulation of the Toyota Prius and General Motors Two-Mode Power-Split HEV Powertrains', *SAE International Journal of Engines*, 4(1), pp. 1281–1297. doi: 10.4271/2011-01-0948.
- DRL (2019) *Models/Emissions/PHEMlight - SUMO Documentation*. Available at: <https://sumo.dlr.de/docs/Models/Emissions/PHEMlight.html> (Accessed: 5 May 2020).
- Duarte, G. O. *et al.* (2014) 'Effect of battery state of charge on fuel use and pollutant emissions of a full hybrid electric light duty vehicle', *Journal of Power Sources*. Elsevier, 246, pp. 377–386. doi: 10.1016/J.JPOWSOUR.2013.07.103.
- Duarte, G. O., Gonçalves, G. A. and Farias, T. L. (2014) 'A Methodology to Estimate Real-world Vehicle Fuel Use and Emissions based on Certification Cycle Data', *Procedia* -

- Social and Behavioral Sciences*. Elsevier B.V., 111, pp. 702–710. doi: 10.1016/j.sbspro.2014.01.104.
- Duarte, G. O., Gonçalves, G. A. and Farias, T. L. (2016) ‘Analysis of fuel consumption and pollutant emissions of regulated and alternative driving cycles based on real-world measurements’, *Transportation Research Part D: Transport and Environment*. Pergamon, 44, pp. 43–54. doi: 10.1016/J.TRD.2016.02.009.
- Enang, W. and Bannister, C. (2017a) ‘Modelling and control of hybrid electric vehicles (A comprehensive review)’, *Renewable and Sustainable Energy Reviews*. Elsevier Ltd, 74(October 2018), pp. 1210–1239. doi: 10.1016/j.rser.2017.01.075.
- Enang, W. and Bannister, C. (2017b) ‘Modelling and control of hybrid electric vehicles (A comprehensive review)’, *Renewable and Sustainable Energy Reviews*. Elsevier, 74, pp. 1210–1239. doi: 10.1016/j.rser.2017.01.075.
- Faris, W., Rakha, H. and Elmoselhy, S. A. M. (2014) ‘Impact of Intelligent Transportation Systems on Vehicle Fuel Consumption and Emission Modeling: An Overview’, *SAE International Journal of Materials and Manufacturing*, 7(1), pp. 129–146. doi: 10.4271/2013-01-9094.
- Fiori, C., Ahn, K. and Rakha, H. A. (2016) ‘Power-based electric vehicle energy consumption model: Model development and validation’, *Applied Energy*. Elsevier, 168, pp. 257–268. doi: 10.1016/J.APENERGY.2016.01.097.
- Fiori, C., Ahn, K. and Rakha, H. A. (2018) ‘Microscopic series plug-in hybrid electric vehicle energy consumption model: Model development and validation’, *Transportation Research Part D: Transport and Environment*. Elsevier, 63(May), pp. 175–185. doi: 10.1016/j.trd.2018.04.022.
- Frey, H. C., Zhai, H. and Roupail, N. M. (2009) ‘Regional On-Road Vehicle Running Emissions Modeling and Evaluation for Conventional and Alternative Vehicle Technologies’, *Environmental Science & Technology*, 43(21), pp. 8449–8455. doi: 10.1021/es900535s.
- Ge, M. and Friedrich, J. (2020) *Greenhouse Gas Emissions by Countries and Sectors World Resources Institute*. Available at: <https://www.wri.org/blog/2020/02/greenhouse-gas-emissions-by-country-sector> (Accessed: 12 April 2020).
- Giannouli, M. (2003) ‘COPERT III Computer programme to calculate emissions from road transport. Delivery of Road Transport Emission data for EU 15 country’, (49).
- Graver, B. M., Frey, H. C. and Choi, H.-W. (2011) ‘In-Use Measurement of Activity, Energy Use, and Emissions of a Plug-in Hybrid Electric Vehicle’, *Environmental Science & Technology*. American Chemical Society, 45(20), pp. 9044–9051. doi: 10.1021/es201165d.
- Green Car Congress (2017) *BCG forecasts electrified vehicles to take half of global auto market by 2030; hybrids to dominate - Green Car Congress, 2004-2020 BioAge Group*,

- LLC. Available at: <https://www.greencarcongress.com/2017/11/20171103-bcg.html> (Accessed: 18 April 2020).
- Holmén, B. A. and Sentoff, K. M. (2015) ‘Hybrid-Electric Passenger Car Carbon Dioxide and Fuel Consumption Benefits Based on Real-World Driving’, *Environmental Science & Technology*. American Chemical Society, 49(16), pp. 10199–10208. doi: 10.1021/acs.est.5b01203.
- Hu, J., Frey, H. C. and Washburn, S. S. (2016) ‘Comparison of Vehicle-Specific Fuel Use and Emissions Models Based on Externally and Internally Observable Activity Data’, *Transportation Research Record: Journal of the Transportation Research Board*. SAGE PublicationsSage CA: Los Angeles, CA, 2570(1), pp. 30–38. doi: 10.3141/2570-04.
- IPCC (2014) *Climate Change 2014 Mitigation of Climate Change, Climate Change 2014: Mitigation of Climate Change. Contribution of Working Group III to the Fifth Assessment Report of the Intergovernmental Panel on Climate Change*. doi: 10.1017/CBO9781107415416.
- Jiménez, J. L. *et al.* (1999) ‘Vehicle Specific Power : A Useful Parameter for Remote Sensing and Emission Studies Effect of Driving Conditions on Emissions • Driving conditions may strongly influence emissions’.
- Kim, C. *et al.* (2016) ‘Study on the criteria for the determination of the road load correlation for automobiles and an analysis of key factors’, *Energies*, 9(8), pp. 7–9. doi: 10.3390/en9080575.
- Kühlwein, J. (2016) ‘The impact of official versus real-world road loads on CO2 emissions and fuel consumption of European passenger cars’, *ICCT White Paper*, (May), pp. 1–54. doi: 10.3109/10641963.2013.776564.
- Lah, O. (2017) ‘Sustainable development synergies and their ability to create coalitions for low-carbon transport measures’, in *Transportation Research Procedia*. doi: 10.1016/j.trpro.2017.05.495.
- Lee, S. *et al.* (2013) ‘Modeling and Validation of Power-Split and P2 Parallel Hybrid Electric Vehicles’, *SAE Technical Paper Series*, 1(April 2016). doi: 10.4271/2013-01-1470.
- Liu, J. and Peng, H. (2008) ‘Modeling and Control of a Power-Split’, *Control*, 16(6), pp. 1242–1251. doi: 10.1109/TCST.2008.919447.
- Liu, J., Peng, H. and Filipi, Z. (2005) ‘Modeling and Analysis of the Toyota Hybrid System’, *Proceedings, 2005 IEEE/ASME International Conference on Advanced Intelligent Mechatronics.*, pp. 24–28. doi: 10.1109/AIM.2005.1500979.
- Mansour, C., Haddad, M. and Zgheib, E. (2018) ‘Assessing consumption, emissions and costs of electrified vehicles under real driving conditions in a developing country with an inadequate road transport system’, *Transportation Research Part D: Transport and Environment*. Elsevier, 63(June), pp. 498–513. doi: 10.1016/j.trd.2018.06.012.

- Montazeri-Gh, M. and Mahmoodi-k, M. (2015) ‘Development a new power management strategy for power split hybrid electric vehicles’, *Transportation Research Part D: Transport and Environment*, 37, pp. 79–96. doi: 10.1016/j.trd.2015.04.024.
- Murphey, Y. L. *et al.* (2012) ‘Intelligent hybrid vehicle power control part I: Machine learning of optimal vehicle power’, *IEEE Transactions on Vehicular Technology*, 61(8), pp. 3519–3530. doi: 10.1109/TVT.2012.2206064.
- Onori, S., Serrao, L. and Rizzoni, G. (2016a) *Hybrid Electric Vehicles*. London: Springer London (SpringerBriefs in Electrical and Computer Engineering). doi: 10.1007/978-1-4471-6781-5.
- Onori, S., Serrao, L. and Rizzoni, G. (2016b) *Hybrid Electric Vehicles*. London: Springer London (SpringerBriefs in Electrical and Computer Engineering). doi: 10.1007/978-1-4471-6781-5.
- Organization of the Petroleum Exporting Countries (2017) *2017 OPEC World Oil Outlook*. Available at: <http://www.opec.org> (Accessed: 3 March 2019).
- Pitanuwat, S. *et al.* (2017) ‘Improvement and validation of a commercial power-split hybrid powertrain simulation based on real-world driving data’, *2017 Society of Automotive Engineers of Japan Congress (Autumn) Proceedings*, (No.126-17), pp. 399–407. Available at: https://www.bookpark.ne.jp/cm/jsae/particulars_e.asp?content_id=JSAE-20176072-PDF.
- Pitanuwat, S. *et al.* (2018) ‘Development of Traction Force-Speed Based Fuel Consumption Prediction Model for Hybrid Vehicles’.
- Pitanuwat, S., Aoki, H., Morikawa, T., *et al.* (2019) ‘Development of hybrid vehicle energy consumption model for transportation application – Part1 : Driving power equation development and the coefficient calibration’, (*Under submission preparation process*), pp. 1–15.
- Pitanuwat, S., Aoki, H., Iizuka, S., *et al.* (2019) ‘Development of Hybrid Vehicle Energy Consumption Model for Transportation Applications—Part II: Traction Force-Speed Based Energy Consumption Modeling’, *World Electric Vehicle Journal*, 10(2), p. 22. doi: 10.3390/wevj10020022.
- Pitanuwat, S. *et al.* (2020) ‘Development of Hybrid-Vehicle Energy-Consumption Model for Transportation Applications—Part I: Driving-Power Equation Development and Coefficient Calibration’, *Energies*. Multidisciplinary Digital Publishing Institute, 13(2), p. 476. doi: 10.3390/en13020476.
- Pitanuwat, S. and Sripakagorn, A. (2015) *An Investigation of Fuel Economy Potential of Hybrid Vehicles under Real-World Driving Conditions in Bangkok*, *Energy Procedia*. Elsevier B.V. doi: 10.1016/j.egypro.2015.11.607.

- Rodríguez, R. A. *et al.* (2016) ‘Influence of driving patterns on vehicle emissions: A case study for Latin American cities’, *Transportation Research Part D: Transport and Environment*. Pergamon, 43, pp. 192–206. doi: 10.1016/J.TRD.2015.12.008.
- Sciarretta, A. *et al.* (2012) ‘A control benchmark on the energy management of a plug-in hybrid electric vehicle’, *Control Engineering Practice*, (29). doi: 10.1016/j.conengprac.2013.11.020.
- Sciarretta, A. *et al.* (2014) ‘A control benchmark on the energy management of a plug-in hybrid electric vehicle’, *Control Engineering Practice*. Pergamon, 29, pp. 287–298. doi: 10.1016/J.CONENGPRAC.2013.11.020.
- Song, G., Yu, L. and Tu, Z. (2012) ‘Distribution Characteristics of Vehicle-Specific Power on Urban Restricted-Access Roadways’, *Journal of Transportation Engineering*, 138(2), pp. 202–209. doi: 10.1061/(ASCE)TE.1943-5436.0000318.
- Song, G., Yu, L. and Wu, Y. (2016) ‘Development of Speed Correction Factors Based on Speed-Specific Distributions of Vehicle Specific Power for Urban Restricted-Access Roadways’, *Journal of Transportation Engineering*, 142(3), p. 04016001. doi: 10.1061/(ASCE)TE.1943-5436.0000819.
- Syed, Fazal U *et al.* (2006) ‘Derivation and Experimental Validation of a Power-Split Hybrid Electric Vehicle Model’, *IEEE TRANSACTIONS ON VEHICULAR TECHNOLOGY*, 55(6). doi: 10.1109/TVT.2006.878563.
- Syed, Fazal U. *et al.* (2006) ‘Derivation and Experimental Validation of a Power-Split Hybrid Electric Vehicle Model’, *IEEE Transactions on Vehicular Technology*, 55(6), pp. 1731–1747. doi: 10.1109/TVT.2006.878563.
- Taylor, N. B. (2003) ‘The CONTRAM Dynamic Traffic Assignment Model’, *Networks and Spatial Economics*. Springer, 3(3), pp. 297–322. doi: 10.1023/A:1025394201651.
- Toyota (2013) *Toyota hybrid system THS II*. Available at: <http://www.toyota.co.jp>.
- Toyota Motor Corporation (2019) *Toyota | Global Newsroom | Toyota Motor Corporation Official Global Website*. Available at: <https://global.toyota/en/newsroom/toyota/> (Accessed: 3 March 2019).
- TOYOTA MOTOR CORPORATION (2019) *Toyota sells 1.52 million electrified vehicles in 2017, three years ahead of 2020 target | Corporate | Global Newsroom | Toyota Motor Corporation Official Global Website*. Available at: <https://global.toyota/en/newsroom/corporate/20966057.html> (Accessed: 17 April 2019).
- US EPA (2010) ‘United states environmental protection agency national vehicle and fuel emissions laboratory 2565 plymouth road ann arbor, michigan 48105-2498’, 12(2), pp. 1–8.
- US EPA (2016) *Description and History of the MOBILE Highway Vehicle Emission Factor Model*. Available at: <https://www.epa.gov/moves/description-and-history-mobile-highway-vehicle-emission-factor-model> (Accessed: 5 May 2020).

- US EPA (2019) *Latest Version of MOtor Vehicle Emission Simulator (MOVES)*. Available at: <https://www.epa.gov/moves/latest-version-motor-vehicle-emission-simulator-moves> (Accessed: 5 May 2020).
- US EPA (2020) *Highlights of the Automotive Trends Report*. Available at: <https://www.epa.gov/automotive-trends/highlights-automotive-trends-report#Highlight1> (Accessed: 17 April 2020).
- Wang, J. and Rakha, H. A. (2016) ‘Modeling Fuel Consumption of Hybrid Electric Buses: Model Development and Comparison with Conventional Buses’, *Transportation Research Record: Journal of the Transportation Research Board*, 2539(1), pp. 94–102. doi: 10.3141/2539-11.
- Wu, Y., Song, G. and Yu, L. (2014) ‘Sensitive analysis of emission rates in MOVES for developing site-specific emission database’, *Transportation Research Part D: Transport and Environment*. Elsevier Ltd, 32, pp. 193–206. doi: 10.1016/j.trd.2014.07.009.
- Wyatt, D. W., Li, H. and Tate, J. E. (2014) ‘The impact of road grade on carbon dioxide (CO₂) emission of a passenger vehicle in real-world driving’, *Transportation Research Part D: Transport and Environment*. Pergamon, 32, pp. 160–170. doi: 10.1016/J.TRD.2014.07.015.
- Yao, Z. *et al.* (2013) ‘Statistical Vehicle Specific Power Profiling for Urban Freeways’, *Procedia - Social and Behavioral Sciences*. Elsevier B.V., 96(Cictp), pp. 2927–2938. doi: 10.1016/j.sbspro.2013.08.324.
- Yi, C. *et al.* (2016) ‘Modeling, control, and performance of a novel architecture of hybrid electric powertrain system’, *Applied Energy*. Elsevier, 178, pp. 454–467. doi: 10.1016/J.APENERGY.2016.06.068.
- Zhai, H., Christopher Frey, H. and Roupail, N. M. (2011) ‘Development of a modal emissions model for a hybrid electric vehicle’, *Transportation Research Part D: Transport and Environment*. Pergamon, 16(6), pp. 444–450. doi: 10.1016/J.TRD.2011.05.001.
- Zhang, R. and Yao, E. (2015) ‘Electric vehicles’ energy consumption estimation with real driving condition data’, *Transportation Research Part D: Transport and Environment*. Pergamon, 41, pp. 177–187. doi: 10.1016/J.TRD.2015.10.010.
- Zhang, S. *et al.* (2014) ‘Real-world fuel consumption and CO₂ (carbon dioxide) emissions by driving conditions for light-duty passenger vehicles in China’, *Energy*. Pergamon, 69, pp. 247–257. doi: 10.1016/J.ENERGY.2014.02.103.
- Zhou, M. and Jin, H. (2017) ‘Development of a transient fuel consumption model’, *Transportation Research Part D: Transport and Environment*. Elsevier Ltd, 51, pp. 82–93. doi: 10.1016/j.trd.2016.12.001.